Evaluating Early-Age Volume Change and Performance of Polymer-Modified Belitic Calcium Sulfoaluminate (BCSA) Cements: Field and Lab testing

Anna Mei Saelens Tenhagen

A thesis
submitted in partial fulfillment of the
requirements for the degree of

Master of Science

University of Washington

2025

Committee:

Fred Aguayo

Travis Thonstad

Program Authorized to Offer Degree:

Civil and Environmental Engineering

University of Washington

Abstract

Evaluating Early-Age Volume Change and Performance of Polymer-Modified Belitic Calcium Sulfoaluminate (BCSA) Cements: Field and Lab testing

Anna Mei Saelens Tenhagen

Chair of the Supervisory Committee:
Fred Aguayo
Civil and Environmental Engineering

Bridge deck cracking is an increasingly prevalent issue, with limited repair times due to mobility and safety constraints restricting the use of conventional high-early-strength concrete (HESC). This study developed a HESC overlay mix using a belitic calcium sulfoaluminate (BCSA) cement-based system and identified key challenges to its reliable field implementation. Four BCSA systems were evaluated for fresh properties, mechanical strength, and durability performance: CSA with Integral Low-PTM (CSAP), CSA with Liquid Low-PTM (LLP), and latex-modified CSA at 25% (LM25) and 100% (LM100) of the standard latex quantity. The CSAP and LLP mixes were applied as overlays on mini-bridge decks to assess their performance and compatibility with existing substrates under simulated field conditions. In laboratory testing, LLP showed comparable or better strength to CSAP, improved durability over the latex-modified mixes, reduced shrinkage, better air content, and acceptable workability. However, on mini-bridge decks, LLP exhibited significant cracking and underdeveloped mechanical properties. While laboratory results indicate potential for both LLP and CSAP, further research is needed to

evaluate the long-term durability and mechanical performance under field conditions. A deeper understanding of the interactions between polymer types and air-entraining admixtures is also essential to improve performance and ensure reliable application.

Table of Contents

LIST OF TABLES

LIST OF FIGURES

LIST OF SYMBOLS AND ABBREVIATIONS

Acronyms and Abbreviations

Short Form	Meaning
ACI	American Concrete Institute
AEA	Air-entraining admixture
Aft	AluminoFerrite trisulfate
ASTM	American Society of Testing and Materials
BCSA	Belitic calcium sulfoaluminate
BSG	Bulk specific gravity
CA	Coarse aggregate
CoTE	Coefficient of thermal expansion
CSA	Calcium Sulfoaluminate
DEF	Delayed ettringite formation
FA	Fine aggregate
HRWR	High range water reducer
moc	By mass of cement
MOE	Modulus of elasticity
MOR	Modulus of rupture

Acronyms and Abbreviations (continued)

Short Form	Meaning
NMSA	Nominal maximum size aggregate
OD	Oven dried
OPC	Ordinary Portland cement (same as PC)
PC	Portland cement (same as OPC)
PLA	Polylactic acid
PLC	Portland limestone cement
PShC	Plastic shrinkage cracking
RH	Relative humidity
SCM	Supplementary cementitious material
SSD	Saturated surface dry
UHPC	Ultra high-performance concrete
Vp/Vv	Volume-of-paste to volume-of-voids ratio
W/C	Water-to-cement ratio
WR	Water reducer
WSDOT	Washington State Department of Transportation

Cement Chemist Notation

Cement Chemist Notation	Name	Chemical Formula
A	Alumina	Al_2O_3
C	Lime (Calcium oxide)	CaO
F	Ferric oxide	Fe_2O_3
H	Water	H_2O
S	Silica (Silicon dioxide)	SiO_2
$\overline{S}$	Sulfate	SO_3
AH_3	Aluminum hydroxide	$Al(OH)_3$
CH	Lime (Calcium hydroxide)	$Ca(OH)_2$
C-S-H	Calcium silicate hydrate	$Ca_xSi_yO_z \cdot nH_2O$
$C\overline{S}$	Calcium sulfate	$CaSO_4$
$C\overline{S}H_{0.5}$	Hemihydrate	$CaSO_4 \cdot 0.5H_2O$
$C\overline{S}H_2$	Gypsum	$CaSO_4 \cdot 2H_2O$
CO_2	Carbon dioxide	CO_2
C_2S	Belite	$2CaO \cdot SiO_2$
C_2ASH_8	Strätlingite	$Ca_2Al_2(SiO_2)(OH)_{10} \cdot 2.5H_2O$
C_3A	Tricalcium aluminate	$2CaO \cdot SiO_2$

Cement Chemist Notation (continued)

Cement Chemist Notation	Name	Chemical Formula
C_3AH_6	Katoite	$Ca_2Al_2(SiO_4)_{1.5}(OH)_6$
C_3S	Alite	$3CaO \cdot SiO_2$
C_4AF	Brownmillerite	$Ca_2(Al,Fe)_2O_5$
$C_4A\bar{S}H_{12}$	Monosulfate	$3CaO \cdot Al_2O_3 \cdot CaSO_4 \cdot 12H_2O$
$C_4A_3\bar{S}$	Ye'elimite	$4CaO \cdot 3Al_2O_3 \cdot SO_3$
$C_6A\bar{S}_3H_{32}$	Ettringite	$Ca_6Al_2(SO_4)_3(OH)_{12} \cdot 26H_2O$

ACKNOWLEDGEMENTS

First and foremost, I would like to express my sincerest appreciation to my advisors, Dr. Fred Aguayo and Dr. Travis Thonstad. Their dedicated mentorship, technical guidance, and unwavering support over the past two years have been instrumental to the completion of this research. The knowledge and insight I have gained under their supervision have not only shaped the content of this thesis but have also contributed significantly to my academic and professional development.

This research would not have been possible without the generous financial support of the Washington State Department of Transportation. I am also sincerely grateful to CTS Cement for donating materials for the project and providing guidance on their proper use. Special thanks to Lafarge Seattle for lending us their freeze-thaw molds and for their assistance in conducting the testing.

I would also like to thank my colleagues and research team members for their collaboration and support. I am especially grateful to Jafet Guerrero-Estrada for initiating the project and onboarding me, Daniel Akerele for his guidance and assistance in conducting many of the tests, and Vania Moreno-Colin for her work on the slant-shear portion and her enthusiastic involvement. Additional thanks to Mo Al-Sharah, Silas Rene, Emelia Swanson, Blair Turpaud, Alena Karpova, and the UW ACI chapter for their collective contributions in the lab.

Finally, I would like to thank my family and friends for their constant love, encouragement, and support throughout this journey and in all of my academic and professional pursuits. Your belief in me continues to inspire and motivate me, and I am deeply grateful to have you in my life.

CHAPTER 1: INTRODUCTION

1.1. Background

Bridge deck cracking is a widespread and persistent issue across the United States, especially in regions like Washington State (WA) where concrete structures are exposed to a combination of mechanical and environmental stressors. While early-age cracking may not immediately compromise structural capacity, it creates pathways for the ingress of deleterious substances such as deicing salts. Over time, this can lead to premature deterioration, increased maintenance needs, and, if unaddressed, compromise the integrity of both the deck and the supporting superstructure.

To mitigate these risks, state department of transportation (DOT) agencies employ a range of bridge preservation strategies, from localized patch repairs to full deck replacement. Concrete overlays are commonly used as an intermediate solution to restore serviceability and extend service life. In some cases, overlays also serve to strengthen bridges by increasing deck thickness, particularly in response to higher traffic demands.

Current overlay options vary, including ultra-high-performance concrete, low-slump concrete, and latex-modified concrete. These materials offer a range of performance characteristics but often fall short when it comes to meeting the demands of today's construction environments. With growing urbanization and increasing traffic volumes, allowable closure times have become more limited, often requiring construction to be completed overnight with minimal disruption. These constraints can pose challenges for traditional cementitious materials, which typically need longer curing periods to perform effectively.

Belitic calcium sulfoaluminate (BCSA) cement, often referred to more broadly as calcium sulfoaluminate (CSA) cement, has emerged as a promising alternative binder due to its rapid setting and early strength development capabilities. In contrast to ordinary portland cement

(OPC), CSA can achieve initial set in as little as 15 minutes and develop compressive strengths exceeding 3,000 psi within three hours of placement. These rapid strength gains are primarily attributed to its finer particle size and a chemical composition that facilitates accelerated ettringite formation during the early stages of hydration. This ettringite-driven expansion may also contribute to mitigating shrinkage-induced cracking. Beyond its performance advantages, CSA cement offers substantial environmental benefits, including a 30–50% reduction in CO_2 emissions from calcination and up to 60% lower energy consumption during production, owing to its lower kiln operating temperatures.

1.2. Motivation

Despite the variety of overlay materials available, agencies like Washington State Department of Transportation (WSDOT) continue to struggle with selecting options that can reliably meet both durability and rapid construction requirements. WSDOT's current prescriptive-based specifications include several overlay types that offer familiarity and ease of implementation. However, these materials often fail to achieve the necessary early-age strength or long-term durability within the tight construction windows typical of overnight closures, especially along heavily trafficked routes. Premature failures of overlays have led to recurring repairs and increased life-cycle costs, creating an urgent need for more effective alternatives.

Given these constraints, CSA cement presents a promising option. Its ability to deliver rapid strength gain, reduce shrinkage cracking, and provide environmental benefits aligns closely with the critical needs of modern bridge preservation efforts. However, CSA remains underutilized in the U.S. due to limited performance data and a lack of established specifications for overlay applications. While only California Department of Transportation (Caltrans) formally recommends CSA for high-early-strength overlays, at least nine other DOTs—including WSDOT—have reported positive experiences using CSA in repair contexts.

The construction of bonded overlays poses unique challenges where adhesion to the existing concrete substrate and compatibility in early-age behavior are critical to long-term performance. The proposed research aims to evaluate the feasibility of CSA-based high-early-strength concrete (HESC) overlays, with particular emphasis on mechanical performance, dimensional stability, and durability. This work seeks to support the development of performance-based guidance and specifications for the use of CSA in accelerated bridge construction and rehabilitation projects.

1.3. Objectives and Tasks

The goal of this research is to develop a performance-based mix design for high-early-strength concrete (HESC) overlays, utilizing a CSA cement-based system specifically for bridge deck applications. A key aim of this study is to identify the challenges or barriers that may hinder the successful and consistent use of HESC for bridge deck overlays in WA. Additionally, this work seeks to establish comprehensive procedures and best practices for the implementation of HESC overlays in the state.

Due to their rapid setting and significant early-age strength development, CSA cements have garnered interest from state agencies as a means to accelerate project timelines and reduce the duration of in-situ concreting operations. These materials hold considerable promise for use in bridge repair and overlay projects, particularly where minimizing traffic disruptions is a priority.

To achieve these objectives, the following tasks will be undertaken:

- **Review of CSA cement systems:** A comprehensive literature review will be conducted on CSA cement-based systems, focusing on the hydration reactions, interactions with admixtures and polymers, as well as their mechanical properties and durability performance.

- **Characterization study:** The mix design variables will be systematically modified to evaluate the effects of different parameters on the fresh properties and overall performance of the CSA cement systems, including workability, air content, and early-age strength development.
- **Field trials:** The CSA cement systems will be tested at a field scale to evaluate their mechanical properties. These systems will also be applied to mini-bridge decks to replicate real-world conditions and assess their performance in practical, large-scale applications.
- **Durability study:** The CSA cement systems will be subjected to various environmental and mechanical stressors, to evaluate their long-term durability and resistance to common bridge deck deterioration mechanisms.
- **Development of recommendations and future work:** Based on the findings from the previous tasks, recommendations for CSA mix design, optimal construction practices, and performance specifications will be developed for bridge rehabilitation projects. Additionally, areas requiring further research or testing will be identified to support future advancements in CSA-based concrete applications.

1.4. Scope and Limitations

This study was developed in coordination with the WSDOT and is intended primarily for application within the Seattle, WA region. The research focuses on evaluating the mechanical, durability, and bond performance of BCSA cement systems. Particular emphasis was placed on the use of polymer-modified BCSA mixtures, aiming to improve durability under conditions typical of bridge deck environments in the Pacific Northwest. A latex-modified BCSA system was used as the control, reflecting its current widespread use in bridge deck overlay applications.

While every effort was made to ensure consistency in testing conditions and methods, some degree of variation is inherent due to the sensitivity of the tests involved. Additionally,

because the study was conducted in a laboratory setting, it was not possible to fully replicate the complexity of real-world bridge deck overlay construction and environmental exposure. Nonetheless, test procedures and material handling were designed to approximate field conditions as closely as possible within the constraints of a controlled environment.

1.5. Thesis Overview

- **Chapter 1: Introduction** outlines the research problem, objectives, and significance of the study. It also defines the scope of the research and provides a summary of the tasks undertaken.
- **Chapter 2: Literature Review** provides an overview of existing research on CSA cement systems, with a focus on their hydration chemistry, interactions with admixtures and polymers, mechanical properties, and durability performance.
- **Chapter 3: Experimental Program** details the materials, mix design variables, and testing methodologies used across the characterization study, field trials, and durability assessments.
- **Chapter 4: Results and Discussion** presents and analyzes the outcomes of both laboratory and field testing, evaluating the performance of the CSA cement systems in terms of strength, durability, and practical application.
- **Chapter 5: Conclusions and Recommendations** summarizes the key findings, discusses their implications for bridge deck rehabilitation, and proposes recommendations for CSA mix design, construction practices, and future research.

CHAPTER 2: LITERATURE REVIEW

2.1. Calcium Sulfoaluminate (CSA) Cements

2.1.1. History of CSA

The origins of Calcium Sulfoaluminate (CSA) cement can be traced back to the pioneering work of Professor Alexander Klein in the 1960s. By utilizing the expansive properties of ye'elimite ($C_4A_3\overline{S}$), Klein aimed to address the issue of drying shrinkage issue commonly found in ordinary or traditional Portland cement (OPC or PC) concrete. His innovative work ultimately led to the development of Type K cement, a supplementary cementitious material (SCM) designed to be added to OPC to compensate for shrinkage related cracking (Bescher & Kim, 2019).

2.1.2. Classification of CSA Cements

Since the initial development of CSA and Type K cement, CSA has evolved into a standalone cement with a variety of compositions, containing different proportions of belite (C_2S), ye'elimite ($C_4A_3\overline{S}$), and calcium sulfates. These variations result in CSA binders with a range of properties, including shrinkage-compensating, rapid setting, self-stressing, or a combination of these characteristics (Bescher & Kim, 2019). Despite these differences in composition and performance, all are categorized as CSA cements. Table 2-1 from Bescher & Kim (2019) summarizes the various compositions of CSA cements, their key traits, and the proposed nomenclature for each.

Table 2-1: Proposed types of CSA cements based on mineralogy reprinted from Bescher & Kim (2019)

CSA Type	CSA [%]	C_2S [%]	$C\overline{S}$ [%]	Other [%]
Type A – Accelerating Additive	35-45	0-20	10-30	5-55
Type B – Belitic CSA	20-30	30-60	5-25	0-35
Type C – Expansive Additive	10-20	10-30	40-60	0-40
Type K – Shrinkage Compensating Cement	1-10	30-50	1-20	20-70

2.2. Belitic Calcium Sulfoaluminate (BCSA) Cements

2.2.1. History and Production of BCSA

Following Klein's work in CSA cements, in 1975, Borje Ost developed a standalone CSA cement known as Belitic Calcium Sulfoaluminate (BCSA) cement. Rich in belite, this cement exhibits low shrinkage and fast strength gain compared to PC (Bescher & Kim, 2019).

Another major advantage of BCSA cement is its reduced carbon footprint during production. The production of PC accounts for approximately 7% of global greenhouse gas emissions (Tan et al., 2020). This is largely due to the high temperature (1500°C) required to form alite (C_3S), the primary binder responsible for early strength gain (Bescher & Kim, 2019; Tan et al., 2020). In contrast, the ye'elimite in BCSA forms at a lower temperature (1250°C) (Tan et al., 2020). Additionally, the inter-grinding of belite and ye'elimite clinker with calcium sulfate is significantly less energy-intensive than the griding of PC clinker due to softer materials, resulting in a further reduction of carbon emissions (Adnan et al., 2022).

Figure 2-1 from CTS Cement Manufacturing Corp. (2022) illustrates the differences in CO_2 emissions from CSA versus PC production. It highlights a 36% reduction in calcination and a 28% in combustion, resulting in a total CO_2 emissions reduction of 33% when using CSA.

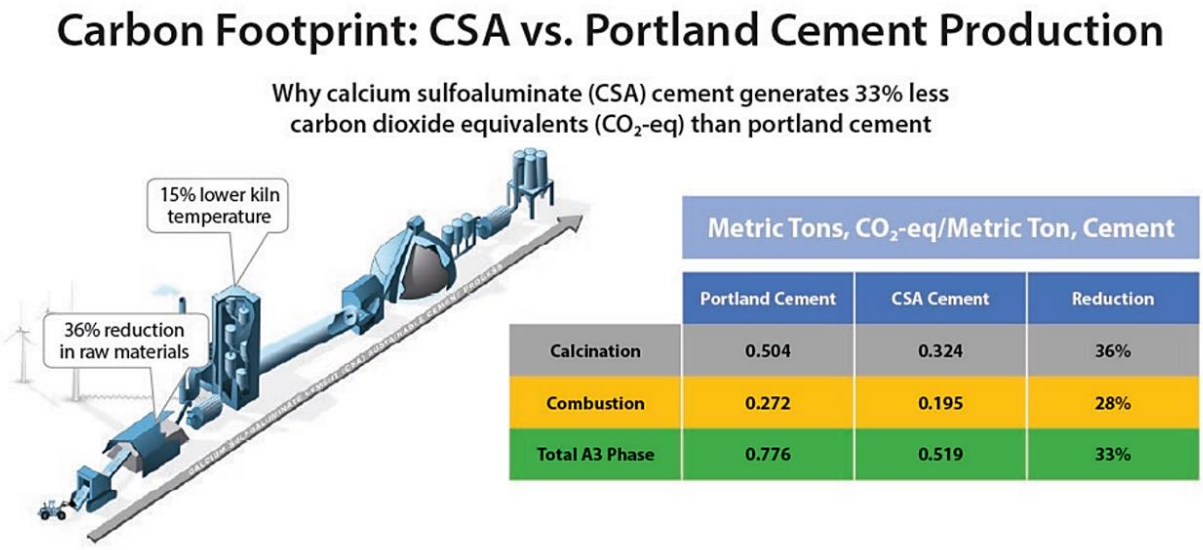

Figure 2-1: Carbon emission comparison of CSA and PC production (CTS Cement Manufacturing Corp., 2022)

2.2.2. Chemical and Mineralogical Composition of BCSA

BCSA cement is produced by inter-grinding belite- and ye'elimite-rich clinker with calcium sulfate. The typical composition of BCSA cement includes, by mass, 20-30% ye'elimite, 30-60% belite, and up to 25% calcium sulfate, which can appear as anhydrite ($C\overline{S}$), gypsum ($C\overline{S}H_2$), or hemihydrate ($C\overline{S}H_{0.5}$) (Adnan et al., 2022). This distinct chemical makeup differentiates BCSA from other CSA cements and traditional PC, influencing its hydration behavior and, ultimately, its mechanical properties. An example of a BCSA cement composition is shown in Table 2-2, adapted from Burris and Kurtis (2018), which compares the compositions of OPC and a belite-rich CSA cement (CSA2).

Table 2-2: Phase composition of OPC and belite-rich CSA2 unhydrated cements adapted from Burris and Kurtis (2018)

Phase	OPC wt% (mole%)	CSA2 wt% (mole%)
Alite (C_3S)	63.0 (59.9)	-
Belite (C_2S)	11.5 (14.5)	39.3 (42.0)
Brownmillerite (C_4AF)	17.6 (15.7)	-
C_3A	2.4 (1.9)	-
Calcite	-	7.2 (13.2)
Anhydrite	1.3 (2.1)	21.1 (28.5)
Bassanite (Hemihydrate)	3.4 (5.1)	3.0 (3.8)
Gypsum	0.7 (0.9)	-
Ye'elimite	-	28.1 (8.5)
Quartz	-	1.3 (4.0)

2.2.3. Hydration of BCSA

BCSA cement undergoes hydration in two major stages that contribute to its early-age and later-age properties. The process begins with the rapid hydration of ye'elimite. In the presence of calcium sulfate, aluminum hydroxide (AH_3) and ettringite ($C_6A\bar{S}_3H_{32}$) are formed (Equation 2-1); in its absence or once all calcium sulfates have been consumed, aluminum hydroxide and monosulfate ($C_4A\bar{S}H_{12}$) are produced instead (Equation 2-2). Although calcium sulfate exists in different forms, anhydrite was assumed for simplicity in Equations 2-1 and 2-2.

$$C_4A_3\bar{S} + 2\ C\bar{S} + 38\ H \rightarrow C_6A\bar{S}_3H_{32} + 2\ AH_3 \quad (2\text{-}1)$$

$$C_4A_3\bar{S} + 18\ H \rightarrow C_4A\bar{S}H_{12} + 2\ AH_3 \quad (2\text{-}2)$$

This early-stage, rapid precipitation of ettringite is responsible not only for the quick setting and strength gain of BCSA systems, but also to a dense microstructure characterized by low permeability and reduced porosity—key factors that improve the concrete's durability (Adnan et al., 2022). However, ettringite can destabilize into monosulfate, particularly at high concrete temperatures (Zhou & Glasser, 2001) or if enough calcium is available, as shown in Equations 2-3 and 2-4, respectively. Conversely, monosulfate can reconvert to ettringite in the presence of water and sulfates—such as during a sulfate attack—in a process known as delayed ettringite formation (DEF) (Wojciech et al., 2024).

$$C_6A\bar{S}_3H_{32} \leftrightarrow C_4A\bar{S}H_{12} + 2\ C\bar{S} + 20\ H \tag{2-3}$$

$$6\ C_2S + 2\ AH_3 + 10\ H + C_6A\bar{S}_3H_{32} \rightarrow 6\ CSH_2 + 3\ C_4A\bar{S}H_{12} \tag{2-4}$$

Although ettringite is often regarded negatively in industry due to DEF and the potential for cracking caused by its expansive nature, it is believed that in BCSA systems, ettringite forms early enough to mitigate these risks (Kim, 2018). Still, the reversible relationship between ettringite and monosulfate can pose durability challenges in later-age concrete if not properly addressed during cement blend and mixture design.

The formation of ettringite and its resulting mechanical properties are also influenced by the dissolution rate of calcium sulfate variants. In a study by Zhang et al. (2020), the effect of calcium sulfate type on the microstructure and properties of sulfoaluminate cement-based grout was investigated, focusing primarily on gypsum and anhydrite. The study found that gypsum dissolves more quickly than anhydrite, leading to the complete formation of ettringite within 2 hours. However, this rapid dissolution can compromise the microstructure, as the resulting ettringite may form unevenly, ultimately weakening the mechanical properties.

In contrast, the slower dissolution rate of anhydrite allows it to continue contributing to ettringite formation during later stages of hydration. This prolonged reaction causes expansion but also promotes a more uniform ettringite structure, which enhances mechanical properties.

The presence of lime (CH) also plays a crucial role in shaping both microstructure and mechanical behavior (Péra & Ambroise, 2004). The following reactions assume gypsum as the calcium sulfate source, based on its faster dissolution compared to anhydrite. Without lime, ye'elimite reacts with gypsum to produce ettringite and aluminum hydroxide (Equation 2-5). In the presence of lime, the reaction yields only ettringite (Equation 2-6).

$$C_4A_3\bar{S} + 2\ C\bar{S}H_2 + 36H \rightarrow C_6A\bar{S}_3H_{32} + 2\ AH_3 \quad (2\text{-}5)$$

$$C_4A_3\bar{S} + 8\ C\bar{S}H_2 + 6CH + 74H \rightarrow 3\ C_6A\bar{S}_3H_{32} \quad (2\text{-}6)$$

Comparing the stoichiometry, Equation 2-6 produces significantly more ettringite per mole of ye'elimite—yielding a 1:8:3 ratio of ye'elimite to gypsum to ettringite—compared to Equation 2-5's 1:2:1 ratio. This increase in ettringite formation through the addition of lime is used in expansive applications, such as shrinkage-compensating and self-stressing cements. Conversely, mixes without lime produce non-expansive cements that offer high early strength, making them suitable for applications requiring rapid mechanical development (Péra & Ambroise, 2004).

The second major stage of BCSA cement hydration is the hydration of belite, which governs the later-age properties of the system. In PC, belite (C_2S) typically makes up only about 10% of the anhydrous phase and hydrates to form calcium silicate hydrate (C-S-H)—a key contributor to strength and durability—and calcium hydroxide (CH) (Equation 2-7). In contrast, BCSA systems often contain at least 35% by mass of belite. In these systems, the presence of aluminum hydroxide (AH_3) instead causes the hydration of belite to form strätlingite (C_2ASH_8),

an important product for long-term strength and durability (Equation 2-8) (Adnan & Thomas, 2025; Winnefeld & Lothenback, 2016).

However, if more belite is present, the amount of strätlingite formed decreases due to dilution. When the belite content exceeds 60% by mass and sufficient calcium oxide is available to stabilize C-S-H and katoite (C_3AH_6), strätlingite becomes increasingly destabilized, as shown in Equation 2-9 (Winnefeld & Lothenback, 2016).

$$C_2S + 2\ H \rightarrow \text{C-S-H} + CH \quad (2\text{-}7)$$

$$C_2S + AH_3 + 5\ H \rightarrow C_2ASH_8 \quad (2\text{-}8)$$

$$C_2S + C_2ASH_8 \rightarrow \text{C-S-H}_2 + C_3AH_6 \quad (2\text{-}9)$$

Furthermore, from a study conducted by Mrak et al. (2021), cements with higher belite content were found to have a lower compressive strength than cements with lower belite as the degree of hydration of belite is lower than ye'elimite, and ettringite is more densifying than strätlingite and C-S-H.

To better visualize and understand the hydration behavior of BCSA cement, the process was simulated by Adnan and Thomas (2025) and is illustrated in Figure 2-2, with the white space representing porosity. Initially, anhydrite and hemihydrate rapidly converted to gypsum. Within 4 days, ye'elimite and gypsum were fully consumed, forming a substantial amount of AFt (AluminoFerrite trisulfate) phases—including ettringite and its variants—as well as a smaller quantity of aluminum hydroxide. Belite hydration accelerated around 24 hours, consuming the aluminum hydroxide produced from ye'elimite hydration and leading to the formation of strätlingite. Once the aluminum hydroxide was depleted, around 42 days, belite hydration continued, producing a small amount of C-S-H.

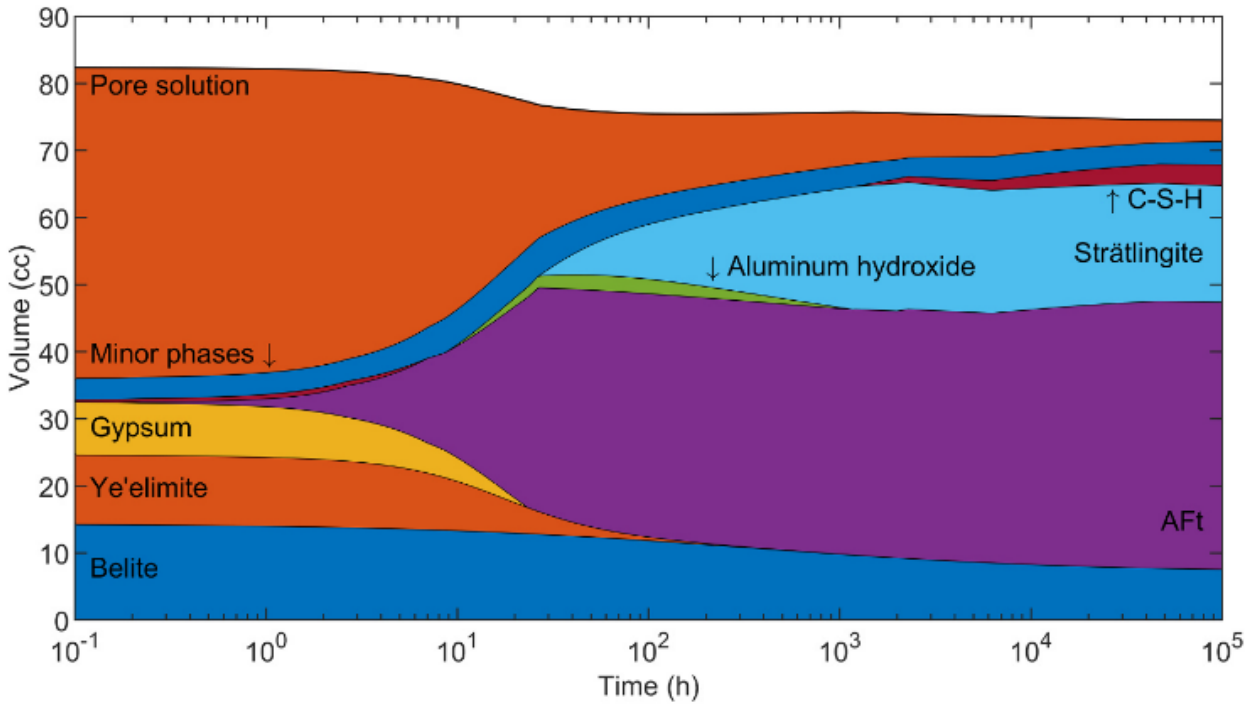

Figure 2-2: Simulated hydration process in the BCSA cement system (Adnan & Thomas, 2025)

However, BCSA cements hydrate more slowly than typical Portland cement (PC), with significant belite (C_2S) hydration not occurring until around three months after casting. By 28 days, only about 20% of the belite phase has typically reacted, increasing to approximately 48% by three months (Bescher & Kim, 2019; Cuberos et al., 2010).

As noted by Ambrose et al. (2023), PC achieves around 70–80% total hydration within the first 28 days, whereas BCSA generally reaches only about 50% in the same period. With extended curing, however, BCSA can approach similar hydration levels to PC, reaching 70–80% by three months. This continued hydration leads to a further reduction in porosity, enhancing mechanical performance and durability. Elevated curing temperatures, such as 40 °C, may also accelerate hydration, offering a more representative assessment of 28-day performance.

Nevertheless, such curing conditions and extended timelines are impractical for conventional construction. While testing during partial hydration may not capture BCSA's full

potential, it provides the most realistic indication of performance within typical construction schedules.

2.2.4. Chemical and Mineral Admixtures Influencing Early-Age Behavior

2.2.4.1. Set Controlling Admixtures

While the rapid set times and strength gaining properties of BCSA are beneficial for the truncation of construction windows and cure time, the short working time is a constructability challenge when trying to increase the scale of repair applications. To manage this, studies have been conducted investigating various set retarders to improve slump flow retention and extend set times. One set retarder that is commonly used is citric acid.

In a study by Burris and Kurtis (2018), the effect of citric acid dosage on the hydration and property development of CSA cement was investigated. Two types of CSA cement were used: one with a lower belite content (CSA1) and another with a higher belite content (CSA2). As seen in Figure 2-3 plotted by Burris and Kurtis (2018), the two CSA cements exhibited different degrees of retardation despite receiving the same citric acid dosage, with the belite-rich CSA2 showing a longer delay in set times.

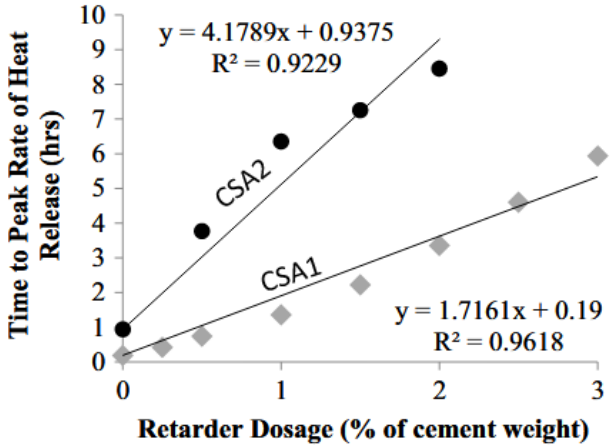

Figure 2-3: Time to peak rate of heat evolution vs. citric acid dosage (Burris & Kurtis, 2018)

The cumulative heat evolved by CSA2 over 48 hours was also studied using isothermal calorimetry, as shown in Figure 2-4 from Burris and Kurtis (2018). As the retarder dosage increased, the initial reaction rate was delayed. However, all samples began to converge by 48 hours. These results suggest that although citric acid affected the initial reaction rates, the retarder dosage did not significantly affect the overall heat of hydration.

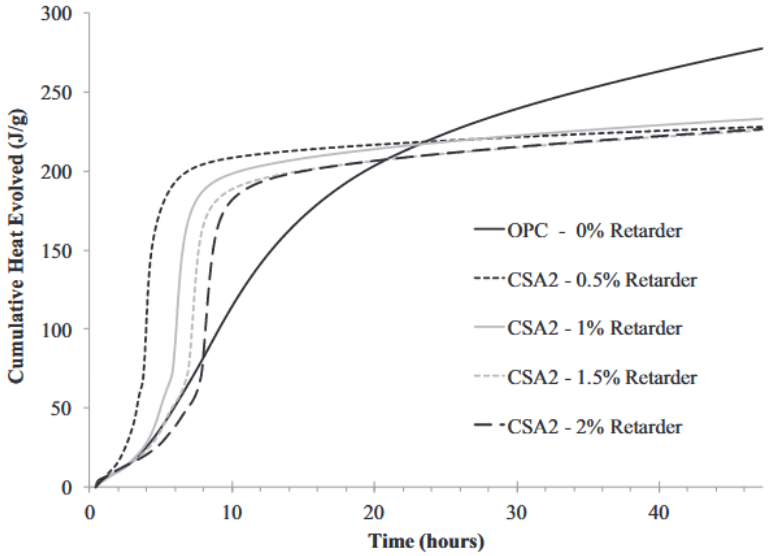

Figure 2-4: Cumulative heat evolution of CSA2 cement pastes (Burris & Kurtis, 2018)

Another study by Soriano (2019) examined the impact of citric acid dosages on the compressive strength of BCSA cement. Figure 2-5 from Soriano (2019) confirms the linear relationship between initial set time and citric acid dosage previously observed by Burris and Kurtis (2018). However, the results also show a general increase in compressive strength after day one with higher citric acid dosages, despite lower early-age strength. This improvement can be attributed to the more uniform formation of ettringite resulting from slower initial reaction kinetics. Additionally, increased citric acid dosage enhanced the workability of the pastes, leading to greater fluidity. This, in turn, reduced porosity and could have further contributed to the observed strength gains at later ages (Soriano, 2019).

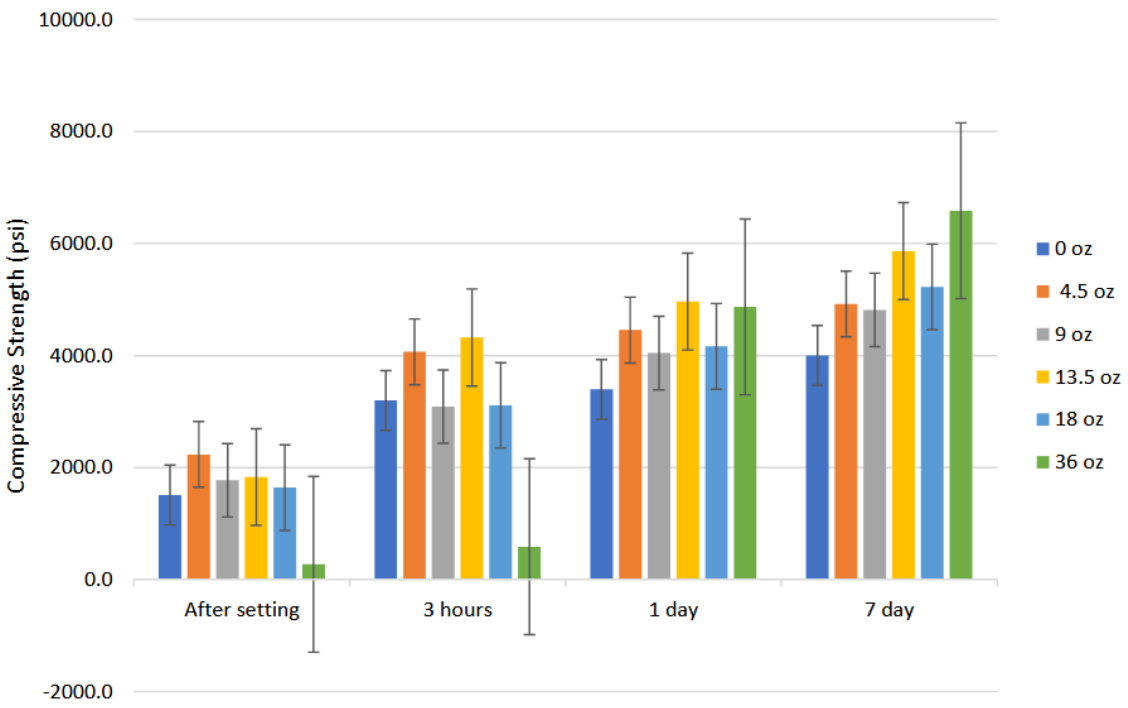

Figure 2-5: Compressive strength results of BCSA cement with varying citric acid dosages (Soriano, 2019)

However, a study by Adnan et al. (2022), which examined the effects of varying citric acid dosages and water-to-cementitious material ratios (w/cm) on the engineering properties of BCSA, found that citric acid had minimal impact on compressive strength, even after three days of curing, as shown in Figure 2-6. Taken together, these studies suggest that while citric acid influences the setting behavior and workability of BCSA systems—potentially affecting long-term strength development—its overall effect on compressive strength varies depending on factors such as dosage, w/cm ratio, curing conditions, and BCSA composition, among others.

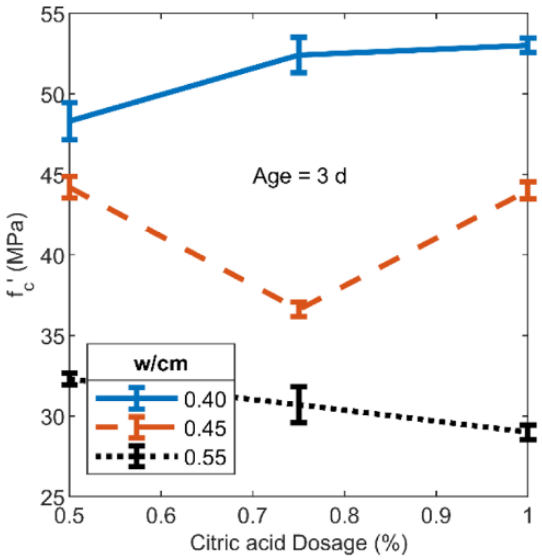

Figure 2-6: Effect of citric acid dosage on compressive strength (Adnan et al., 2022)

Citric acid is not the only set retarder available for CSA cement systems. In a study by Acarturk & Burris (2020), citric acid, tartaric acid, and borax were evaluated at various dosages, both individually and in combination (citric acid with borax, and citric acid with tartaric acid). Figure 2-7 illustrates the relationship between final setting time od CSA pastes and 28-day compressive strength of CSA mortars with different retarder types and dosages. The naming convention “xR” is used, where *x* denotes the dosage or dosage ratio and *R* represents the retarder(s); "0" indicates the control CSA paste with no retarder.

In all cases, increasing retarder dosage led to longer setting times. Among the retarders, borax produced the greatest delay, followed by tartaric acid and then citric acid. However, this increase in setting time came at the expense of compressive strength. Due to its ability to moderately extend workability time with minimal impact on compressive strength, citric acid remains the most commonly used set retarder in practice.

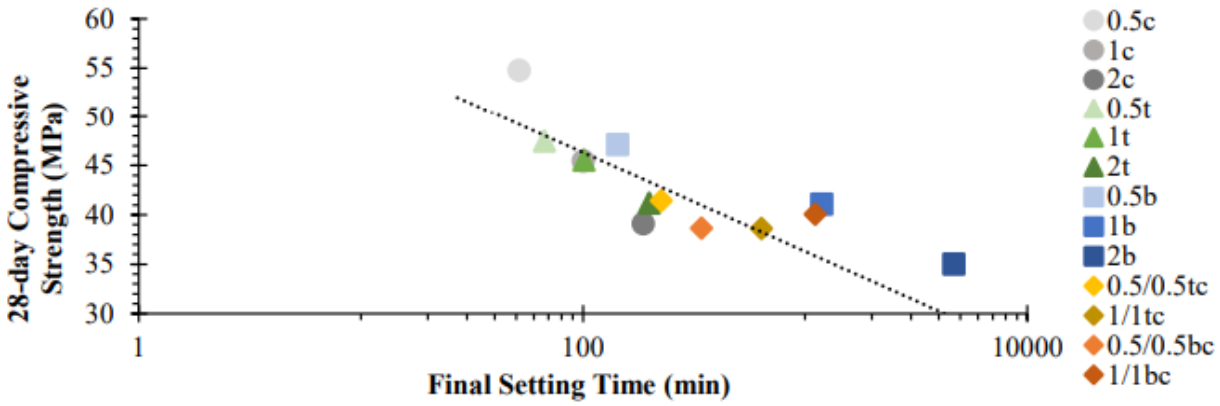

Figure 2-7: Correlation between CSA paste setting time and 28-day mortar strength across various retarder dosages (Acarturk & Burris, 2020)

2.2.4.2. Flow Controlling Admixtures

Water reducing admixtures (WRAs) are commonly used in the concrete industry to improve the fluidity and workability of concrete mixtures without increasing the water content—and often allow the water content to be reduced. By lowering the amount of water while maintaining workability, the water-to-cement ratio (W/C) is reduced, leading to increased strength and durability.

High-range water reducers (HRWR), also known as superplasticizers, offer the same benefits but with significantly greater efficiency. HRWR can reduce water needs by 12% to 30%, producing ultimate compressive strengths greater than 70 Ma (10 ksi). Additionally, HRWR can help minimize drying shrinkage compared to concrete mixtures that rely on higher water content to achieve similar workability levels (Kosmatka et al., 2003). As advancements in HRWR have progressed, the next generation of superplasticizers has been developed using polycarboxylate technology.

A study by Huang et al. (2021) investigated the effects of various HRWRs on the fluidity, hydration, and setting time of ferrite aluminate cements (FAC). The HRWRs evaluated included an aliphatic-based agent (AP), a melamine-based agent (MA), and a polycarboxylate-based agent

(PC). Figure 2-8 from the authors illustrates that the amount of PC admixture required to achieve a given level of fluidity is significantly lower than that of the other admixtures evaluated, demonstrating its superior efficiency.

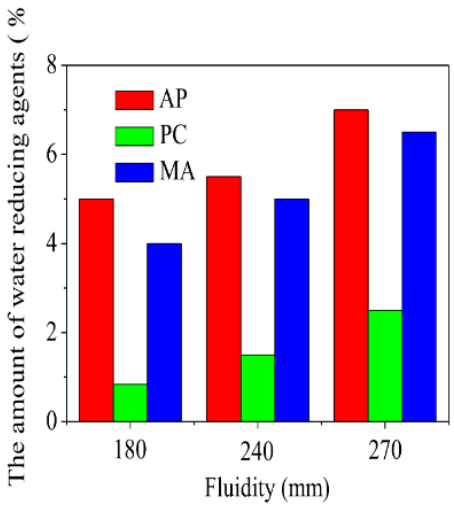

Figure 2-8: Amount of water reducing agent versus flow (Huang et al., 2021)

Figure 2-9 from Huang et al. (2021) shows the initial and final setting times of FAC pastes using the WR dosages required to achieve equivalent fluidity. Notably, the PC-based HRWR significantly extended both the initial and final setting times, with delays of up to 6.08 hours and 7.16 hours, respectively, at a dosage of 2.5%. Despite this substantial retardation, isothermal calorimetry results shown in Figure 2-10 indicate that overall hydration was not significantly impacted by the PC HRWR. In contrast, a greater effect on hydration was observed with the use of the MA-based HRWR.

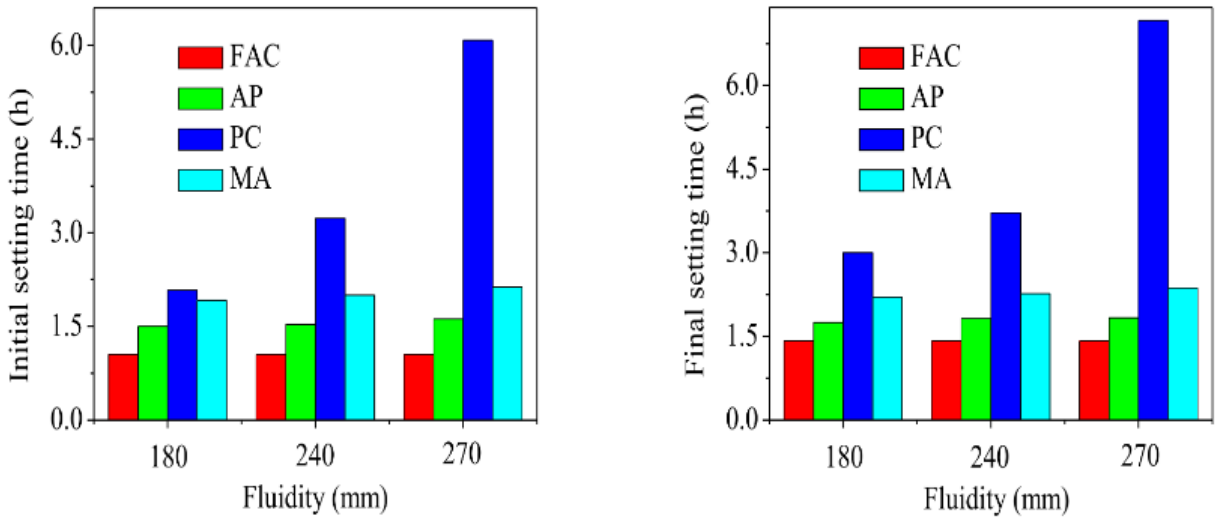

Figure 2-9: The effect of water reducing agent on setting times (Huang et al., 2021)

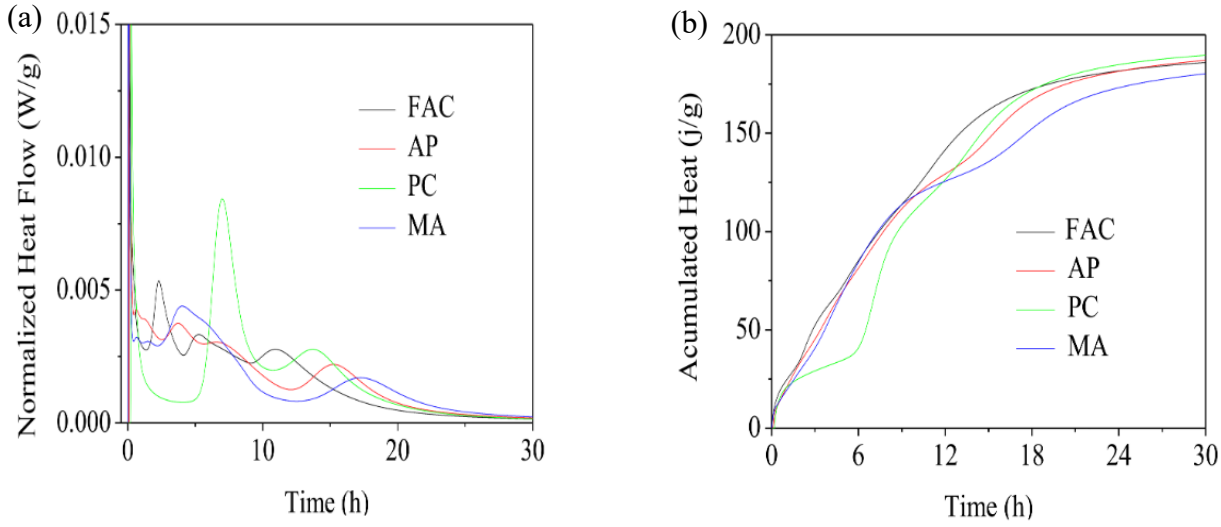

Figure 2-10: Effect of water reducing agents on (a) heat evolution and (b) cumulative released heat (Huang et al., 2021)

A study by Ma et al. (2014) on the compatibility of PC-based HRWR with belite-rich sulfoaluminate cement reported similar findings. The PC-based HRWR began significantly delaying setting times when dosed above 0.075% by mass. Mixtures exceeding this threshold showed up to a 21.5% reduction in 1-day compressive strength, while no significant differences were observed at 3 days. Interestingly, a dosage of exactly 0.075% resulted in a substantial

increase in 28-day compressive strength—up to 44.5%. These results are illustrated in Figure 2-11 from Ma et al. (2014).

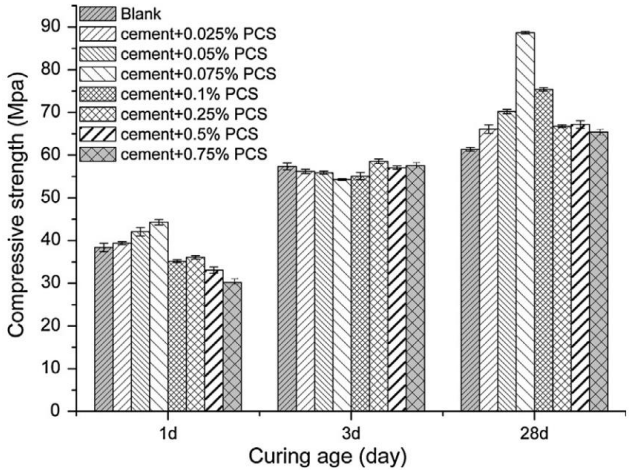

Figure 2-11: Compressive strengths of belitic-rich sulfoaluminate cement with different quantities of polycarboxylate acid-based superplasticizers (PCS) (Ma et al., 2014)

In a more recent study, Belhadi et al. (2021) investigated the combined use of citric acid as a set retarder and PC-based HRWR in CSA cement mixtures, focusing on admixture compatibility. Due to the high reactivity of CSA, fluidity provided by HRWR is rapidly lost; however, this effect can be mitigated by set-retarding admixtures such as citric acid.

The study found that citric acid slows the dissolution of ye'elimite and anhydrite, thereby delaying the formation of ettringite and other hydration products. This delay allows the PC-based HRWR to better maintain its dispersing efficiency and reduce the rapid loss of fluidity. However, the study also revealed competitive adsorption between citric acid and PC-based HRWR, with citric acid preferentially adsorbing onto cement particles and thereby hindering the HRWR's effectiveness in maintaining initial fluidity.

Figures 2-12 and 2-13 from Belhadi et al. (2021) illustrate the interaction mechanisms of polycarboxylate superplasticizers (PCE) alone and in combination with citric acid (AC), respectively. When used alone, PCE absorbs onto the surface of cement particles, and its side

chains cause repulsive spacing that promotes dispersion and enhances early fluidity. As hydration progresses, the formation of hydrates covers these side chains, reducing PCE's dispersing capacity over time. When PCE is combined with AC, highly charged $[Ca(citrate)_2]^{4-}$ complexes—formed by the binding of the citric acid's carboxylate groups ($-COO^-$) with Ca^{2+}—rapidly adsorb to cement surfaces. This limits the initial adsorption of PCE and reduces its early dispersing effect. However, because AC slows hydration, fewer hydrates form initially, allowing more PCE to adsorb gradually and maintain its dispersing function over a longer period.

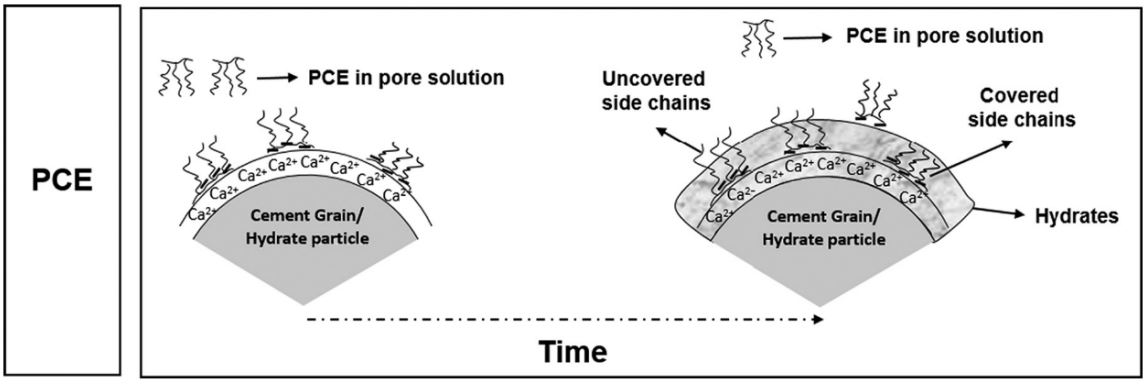

Figure 2-12: Interaction mechanism of polycarboxylate superplasticizers (PCE) (Belhadi et al., 2021)

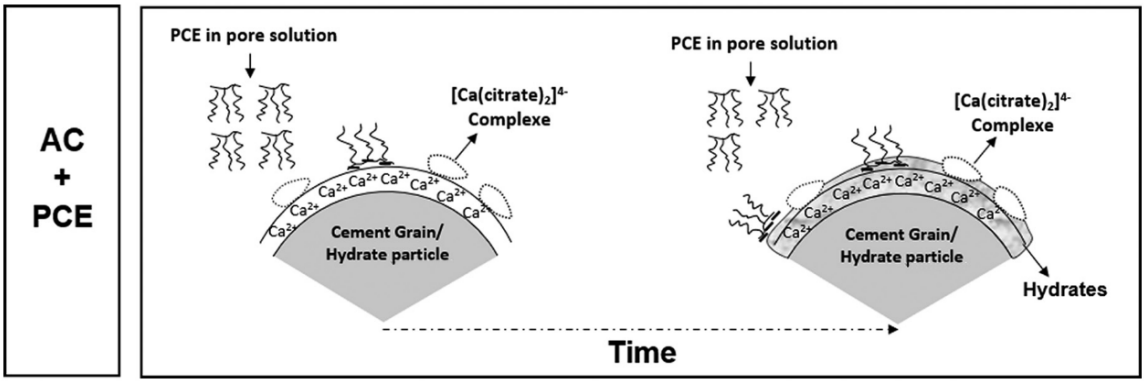

Figure 2-13: Interaction mechanism of citric acid (AC) and polycarboxylate superplasticizers (PCE) (Belhadi et al., 2021)

Figure 2-14 from the authors presents the isothermal calorimetry results from this study. One key finding is that the set delay caused by citric acid and PC HRWR is not cumulative;

instead, it is primarily influenced by citric acid, with only a minor contribution from the PC HRWR. Additionally, the isothermal calorimetry data from this study appear to contradict earlier research, as the results showed that both citric acid and PC HRWR reduce the total hydration of CSA, even when used individually.

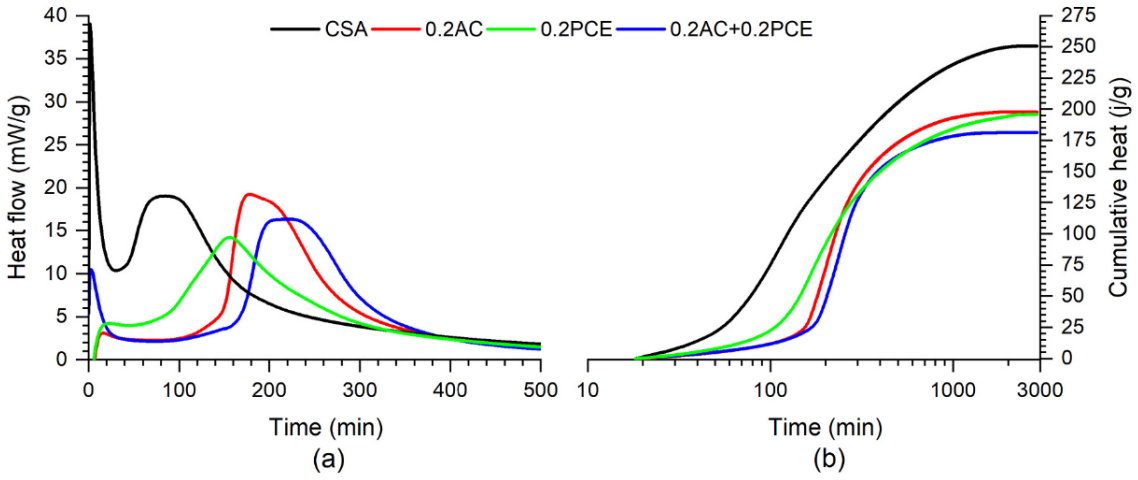

Figure 2-14: (a) Heat evolution and (b) cumulative released heat of CSA with and without citric acid (AC) and/or polycarboxylate superplasticizers (PCE) (Belhadi et al., 2021)

2.2.4.3. Air Controlling Admixtures

Air voids are an important component of concrete mixtures, particularly in cold climates where the concrete is exposed to freeze-thaw cycles. These microscopic voids provide space for expanding water during freezing, which helps reduce internal pressure and prevents cracking.

The volume of air voids in a mix is influenced by several variables, including the type and dosage of air-entraining admixture (AEA), the proportion of fine aggregate, supplementary cementitious materials (SCMs), and the chemical composition of the cement. Among these factors, AEA and fine aggregate content typically have the greatest impact.

During mixing, air bubbles naturally form in the concrete. The role of AEA is not to generate these bubbles, but to stabilize them. Two processes contribute to air incorporation during mixing. First, a vortex action that draws in air, dispersing and breaking it into smaller

bubbles through shearing action. Second, the fine aggregates act as a "three-dimensional screen," helping to entrap and retain air within the mix. These processes occur regardless of whether an AEA is used, but with an AEA, the air content increases, and the bubbles become smaller and more stable (Dolch, 1996). However, AEA dosage generally follows a parabolic relationship with air content: as dosage increases, air content increases up to a certain point, beyond which it levels off or may even decline (Dolch, 1996).

Different AEAs have distinct chemical compositions, which affect their performance and interaction with concrete. The two most common types are vinsol resin-based and synthetic detergent-based admixtures. Vinsol resin is an insoluble residue derived from pine stump processing and is composed of phenolics, carboxylic acids, and other organic compounds. When neutralized with sodium hydroxide, it becomes water-soluble and is commonly used as a base in AEA formulations. Synthetic detergents, typically alkyl aryl sulfonates, are surfactants produced by combining complex petroleum residues with benzene, followed by sulfonation and neutralization to create a water-soluble salt (Dolch, 1996).

Understanding the chemical interactions of AEAs with cement and other admixtures is essential for evaluating their effectiveness. Yang et al. (2022) investigated the effects of AEA on the pore structure and sulfate resistance of BCSA (referred to as CSAB in the study). Four mortar mixes were prepared and stored in either deionized water (DI) or a sodium sulfate solution: OPC, CSAB cement, CSAB cement with fly ash, and CSAB cement with AEA (CSAB+AIR). Due to the absence of coarse aggregates, mortars typically have higher air content; thus, the air content of the non-entrained CSAB mixture was 9%. For the CSAB mixtures with AEA, the synthetic AEA SikaControl® AIR-160 was used at a dosage of 10 mL/100 kg cement, resulting in a mortar air content of 9.4%.

Despite this slight increase in air content, the performance of CSAB+AIR samples remained largely unchanged under both storage conditions. AEAs are commonly used to modify the pore structure of concrete, improving its resistance to freeze-thaw damage. However, no significant differences in length change were observed between the CSAB and CSAB+AIR samples, despite potential changes in pore structure.

As shown in Figure 2-15 from the Yang et al. (2022), all samples experienced notable expansion within the first 3 days, followed by stabilization with no further expansion throughout the testing period. Additionally, none of the samples exceeded the 0.05% ACI expansion limit. Both sets of samples also maintained sufficient pore volume to prevent damage from salt crystallization, further indicating that the addition of AEA did not affect the performance of CSAB.

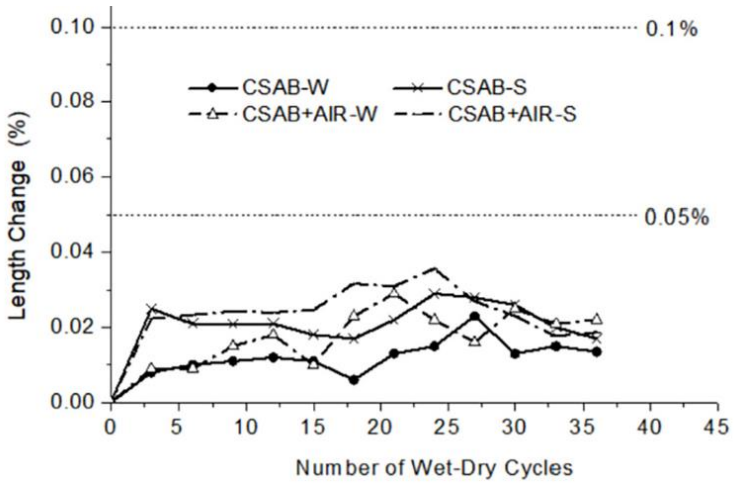

Figure 2-15: Length changes of CSAB and CSAB+AIR samples immersed in DI water (-W) and sodium sulfate solution (-S) adapted from Yang et al. (2022)

While the CSAB+AIR samples showed a slight increase in air content, such effects are not always achievable, especially in systems incorporating fly ash or other carbon-rich supplementary cementitious materials (SCMs) as AEAs tend to be adsorbed by carbon. Although

the dosage may be increased to compensate for the loss, the resulting entrained air is largely variable.

Pederson et al. (2008) explain that it is the unburned carbon—rather than the inorganic mineral content—of fly ash that is responsible for the adsorption of AEAs. A significant portion of the carbon surface is non-polar, unlike the polar surface of the inorganic particles. This difference in polarity creates active adsorption sites for the hydrophobic portion of the surfactants, which leads to competition at the air/water interface. The authors illustrate this interaction in Figure 2-16, where the small circles represent the polar end of the AEAs, and the tails represent the hydrophobic ends. The black irregular shape, representing a carbon particle, is shown to adsorb many of the AEAs that would have otherwise contributed to the formation of air bubbles.

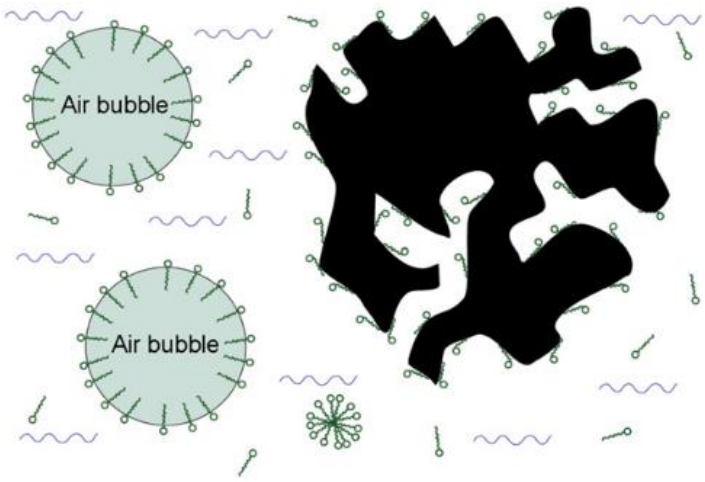

Figure 2-16: Adsorption sites for AEAs at air/water interface and at carbon surface (Pedersen et al., 2008)

While the interaction between carbon and AEA has been consistently observed, the type of AEA can also influence the degree of adsorption. In a study by Wang et al. (2023), three types of AEAs—one a vinsol resin based (AEA1) and two synthetic (AEA2 and AEA3)—were tested with two different polycarboxylate superplasticizers (SPs) to evaluate how admixture

combinations affect the formation and stability of air bubbles in Class F fly ash-blended cement. The study found that AEA1 generated more foam than the synthetic AEAs. Moreover, air bubble stability in fresh concrete was significantly affected by the compatibility between AEAs and SPs; AEA1 consistently produced more stable air bubbles than the synthetic AEAs. Together, these findings highlight how the type of AEA can significantly affect the quantity and stability of air voids in a mix.

While the role of carbon in AEA adsorption and AEA type has been explored, the influence of other admixtures—particularly polymers—is not well understood. Latex, a common polymer used in concrete, has inherent air-entraining properties and therefore is typically not used with AEAs, as discussed section 2.2.5. However, various other types of polymers exist, and research on their interactions with AEAs remains limited. Further investigation is needed to clarify how different polymer types affect AEA performance in cementitious systems.

2.2.5. Polymer-Modified CSA/BCSA Cements

Polymer-modified concrete has become the preferred option for bridge deck overlays by State Departments of Transportation nationwide, due to its enhanced durability and mechanical properties compared to conventional hydraulic cement. Notable improvements include better resistance to freeze-thaw cycles, reduced chloride penetration, and stronger bond strengths between the overlay and substrate. The addition of polymers in concrete has been linked to significantly longer overlay service lives, ranging from 14 to 50 years (Deo et al., 2022).

Styrene-butadiene mortar mixes were first developed by the Dow Chemical Company in 1975 and later used in concrete mixes for rehabilitation projects during the 1970s, following lab tests that demonstrated their ability to inhibit chloride ingress (Clear & Chollar, 1978). Styrene-butadiene has since become the standard polymer used in the production of latex-modified concrete. Unique properties of fresh latex-modified concrete include the ability to achieve good

workability with lower water content and the elimination of the need for air entrainment, as air is naturally trapped during the mixing process (L. A. Kuhlmann, 1993). The widespread use of styrene-butadiene in latex-modified concrete and its benefits have sparked significant interest among researchers, leading to studies on the performance of latex-modified CSA concrete.

A study by Lin et al. (2018) examined the performance of latex-modified CSA using various latex polymers and dosages. The effectiveness of each polymer was assessed based on its impact on durability, workability, and mechanical properties of CSA mortar mixes. The study used three types of latex polymers: styrene-butadiene rubber (SBR), styrene acrylic ester (SAE), and polyacrylic ester (PAE). Results varied depending on the polymer type and polymer-to-cement ratio used as shown in Figure 2-17 from the authors. For improving workability in CSA, the study found that higher dosages of all three polymer latexes led to water-reduction rates, with SBR and PAE performing similarly well.

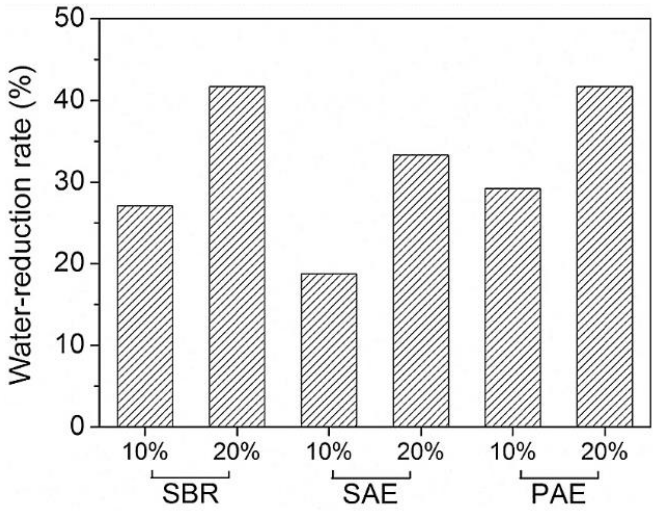

Figure 2-17: Water-reduction rates of latex-modified CSA cement for varying polymer types and polymer-to-cement ratios (Li et al., 2018)

Another observation was that SAE latex caused the greatest delay in set times, while PAE latex showed no effect on setting. The mechanical strength properties of CSA were also

influenced, with all polymer latexes enhancing both compressive and flexural strengths, with SBR performing the best. The inclusion of latex polymers led to reduced drying shrinkage, improved resistance to water capillary absorption, and increased durability against sulfate attack and carbonation. However, SBR was the only polymer latex to show improvements in freeze-thaw cycle resistance, although it had minimal impact on drying shrinkage.

2.2.6. Hardened Properties

After the citric acid retardation period, rapid ettringite hydration initiates setting, with final set occurring within a few hours. This rapid early formation of ettringite in BCSA is what drives quick setting and strength development, while also creating a dense microstructure with low permeability and reduced porosity.

The early-age mechanical properties of BCSA concrete with varying citric acid dosages and water-to-cementitious material ratios (w/cm) have been extensively researched by Adnan et al. (2022). Figure 2-18 from their study illustrates the evolution of compressive strength overtime, expressed as a ratio to its 28-day strength. The data are grouped by w/cm, as citric acid dosage was found to have negligible effect on strength development—contrasting the findings from Soriano (2019), as discussed in section 2.2.4.1.

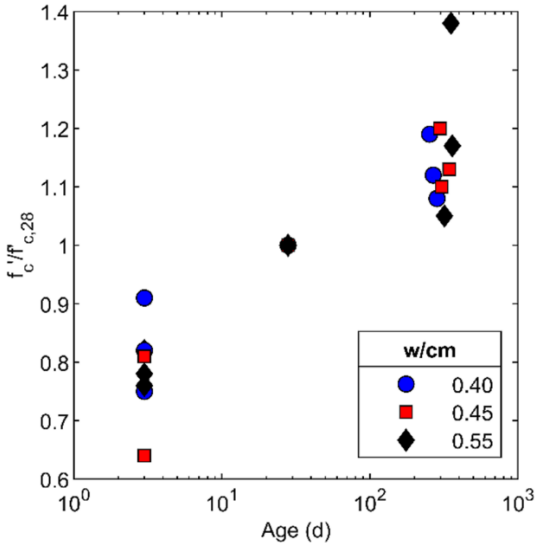

Figure 2-18: Compressive strength of BCSA vs age for varying w/cm (Adnan et al., 2022)

The compressive strength showed the expected trend of increased strength over time, with the mixes achieving approximately 78.9% of their 28-day strength within the first three days. Strength development continued beyond 28 days, ultimately surpassing the 28-day benchmark by an average of 15.8%. This trend aligns with previous studies demonstrating the long-term evolution of BCSA concrete's mechanical properties, even over decades of service (Bescher & Kim, 2019). The continued strength gain at later ages is primarily attributed to the gradual hydration of the belite phase into strätlingite and calcium silicate hydrate.

Adnan et al. (2022) also investigates the modulus of elasticity, with their findings presented in Figure 2-19. These results are evaluated against the range of values predicted by the ACI 318 (A.C.I. Committee, 2019), CSA A23 (CSA, 2004), and EC-2 (En 1992-1-1, 2004) code equations and fitted to a free power and square root model. It is important to note that the "code region" represents the span between the highest and lowest estimates across these codes for a given compressive strength, rather than an uncertainty range for a single standard.

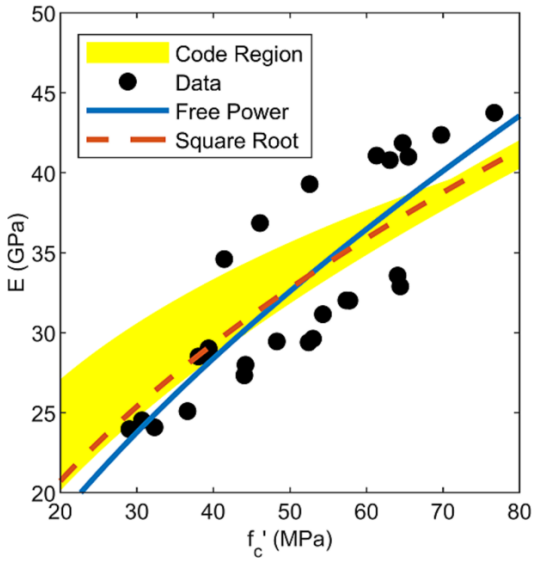

Figure 2-19: Modulus of elasticity of BCSA (Adnan et al., 2022)

The data show that the modulus of elasticity increases with compressive strength, as expected. This trend may be attributed to the evolving nature of the hydration products: while early-age ettringite formed from ye'elimite hydration contributes to initial stiffness, later-age phases such as strätlingite and calcium silicate hydrates, formed through belite hydration, may exhibit greater stiffness and contribute to the continued increase in elastic modulus over time.

The splitting tensile strength followed a similar increasing trend with compressive strength as observed for the modulus of elasticity, as shown in Figure 2-20. On average, the splitting tensile strength was 7.6% of the corresponding compressive strength. In a similar study on the mechanical properties of repair materials—including three different rapid repair CSA mixtures and a CSA-latex blend—Dornak (2014) reported comparable splitting tensile values, with the CSA mixtures averaging approximately 8% of the 28-day compressive strength.

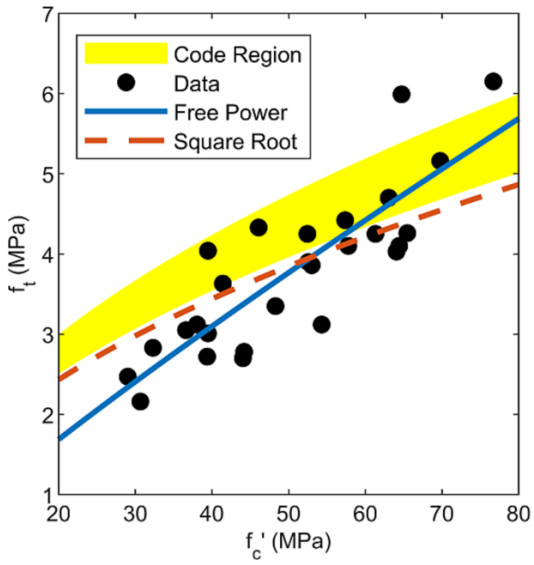

Figure 2-20: Splitting tensile strength of BCSA (Adnan et al., 2022)

According to Mehta & Monteiro (2014), as the compressive strength of concrete increases, the typical assumption that tensile strength is 10% of the compressive strength becomes less accurate. For high-strength concrete, tensile strength values as low as 7–8% of the compressive strength have been observed, as noted by Adnan et al. (2022) and Dornak (2014).

This suggests that higher compressive strength is associated with increased brittleness, which impacts tensile strength more significantly than compressive strength. This relationship may be applicable to BCSA, given it demonstrated high early-age compressive strength.

Dornak (2014) also evaluated the flexural strength of CSA mixtures and found that all tested mixes met the Texas Department of Transportation's (TxDOT) minimum 28-day modulus of rupture requirement of 620 psi for concrete pavements. However, compared to mixtures composed primarily of Portland limestone cement (PLC), the CSA mixtures exhibited significantly lower flexural strengths.

In another study, Markosian et al. (2021) tested a full-scale precast, prestressed BCSA concrete bridge girder. When tested at mid-span, the girder achieved an ultimate moment capacity of 1290 kip-ft (1749.01 kNm), with failure occurring due to shear or bond rather than flexure. This suggests that the girder's full flexural potential may not have been reached during testing.

Field data from the Seattle-Tacoma (Sea-Tac) International Airport runway also demonstrates the long-term flexural performance of BCSA. During slab replacements in 1997, the BCSA slabs were designed to achieve a flexural strength of 498.92 psi (3.44 MPa) within 4 hours, with a design life of 20 years. However, after 15 years of service, the slabs were retested and showed substantial strength gains, reaching a flexural strength of 1160.3 psi (8.0 MPa) (McNerney et al., 2020).

These mechanical properties can be attributed to the dense and refined pore structure of BCSA cement, which results from the early formation of ettringite during hydration. The microstructure reduces the concrete's permeability and porosity, improving its durability and resistance to chemical attack and freeze-thaw cycles (Adnan et al., 2022). However, a study by De Bruyn et al. (2017) found that although the pores were smaller, with nearly half the measured

surface area corresponding to pores smaller than 0.16 in μin (4 nm) diameter, the CSA cement paste microstructures were coarser than those of PC pastes.

De Bruyn et al. (2017) used mercury intrusion and nitrogen sorption porosimetry to investigate the pore structure of CSA and PC pastes at varying w/c ratios. CSA cement showed a unimodal pore distribution with a broad shoulder, while Portland cement exhibited a bimodal pattern with a secondary jump at 0.39–0.79 μin (10–20 nm) (Figure 2-21), suggesting coarser pore structure. This difference may be linked to the degree of hydration of the cement.

In CSA cement, the Belitic C_2S phase might not hydrate as completely as the C_2S and C_3S phases in PC, likely due to the rapid formation of ettringite, which consumes water early on. This limits the availability of water for further hydration, reducing overall porosity and slowing the penetration of additional curing water, leaving capillaries in the matrix once the concrete hardens.

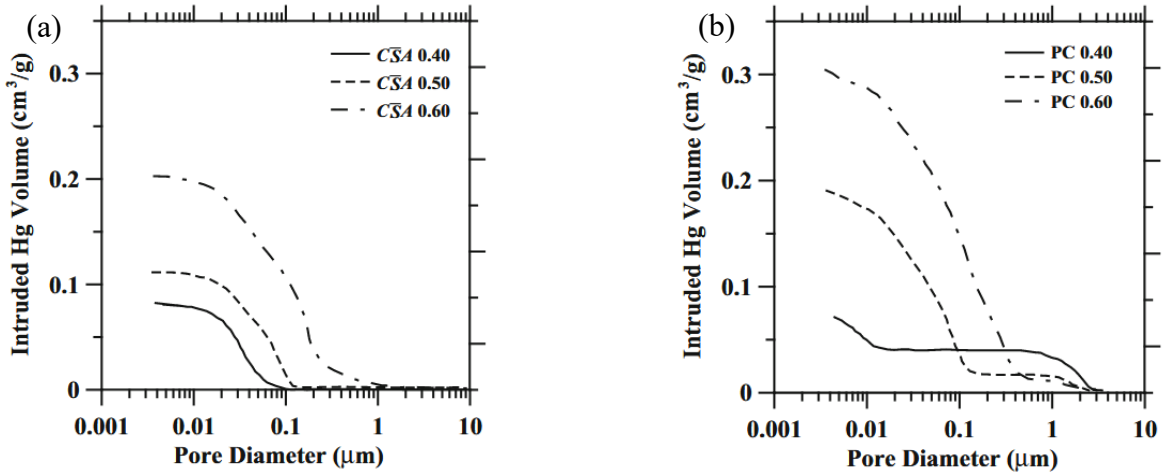

Figure 2-21: Cumulative plots of intruded Hg volume versus pore diameter for (a) CSA cements and (b) Portland cements (De Bruyn et al., 2017)

Despite the coarse pore structure, the overall pore size is small and dense. The balance between these two factors may contribute to a more stable microstructure, potentially reducing ion mobility and contributing to long-term durability. In addition to pore structure, the pore

solution of CSA concrete has been measured at a pH of 10.8, compared to 12.5 in PC systems. This lower alkalinity suggests a reduced potential for steel passivation, as the corrosion of embedded steel is closely linked to the high pH of the pore solution (Carsana et al., 2018).

2.2.7. Other Variations of CSA/BCSA Cements

Aside from BCSA, of the different types of CSA, Type K is the most used and well documented. This type of CSA is popular for its shrinkage compensating effect as it offsets the natural shrinkage that occurs in Portland cement (PC) concrete. In a study by Dhahir & Marx (2023), the use of Type K CSA cement was blended with PC at varying percentages (10%, 12.5%, 15%, 17.5%, and 20%) with the goal of developing an expansive concrete for chemical prestressing applications. Specimens were cured under wet-dry and dry-wet conditions to understand the deformation and mechanical effects of curing on the mixtures. The deformation results from the wet-dry and dry-wet conditions are shown in Figures 2-22 and 2-23, respectively.

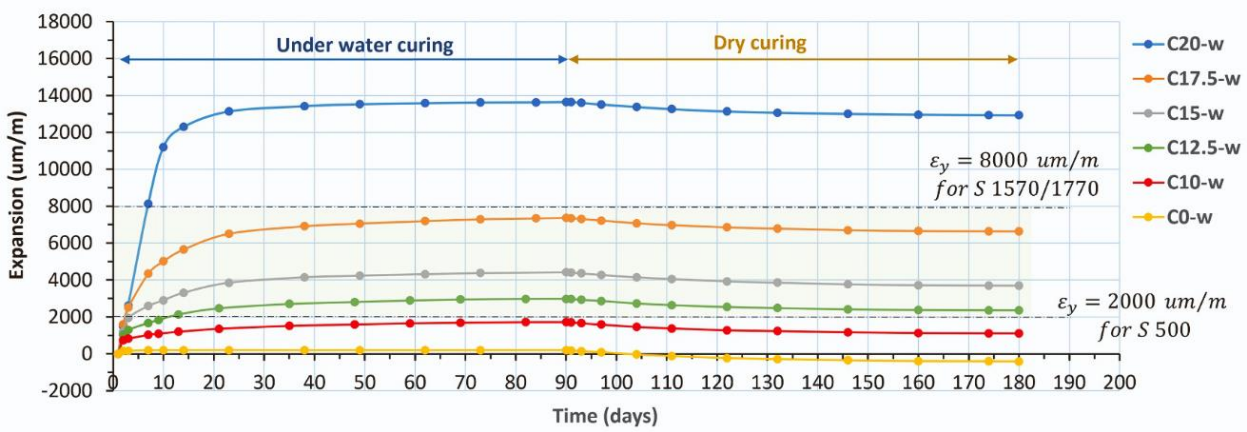

Figure 2-22: Deformation measurements of mixtures with varying Type K CSA cement repla cured under wet-dry conditions (Dhahir & Marx, 2023)

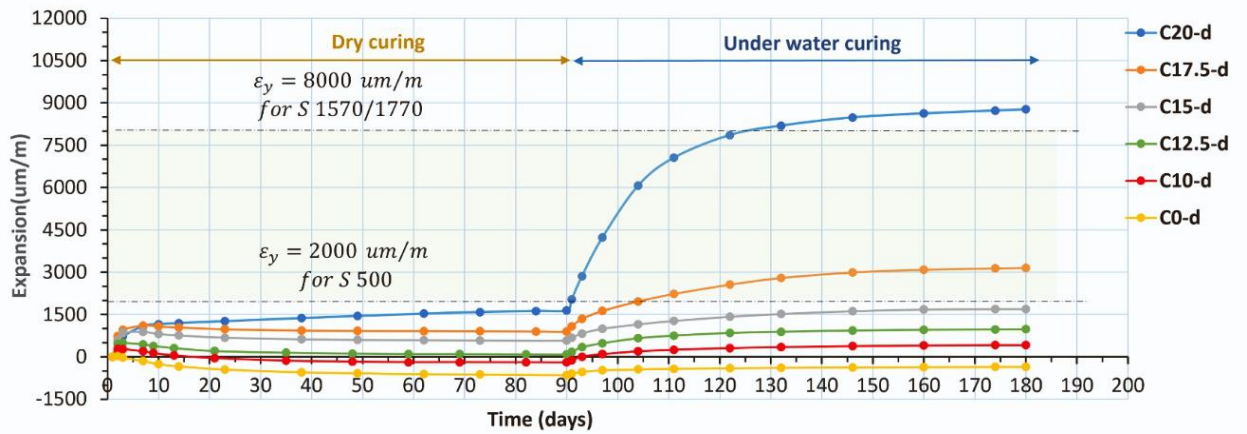

Figure 2-23: Deformation measurements of mixtures with varying Type K CSA cement repla cured under dry-wet conditions (Dhahir & Marx, 2023)

It was found that under the wet-dry curing and high CSA dosages (17.5–20%), the concrete experienced significant expansion of approximately 7.3–14 mm/m, but also a significant decrease in mechanical properties. This decrease was attributed to internal microcracking and was especially evident in the 20% CSA replacement specimen as cracks were visible and specimens showed deformation (curved) due to the high expansion.

On the other hand, while lower CSA replacement ratios (10% and 12.5%) also showed high expansion rates of 1.7 mm/m and 3.0 m/mm, respectively, their mechanical properties were similar to that of just PC in the study. It was also noted that most of the expansion for all of the mixtures occurred in the first 15 days and that the expansion behavior varies nonlinearly with different CSA replacement ratios.

Under dry conditions, all CSA mixtures exhibited rapid expansion during the first 3 days, but this expansion nearly stopped as contraction due to shrinkage began. Despite this, the overall expansion of the dry-cured mixtures was 10-20% lower compared to those cured in water. When water was reintroduced, re-expansion began immediately due to unreacted CSA. This re-expansion can significantly reduce the mechanical properties of the concrete. However, the effect

became less pronounced as the CSA replacement ratio decreased, as the extend of re-expansion was also dependent on the replacement ratio.

This portion of the study emphasizes the importance of fully curing this expansive concrete, particularly during the first two weeks. If there is insufficient water during curing, re-expansion will occur when the concrete comes in contact with water again, potentially damaging its mechanical properties.

In addition to the CSA cements defined by Bescher & Kim (2019), new blends are being developed to further utilize the various benefits CSA has to offer. One such blend, known as supersulfated BCSA (SBCSA), was recently developed and studied by Deo et al. (2023). The authors aimed to modify the balance between CSA and $C\overline{S}$ to create a cement capable of generating controlled expansion while maintaining sufficient strength to prevent structural damage. Developed by mixing commercially available BCSA (80% by weight) with pure, finely ground anhydrite (20% by weight), SBCSA integrates principles from both BCSA and Type K cements to create a fast-setting, expansive binder that is entirely free of Portland cement (PC). Figure 2-24 from the authors illustrates the intended dimensional behavior of SBCSA mortars compared to BCSA, Type K, and PC mortars.

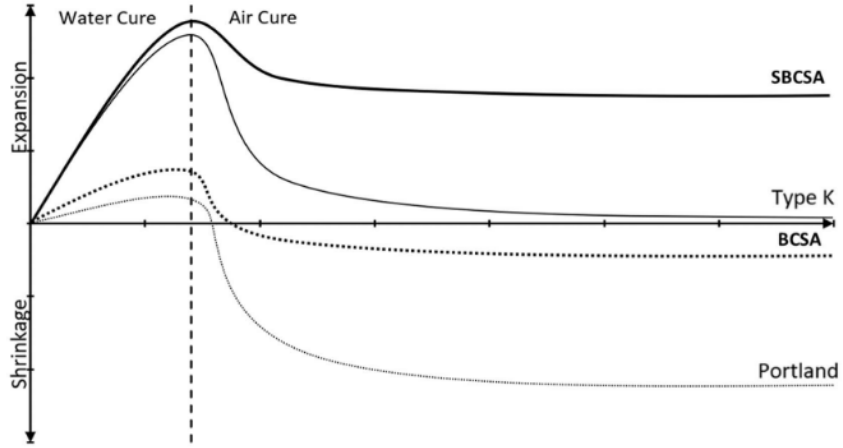

Figure 2-24: Schematic expansion and drying shrinkage for PC, Type K, BCSA, and SBCSA mortars (Deo et al., 2023)

SBCSA was comprehensively tested for its hydration kinetics, phase development, and mechanical properties to provide a holistic understanding of how it differs from conventional BCSA. In addition to testing standard mortar and concrete mixtures, steel fibers were incorporated to assess the potential of SBCSA for chemical prestressing applications. Overall, SBCSA demonstrated significant improvements in strength while maintaining net positive expansion.

As seen in Figure 2-25, SBCA exhibited significant expansion, particularly within the first 14 days. While SBCSA and BCSA exhibit very different expansion behavior under water curing, both showed similarly limited drying shrinkage compared to OPC. This contrasts with the behavior of Type K cement, which includes Portland cement, whereas SBCSA is PC-free. This fundamental difference in composition contributes to SBCSA's unique shrinkage and expansive behavior.

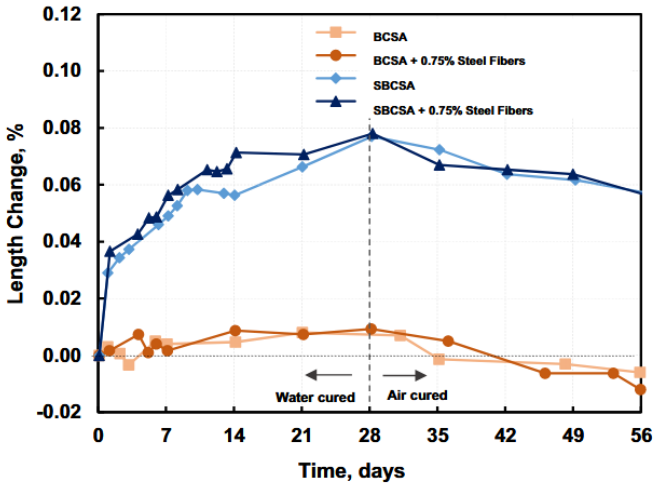

Figure 2-25: Unrestrained expansion of BCSA and SBCSA concrete bars (Deo et al., 2023)

As shown in Figures 2-26 and 2-27, SBCSA concrete specimens exhibited significant improvements in both compressive and flexural strength compared to BCSA. Although SBCSA

showed lower compressive strengths at early ages, substantial strength gains were observed after 3 days, outperforming BCSA by 50% at 28 days. In terms of flexural strength, SBCSA consistently demonstrated higher strength than BCSA at almost all test ages. The increased modulus of rupture in SBCSA was attributed to the additional formation of ettringite produced after 4–5 days of curing.

Hydration phase analysis revealed that SBCSA contained approximately 28% more ettringite at 28 days compared to BCSA. This increase in ettringite formation correlates with the observed improvements in both compressive and flexural strength and is believed to results from the enhanced reactivity of belite in the presence of additional anhydrite.

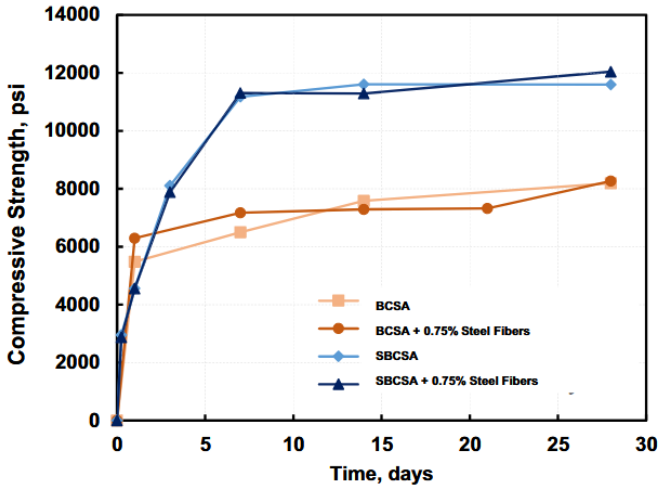

Figure 2-26: Compressive strength of BCSA and SBCSA concrete cylinders (Deo et al., 2023)

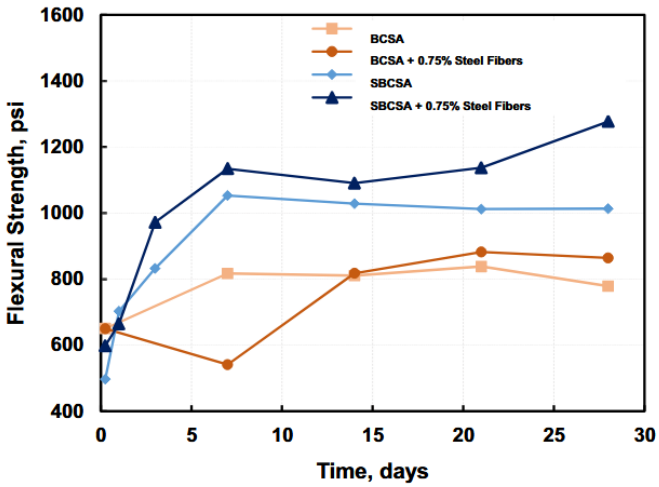

Figure 2-27: Flexural strength of BCSA and SBCSA concrete beams (Deo et al., 2023)

SBCSA shows strong potential for a range of applications due to its increased ettringite formation, which drives significant gains in both compressive and flexural strength. Combined with its controlled expansion and minimal shrinkage, this enables new design possibilities. Additionally, unlike Type K cement, which is added to Portland cement, SBCSA is entirely Portland-free, offering improved sustainability.

2.3. Durability Performance of CSA/BCSA Binders

2.3.1. Early-Age Shrinkage

Volume change is a critical factor affecting the compatibility between an overlay and substrate, as well as the overall performance of concrete. Due to its rapid hydration mechanisms compared to OPC, BCSA cement exhibits distinct shrinkage behaviors during the initial stages of curing. Early-age shrinkage can significantly contribute to the development of microcracks, which may compromise long-term durability and mechanical strength.

Among the various types of early-age shrinkage, autogenous shrinkage is particularly significant in CSA systems as they are commonly used with low water-to-cement (W/C) ratios. Autogenous shrinkage, also known as autogenous deformation or bulk strain, refers to the

volume change caused by cement hydration when no external forces are applied. With low W/C ratios there is typically insufficient water for full hydration, leading to self-desiccation. The water required for full hydration is determined by the stoichiometry of the cement; for OPC, the stoichiometric W/C is approximately 0.40-0.42, while it can be as high as 0.75 for CSA cement (Winnefeld & Lothenbach, 2010).

When there is insufficient water, self-desiccation occurs as mixing water is consumed during hydration. This reduces the amount of free water in the pore structure, leading to the development of self-induced stresses. These stresses, in turn, drive autogenous shrinkage and can ultimately result in cracking. At the same time, low W/C ratios for CSA concrete are essential for producing stable mixes that prevent segregation and meet the necessary mechanical property requirements (Sirtoli et al., 2020).

Sirtoli et al. (2020) investigated the volume changes of mortars containing CSA cement (CSA), limestone Portland cement (PC), and a 50/50 blend by mass of the two cements (MIX). The autogenous shrinkage results of the study are presented in Figure 2-28. The CSA mortar showed the greatest autogenous shrinkage, with the Mix mortar in between it and the PC mortar. The significant shrinkage observed in both the CSA and, to a lesser extent, the PC mortars indicate self-desiccation, as the W/C of the mixes were 0.5 and 0.45, respectively—much lower than the required 0.75. Additionally, it was also noted that the MIX mortar exhibited a bi-modal shrinkage pattern, suggesting a potential risk of cracking both during the early stages of curing and at later ages.

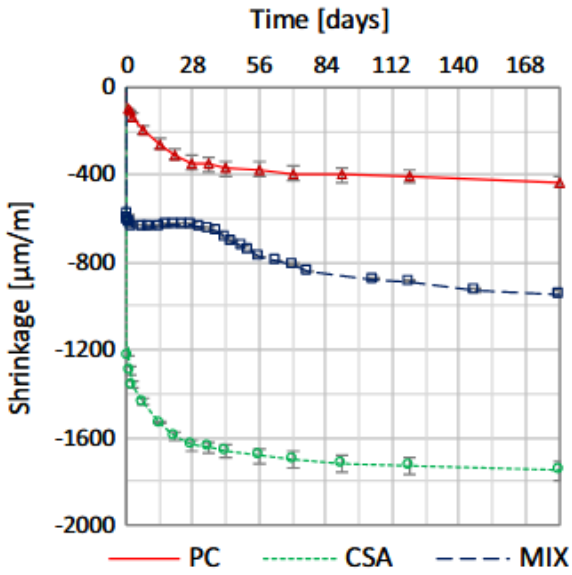

Figure 2-28: Autogenous shrinkage evolution of CSA (Sirtoli et al., 2020)

Plastic shrinkage cracking (PShC) is another common early-age problem in concrete. Occurring within the first few hours after casting, PShC is especially prevalent in large surface applications like pavements and slabs exposed to hot, dry, and windy conditions. The primary cause of PShC is rapid surface water evaporation, which creates capillary forces that, when restrained, generate internal stress and causes cracks, particularly at points where air penetrates the concrete. Factors like evaporation rate, bleeding, material properties, setting time, and construction practices influence PShC, with evaporation and bleeding having the most direct effects. If not properly controlled, PShC can significantly compromise the durability of concrete structures. Cracks formed during early stages provide pathways for corrosive agents to penetrate the concrete, accelerating deterioration and reducing structural integrity (Combrinck & Boshoff, 2015).

Combrinck & Boshoff (2015) studied the mechanisms of plastic shrinkage, focusing on setting time and bleeding. Four mixes were tested: a standard OPC concrete mix (MS), one with retarded setting (MR), one with accelerated setting (MA), and one designed to increase bleeding

(MB). Figure 2-29 presents the results of the four mixes, while Figure 2-30 illustrates the typical PShC observed by the authors.

It was found that PShC consistently began after initial setting and stabilized before final setting, with air entry occurring just before or at the initial set. After final setting, cracks widened more slowly due to drying shrinkage, which begins only after final setting. While evaporation plays a major role, bleeding also significantly influenced the PShC severity. The mix designed to enhance bleeding (MB) showed reduced cracking, whereas the mix intended to accelerate setting (MA) exhibited increased cracking. In contrast, delaying the setting time reduced cracking.

These findings differ from other studies, some of which reported opposite trends or found an inexplicable relationship between admixtures and PShC. This highlights the need for further research, particularly for CSA cement, which sets rapidly and typically exhibits less bleeding than OPC.

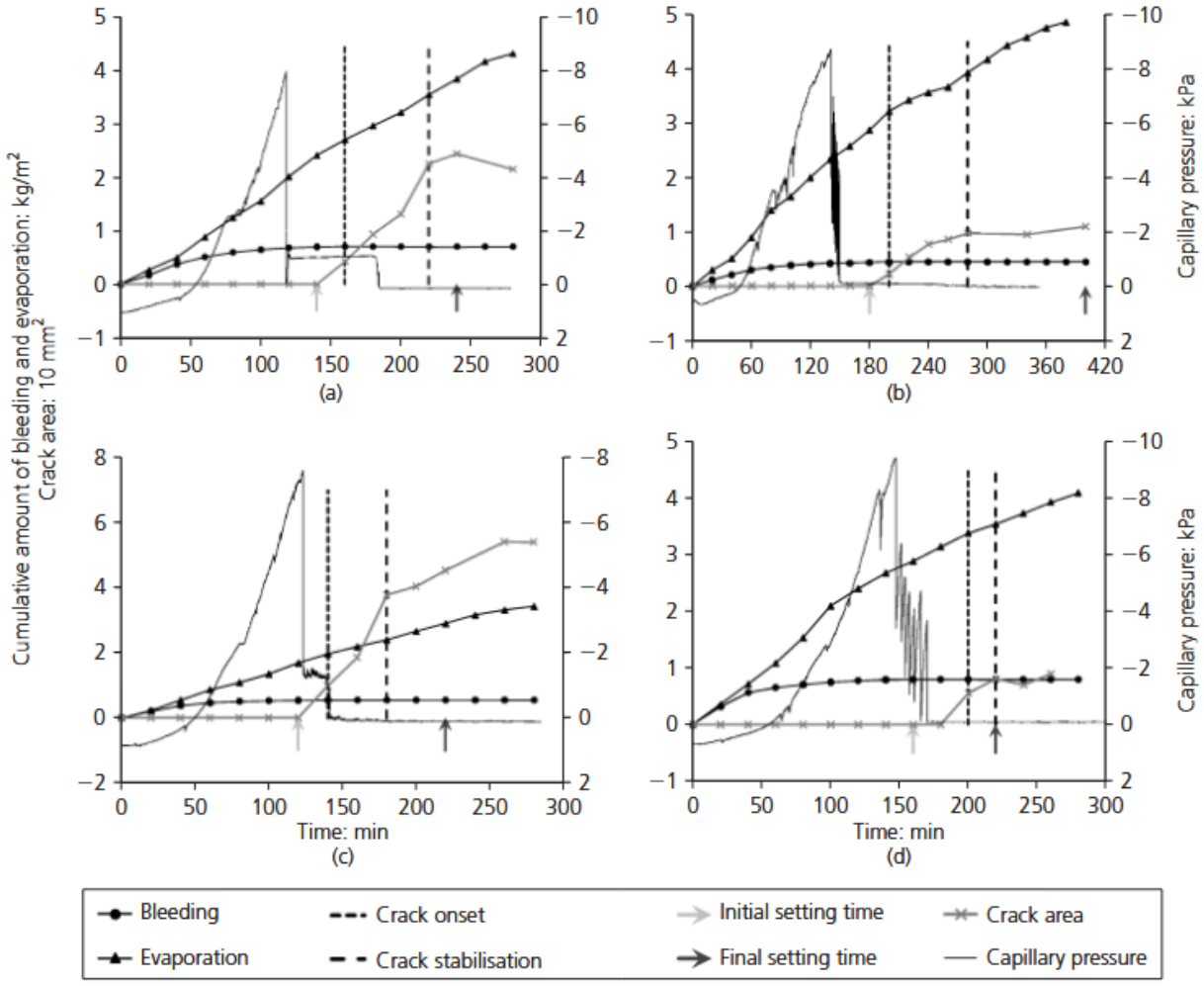

Figure 2-29: Cumulative amount of bleeding and evaporation, crack area, and capillary pressure plotted against time for (a) standard OPC mix (MS), (b) retarded mix (MR), (c) accelerated mix (MA), and (d) increased bleeding mix (MB) (Combrinck & Boshoff, 2015)

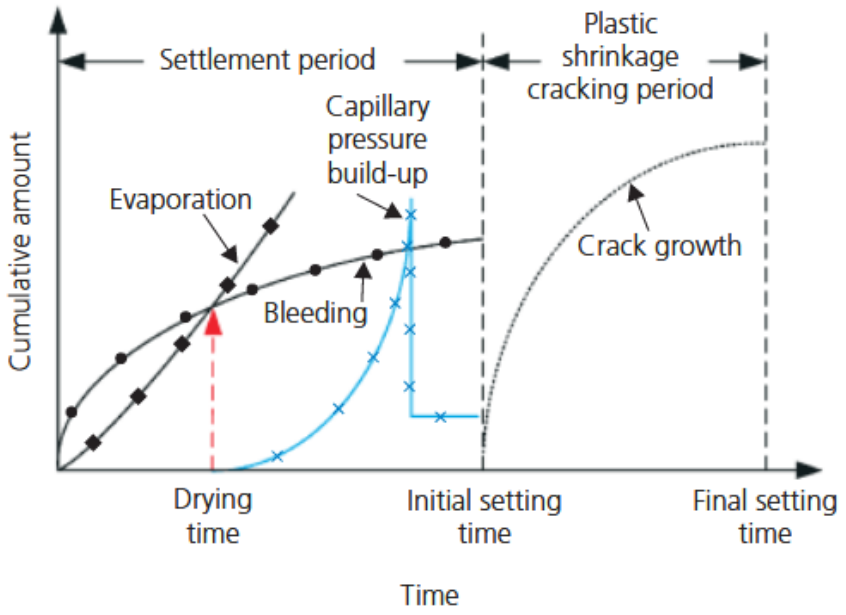

Figure 2-30: Typical plastic shrinkage cracking behavior integrity (Combrinck & Boshoff, 2015)

In addition to autogenous and plastic shrinkage, drying shrinkage is another important deformation mechanism in concrete. It is measured under drying conditions, where moisture loss to the environment induces volume change. Typically, the measured deformation typically reflects the combined effects of autogenous and true drying shrinkage.

In the same study by Sirtoli et al. (2020), the drying shrinkage of CSA, PC, and a mix of the two cements (MIX) was also studied under different relative humidity (RH) conditions (36%, 57%, 70% and 90%). To simulate real-world concrete applications, samples were not demolded for the first 24 hours. Instead, autogenous shrinkage specimens were used to supplement the data for the initial 24 hours at the same RH conditions. Additionally, mass loss of the specimens was recorded to monitor changes in water content over time and to correlate these changes with drying shrinkage. The drying shrinkage results are presented in Figure 2-31, along with the baseline autogenous data from Figure 2-28 for comparison.

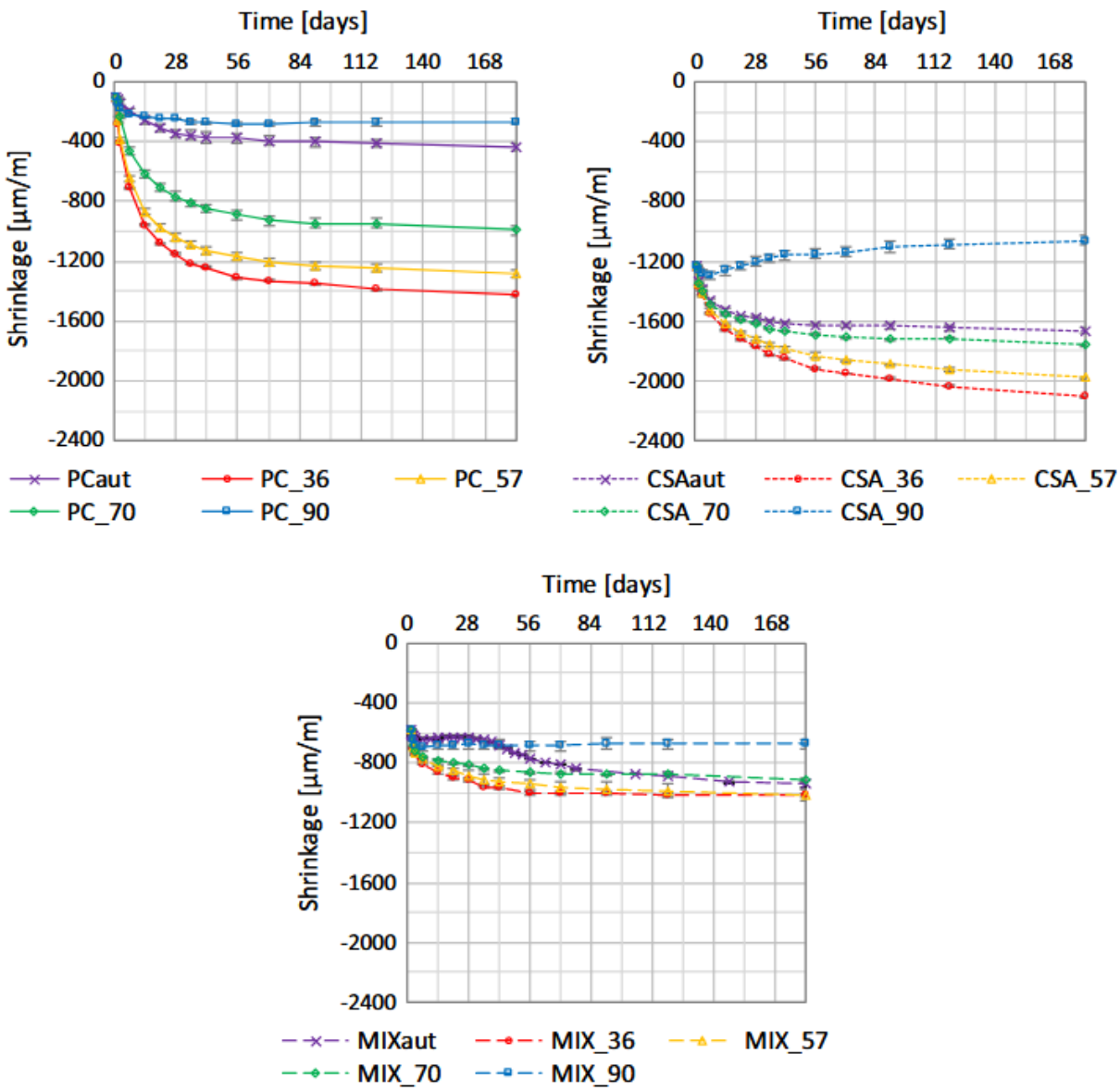

Figure 2-31: Shrinkage evolution as a combination of autogenous condition before 24 hours and drying at different relative humidities after 24 hours (Sirtoli et al., 2020)

For all specimens, greater mass loss and shrinkage were observed as the environmental RH decreased. This trend is attributed to the environmental RH being lower than the internal RH, causing water to evaporate from the specimens and resulting in mass loss. Conversely, when the internal RH falls below the environmental RH due to self-desiccation, the specimens begin to

absorb moisture, leading to mass gain. This behavior explains the mass increase observed in mortars stored at 90% RH, particularly in CSA mortars.

It is important to note that the majority of shrinkage develops very early, especially for CSA. In a similar study by Ke et al. (2022), CSA concrete was shown to have experienced over 85% of the total shrinkage measured at 28 days within the first 2 hours of setting. During the subsequent humidity decline stage, less than 15% of the total 28-day shrinkage develops. This highlights the critical role of early moisture loss and internal RH evolution in governing long-term shrinkage behavior.

However, the relationship between environmental RH and moisture behavior is more complex than that between self-desiccation and autogenous shrinkage. This complexity comes from the non-uniform drying-induced shrinkage caused by moisture gradients that form immediately after exposure. The resulting moisture and shrinkage profiles are influenced by several factors: the initial internal RH at the time of exposure, the ambient RH, moisture diffusion within the sample, and ongoing self-desiccation and autogenous shrinkage.

Additionally, the use of admixtures can influence the shrinkage of concrete. In a study by Li et al. (2018) that specifically investigated the effects of various polymer latex on CSA cement mortar shrinkage, it was found that increasing the amount of latex reduced shrinkage. Three different polymer latexes were studied: styrene butadiene rubber (SBR), styrene acrylic ester (SAE), and polyacrylic ester (PAE). The shrinkage results for these mixes are presented in Figure 2-32.

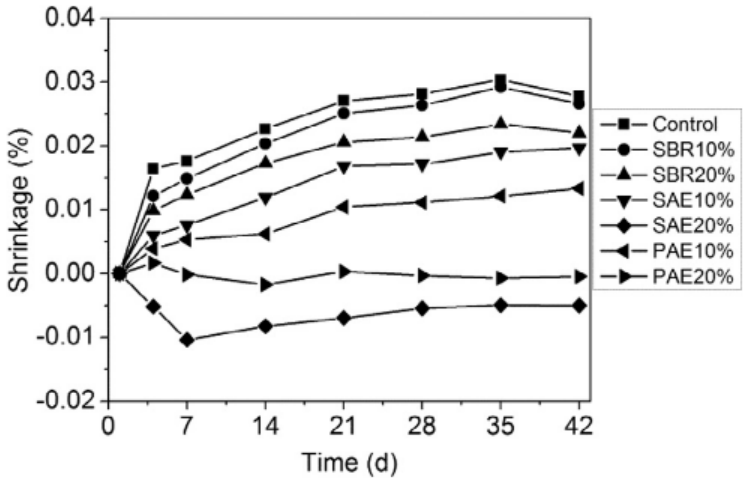

Figure 2-32: Shrinkage of polymer latex modified CSA cement mortar (Li et al., 2018)

It was found that an increase in latex for any of the polymers led to reduced shrinkage, with PAE producing the greatest reduction and SBR the least. It was hypothesized that the polymer films formed within latex-modified mortars act like "micro-fibers" within the matrix, helping to limit shrinkage development. Furthermore, these films can block pores and refine the internal pore structure of the cement matrix, reducing water evaporation and further minimizing shrinkage.

2.3.2. Freeze-Thaw

Freeze-thaw resistance is a critical durability concern for concrete exposed to cyclic freezing and thawing conditions. During freezing, water within the concrete's pore structure expands, generating internal stresses that can lead to microcracking, surface scaling, and ultimately, structural deterioration. The microstructure of concrete—including pore size distribution, connectivity, and overall porosity—plays a significant role in its ability to withstand freeze-thaw damage. A well-refined microstructure with a controlled air-void system can mitigate internal pressures by providing space for ice expansion. Additionally, shrinkage mechanisms, such as autogenous and drying shrinkage, influence the initial microstructural state

of concrete by promoting internal tensile stresses and microcrack formation, which can further compromise freeze-thaw performance.

De Bruyn et al. (2017) conducted freeze-thaw testing on CSA cement concrete and PC concrete with two different coarse aggregates: one reportedly very good freeze-thaw performance (G) and another with very poor freeze-thaw resistance (B). The results, expressed as relative dynamic modulus (RDM) and percentage weight loss (PWL), are presented in Figure 2-33. According to the testing standard ASTM C666 (ASTM International, 2003), the test should be stopped when the RDM falls below 60%, as specimens are then considered non-durable under freeze-thaw conditions. However, the authors continued testing beyond this threshold until it was no longer possible to measure the RDM.

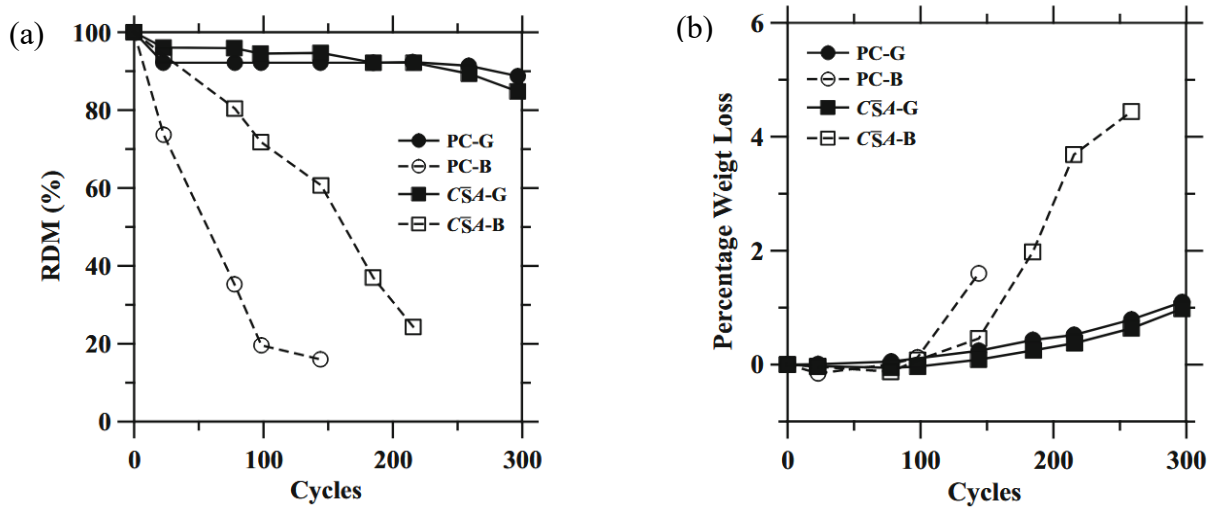

Figure 2-33: (a) Relative dynamic modulus and (b) percent weight loss results for freeze-thaw test of CSA cement and PC concrete (De Bruyn et al., 2017)

For the mixes made with the good-quality coarse aggregate, both CSA and PC concrete remained durable, maintaining over 60% RDM through 300 cycles; however, closer inspection revealed more severe scaling in the PC specimens. For the mixes made with the poor-quality coarse aggregate, the PC concrete (PC-B) dropped below 60% RDM after about 50 cycles, while

the CSA concrete (CSA-B) maintained over 60% RDM until approximately 150 cycles. Both mixes exhibited surface scaling after 144 cycles, as reflected by a steady increase in percent weight loss (PWL).

Although both concretes with the poor aggregate ultimately considered non-durable, the CSA concrete demonstrated roughly 300% improvement in freeze-thaw resistance compared to the PC concrete. These findings suggest that while marginal-quality aggregates (worse than aggregate G but better than aggregate B) are typically unsuitable for use with PC in freeze-thaw environments, they may perform adequately when combined with CSA cement. Since such aggregates are generally less expensive, CSA cement could enable the production of durable, freeze-thaw-resistant concrete at a lower cost.

A study by Li et al. (2018) also looked at the freeze-thaw resistance of CSA cement mortar but with the polymer latexes: SBR, SAE, and PAE. Speciemens were subjected to 56 freeze-thaw cycles then measured for their flexural and compressive strengths. The durability performance of the mixes was evaluated by calculating a durability coefficient ($\Gamma_{F\text{-}T}$) which was calculated by the ratio of the flexural and compressive strength with and without freeze-thaw attack. These coefficients are presented in Figure 2-34.

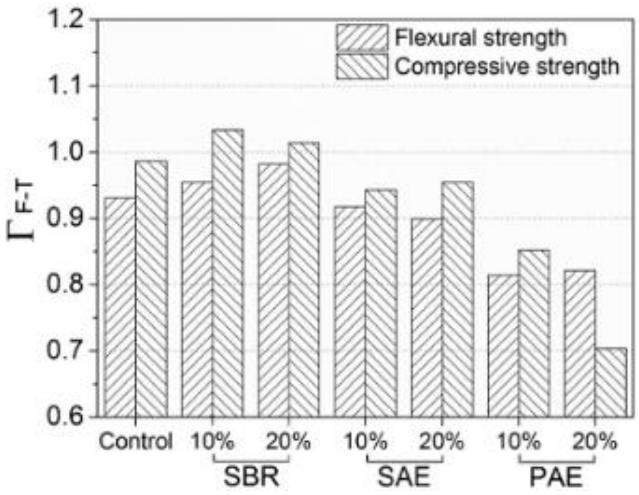

Figure 2-34: Coefficient of freeze-thaw cycle resistance for latex-modified CSA cement mortars (Li et al., 2018)

Among all tested mixes, SBR-modified mortar demonstrated the best resistance to freeze-thaw cycles, whereas PAE-modified mortar exhibited the poorest performance. It was also noted that the compressive strength $\Gamma_{F\text{-}T}$ was generally higher than the flexural strength $\Gamma_{F\text{-}T}$, except for mortars with 20% PAE. Overall, SBR latex enhanced the freeze-thaw durability of CSA, while PAE latex significantly reduced freeze-thaw resistance. This indicates that the chemistry of the polymer and its interaction with CSA can vary depending on the type of polymer used, significantly affecting the performance of CSA concrete.

2.3.3. Salt Scaling

Similar to freeze-thaw resistance, salt-scaling resistance refers to concrete's ability to withstand freeze-thawing cycles in the presence of deicing salt solution. Salt scaling leads to the flaking or peeling of the concrete's surface layer and can be influenced by several factors, including cement composition, W/C ratio, and surface finishing.

Cements with low C_3A and low alkali content have been found to offer better resistance to salt scaling by helping maintain a stable air-entrainment system. Additionally, lowering the W/C ratio decreases porosity and increases strength, both of which improve scaling resistance. As for the surface finish, if finishing occurs while bleed water remains, it can be mixed back into the surface, increasing the surface W/C ratio and weakening the surface strength. On the other hand, excessive finishing can remove air from the surface layer, making the concrete more vulnerable to freeze-thaw damage. Given their typically low C_3A content and frequent use of low W/C ratios, CSA-based systems may therefore exhibit strong resistance to salt scaling (Moffatt, 2016).

Moffatt (2016) evaluated the salt-scaling resistance of ettringite-based concrete of laboratory scale specimens or slab specimens exposed to natural weathering. The following cements were subjected to NaCl solution applied in the lab for 50 freeze-thaw cycles or after each snow fall outside at the University of New Brunswick: a ternary system with PC, calcium aluminate cement (CAC), and calcium sulfate (C$), labeled PC-CAC-C$; a belite-rich CSA cement system (C$A(1)-C2S); a standard CSA cement system blended with PC (C$A(2)-PC); and as controls, ordinary Portland cement (PC) and a high-early strength Portland cement (HEPC). The performance of these mixes were evaluated according to ASTM C672 (ASTM International, 1998) and compared to the Canadian standard, BNQ NQ 2621-900, with results shown in Figure 2-35.

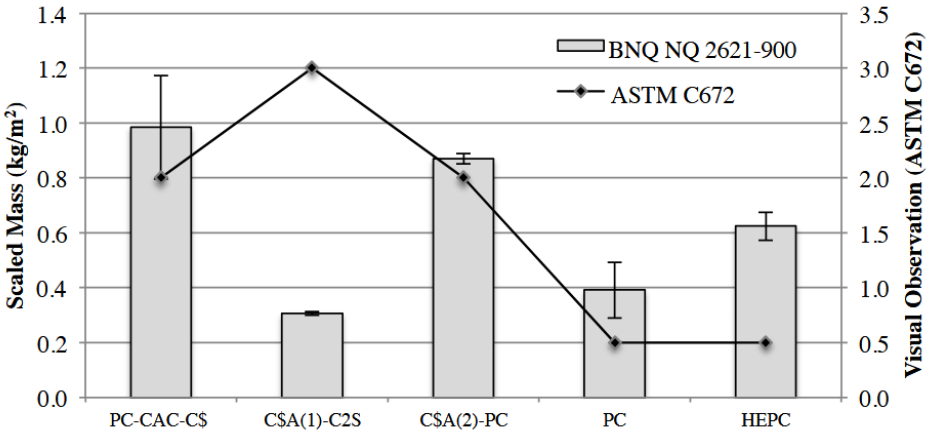

Figure 2-35: Freeze-thaw performance of the laboratory scale ettringite-based cement systems (Moffatt, 2016)

In the laboratory tests, the PC-CAC-C$ and C$A(2)-PC mixes exhibited the highest mass loss, nearing the typical failure threshold of 1 kg/m^2. In contrast, the C$A(1)-C2S and PC mixes showed the least scaling. However, after approximately three years and fifth treatments in the field exposure tests, the trends reversed: C$A(1)-C2S performed the worst, while PC and HEPC showed the best durability.

The discrepancy between laboratory and field results was attributed to factors such as the harsher, accelerated conditions in the lab (rapid freezing/thawing and optimized salt exposure), differences in curing time (14 days in lab vs. 28 days in the field), and the sensitivity of ettringite-based systems to handling during early setting. These findings highlight that while CSA-based systems may show promise under controlled conditions, their long-term durability against salt-scaling in real-world environments requires careful attention to curing practices and early-age handling to ensure consistent performance.

CHAPTER 3: EXPERIMENTAL PROGRAM

3.1. Materials

3.1.1. Cements

This project aimed to characterize and compare the performance of polymer-modified CSA cement against unmodified CSA cement. Two proprietary polymer-modified CSA cements were evaluated—both identical in composition except for the method of polymer incorporation: one contained the polymer as a mineral admixture that was inter-ground and blended in the cement during production (integral Low-P™), while the other used a separate chemical admixture (Liquid Low-P™). It is important to note that the integral Low-P™ mix also included a powdered HRWR as part of its formulation. Latex-modified CSA cement was chosen as the polymer-modified control for this study, as it represents a common approach to concrete overlays for bridge decks.

The cement information and IDs are listed in Table 3-1. Note that while the cement used in this project is specifically BCSA, it is common in the industry to use BCSA and CSA interchangeably, as CSA serves as the umbrella term for this classification of cement. Therefore, these terms will be used interchangeably throughout the thesis.

Table 3-1: Summary of Cements

Cement ID	Description
CSAP or P	BCSA with integral Low-P^{TM} polymers
CSA-LLP or LLP	BCSA with Liquid Low-P^{TM} admixture
CSA-LM or LM	BCSA with latex admixture

3.1.2. Aggregates

For this project, two coarse aggregates (CA) were used: a 3/4" nominal maximum size aggregate (NMSA) rock and a 3/8" NMSA pea gravel. A single fine aggregate (FA), river sand, was used throughout the project. All aggregates used were locally sourced from DuPont, WA. The pea gravel and sand used have been extensively tested in previous research projects at the University of Washington, providing gradations for both aggregates. Figure 3-1 shows the gradation of the sand compared to the ASTM C33 (ASTM International, 2024b) fine aggregate requirements to confirm compliance.

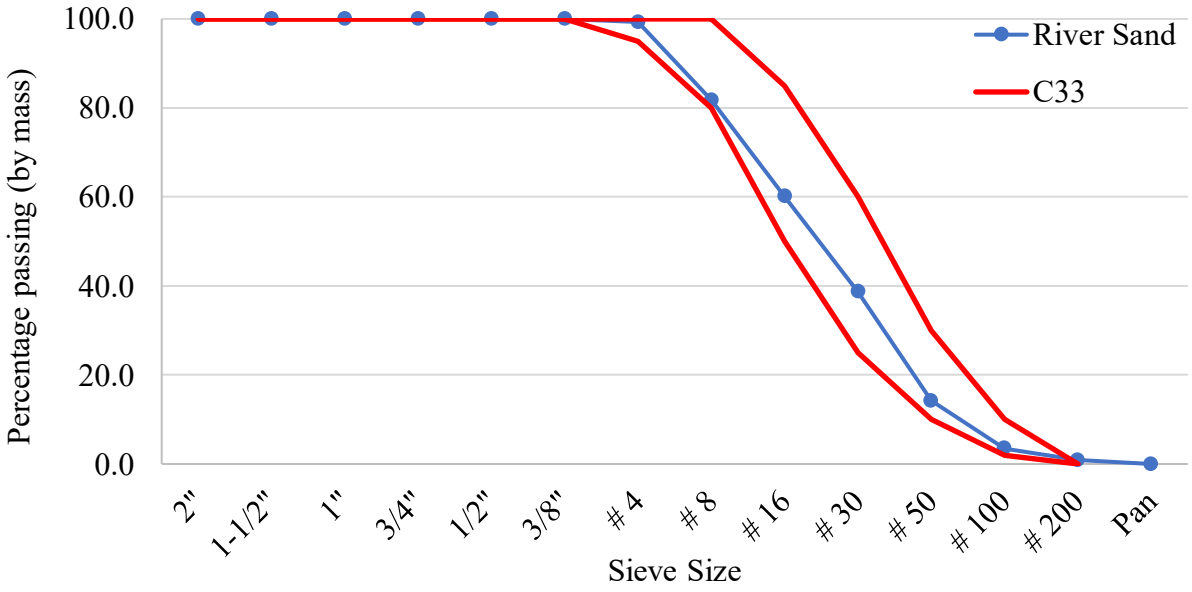

Figure 3-1: River sand gradation

Figure 3-2 compares the pea gravel gradation to the ASTM C33 requirements for Size 7 and Size 8 aggregate classifications. This figure shows that the aggregate tested slightly out of bounds for both classifications. This difference may be due to material loss during sieving or non-representative sampling from laboratory supersacks.

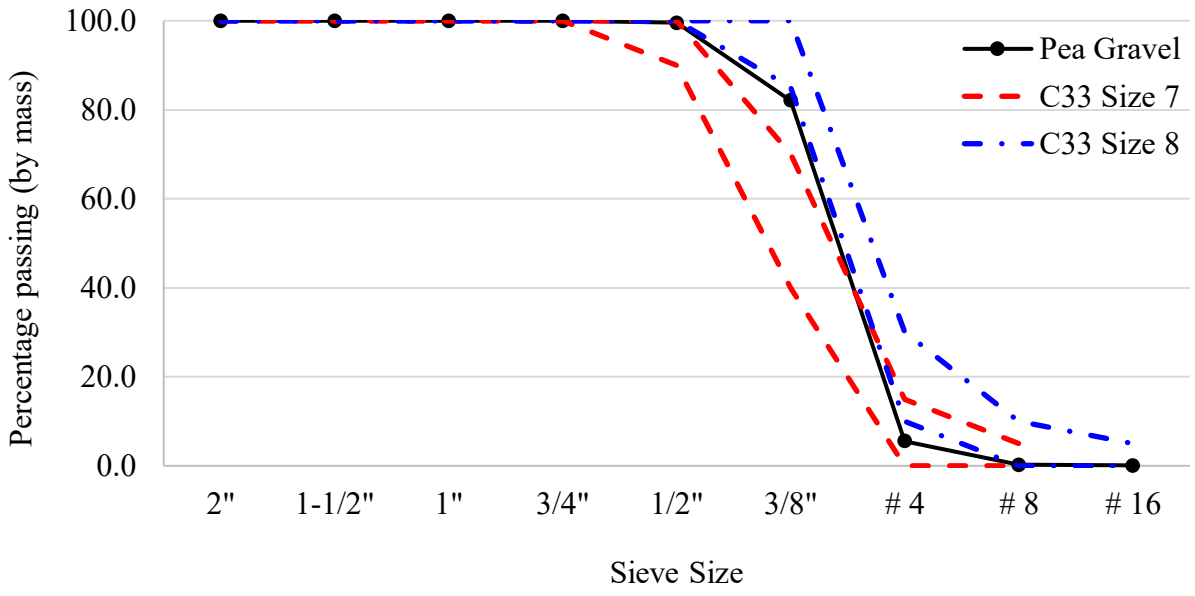

Figure 3-2: Pea gravel gradation

A sieve analysis of the 3/4" rock was conducted in accordance with ASTM C136 (ASTM International, 2019a) and is shown in Figure 3-3, along with the gradation requirements for Size 56 aggregate from ASTM C33. The rock falls slightly out of bounds for the 1/2" sieve size. Similar to the pea gravel, this deviation may be due to material loss during sieving or non-representative sampling from laboratory supersacks.

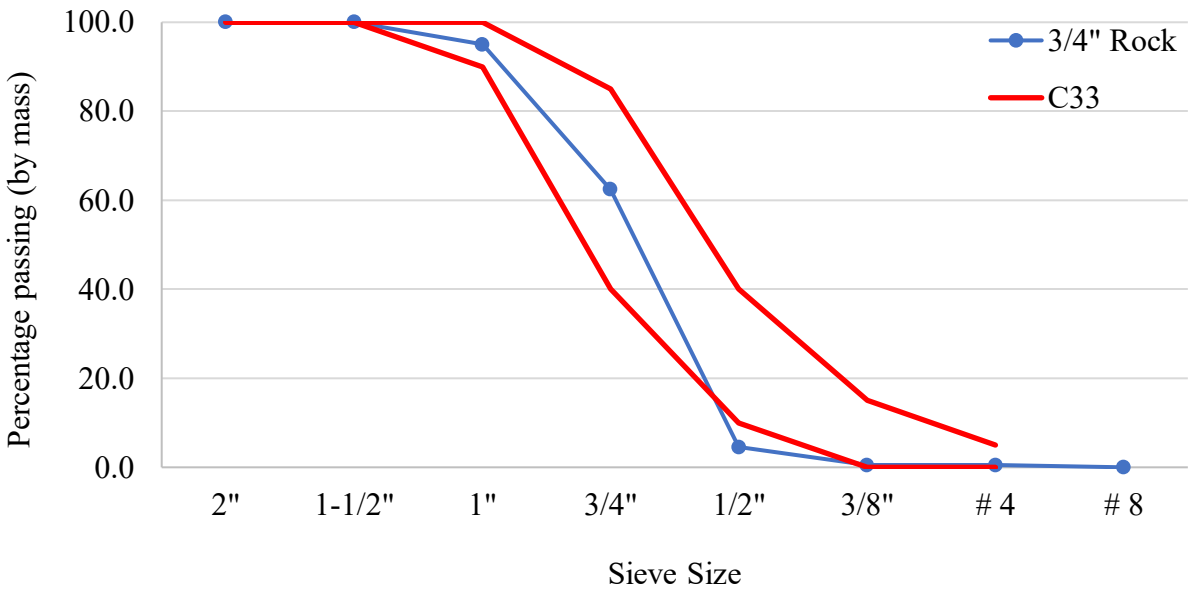

Figure 3-3: 3/4" Rock gradation

The 3/4" rock was also characterized for its oven-dried (OD) and saturated surface dry (SSD) bulk specific gravity (BSG) and absorption capacity following ASTM C127 (ASTM International, 2015). Previous research work at the University of Washington had already established the absorption capacities and OD specific gravities for the pea gravel and river sand. These recorded values were used to determine mixture proportions and moisture corrections. Table 3-2 summarizes the properties of the aggregates used.

Table 3-2: Aggregate Properties

Aggregate	11	Specific Gravity (OD)	Specific Gravity (SSD)	Absorption Capacity (%)	Dry Rodded Unit Weight (lb/ft^3)
Rock (3/4" NMSA)	56	2.69	2.71	0.88	110.8
Pea Gravel (3/8" NMSA)	7, 8	2.68	2.71	1.12	110.8
River Sand	ASTM C33	2.65	2.71	2.10	111.2

[1] (ASTM International, 2024b)

3.1.3. Chemical and Mineral Admixtures

A variety of admixtures were utilized in this project to achieve targeted concrete properties, such as air-entraining admixtures (AEA), high-range water reducers (HRWR), set retarders, and polymers. A summary of the different admixtures used is provided in Table 3-3. Several AEAs were tested to address challenges with air-entraining Low-P™ polymer-modified mixtures. For most of the mixtures evaluated under this project, a vinsol resin-based AEA, MasterAir® VR 10, was used. Additionally, the vinsol resin-based AEA, Daravair® 1000, and synthetic-based AEAs, such as MasterAir® AE 90 and MasterAir® AE 200, were also utilized for certain portions of the project.

All high-range water reducers (HRWR) used to achieve the desired workability were polycarboxylate-based admixtures. However, due to variations in performance based on chemical composition, two different HRWRs were tested: MasterGlenium® 7920 and ADVA Cast® 195. Both HRWRs meet the ASTM C494 (ASTM International, 2024d) standards for Type A (water-reducing) and Type F (high-range water-reducing) admixtures. When using both AEAs and HRWRs, it is important to use admixtures from the same manufacturer, as chemical incompatibility may occur. As a result, MasterGlenium® 7920® was paired with MasterAir® VR 10, MasterAir® AE 90, MasterAir® AE 200, while ADVA Cast® 195 was only used with Daravair® 1000.

Citric acid was used to control the set times of the BCSA concrete mixtures. The dosage rates varied for each mixture design, with an initial baseline dosage rate of 0.25 lbs/cwt, which was then adjusted as needed. The citric acid used was an anhydrous fine granular powder that was dissolved into the batch water after the aggregate reached saturated surface dry conditions.

Two different polymer admixtures were used for this project: Liquid Low-P™ and STYROFAN® 1186. Liquid Low-P™ is a proprietary polymer designed to produce low-

permeability concrete, which helps inhibit the corrosion of reinforcement steel. It is reported to be 50% solids by mass, with recommended addition rates as low as 10.0 fl oz/cwt. STYROFAN® 1186 is a styrene-butadiene emulsion polymer used to produce latex-modified BCSA concrete, and it is reported to be 48% solids by mass. According to ACI 548.4-11 (American Concrete Institute, 2012), the current standard for latex-modified CSA concrete overlay mixes is 3.5 gallons of latex per sack (94 lbs) of cement (American Concrete Institute, 2009). This rate is nearly 50 times higher than that for Liquid Low-P™. Due to the significant difference in dosage rates, water adjustments were made for mixes containing STYROFAN® 1186 to account for the water content in the polymer and ensure the design water-to-cement ratio (W/C) was maintained.

Table 3-3: Summary of Admixtures

Admixture	ID	Type	Use
MasterAir® VR 10	VR10	AEA (vinsol resin)	Air content
MasterAir® AE 90	AE90	AEA (synthetic)	Air content
MasterAir® AE 200	AE200	AEA (synthetic)	Air content
Daravair® 1000	DA1000	AEA (vinsol resin)	Air content
MasterGlenium® 7920	MG7920	HRWR (polycarboxylate)	Workability
ADVA Cast® 575	AD575	HRWR (polycarboxylate)	Workability
Citric Acid	-	Anhydrous fine granular powder	Retarder
Liquid Low-P™	LLP	Polymer	Durability
STYROFAN® 1186	Latex	Styrene-butadiene emulsion polymer	Durability

3.2. Laboratory Testing

3.2.1. Developing a Preliminary CSA Overlay Mixture Design

The preliminary CSA overlay mixture design used in this project was originally developed as part of Guerrero-Estrada (2024). This design focused on optimizing aggregate

gradation and workability by ensuring sufficient paste-to-aggregate ratios while maintaining a target compressive strength. The initial design incorporated the Tarantula curve and Power 45 curve for aggregate optimization, along with a modified void ratio approach to achieve desired workability while minimizing the paste quantity. Following this preliminary design, further modifications were made to investigate the effects of different mix variables on both fresh and hardened properties, providing a comprehensive understanding of its behavior and potential improvements.

3.2.1.1. Modified Void Ratio for Paste/Aggregate Optimization

The preliminary mixture design was initially developed based on the strength data of the concrete substrate, serving as a baseline for target strength. The substrates used in this project were originally constructed as part of Guerrero-Estrada (2024). High target strengths were established as indicators of potential bond performance, leading to a BCSA mixture with a low water-to-cement ratio. Mixture proportions and paste contents were optimized using performance-based mixture proportioning, ensuring efficient material utilization while producing concrete that met the required specifications (Taylor et al., 2015)

Performance-based mixture proportioning is an iterative process that involves optimizing both aggregate and paste quantities. The process begins with a sieve analysis to determine the gradations of the as-received fine and coarse aggregates following ASTM C136 (ASTM International, 2019a). The resulting aggregate gradations are then entered into a spreadsheet designed to determine the optimal combination of the two aggregates for the chosen gradation system using the Excel solver function. According to Taylor et al. (2015) recommendations, the aggregate gradation was proportioned within the Tarantula Curve while aiming to stay close to the Power 45 curve.

Once the optimal coarse and fine aggregate blended proportions are identified, the aggregate void percentage is calculated using a modified ASTM C29 (ASTM International, 2023a) procedure. In this step, the coarse and fine aggregates are blended according to the previously determined proportions and tested accordingly.

Cement paste properties, as specified in the requirements, along with binder properties, were input into the process. These inputs included W/C ratios and air contents. An additional key input was the volume-of-paste to volume-of-voids (Vp/Vv) ratio, which determines the amount of paste needed to fill the voids left by the aggregate proportions and sufficient lubrication for the desired workability. The spreadsheet generated batch quantities as outputs, and trial mixes were prepared to evaluate the effectiveness of the mixture design. The Vp/Vv ratio was adjusted iteratively based on the results of these trial mixes. Whenever new aggregate proportions were selected, the percentage of voids in the aggregate blends was recalculated, and a new mixture was designed.

This iterative process of adjusting the Vp/Vv ratios and aggregate proportions continued until satisfactory results were achieved, with the primary objective being to minimize the paste content to produce a slump range of 1-3 inches without the addition of HRWR. Thereafter, the process allowed for flexibility in further adjusting the workability as needed by adding HRWR. Along with achieving the desired workability, a compressive strength ranging between 7-9 ksi by 7 days was targeted, as the concrete substrate's design strength at the time of testing was 9 ksi.

It is important to note that the performance-based mix design spreadsheet was originally designed for concrete pavement mixtures using NMSA of 3/4" or larger. Since pea gravel (3/8" NMSA) was used in this study, the spreadsheet had to be modified to accommodate the smaller aggregate materials. Additionally, the Tarantula curves were not developed for such NMSA values, so the minimization of the Power 45 curve was prioritized to achieve a densely packed

aggregate structure, which positively impacts strength and durability. Deviations from the recommended Vp/Vv ratios provided in the study were also necessary because the spreadsheet was developed using Portland cement as the binder. The use of BCSA required adjustments due to its unique workability properties, including its fast-setting nature and rapid slump loss.

3.2.2. Characterization Study

The preliminary phase from Guerrero-Estrada (2024) established baseline mixes that achieved the desired aggregate gradation, workability, and strength. Building on these mixes, this part of the project further investigated the influence of aggregate size and ratio, as well as AEA type and dosage, on the performance of CSA concrete. Based on WSDOT's 2025 Standard Specifications (2025) for air content of concrete Class 4000D decks and modified concrete overlays a target fresh air content of 5.5% ± 1.5% was chosen. However, a common challenge with polymer modified CSA cement is achieving this target fresh air content; therefore, this study focused on evaluating AEA dosage and type to achieve target fresh air content while maintaining sufficient workability, strength, and durability characteristics.

3.2.2.1. Test Matrix

Expanding on the initial evaluation and optimization of the preliminary CSA mixes, additional experimental work was conducted to assess the effects of various mix design parameters. These parameters included:

a. Coarse-to-fine aggregate ratio
b. Maximum coarse aggregate size
c. Air-entraining admixture dosage
d. Air-entraining admixture type
e. Latex modifier dosage

The first four parameters (a) through (d) were studied sequentially. Parameters (a) and (b) were tested on each of the CSA systems: CSAP, CSA-LLP, and CSA-LM, while parameters (c) and (d) were only assessed on CSAP and CSA-LLP, as air-entrainment is primarily an issue in Low-PTM polymer-modified CSA systems; CSA-LM was excluded from this experimental program due to its inherent air-entraining properties. The latex modifier dosage (e) was studied separately to isolate its specific effect on fresh and hardened properties.

Phase I of the testing program involved evaluating parameters (a) maximum coarse aggregate size and (b) coarse-to-fine aggregate ratio. The aggregates used in the preliminary CSA mixes include an ASTM C33 (ASTM International, 2024b) river sand and 3/8" NMSA pea gravel, which are suitable for concrete overlay toppings with a minimum depth of 1.5". To assess CSA's suitability for thicker overlay toppings, mixtures were tested with 3/4" NMSA (Grade No. 56 stone) during the first phase of the characterization testing program. Additionally, the coarse-to-fine aggregate (CA/FA) ratio by mass was adjusted to 60/40 to align with common gradations used for concrete pavement mixtures. Finally, 4x8-inch cylinders were used for these mixes to accommodate the larger 3/4" aggregate size, while 3x6-inch cylinders were used for all other mixes.

A reoccurring issue with CSA mixes is their low air content. Specifically, CSA mixtures incorporating either integral Low-P (CSAP) or Liquid Low-P (CSA-LLP) have not been able to achieve the target fresh air content range of 4–7% in the concrete. One potential improvement is adjusting the CA/FA ratio, as increasing the proportion of fine aggregate in a mix will typically result in higher air content. The fine aggregate acts as a "screen," capturing air during mixing and creating voids filled with paste and air bubbles, thereby efficiently generating air within the mixture (Dolch, 1996). To test this hypothesis, river sand and 3/8" NMSA were blended at coarse-to-fine aggregate ratios of 45/55 and 35/65 in the first phase as well.

The dosage of air-entraining admixture (AEA) also affects the air content of concrete. In Phase II of the testing program, VR10 was added to the selected aggregate blend from Phase I at dosages of 1.0% and 1.75% by mass of cement (moc) for CSAP mixes, and at 1.75% and 2.5% moc for CSA-LLP mixes. After assessing the influence of dosage and selecting an optimal amount, Phase III involved testing various synthetic and vinsol resin-based AEA products to evaluate their interactions with CSA and aggregates, as these variations may impact air content.

The last phase, Phase IV, focused on latex modifier dosage. In this phase, the aggregate size and blend remained consistent with the preliminary CSA-LM mixture, with only the latex quantity adjusted. The ACI 548.4-11 standard (American Concrete Institute, 2012) specifies 3.5 gallons of latex per sack (94 lbs) of cement, a requirement that has remained unchanged for decades despite limited supporting data for modern cements, especially BCSA. Meanwhile, CSA-LLP requires only 10 fl-oz/cwt, significantly less than the standard latex dosage. To reduce material costs and overall material usage, and to determine whether a reduced latex quantity could achieve comparable performance to the Liquid Low-P™ product, latex dosages were tested at 25% and 50% of the standard dosage—equivalent to 0.875 gal/sack and 1.75 gal/sack, respectively. Table 3-4 presents the mix matrix used to characterize the influence of various variables on CSA mixtures.

Table 3-4: Characterization mix matrix summary

Phase	Mixture ID	NMSA	CA/FA Blend	AEA Type	Dosage (% moc)	Latex (% of standard dosage)
Phase I: Coarse-to-fine aggregate ratio & Maximum coarse aggregate size	P_3/4"	3/4"	60/40	VR10	0.50	N/A
	LLP_3/4"	3/4"	60/40	VR10	0.50	N/A
	LM_3/4"	3/4"	60/40	N/A	N/A	100
	P_48.9/51.1	3/8"	48.9/51.1	VR10	0.50	N/A
	LLP_48.9/51.1	3/8"	48.9/51.1	VR10	0.50	N/A
	LM_48.9/51.1	3/8"	48.9/51.1	N/A	N/A	100
	P_45/55	3/8"	45/55	VR10	0.50	N/A
	LLP_45/55	3/8"	45/55	VR10	0.50	N/A
	LM_45/55	3/8"	45/55	N/A	N/A	100
	P_35/65	3/8"	35/65	VR10	0.50	N/A
	LLP_35/65	3/8"	35/65	VR10	0.50	N/A
	LM_35/65	3/8"	35/65	VR10	N/A	100
Phase II: Air-entraining admixture dosage	P_1.0%	3/8"	48.9/51.1	VR10	1.00	N/A
	P_1.75%	3/8"	48.9/51.1	VR10	1.75	N/A
	LLP_1.75%	3/8"	48.9/51.1	VR10	1.75	N/A
	LLP_2.5%	3/8"	48.9/51.1	VR10	2.50	N/A
Phase III: Air-entrining admixture type	P_AE90	3/8"	48.9/51.1	AE90	1.75	N/A
	P_AE200	3/8"	48.9/51.1	AE200	1.75	N/A
	P_DA1000	3/8"	48.9/51.1	DA1000	1.75	N/A
	LLP_AE90	3/8"	48.9/51.1	AE90	1.75	N/A
	LLP_AE200	3/8"	48.9/51.1	AE200	1.75	N/A
	LLP_DA1000	3/8"	48.9/51.1	DA1000	1.75	N/A
Phase IV: Latex modifier dosage	LM_25%	3/8"	48.9/51.1	N/A	N/A	25
	LM_50%	3/8"	48.9/51.1	N/A	N/A	50

3.2.2.2. Mixture Proportions

The following tables present the mixture proportions used in each phase of the characterization study. All mixes were designed with a W/C of 0.32 unless otherwise specified. AEA, HRWR, and citric acid were adjusted as needed for workability and working time, except when specifically studied. AEA was typically dosed at 0.50% by mass of cement, and HRWR dosage typically ranged between 0.25–1.00% by mass of cement, while citric acid typically ranged between 0.15–0.25% by mass of cement. It is important to note that dosages of admixtures were determined as percentages of cement mass but are reported here in fl-oz/cwt, following common practice. Table 3-5 presents the mixture proportions for the aggregate size study of Phase I, while Tables 3-6, 3-7, and 3-8 show the mixture proportions for the aggregate blend portion of Phase I. The blend shown in Table 3-6 reflects the optimized mixture developed using the modified void ratio method.

Table 3-5: Mixture proportions for 3/4" nominal maximum coarse aggregate size study

Mixture	BCSA (lb/yd^3)	Rock (lb/yd^3)	River Sand (lb/yd^3)	Water (lb/yd^3)	Latex (lb/yd^3)	LLP (fl-oz/cwt)
P_3/4"	648	1,881	1,254	207	0	0
LLP_3/4"	648	1,881	1,254	207	0	10
LM_3/4"	648	1,726	1,150	101	205	0

Table 3-6: Mixture proportions for 48.9/51.1 coarse-to-fine aggregate study

Mixture	BCSA (lb/yd^3)	Pea Gravel (lb/yd^3)	River Sand (lb/yd^3)	Water (lb/yd^3)	Latex (lb/yd^3)	LLP (fl-oz/cwt)
P_48.9/51.1	648	1,521	1,589	207	0	0
LLP_48.9/51.1	648	1,521	1,589	207	0	10
LM_48.9/51.1	648	1,395	1,458	101	205	0

Table 3-7: Mixture proportions for 45/55 coarse-to-fine aggregate study

Mixture	BCSA (lb/yd^3)	Pea Gravel (lb/yd^3)	River Sand (lb/yd^3)	Water (lb/yd^3)	Latex (lb/yd^3)	LLP (fl-oz/cwt)
P_45/55	648	1,399	1,710	207	0	0
LLP_45/55	648	1,399	1,710	207	0	10
LM_45/55	648	1,284	1,569	101	205	0

Table 3-8: Mixture proportions for 35/65 coarse-to-fine aggregate study

Mixture	BCSA (lb/yd^3)	Pea Gravel (lb/yd^3)	River Sand (lb/yd^3)	Water (lb/yd^3)	Latex (lb/yd^3)	LLP (fl-oz/cwt)
P_35/65	648	1,087	2,019	207	0	0
LLP_35/65	648	1,087	2,019	207	0	10
LM_35/65	648	997	1,852	101	205	0

From the results of Phase I of the characterization study, pea gravel and a CA/FA ratio of 48.9/51.1 were selected for the subsequent phases due to their superior compressive strength results as shown in sections 4.1.1.1 and 4.1.1.2. Table 3-9 presents the mixture proportions for

Phase II. In this phase, VR10 was added to CSAP and CSA-LLP at varying dosages to evaluate the influence of air-entraining admixture (AEA) dosage on the air content of the mixtures.

Table 3-9: Mixture proportions for air-entraining admixture dosage study

Mixture	BCSA (lb/yd^3)	Pea Gravel (lb/yd^3)	River Sand (lb/yd^3)	Water (lb/yd^3)	LLP (fl-oz/cwt)	VR10 (% moc)
P_1.0%	648	1,521	1,589	207	0	1.00
P_1.75%	648	1,521	1,589	207	0	1.75
LLP_1.75%	648	1,521	1,589	207	10	1.75
LLP_2.5%	648	1,521	1,589	207	10	2.50

For Phase III of the characterization study, an AEA dosage of 1.75% by mass of cement was selected for future testing due to increased fresh air content while maintaining compressive strength results as shown in section 4.1.1.3.Tables 3-10 and 3-11 present the mixture proportions for the CSAP and CSA-LLP mixes used in the study of AEA type, respectively. For subsequent testing, VR10 was selected based on its balanced performance in air entrainment, strength, and workability shown in section 4.1.1.4.

Table 3-10: Mixture proportions for CSAP air-entraining admixture type study

Mixture	BCSA (lb/yd^3)	Pea Gravel (lb/yd^3)	River Sand (lb/yd^3)	Water (lb/yd^3)	AE90 (% moc)	AE200 (% moc)	DA1000 (% moc)
P_AE90	648	1,521	1,589	207	1.75	0	0
P_AE200	648	1,521	1,589	207	0	1.75	0
P_DA1000	648	1,521	1,589	207	0	0	1.75

Table 3-11: Mixture proportions for CSA-LLP air-entraining admixture type study

Mixture	BCSA (lb/yd^3)	Pea Gravel (lb/yd^3)	River Sand (lb/yd^3)	Water (lb/yd^3)	LLP (fl-oz/cwt)	AE90 (% moc)	AE200 (% moc)	DA1000 (% moc)
LLP_AE90	648	1,521	1,589	207	10	1.75	0	0
LLP_AE200	648	1,521	1,589	207	10	0	1.75	0
LLP_DA1000	648	1,521	1,589	207	10	0	0	1.75

Table 3-12 presents the mixture proportions for the Phase IV of the characterization study, in which varying levels of latex modifier dosage were evaluated. Note that the W/C for the CSA-LM mixtures with 25% and 50% of the standard dosage was increased to 0.38. This adjustment was necessary because the reduction in latex led to a decrease in water content from the polymer, requiring additional water to compensate for the loss.

Table 3-12: Mixture proportions for latex modifier dosage study

Mixture	BCSA (lb/yd^3)	Pea Gravel (lb/yd^3)	River Sand (lb/yd^3)	Water (lb/yd^3)	Latex (lb/yd^3)	W/C
LM_25%	648	1,439	1,504	220	51	0.38
LM_50%	648	1,408	1,471	193	103	0.38
LM_100%	648	1,395	1,458	101	205	0.32

After the characterization phase of the project, four mixture designs were selected for further study in the experimental program. These mixture designs are presented in Table 3-13. Pea gravel with a coarse-to-fine ratio of 48.9/51.1 was used in all mixes. For the CSAP and CSA-LLP mixes, VR10 was chosen as the air-entraining admixture at a dosage of 1.75% by mass of cement. To examine the effects of varying latex dosages, two latex modified mixes were studied: one with 100% (LM100) of the standard dosage and another with 25% (LM25) of the standard dosage. The W/C was 0.32 for all mixes, except for LM25, which had a ratio of 0.38.

Table 3-13: Final mixture proportions

Mixture	BCSA (lb/yd^3)	Pea Gravel (lb/yd^3)	River Sand (lb/yd^3)	Water (lb/yd^3)	Latex (lb/yd^3)	LLP (fl-oz/cwt)	VR10 (% moc)
CSAP	648	1,521	1,589	207	0	0	1.75
LLP	648	1,521	1,589	207	0	10	1.75
LM100	648	1,395	1,458	101	205	0	0
LM25	648	1,439	1,504	220	51	0	0

3.2.2.3. Slump Test

Immediately after mixing, the slump of each mix was measured in accordance with ASTM C143 (ASTM International, 2020) to determine the maximum possible workability, given the expedited setting time of CSA cement. Since this is a fresh property, it was measured once per mix, and no error bars were included. For each mixture, a slump range of 4–6 inches was targeted based on WSDOT's 2025 Standard Specifications (2025) for slump of concrete Class 4000D decks and modified concrete overlays. At this time, the mix temperature was also measured to obtain an early concrete placement temperature reading, as CSA cement is known for its rapid heat release during setting.

3.2.2.4. Air Content Test

Following the concrete slump test, the air content of the mix was measured in accordance with ASTM C231 (ASTM International, 2024c), with a target air content of 5.5% ± 1.5% based on WSDOT's 2025 Standard Specifications (2025) for air content of concrete Class 4000D decks and modified concrete overlays. Since air content is a fresh property, it was measured only once per mix, and no error bars were included. The unit weight (i.e., fresh concrete density) of the mixtures was also recorded using the air content pot before the test began.

3.2.2.5. Compressive Strength

While the concrete slump and air content tests were being conducted, cylinder specimen molds were simultaneously filled in accordance with ASTM C31 (ASTM International, 2024a). 3x6-inch cylinder molds were used for all mixes, except those with a 3/4" NMSA. For these mixes, 4x8-inch cylinders were used to accommodate the larger aggregate size.

The cylinders were covered with plastic lids to prevent moisture loss and left to cure for 24 hours before being demolded and transferred to a saturated lime-water bath to continue curing until testing. The test ages were 2, 3, and 4 hours, as well as 1, 3, 7, and 28 days. For each test

age, three specimens were tested following ASTM C39 (ASTM International, 2023b), and error bars were included to represent the variation at each test age. Specimens tested for early-age strength—just a few hours after mixing—were demolded and tested immediately. The target compressive strength was 3,000 psi within 3 hours.

3.3. Field Trials

To evaluate the effectiveness of the CSA mixtures in a field-scale application, overlays were cast on mini-bridge deck substrates designed to replicate conventional Washington State Department of Transportation (WSDOT) bridge decks. A key focus of this study was assessing the compatibility between the overlays and substrates, particularly in terms of bond strength and volume stability over time. Additionally, the mechanical properties of the mixes were examined under less controlled field mixing conditions to better understand their real-world performance and potential limitations.

3.3.1. Substrate Design and Construction

The substrates used in this project were originally constructed as part of Guerrero-Estrada (2024). The substrates were cast over a year prior to the addition of the CSA overlays and have since been outside untouched and unprotected to the elements.

3.3.1.1. Mixture Proportions

The chosen substrate concrete mixture design needed to represent existing bridges that may require repairs or rehabilitation. To achieve this, the 2004 WSDOT concrete bridge deck specification, known as “Concrete Class 4000D,” was selected (Washington State Department of Transportation, 2004). This historical, prescriptive concrete specification ensured the project remained focused on bridge deck rehabilitation, as bridges requiring protective overlays are typically at least 20 years old. A local ready-mix producer with an approved 2004 WSDOT concrete class 4000D mixture design was utilized in this project which consisted of a local

ASTM C595 Type I-L cement, fly ash, and a W/C of 0.34. The AEA used was DARAVAIR® 1000, and the HRWR used was ADVA® 195. Additionally, the water-reducing admixture (WR), WRDA® 64 was incorporated into the mix.

Table 3-14: Approved 2004 WSDOT concrete substrate mix design

Mixture	Type I-L Cement (lb/yd^3)	Fly Ash (lb/yd^3)	3/4" Rock (lb/yd^3)	River Sand (lb/yd^3)	Water (lb/yd^3)	AEA (fl-oz/cwt)	WR (fl-oz/cwt)	HRWR (fl-oz/cwt)	W/C
Substrate	660	75	1,735	1,243	250	2.12	3.48	4.64	0.34

3.3.1.2. Formwork and Dimensions

Six mini-bridge decks were used in this project. Five of them measured 3'x6'x7.5". The sixth deck was cast and screeded only up to the top mat of the rebar, leaving it partially exposed and resulting in the dimensions of 3'x6'x7.25". Figure 3-4 shows the formwork and dimension of the mini-bridge deck substrates, while Figure 3-5 shows the reinforcement layout as drawn by Guerrero-Estrada (2024).

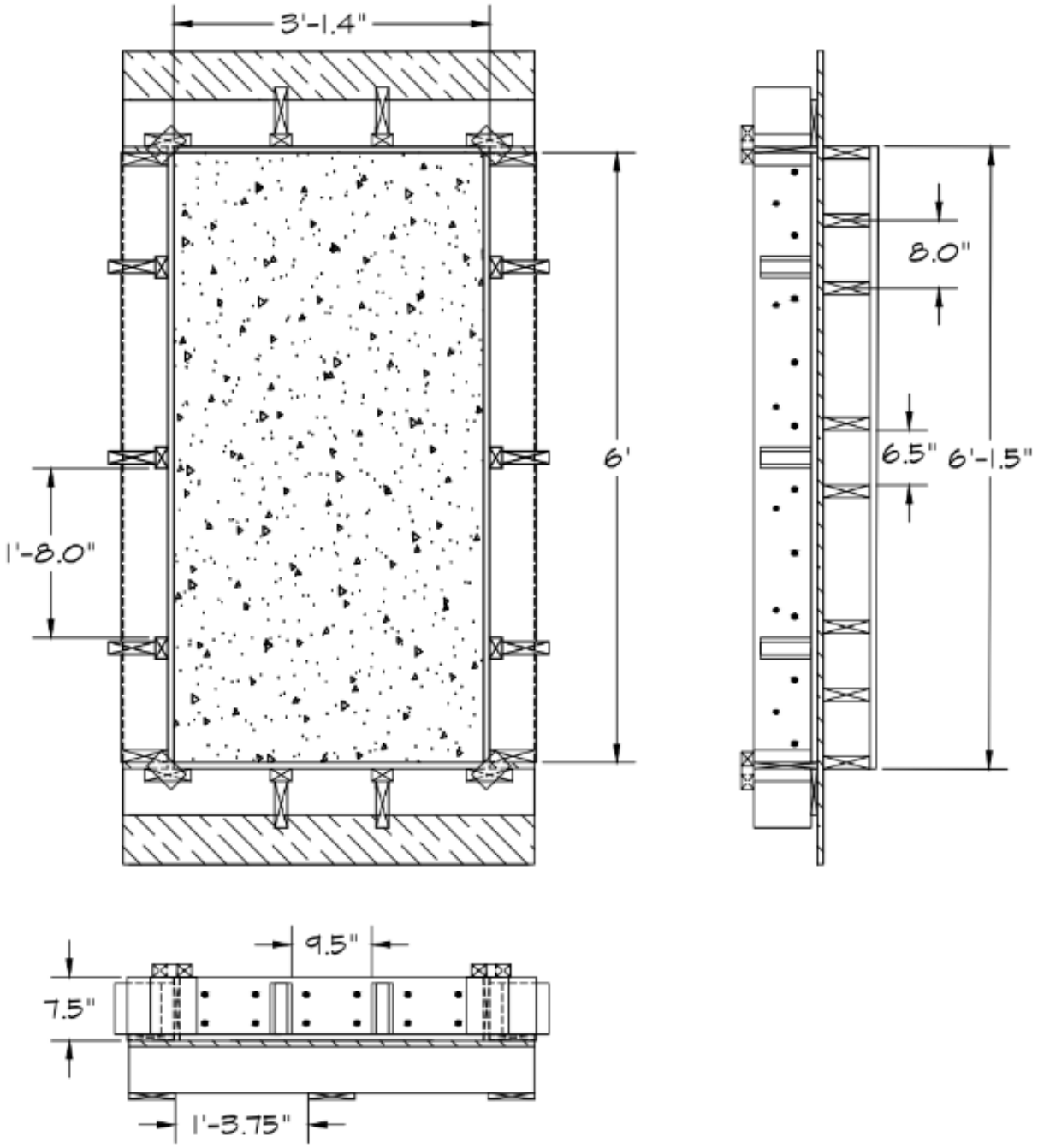

Figure 3-4: Formwork and dimensions of the mini-bridge deck substrates (Guerrero-Estrada, 2024)

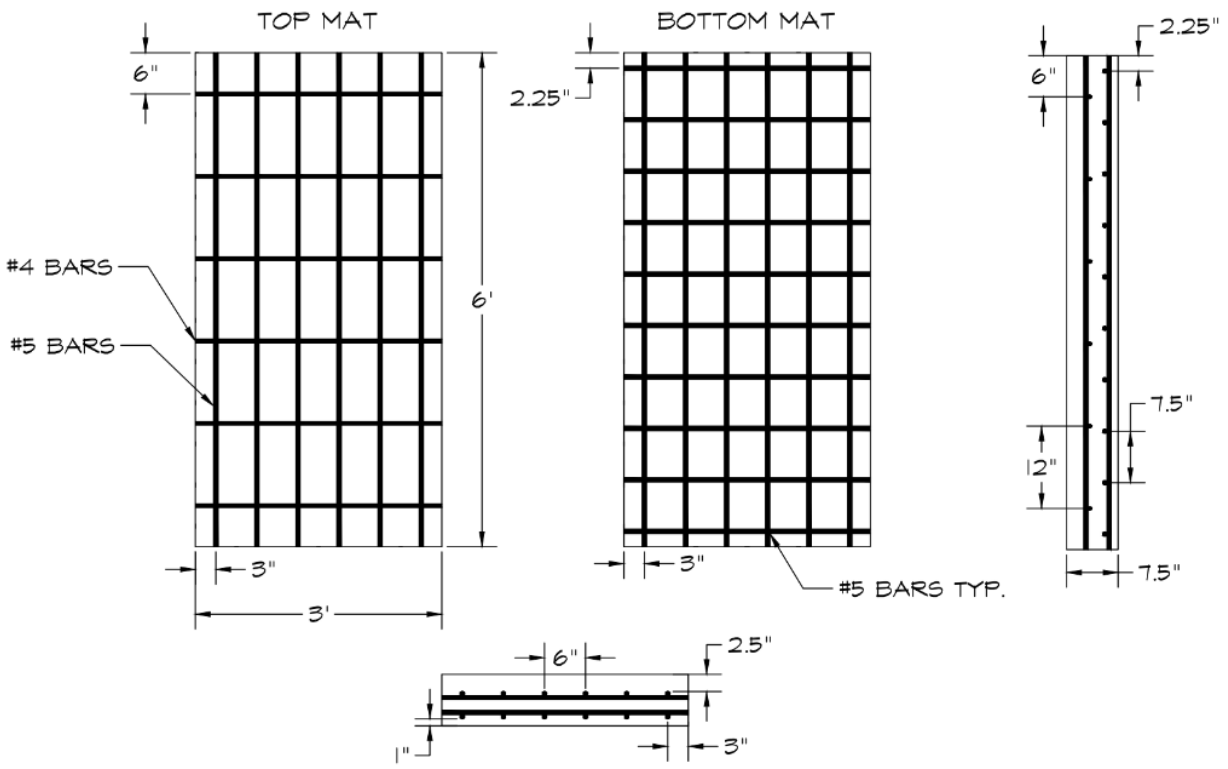

Figure 3-5: Reinforcement layout of the mini-bridge deck substrates (Guerrero-Estrada, 2024)

3.3.1.3. Casting

Once the formwork for the mini-bridge deck substrates was completed, the substrate mixture design was finalized, and the required concrete volume was calculated. A local ready-mix supplier was then contacted for delivery and 3.5 cubic yards of Concrete Class 4000D that met 2004 WSDOT standard specifications were provided. The pour took place at 1:00 PM on September 19, 2023, under partly cloudy skies, with an ambient temperature of 65°F and no wind gusts.

The concrete was poured in a single lift and consolidated with interval vibration. A 2"x6" screed was used to strike off the excess material, followed by smoothing with magnesium hand floats. Once the surface became firm to the touch, surface retarders were applied to the substrates using a pump sprayer. The concrete was then left to cure overnight. Additional details on the

surface retarders used are provided in section 3.3.1.4. Figure 3-6 show the substrates during casting (Guerrero-Estrada, 2024).

Figure 3-6: The substrate decks during casting (Guerrero-Estrada, 2024)

3.3.1.4. Surface Preparation

In practice, hydro demolition is used on bridge decks to improve surface texture and enhance the bond between the overlay and substrate. However, due to its high cost and the challenges of replicating this process in a lab setting, surface retarders were used instead.

To simulate different surface preparation conditions, the top surfaces of the slabs were treated with two different spray-on surface retarders, creating distinct surface textures. The retarders used were Top-Cast® 05, which produced a sandblast finish, and Top-Cast® 150, which created an exposed aggregate finish with an etch depth of 3/8" to 5/8". The sandblast (SB) finish surface retarder had a blue-tinged color, while the exposed aggregate (EA) finish surface retarder had a green-tinged color.

After casting, once the surface was firm to the touch, surface retarders were applied to the substrates using a garden sprayer. The SB surface retarder was applied to two of the mini-bridge

deck substrates, while the other four, including the deck with exposed rebar (ER), received the EA surface retarder. The decks with the surface retarders applied are shown in Figure 3-7.

Figure 3-7: Mini-bridge decks with surface retarders applied (Guerrero-Estrada, 2024)

The next day, the top surface was cleaned with a pressure washer and a metal wire brush to remove any unhardened cement paste and expose the surface etching. After the final set and completion of pressure washing, the specimens were covered with a tarp and wet burlap. The resulting exposed aggregate and sandblast surface finishes are shown in Figures 3-8 and 3-9, respectively (Guerrero-Estrada, 2024).

Figure 3-8: Exposed aggregate etching (Guerrero-Estrada, 2024)

Figure 3-9: Sandblast etching (Guerrero-Estrada, 2024)

3.3.2. Overlay Design and Construction

More than a year after the initial construction of the substrates, CSA concrete overlays were cast on top of them; the overlays are the primary focus of this project. Two different mixtures were used to evaluate differences in bonding and mechanical properties at a field scale. Additionally, several decks were instrumented with strain gauges to monitor volume changes in the overlays over both short- and long-term periods.

3.3.2.1. Mixture Proportions

For the CSA overlays of the mini-bridge decks, CSAP and LLP were used to compare the effects of integrated Low-P™ and Liquid Low-P™ on the concrete's mechanical properties and overall effectiveness as an overlay. Due to the rapid setting time of CSA, a volumetric mixing truck was used to pour the overlays. As a result, the final mixtures varied slightly from the original designs, as adjustments were made during the pour to accommodate workability and setting time.

Additionally, the aggregate and admixtures used were supplied by the contracted volumetric mixing company, so the admixture products in these mixes differ from those typically

used in the laboratory. The AEA used was the synthetic surfactant DarCole Synthetic Air 110, and the HRWR was DarCole Superflow 1443. The original mixture designs for the overlays are presented in Table 3-15, and the final batched overlay mixtures are presented in Appendix A: Field Trials.

Table 3-15: Original mini-bridge deck overlay mixture designs

Mixture	BCSA (lb/yd^3)	Pea Gravel (lb/yd^3)	River Sand (lb/yd^3)	Water (lb/yd^3)	LLP (fl-oz/cwt)	W/C
CSAP	658	1,535	1,563	220	0	0.35
LLP	658	1,520	1,548	220	10	0.36

3.3.2.2. Formwork and Dimensions

Overlays of at least 2" were planned for the substrates. To achieve this, formwork was retroactively constructed and attached to the substrates. The overlay formwork drawings for the deck without exposed rebar are shown in Figure 3-10, while the drawings for the one with exposed rebar are shown in Figure 3-11. The forms were secured by bolting them to the substrates using drop-in anchors. Holes were drilled into each substrate—one on each short side and three on each long side—where the drop-in anchors were installed, as shown in Figure 3-12a. The forms were then attached using bolts and washers, with the corners further secured with screws, as shown in Figure 3-12b. Any gaps were sealed with caulk. Figure 3-13 shows the completed overlay formwork for all the decks.

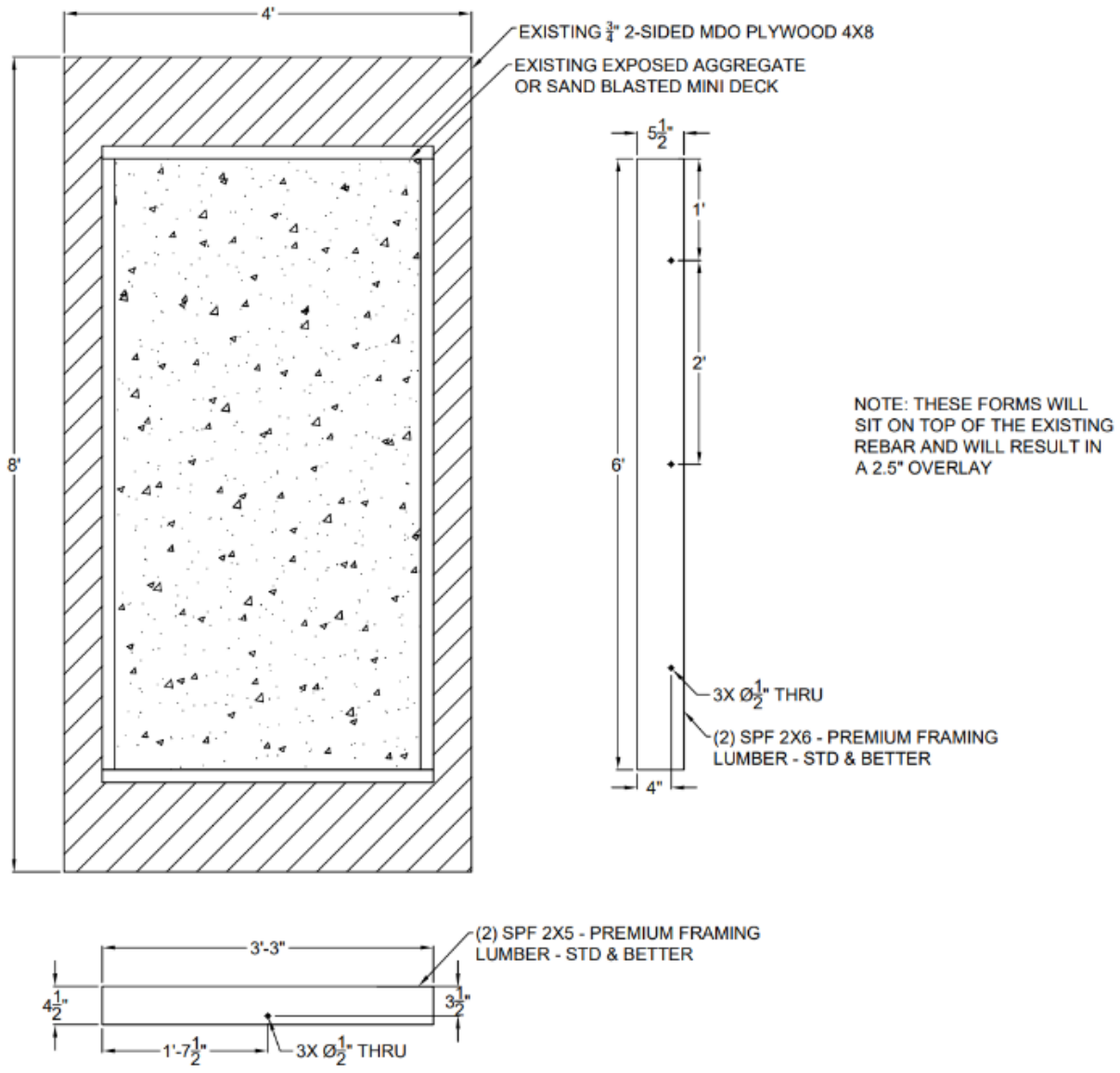

Figure 3-10: Overlay formwork drawings and dimensions for the decks without exposed rebar

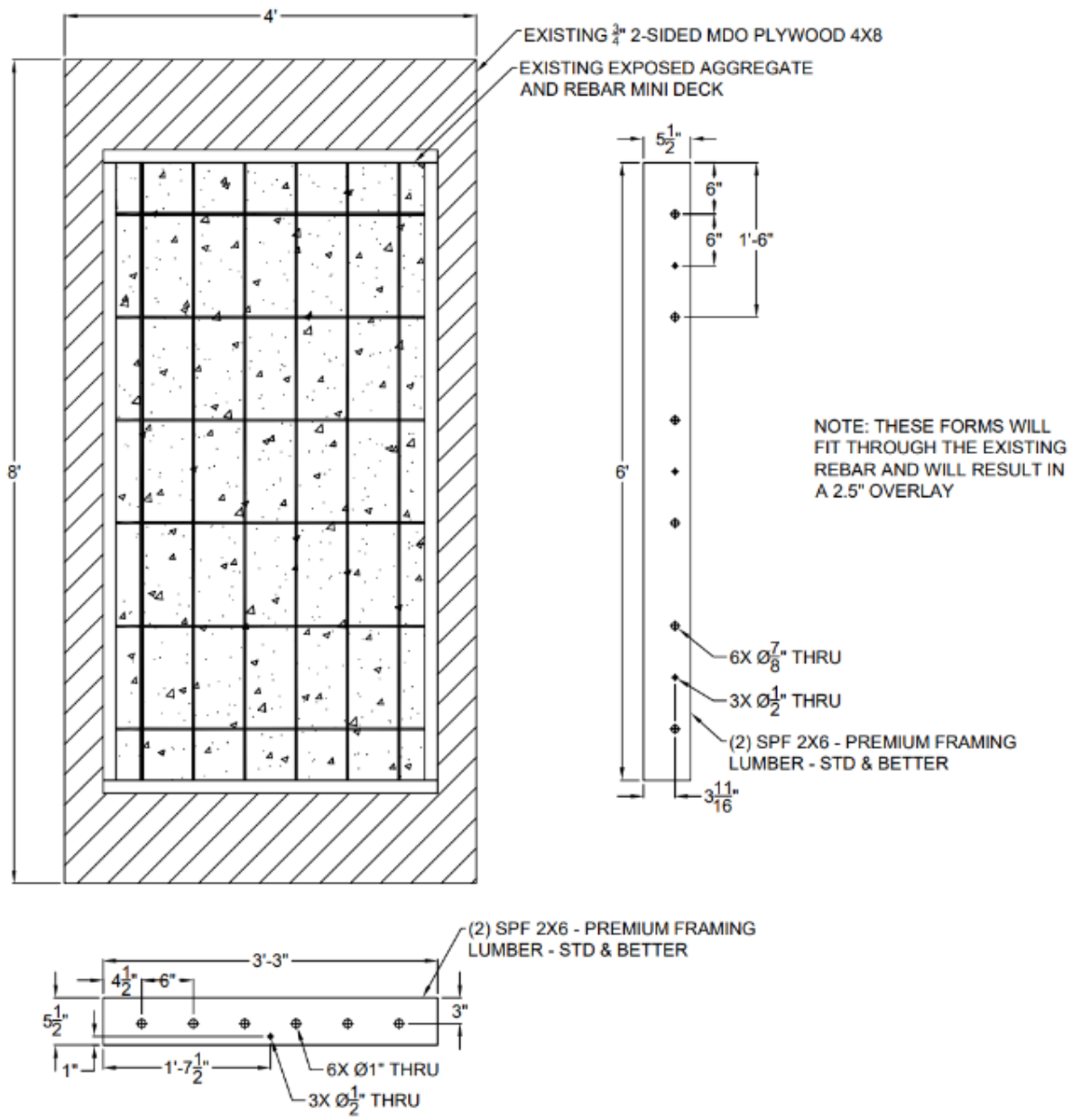

Figure 3-11: Overlay formwork drawings and dimensions for the deck with exposed rebar

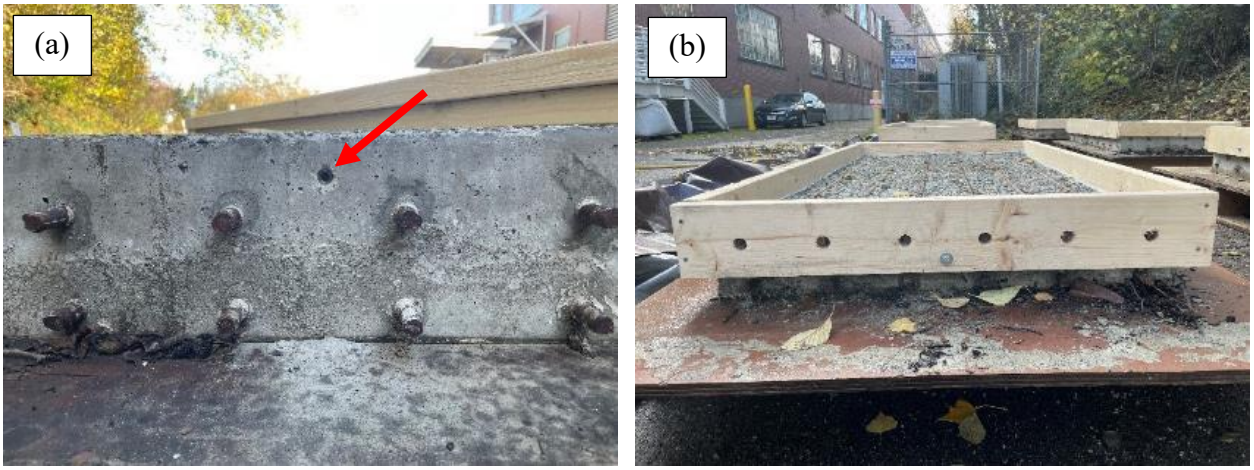

Figure 3-12: (a) Drop-in anchor set in the substrate, and (b) forms fully secured to the deck

Figure 3-13: Completed formworks for all overlays

The formwork had a slight height difference of approximately 0.5" between the long and short sides. During casting, the concrete was screeded to the raised side, resulting in overlays of approximately 2.5" for all decks, except for the exposed rebar deck, which had a 3" overlay.

3.3.2.3. Instrumentation

To monitor strain and temperature in the concrete, strain gauges were installed on four of the six decks. Concrete embedded strain gauges (CESGs) measured strain in the overlays, while arc-welded strain gauges (AWSGs) monitored strain at the interface between the substrate and

the overlay. Figure 3-14 shows the mini-bridge deck IDs, their overlay type, surface finish, and the instrumentation of each deck, while Figure 3-15 shows which decks the IDs correspond to.

D2_LLP_SB (none)	D4_LLP_EA (CESG, AWSG)	D6_CSAP_EA (none)
D1_CSAP_SB (CESG)	D3 _CSAP_EA (CESG, AWSG)	D5_CSAP_ER (CESG)

Figure 3-14: Mini-bridge deck IDs, their overlay type, surface finish, and instrumentation layout

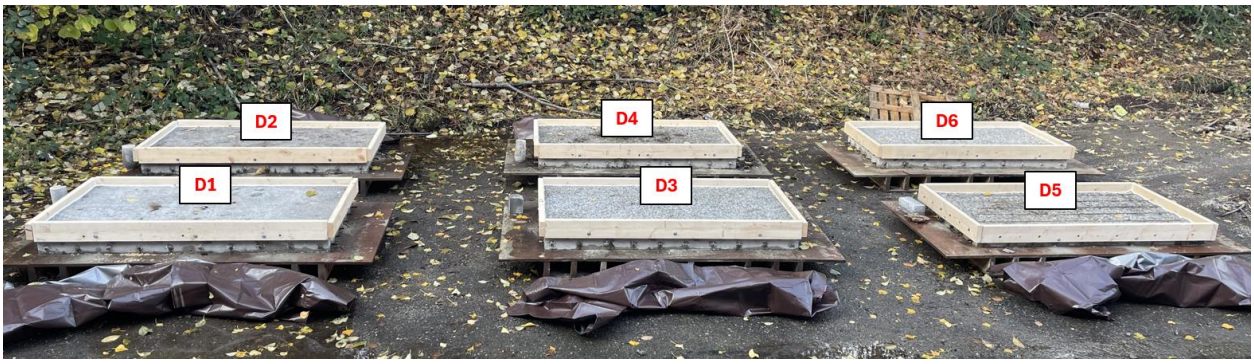

Figure 3-15: Mini-bridge deck IDs and the decks with which they correspond

3.3.2.3.1. Concrete-Embedded Strain Gauges

For the concrete-embedded strain gauges (CESGs), two spacers were used to support each gauge above the substrate and within the overlay. The spacers were epoxied to the substrate surface and the center of the strain gauge positioned at the midpoint of the deck and oriented along its length. Figure 3-16 provides a close-up view of a CESG installation.

Figure 3-16: Close-up of a concrete-embedded strain gauge installation

3.3.2.3.2. Arc-Welded Strain Gauges

The arc-welded strain gauges (AWSGs) were positioned approximately 1' away from the CESG and aligned in the same direction. For the AWSGs, rectangular slots were cut and chipped into the deck, and holes were drilled into the substrate to accommodate the gauge supports. The bolt ends of the supports were epoxied into the holes, ensuring that the strain gauges were flush with the surface of the substrate. A close-up of an AWSG installation is shown in Figure 3-17.

Figure 3-17: Close-up of an arc-welded strain gauge installation

To prevent concrete from interfering with the movement and readings of the AWSGs, low-modulus foam was used to encase them. The foam was pliable enough not to impede

concrete placement, yet secure enough to protect the strain gauges. Figure 3-18 shows the strain gauges before and after the foam was applied.

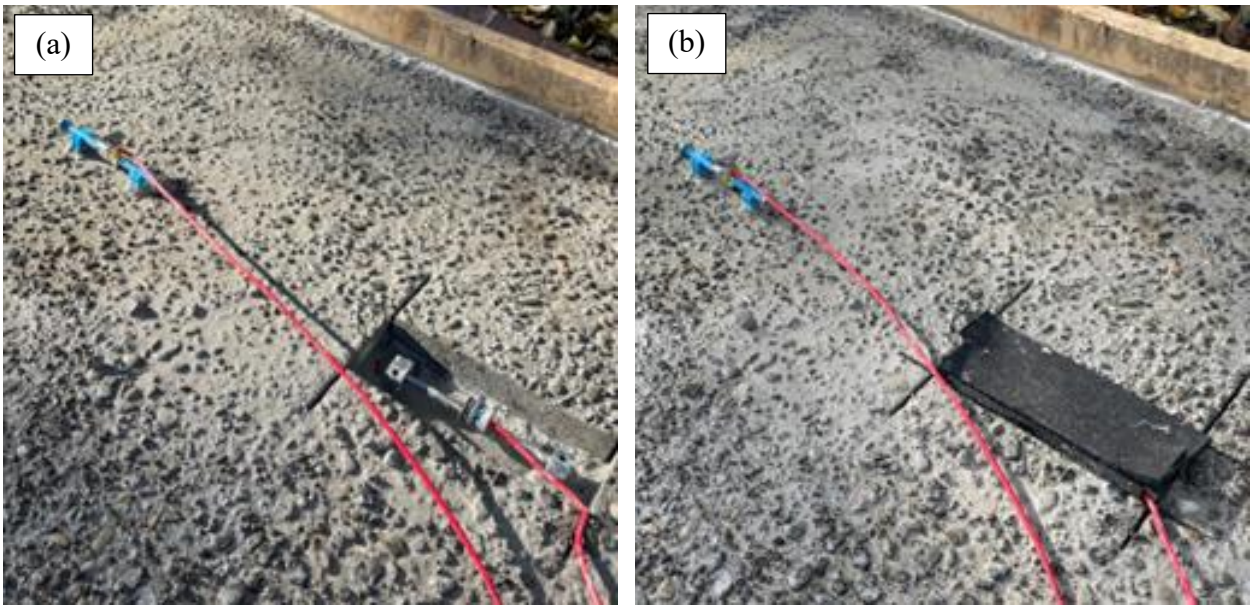

Figure 3-18: Strain gauges (a) before and (b) after the addition of foam

3.3.3. Casting

Once the formwork for the mini-bridge deck overlays was completed, the CSAP and LLP overlay mixture designs were finalized, and the required concrete volume of each calculated. A local volumetric mix truck was contracted for the pour and assisted in mixing and casting. The pours for the LLP and CSAP overlays took place at 2:35 PM and 3:20 PM, respectively, on November 15, 2024, under mostly clear skies, with day and evening temperatures of 48°F and 45°F, respectively, and minimal wind gusts.

On the morning of the pours, the decks were power washed to remove any debris and then wet vacuumed to make the decks saturated surface dry. During this process, extra care was taken to protect the strain gauges from damage. Aside from the power washing and wet vacuuming, no additional preparation was done for the exposed rebar deck.

For each mix, the concrete was poured in one layer and consolidated using internal vibration, taking care not to disrupt the strain gauges that were placed. Excess material was struck off with a 2"x4" screed, and the surface was then smoothed with magnesium hand floats. The casting and screeding of one of the decks is shown in Figure 3-19. While the decks of each pour were being cast, fresh property testing was conducted, and beam and cylinder samples were filled simultaneously, as shown in Figure 3-20. Each mix was placed within an hour.

Figure 3-19: Casting (a) and screeding (b) of the mini-bridge deck overlays

Figure 3-20: (a) Fresh property testing and filling of cylinders, and (b) filling of beams

After reaching initial set, the decks were wet-cured with burlap, as shown in Figure 3-21a. The burlap and forms were removed 24 hours after casting, as shown in Figure 3-21b. The field samples were also covered with burlap and left outdoors for 24 hours before being demolded and transferred to a saturated limewater curing tank for further testing. Samples tested at early ages, within hours after pouring, were demolded at the time of testing.

Figure 3-21: (a) The mini-bridge decks curing under burlap, and (b) the decks 24 hours later with burlap and forms removed

3.3.4. Field-Scale Tests

Field-scale specimens from the CSAP (CSAP_deck) and LLP (LLP_deck) overlay mixes were cast during their respective pours to monitor the evolution of their mechanical properties over time. Additionally, field-scale specimens for the CSAP, LLP, LM100, and LM25 mixes were cast in the laboratory under more controlled conditions, allowing for a more precise direct comparison of the four mixes.

All specimens were prepared in accordance with ASTM C31 (ASTM International, 2024a). Specimens cast during the CSAP and LLP overlay mixes were prepared outdoors,

covered with damp burlap after reaching initial set, and left outside to cure. The specimens cast in the laboratory were covered with plastic after final set to retain moisture and cured inside the lab. 24 hours after casting, the specimens were removed from their molds and placed in a saturated lime-water bath for further curing, unless otherwise specified. Specimens were tested at their designated test ages following the corresponding ASTM testing procedures. For early-age strength tests, samples were demolded and tested immediately. In addition to hardened properties, fresh properties were taken at time of casting for all mixes.

Table 3-16 summarizes the tests conducted, specimen sizes, testing ages, number of specimens per test age, and the corresponding ASTM standards for the field-scale tests of each mixture.

Table 3-16: Summary of field-scale tests for each mixture

Test	Specimen Size	Test Ages	Specimens Per Test Age	ASTM
Compression Strength	4"x8"	2, 3, 4hr & 1, 3, 7, 28, 181d	3	C39[1]
Split Tensile Strength	4"x8"	1 & 28d	2	C496[2]
Flexural Strength	4"x4"x14"	1 & 28d	2	C78[3]
Dry Shrinkage	3"x3"x11.25"	1, 4, 7, 14, 28d & 8, 16, 32, 64w	3	C157[4]
Modulus of Elasticity	4"x8"	1, 7, 28d	1	C469[5]

[1] (ASTM International, 2023b)
[2] (ASTM International, 2017b)
[3] (ASTM International, 2022a)
[4] (ASTM International, 2017a)
[5] (ASTM International, 2022b)

3.3.4.1. Fresh Concrete Testing

The slump and air content of the mixes were measured immediately after the start of their respective pours. Slump measurements followed ASTM C143 (ASTM International, 2020),

while the air content was measured according to ASTM C231 (ASTM International, 2024c). Additionally, the unit weight and temperature at the time of placement was recorded.

3.3.4.2. Compressive Strength

To evaluate the short-term and long-term compressive strength of the mixes, 4x8-inch cylinder specimens were tested at 2, 3, and 4 hours, as well as at 1, 3, 7, 28, and 181 days. Three specimens were tested at each age in accordance with ASTM C39 (ASTM International, 2023b), with error bars indicating variability. The test setup is shown in Figure 3-22.

Figure 3-22: Compressive strength test setup

3.3.4.3. Split Tensile Strength

Two 4x8-inch cylinders specimens were tested at 1 day and 28 days to compare the split tensile strength development of the mixtures. The testing procedures followed ASTM C496 (ASTM International, 2017b) and the test set up is shown in Figure 3-23. No error bars were included for this test, as only two specimens were tested per test age.

Figure 3-23: Split tensile strength test setup

3.3.4.4. Flexural Strength

To determine the flexural strength of the mixtures, the ASTM C78 (ASTM International, 2022a) testing procedures were followed. To compare the strength development, two 4"x4"x14" beam specimens were tested at 1 day and 28 days. The specimens were marked according to standard procedures and aligned in the test setup for the third-point loading method, as shown in Figures 3-24 and 3-25. The modulus of rupture (MOR) was then calculated using the appropriate equation, depending on the location of the fracture. No error bars were reported for this test, as only two specimens were tested per test age.

Figure 3-24: Flexural strength specimens marked for the third-point loading method

Figure 3-25: Third-point loading method test setup for flexural strength

3.3.4.5. Modulus of Elasticity

The modulus of elasticity (MOE) of the mixtures was measured following ASTM C469 (ASTM International, 2022b) testing procedures. The MOE was recorded at 1, 7, and 28 days using one 4x8-inch cylinder. At each test age, the specimen was loaded three times to 40% of the ultimate load experienced by other cylinder specimens tested at the same age. Data from the first

loading were discarded, and only the last two loadings were recorded and averaged. Figure 3-26 shows the test setup.

Figure 3-26: Modulus of elasticity test setup

3.3.4.6. Drying Shrinkage

The drying shrinkage of the mixtures was monitored over both short-term and long-term periods using three 3"x3"x11.25" prism specimens tested at 1, 4, 7, 14, and 28 days, as well as 8, 16, 32, and 64 weeks, following testing procedures outlined in ASTM C157 (ASTM International, 2017a). After being demolded 24 hours after casting, the shrinkage prism specimens were stored in the open air in the laboratory at 23° C and a relative humidity of 50%. The setup for this test is shown in Figure 3-27.

Figure 3-27: Dry shrinkage test setup

3.3.4.7. Coefficient of Thermal Expansion (CoTE)

The coefficient of thermal expansion (CoTE) measures how much a material expands or contracts with temperature fluctuations. In concrete pavements, CoTE plays a crucial role in performance, as uniform temperature changes influence joint movement, while temperature gradients through the slab thickness can cause curling. Precise CoTE measurements help improve predictions of slab movement and stress development resulting from temperature variations.

Two 4x8-inch cylinder specimens of the following mixes were tested: CSAP, LLP, LM100, LM25. The CSAP and LLP specimens were taken from the mix used for the outside mini-bridge deck pours. All specimens were cured for at least 24 hours. To fit the specimens inside the testing frame, ½" was cut off from both the top and bottom of each cylinders, resulting in an overall length of 7". The specimens were then carefully placed inside the testing frame and

submerged in water. Following AASHTO T336 (AASHTO Association, 2022) procedures and a testing temperature range of 10°F to 50°F, the CoTE of the specimens was determined.

3.3.5. Mini-Bridge Deck Monitoring

Various methods were used to assess the overlays' performance over short- and long-term periods. Of particular interest was the bonding compatibility between the overlays and substrates, as well as the volume change of the overlays—key indicators of their potential suitability for industry applications.

3.3.5.1. Concrete Embedded and Arc-Welded Strain Gauges

The concrete embedded strain gauges (CESGs) and arc-welded strain gauges (AWSGs) from all the decks were connected to a central, weatherproof data logger. The CESGs measured the strain experienced by the CSA overlays, while the AWSGs measured the strain experienced by the substrate at the overlay-substrate interface. Both types of strain gauges also recorded the temperature of the concrete in which they were embedded, and the data logger recorded the ambient temperature.

After installation, all strain gauges were calibrated according to the manufacturer's specifications and set to mid-range to accommodate potential concrete expansion and contraction. Data logging began several hours before the pour and continued at 1-minute intervals for the first seven days after casting the overlays. After seven days, the data was retrieved, and the logging interval was adjusted to every 30 minutes. Long-term data continued, with data being retrieved approximately every two to three months after casting.

3.3.5.2. Crack Mapping

In addition to strain gauges, the volume change of the overlays was visually recorded through manual crack mapping. A 1'x1' grid was drawn on the decks, with boxes numbered 1 through 18. Using a crack width gauge card and a magnifying glass, cracks were identified,

measured, and marked with a permanent marker. Each crack was documented based on its width, direction, and corresponding grid box. The labeling and orientation conventions used for the deck grids are shown in Figure 3-28.

Crack mapping was conducted 1.5 weeks after casting and repeated approximately two and five months later. New cracks that appeared after the initial assessment were marked in a different color to distinguish between observation periods.

		←	Vertical	→		
↑	1	2	3	4	5	6
Transverse	7	8	9	10	11	12
↓	13	14	15	16	17	18

Figure 3-28: Crack mapping labeling and orientation conventions for the mini-bridge decks

3.4. Durability Study

CSA cements are gaining recognition for their rapid strength development, low shrinkage, and reduced carbon footprint compared to OPC. Their low permeability has been shown to enhance resistance to chemical ingress and freeze-thaw damage, suggesting potential advantages in durability. However, despite these promising characteristics, further research is needed to comprehensively assess their long-term performance under various environmental and mechanical conditions.

3.4.1. Autogenous Deformation

Bulk strain, also known as autogenous shrinkage or deformation, occurs in the absence of external forces and results from cement hydration. In conventional concrete, autogenous deformation is generally negligible. However, the chemical reactions of CSA require further research, as they could potentially be significant, leading to the formation of micro- and macro-cracks that may compromise strength, durability, and aesthetics. Autogenous deformation is also particularly problematic in low W/C mixes, which are commonly used with CSA. The low water

content causes self-desiccation, a phenomenon where the concrete loses water due to the internal consumption by hydration reactions, leading to shrinkage and increased risk of cracking.

Following ASTM C1698 (ASTM International, 2019b), the autogenous deformation of cement pastes and mortar systems were studied using sealed, corrugated plastic tubes, which allow the unrestrained expansion and contraction in a closed environment. Two series of this test were conducted: one with mortar specimens and another with paste specimens.

In the first series, concrete specimens were wet-sieved through a #4 sieve to obtain the mortar fraction with a NMSA of 4.75 mm and then stored at 23°C. In the second series, cement paste specimens were prepared using a mixture design specifically modified to eliminate aggregates and were mixed according to ASTM C305 (ASTM International, 2019b). The mixture designs for the pastes are presented in Table 3-17. All other test procedures remained the same. This version of the test was iterated three times, with the specimens stored at different isothermal testing temperatures: 23°C, 10°C, and 35°C.

Table 3-17: Mixture proportions for cement pastes

Mixture	BCSA (g)	Water (g)	Latex (g)	LLP (g)
CSAP	1,500.00	480.00	0.00	0.00
LLP	1,500.00	480.00	0.00	9.75
LM100	1,500.00	450.96	55.85	0.00
LM25	1,500.00	517.74	13.96	0.00

For each test version and iteration, three specimens of the following mixes were cast: CSAP, LLP, LM100, and LM25. Testing ages included final set, 2, 3, and 4 hours, as well as 1, 3, 7, and 28 days. The time to final set was determined using a penetrometer in accordance

with ASTM C403 (ASTM International, 2023c) and was defined as reaching a strength of 4,000 psi.

The specimen length at each test age was recorded using a dilatometer bench designed for the corrugated specimen molds. Before each set of length readings, a reference bar was placed in the dilatometer and zeroed to ensure accuracy. Specimens were carefully placed in the dilatometer in the same orientation for each reading for consistent data collection. Figure 3-29 shows a specimen aligned in the dilatometer, with the reference bar below the setup.

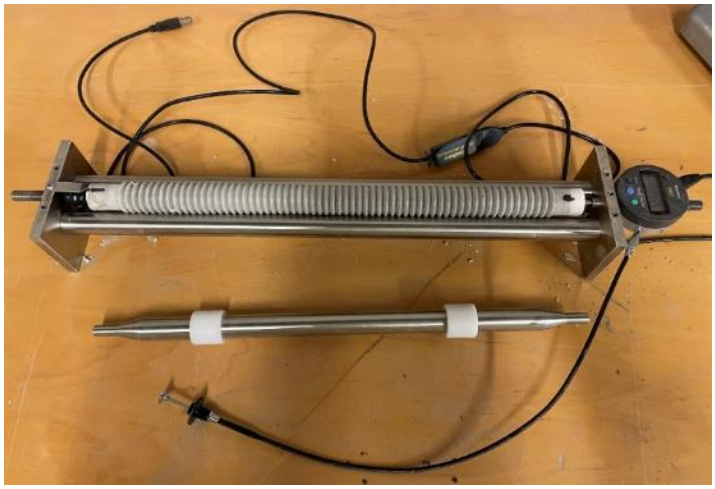

Figure 3-29: Dilatometer bench set up with specimen and reference bar

3.4.2. Plastic Shrinkage

Plastic shrinkage refers to the shrinkage that occurs when freshly placed concrete loses moisture rapidly while still in its plastic, unset state. In accordance with ASTM C1579 (ASTM International, 2021), this test was conducted to evaluate the surface cracking in concrete panels and compare the plastic shrinkage cracking behavior of the following concrete mixtures: CSAP, LLP, LM100, and LM25. It is important to note that this is a modified version of the test, as the original test was intended to evaluate plastic shrinkage reduction in fiber-reinforced concrete. For this study, the test parameters and conditions have been adapted to assess the plastic shrinkage in BCSA concrete.

Two specimens of each mixture were cast in 14"x22"x4" rectangular molds fitted with a single sheet of bent metal at the bottom, as shown in Figure 3-30. The bent metal created stress risers that concentrated stress in specific locations, accelerating crack formation.

Figure 3-30: Plastic shrinkage test molds

After casting, the panels were placed inside an environmental chamber designed to meet the standard's criteria. The chamber was equipped with two fans with two heating elements, an anemometer, a scale, and an evaporation monitoring pan. A fan was positioned in front of each panel to ensure even wind distribution, and the specimens were elevated on a pallet to further enhance airflow.

The heating elements were placed in front of the fans to heat the air blown into the chamber and were automatically regulated by a temperature regulator to maintain the required test temperature. The anemometer was positioned above one of the panels and recorded the temperature, windspeed, and relative humidity to ensure a stable environment for the specimens.

Initial testing showed that the relative humidity inside the chambers was lower than required, so pans of water were added to increase moisture levels. Despite adding more water pans, the relative humidity remained below the standard. However, measurements from the evaporation monitoring pan indicated an evaporation rate of 1.06 $kg/m^2/h$, which exceeds the minimum required rate specified in ASTM C1579 (ASTM International, 2021). Therefore, for

the purposes of this project, the observed relative humidity was considered acceptable for the test panels and was accounted for during data analysis.

Figures 3-31 and 3-32, show the environmental chamber fully opened and with the lid closed, respectively. Note that the light sockets on the lid seen in Figure 3-31 were from a previous iteration of the test setup and were not used in the final version.

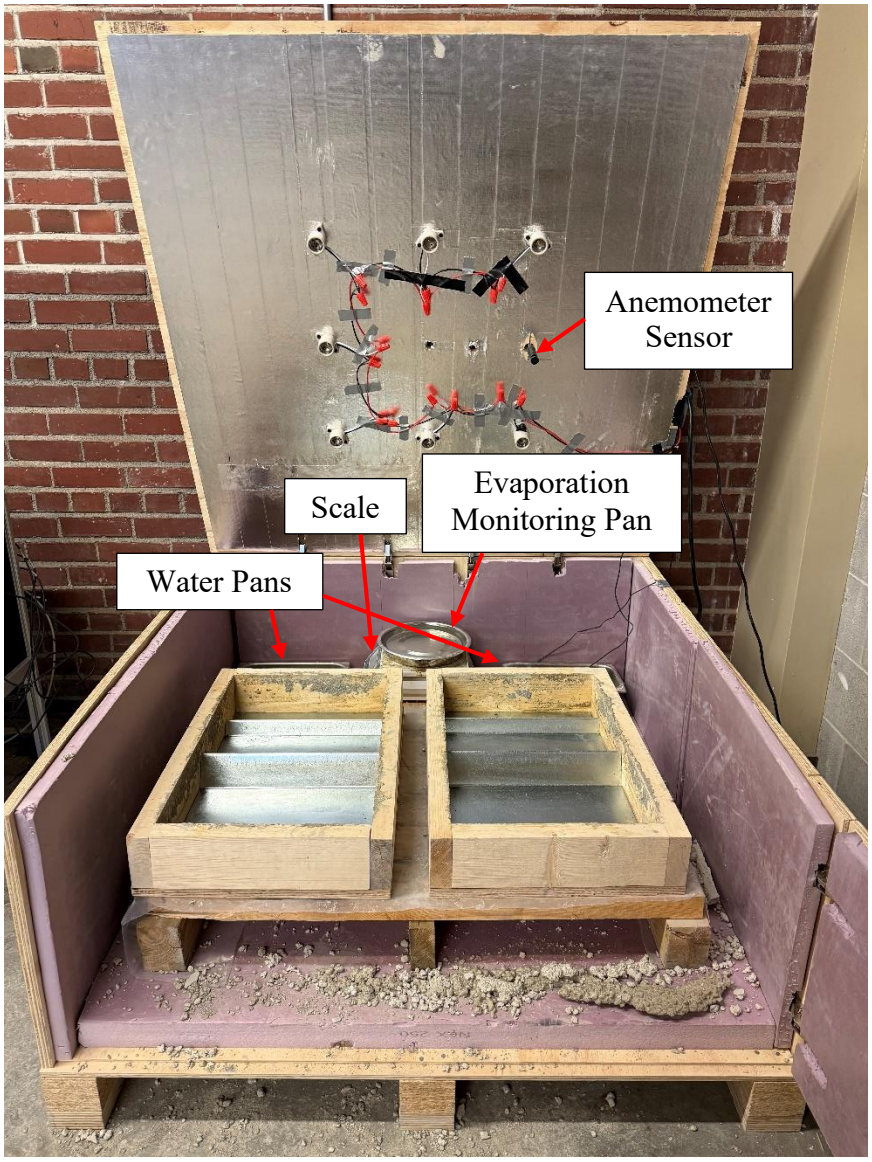

Figure 3-31: Plastic shrinkage environmental chamber fully open

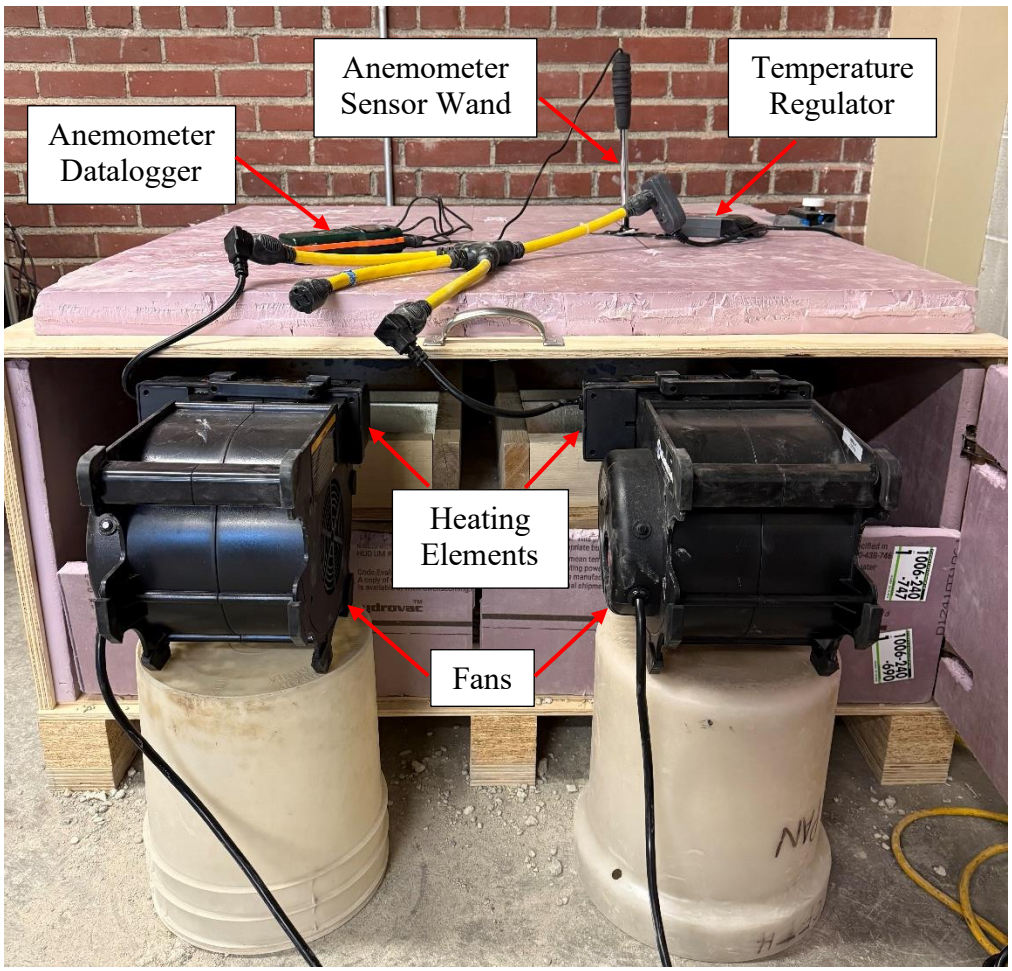

Figure 3-32: Plastic shrinkage environmental chamber with lid closed

Specimens were placed and closed in the environmental chamber immediately after casting and remained inside until final set. The final set was determined according to ASTM C403 (ASTM International, 2023c) under the same conditions as the specimen testing. Specimens were considered to have reached the final set upon attaining a strength of 4,000 psi. After final set, the specimens were removed from the environmental chamber and stored at 23°C ± 2°C under plastic wrap. At the end of the test, total water loss from the monitoring pan was recorded to ensure the evaporation rate met the test standards. 24 hours after mixing, the number and width of cracks were quantified, and an average was calculated.

3.4.3. Freeze-Thaw Resistance

This test evaluates the ability of concrete specimens to withstand rapidly repeating cycles of freezing and thawing. Two specimens of each of the following mixes were cast in 3"x4"x16" molds: CSAP, LLP, LM100, and LM25. The specimens were first cured in saturated limewater for 14 days before being placed in a freeze-thaw chamber onsite at Lafarge in Seattle, WA. Preparation and testing procedures were conducted by Lafarge and followed ASTM C666 (ASTM International, 2003), Procedure A, for up to 300 freeze-thaw cycles. At each testing interval, the fundamental transverse frequency was measured for each specimen.

3.4.4. Salt-Scaling Resistance

This test evaluates the scaling resistance of concrete specimens subjected to freeze-thaw cycles in the presence of deicing chemicals. Following ASTM C672 (ASTM International, 1998), two specimens of each of the following mixes were cast in 8"x9"x3.5" molds: CSAP, LLP, LM100, and LM25. The specimens were struck off, and the surface was finished with a medium-stiff brush.

After curing and removal from the molds, the specimens were cured in a saturated lime-water bath for 14 days, followed by 14 days of air storage. During the air storage period, 1" PVC pipes were glued to the surface of the specimens to create a dike capable of maintaining a brine pond, resulting in a surface area of 56 in^2. Figure 3-33 shows all the salt-scaling specimens with the dike attached, while Figure 3-34 provides a close-up view of a single specimen.

Figure 3-33: Salt-scaling specimens with dikes

Figure 3-34: Close-up of salt-scaling specimen with dike

The specimens were subjected to 50 freeze-thaw cycles, with the surface flushed and visually examined every five cycles. Water was added as needed between cycles to maintain the proper solution depth, and any leaks in the dike seal were repaired with glue. During visual examinations, the surface conditions of the specimens were assessed and assigned a rating based on the standard's scale.

3.4.5. Slant-Shear Test

The slant-shear test followed ASTM C882 (ASTM International, 2023d), which typically uses 30° slant-shear dummies as the standard for determining the bonding strength of systems with Portland-cement concrete substrates. However, to study the influence of interface angle on material bonding behavior, this project investigated bond strength at 30°, 45°, and 60° interfaces for the CSAP and LLP overlay mixtures with a concrete substrate. Specimens were tested at 7 and 14 days for each angle and mix combination. Four specimens were tested at each age: two 3x6-inch cylinders and two 4x8-inch cylinders. The test matrix is shown in Figure 3-35.

Additionally, to measure the strength of each individual mixture (substrate, CSAP, and LLP), four full cylinders were cast per mix and tested at 7 days. This ensured that the substrate was sufficiently strong for failures to occur at the substrate-overlay interface rather than within the substrate itself.

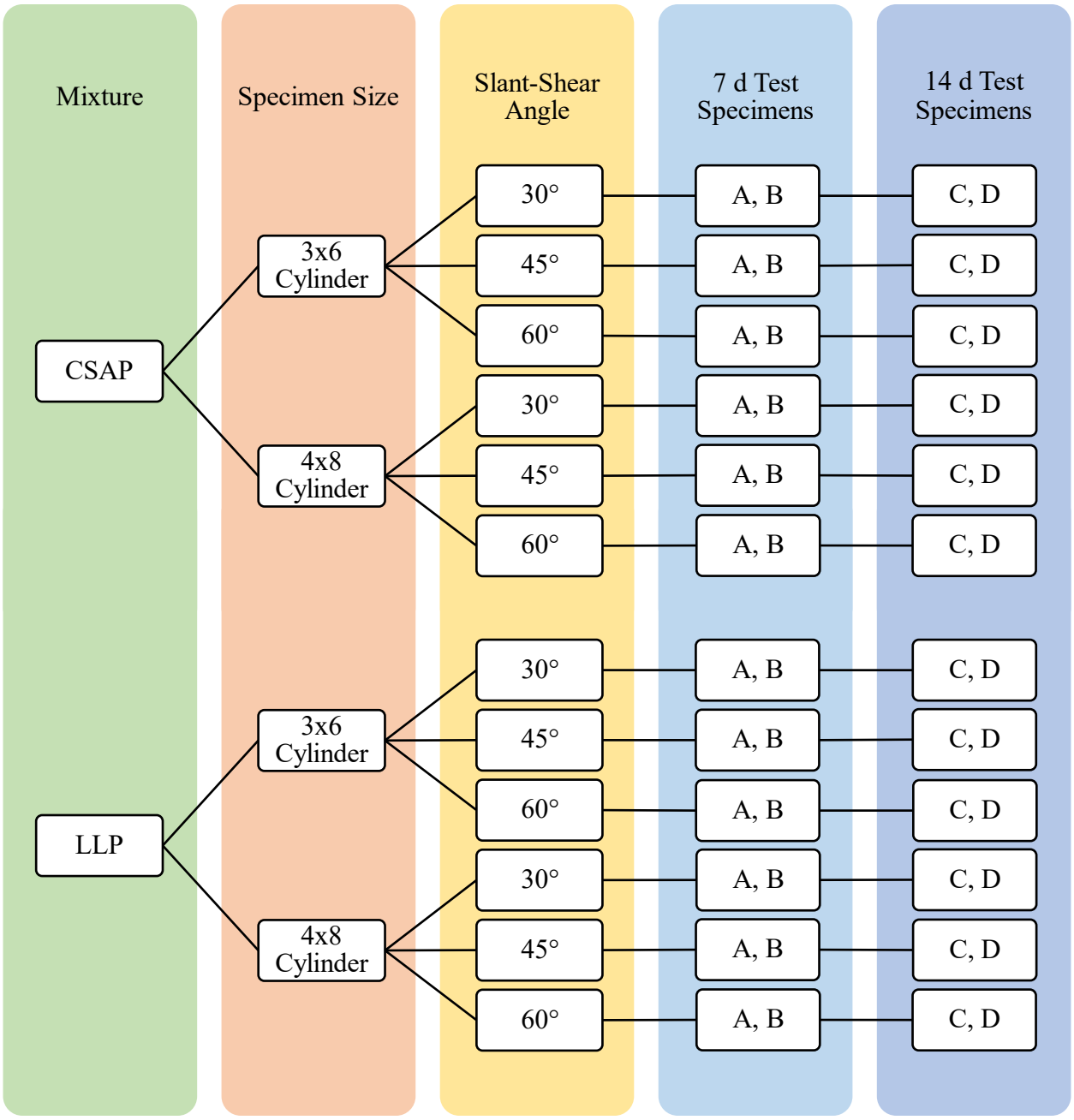

Figure 3-35: Slant-shear testing matrix

The dummy sections were 3D-printed using polylactic acid (PLA) filament for each angle. The dummy sections were inserted into the cylinders, and any gaps were caulked to create a seal. A surface retarder, Top-Cast® 150, was then applied to the exposed face of the dummy section to achieve an exposed aggregate finish with an etch depth of 3/8" to 5/8". An exposed aggregate finish was chosen over the less severe sandblasted finish because it provided better bonding between the substrate and CSA overlays.

Figure 3-36 shows example cylinders with the dummy sections inserted, caulked, and coated with surface retarder. Once the surface retarder had dried, the cylinders were overlayed with the CSA mixes that were then consolidated with 1 lift, rodded 25 times with a 3/8" rod, and screeded. The cylinders were then covered with plastic to prevent moisture loss and left to cure.

Figure 3-36: Example slant-shear cylinders prepared for substrate casting

After 24 hours, the cylinders were demolded, the dummy sections and PLC substrates separated, and the surface retarder removed. A sample of finished substrates is shown in Figure 3-37. The substrates were then cured in a saturated lime-water bath. After 3 days of curing,

substrates were tested for strength to ensure they would reach at least 4000 psi by 7 days, allowing failure to occur at the substrate-overlay interface rather than within the substrate.

Over one week after casting the substrates, they were placed back into cylinder molds, and the CSA mixes were cast on top and cured using the same method. Both CSA mixes were cast the same day. Samples of finished cylinders at the three different interface angles are shown in Figure 3-38. 7 and 14 days after the CSA mixes were cast, the cylinders were tested for compression strength, from which the bond strength was calculated.

Figure 3-37: Sample of finished substrates

Figure 3-38: Finished cylinder samples at the three different angles, arranged from left to right: 30°, 45°, and 60°

CHAPTER 4: RESULTS AND DISCUSSION

4.1. Laboratory Testing

4.1.1. Characterization Study

The preliminary optimization phase of Guerrero-Estrada (2024) established baseline mixes targeting aggregate gradation, workability, and strength based on the modified void ratio method by Taylor et al. (2015). Building on this, the current study examined the influence of aggregate size and ratio, admixture type and dosage, on the performance of CSA concrete.

Testing was divided into four phases. Phase I focused on aggregate modifications, specifically the nominal maximum size aggregate (NMSA) and the coarse-to-fine aggregate ratio (CA/FA). Phase II adjusted the dosage of the air-entraining admixture (AEA) VR10, and Phase III varied the AEA type—both using the optimized aggregate combination established in Phase I. Phase IV, limited to the latex-modified CSA concrete mixtures, investigated the impact of different latex dosages.

The target compressive strength at 4 hours was set at 4,000 psi, with a fresh air content of 5.5% ± 1.5%. The strength target was based on early-opening benchmarks for concrete pavements identified in two surveys of state agency specifications (Cavalline et al., 2020; Van Dam et al., 2005). The air content target was selected based on WSDOT's 2025 Standard Specifications (2025) for Class 4000D decks and modified concrete overlays. For reference, the target strength and lower bound air content range are marked in red on the corresponding figures.

4.1.1.1. Influence of Coarse-to-Fine Aggregate Ratio

The compressive strength and air content of the CA/FA portion of Phase I are presented in Figure 4-1. The air content generally increased with a higher proportion of fine aggregate, with all 35/65 mixes achieving 4.5% air content. These results are consistent with Dolch (1996), who noted that the fine aggregates form a "screen" that traps air within the mix, thus increasing

the proportion of fine aggregates in a mix will increase the air content. However, the 35/65 mixes exhibited the lowest compressive strength, likely due to the reduced coarse aggregate content, which plays a key role in load transfer and strength development. Additionally, the higher fine aggregate content likely increased air entrainment—as intended—which further contributed to strength loss. Notably, ultra-high-performance concrete (UHPC) achieves exceptional strength without coarse aggregate, but this is enabled by extremely high cement contents, often exceeding 1000 lbs per cubic yard

The 48.9/51.1 blend, derived from the modified void ratio approach, and the 45/55 blend showed only minor differences in the CSAP and LM mixes. In the LLP mixes, both blends exhibited comparable early-age strength; however, by 7 days, the 48.9/51.1 blend outperformed the 45/55 blend. This indicates that even small adjustments in the CA/FA ratio can lead to measurable improvements in long-term strength development.

Although the two blends are similar in proportion, the slight shift toward a coarser gradation in the 48.9/51.1 mix likely enhanced packing density without significantly affecting air content, thereby refining the concrete microstructure. These results not only contributed to higher strength but also support the validity of the modified void ratio approach in optimizing aggregate proportions for improved performance and potential long-term durability.

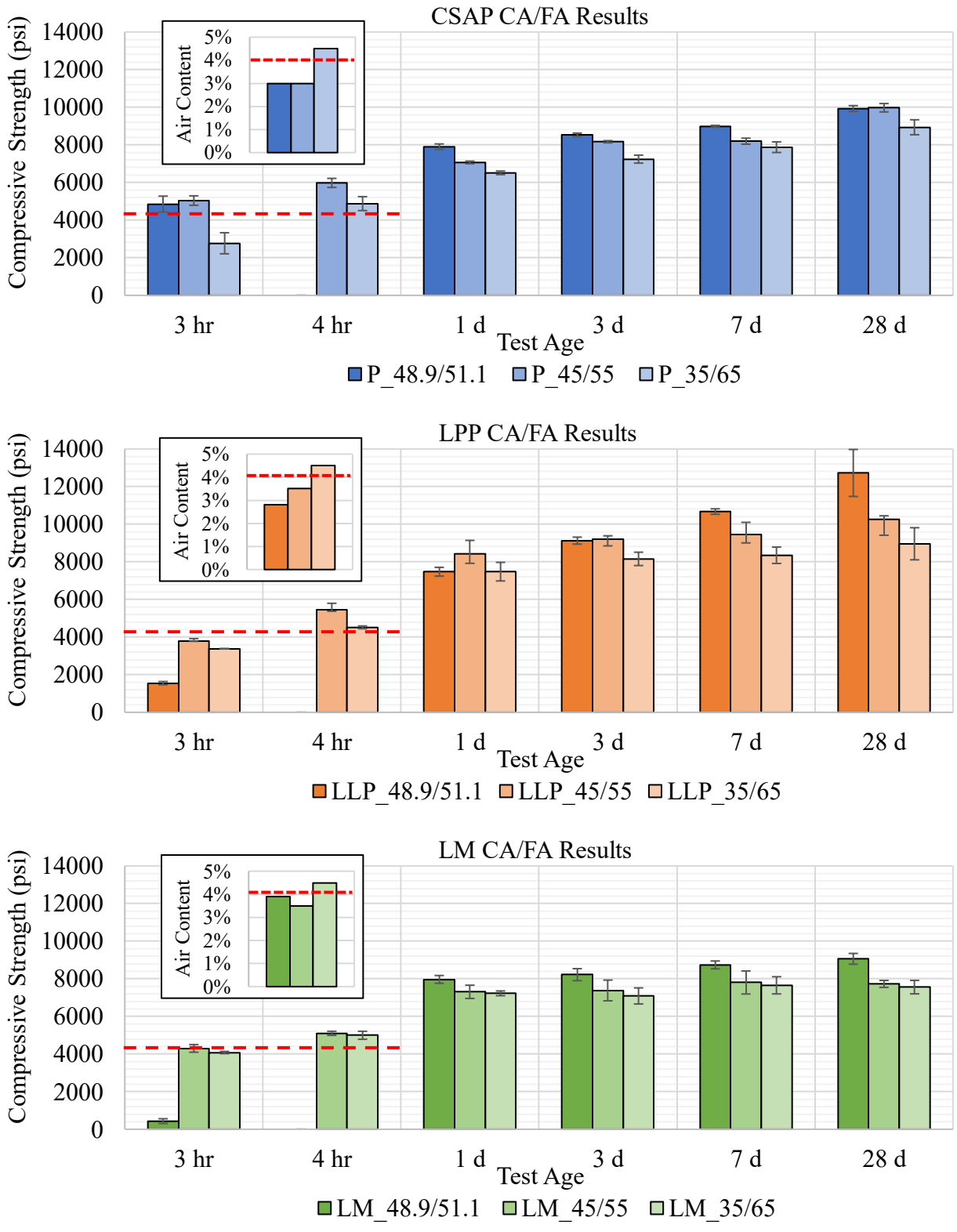

Figure 4-1: Compressive strength and air content of the coarse-to-fine aggregate study

4.1.1.2. Influence of Maximum Coarse Aggregate Size

Figure 4-2 presents the compressive strength and air content of the 3/4" NMSA mixtures from Phase I. To align with common gradations for mixes using this NMSA, the CA/FA ratio was adjusted to 60/40 in these mixtures. When comparing the air content of the 3/4" NMSA to the air content of the 3/8" NMSA in Figure 4-1, the 3/4" NMSA consistently achieved the lowest air content among all the mixes, with values ranging from approximately 1.75% to 2.25%. This suggests that the larger aggregate size of the 3/4" NMSA may result in less air entrainment within the mix, possibly due to the reduced surface area available for AEA to act upon. The reduction in fine aggregate likely further contributed to the low air content, as fine particles are essential for creating a matrix capable of stabilizing entrained air bubbles. Additionally, the decreased air content may be attributed not only to the lower fine aggregate proportion but also to a likely poorer overall gradation associated with the larger NMSA.

Importantly, no AEA was used in these LM mix, as latex has air entraining properties. Despite this, the 3/4" NMSA LM mix still resulted in low air contents, emphasizing the critical role of fine aggregate in facilitating air entrainment. The observed reduction in air content may have implications for durability, as lower air contents are typically associated with decreased freeze-thaw resistance.

The 3/4" NMSA also generally exhibited weaker strength than both the 48.9/51.1 blend and the 45/55 blend in the CSAP and LLP mixes. The higher proportion of smaller aggregates likely contributed to better packing density, particle interlocking, and hydration, resulting in stronger mixes. In contrast, the larger aggregate in the 3/4" aggregate mixes likely created a less dense microstructure leading to weaker compressive strength. However, in the LM mix, the 3/4" NMSA performed similarly to the blends with 3/8" NMSA, suggesting that latex modification

improved the strength of the interfacial transition zone between the paste and aggregate, thereby maintaining compressive strength despite the lower air content.

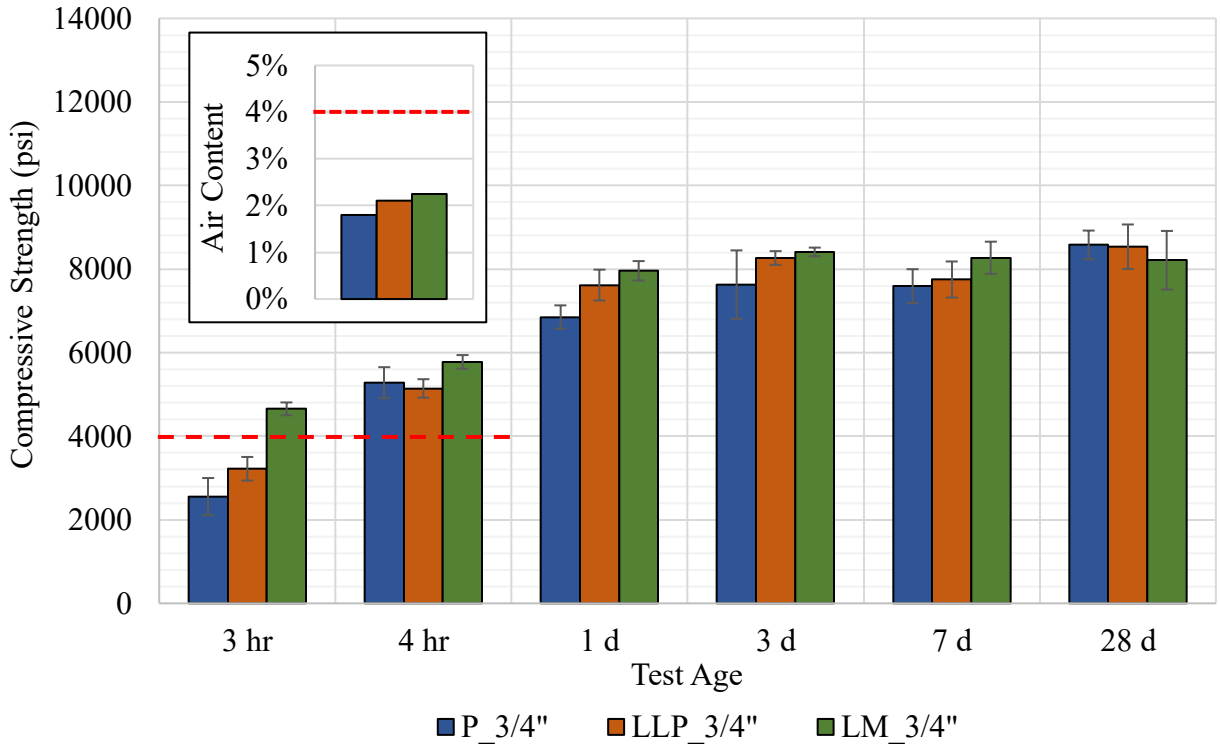

Figure 4-2: Compressive strength and air content of the maximum coarse aggregate study

Figure 4-3 presents a trellis plot comparing permutations of CSA system, NMSA, aggregate blend (expressed as fine aggregate content), air content, and 28-day compressive strength. Scatter plots, jitter plots, bar graphs, and histograms visualize the relationships among variables. In the jitter plots, darker regions reflect overlapping points and higher data concentrations. A red dashed line marks the minimum target air content of 4%.

On average, mixes achieved 60% of their 28-day strength at 4 hours (SD = 0.066), making the 4-hour target of 4000 psi equivalent to 6700 psi at 28 days. This benchmark is also marked with a red dashed line.

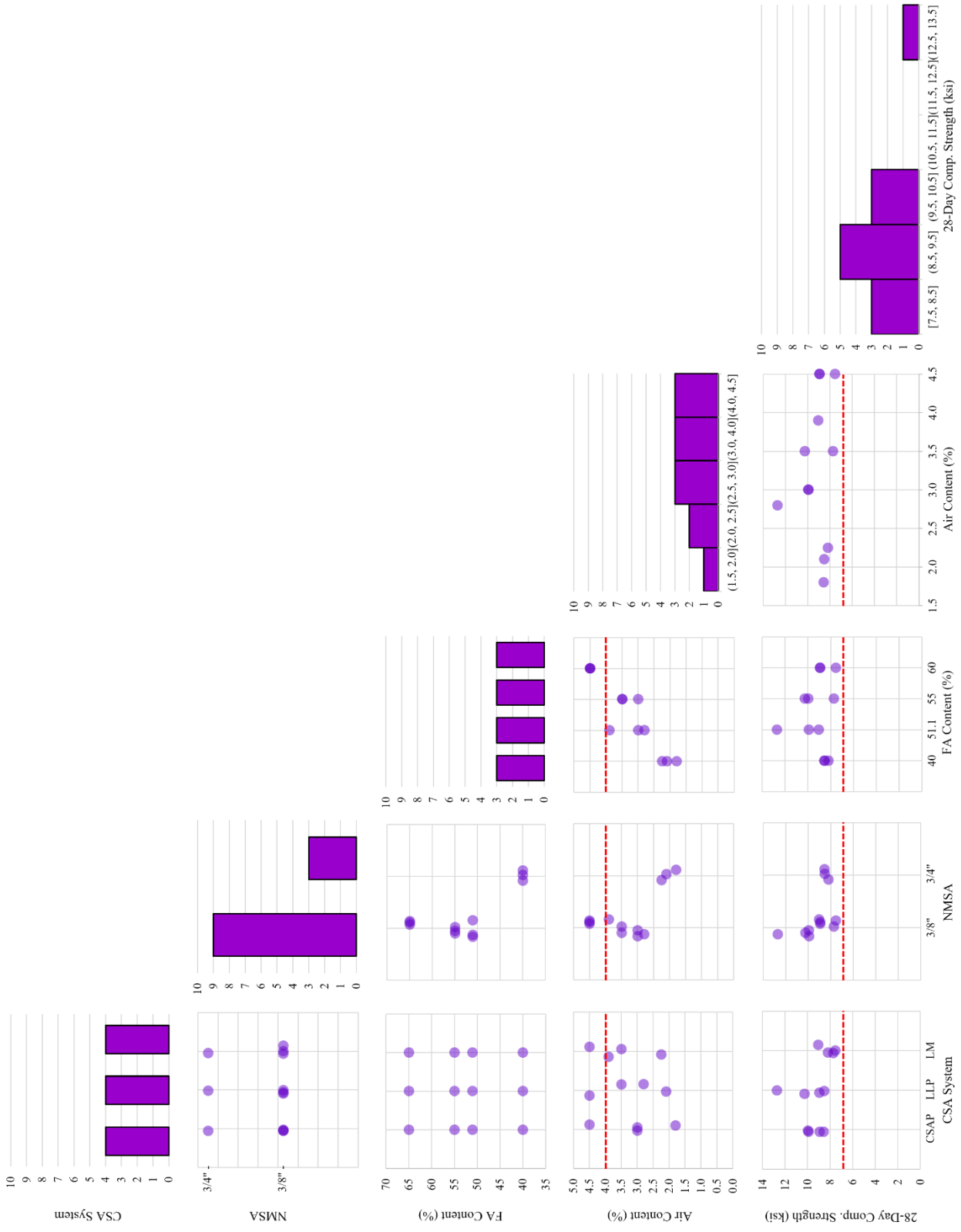

Figure 4-3: Trellis plot of CSA aggregate parameters and performance metrics

Similar to observations by Dolch (1996), a positive trend was observed between FA content and air content, with only the mixes containing 60% FA exceeding the target minimum air content. In contrast, compressive strength showed a negative trend with increasing FA content. Notably, all mixes with a 3/4" NMSA had the lowest air contents and lower compressive strengths. However, all mixes exceeded the 28-day strength equivalent to a 4-hour strength of 4000 psi, indicating they met the reopening strength requirement.

4.1.1.3. Influence of Air-Entraining Admixture Dosage

For Phase II and III involving AEA dosage and type, the coarse-to-fine aggregate ratio of 48.9/51.1 with a 3/8" NMSA was used. Despite the 35/65 blend having the highest air content, the 48.9/51.1 blend exhibited the greatest strength gain by the end of the test period and maintained air content similar to that of the 45/55 blend.

Figure 4-4 presents the compressive strength and air content results for the Phase II mixes. The AEA dosage and type will also influence the air content of the concrete. In Phase II, VR10 was added at dosages of 1.0% and 1.75% by mass of cement (moc) for CSAP mixes, and at 1.75% and 2.5% by moc for CSA-LLP mixes. Increasing the AEA dosage had no measurable effect on air content in the CSAP mix. However, the LLP mix showed a slight decrease in air content at the higher AEA dosage—a counterintuitive result that may be due to destabiliization of air voids at increased AEA levels.

These trends are consistent with the parabolic relationship between AEA dosage and air content described by Dolch (1996), where the air content increases up to a certain point and then levels off or decreases. For the CSAP mix, air content appeared to plateau after the 1.0% dosage, as indicated by the similar results at 1.75%. In the LLP mix, the parablic relationship is more evident, with air content decreasing beyond the peak dosage of 1.75%.

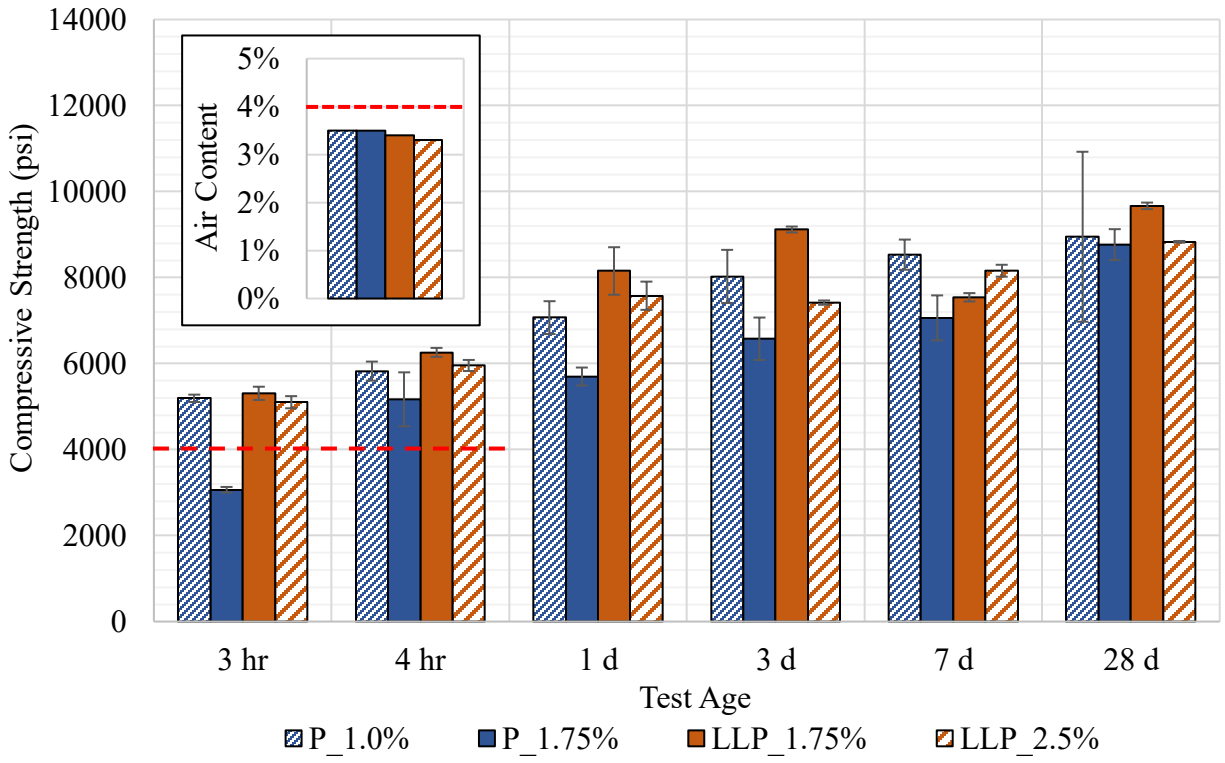

Figure 4-4: Compressive strength and air content of the air-entraining admixture dosage study, all with VR10 and dosed by mass of cement

Regarding compressive strengths, the CSAP mix with a 1.0% dosage consistently outperformed the mix with a 1.75% dosage. However, by 28 days, both mixes exhibited comparable strength. In contrast, for the LLP mixes, the 1.75% dosage generally resulted in greater strength than the 2.5% dosage. It is worth noting that the CSAP 1.0% dataset showed a relatively large standard deviation of 1976 psi at 28 days, which may indicate variability in performance of sampling inconsistencies. The lower compressive strength observed for the LLP mix with 1.75% at 7 days may be due to a sampling anomaly, as the trend seen at earlier ages continued at 28 days. These trends from both mixes may indicate an overdosage effect, where excess AEA could disrupt the microstructural matrix or reduce paste cohesion.

An AEA dosage of 1.75% was chosen for future testing, as it resulted in higher air content and a strong mix for LLP. It also had an insignificant impact on air content for CSAP

and showed comparable strength at 28 days to the CSAP mix with 1.0% AEA. This suggests that 1.75% represents an effective balance between air content and mechanical performance for both binder systems.

4.1.1.4. Influence of Air-Entraining Admixture Type

Figure 4-5 presents the compressive strengths and air content from Phase III, along with the results of the 1.75% VR10 dose mixes for comparison. In addition to AEA dosage, various synthetic and vinsol resin-based AEA products were tested as their compatibility with the CSA and aggregates, which could potentially affect air content. The P_VR10 data shown in Figure 4-5 is the same data labeled as P_1.75% in Figure 4-4 from Phase II, and was relabeled here to focus on the particular admixture used.

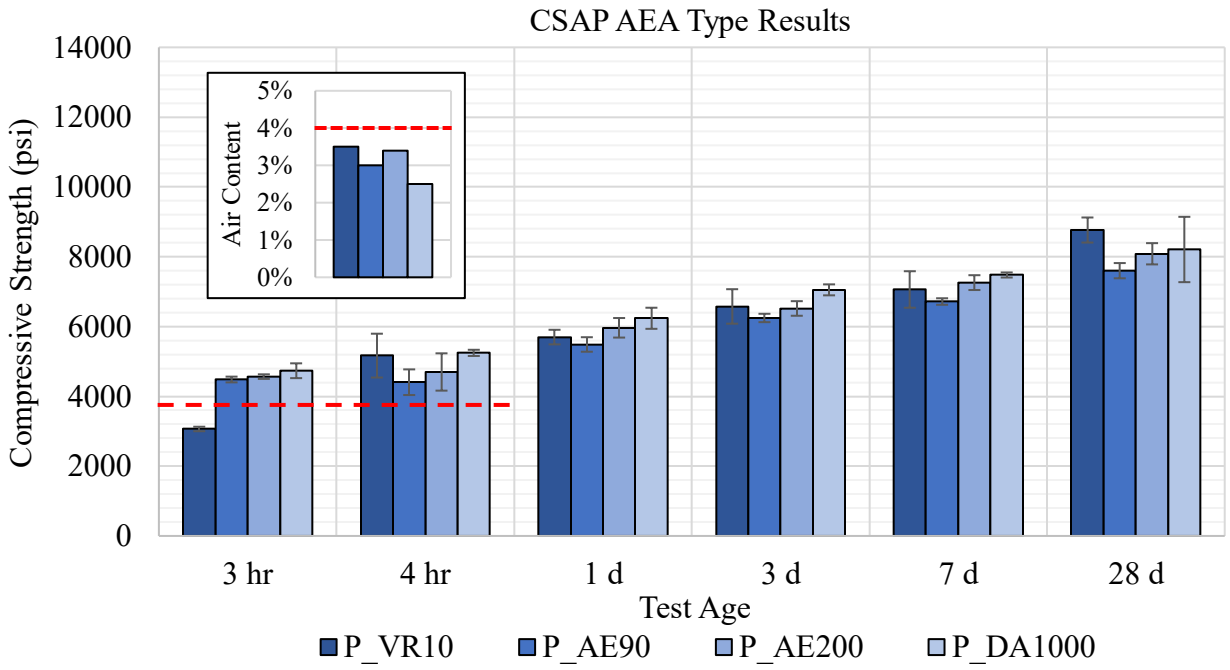

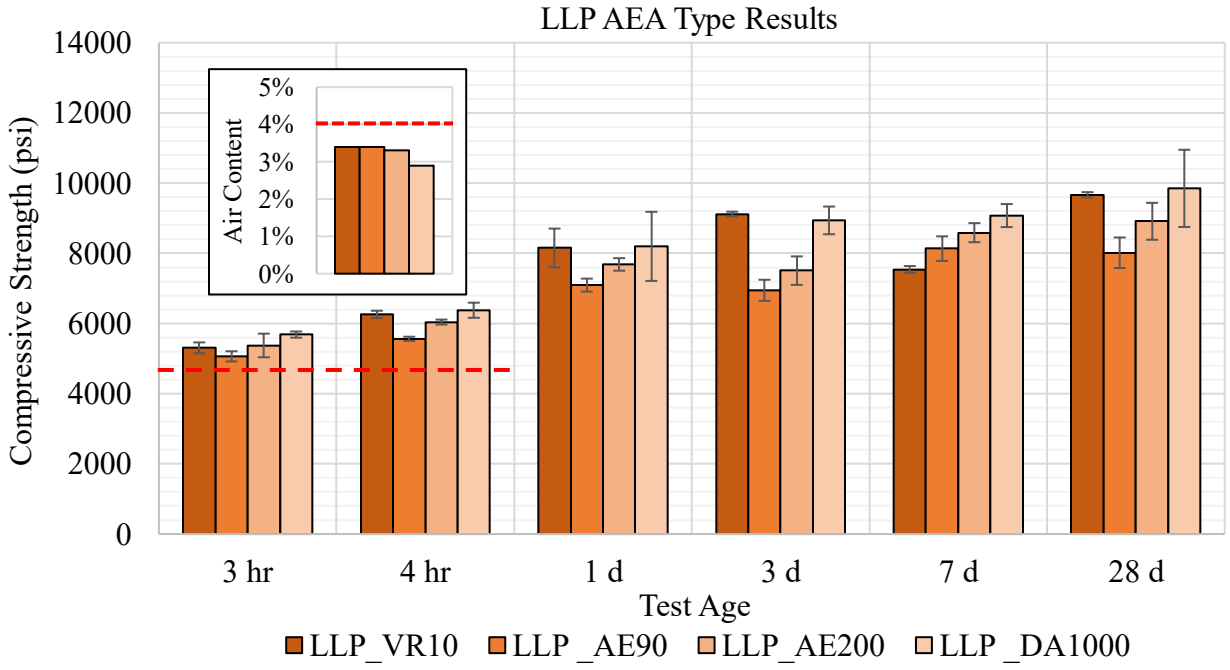

Figure 4-5: Compressive strength and air content of the air-entraining admixture type study, all dosed at 1.75% by mass of cement

It was found that the vinsol resin-based VR10 and the synthetic AE200 produced approximately the same amount of air—around 3.5%—in both CSA systems. However, the vinsol resin-based AEA, DA1000, resulted in the lowest air content among all AEAs tested for

both systems, with values between 2.5% and nearly 3%. While this difference may partly reflect normal mix-to-mix variation, it still highlights that AEAs sharing the same base material can have distinct chemical formulations that significantly affect their interaction with cement and aggregates.

The synthetic AEA AE90 produced more air in the LLP system than in the CSAP system, with a similar trend observed for DA1000, where the CSAP system generated less air compared to LLP. This suggests a potential interaction between the Low-P™ polymer and the AEA that varies depending on whether the polymer is incorporated as a liquid admixture (LLP) or as an interground powder (CSAP). Since the Low-P™ polymer used in both systems is proprietary, its exact formulation and influence on air content remain unknown.

One possible mechanism for the reduced air content is the adsorption of AEA molecules onto polymer particles, similar to the adsorption of AEA by carbon particles reported by Penderson et al. (2008). The powdered polymer may present a non-polar surface that promotes surfactant adsorption, a behavior that does not appear to occur when the polymer is introduced in liquid form. However, due to the unknown polymer formulation, this hypothesis remains speculative.

However, the negligible difference in air content between systems for VR10 and AE200 suggests that this adsorption interaction may be specific to certain AEA formulations, or that the observed trends are due to other, unrelated factors. Further research is needed to identify the mechanisms governing AEA-polymer interactions and their influence on air entrainment behavior in CSA systems.

During the testing period, the vinsol resin-based AEAs generally exhibited comparable or greater strength than the synthetic-based AEAs, similar to the findings reported by Wang et al. (2023). The synthetic AEA, AE90, consistently showed the lowest strength among all mixes for

both CSAP and LLP. Among the vinsol resin-based AEAs, VR10 tended to result in slightly lower strengths in the CSAP mixes until 28 days, at which point it surpassed DA1000. In contrast, VR10 and DA1000 produced comparable strength throughout the entire testing period for the LLP mixes.

Figure 4-6 presents the HRWR dosages and corresponding slump values for mixes tested in Phases II and III. Percent labels indicate VR10 dosage, and striped bars mark mixes with AEA dosages other than the standard 1.75% by moc. Different HRWRs were used to ensure compatibility with the specific AEA used in each mix. This adjustment, along with variations in AEA type and dosage, likely influenced both air content and workability. The target slump range was 4–6 inches, with upper and lower bounds marked in red for reference. In the figure, the mixes labeled with percentages represent Phase II mixtures containing VR10 at varying dosages.

All mixes began with an initial HRWR dosage in the mix design, ranging from 0.25–1.00% by moc. It is important to use the AEA and HRWR from the same manufacturer to avoid chemical incompatibilities. As a result, MG7920 was paired with the VR10, AE90, and AE200 AEAs, while AD575 was used with the DA1000 AEA. It is also worth noting that the CSAP cement system contains a powdered HRWR as part of its formulation.

During mixing, additional HRWR was incrementally added as needed to achieve workable consistencies, resulting in variable dosages across mixtures. Although the absolute HRWR volumes differed, the relative dosages and their influence on slump provide insight into admixture interactions. The HRWR dosage (in fl-oz) is shown in red above each bar to facilitate comparison across mixes.

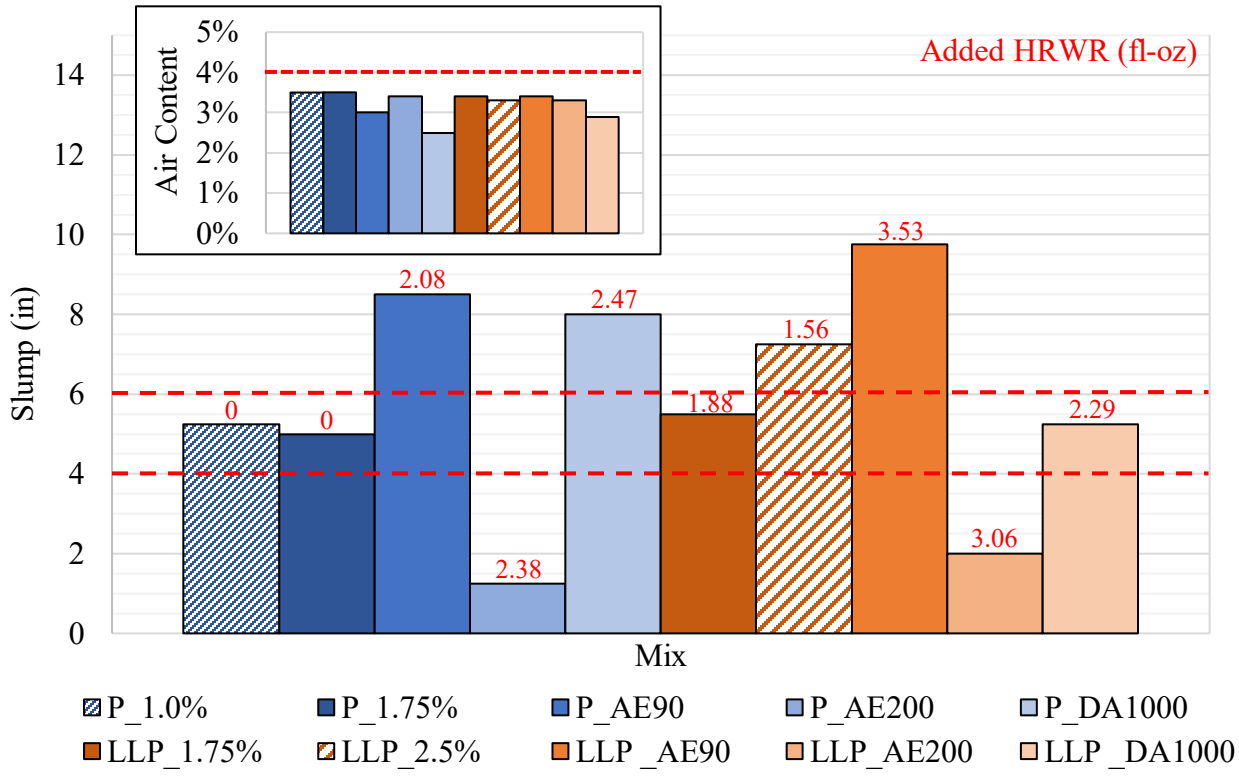

Figure 4-6: Workability and air content for different AEA types and dosages

Regarding workably, the results indicate clear distinction in the influence of the different admixtures, driven largely by differences in chemical composition and their interaction with the cementitious system. Mixes incorporating AE200 exhibited the lowest slump, even with the addition of 2.38 to 3.06 fl-oz of HRWR. Despite AE200 and AD575 coming from the same manufacturer, the HRWR's inability to restore workability highlights their limited chemical compatibility, possibly due to adverse interactions that destabilize air bubbles or hinders their efficiency.

In contrast, AE90 produced the highest slump values, despite requiring less HRWR—for example, the addition of 2.08 fl-oz in the CSAP mix achieving over 8 inches in slump, compared to AE200's 2.38 fl-oz yielding under 2 inches of slump in the same system. This favorable performance suggests a chemical composition that supports stable bubble formation, improved dispersion, and reduced inter-particle friction. The enhanced workability of mixes with AE90

indicate strong compatibility of the AEA and HRWR with the cement systems at a molecular level.

DA1000, a vinsol resin-based AEA, produced moderate to high slump values (5.25 to 8 inches) but required slightly higher HRWR dosages (2.29 to 2.47 fl-oz). In contrast, VR10 achieved a moderate slump of approximately 5 inches in the CSAP system without any additional HRWR, and 5.5 to 7.25 inches in LLP mixes with only 1.56 to 1.88 fl-oz of HRWR. The workability observed in the CSAP system is likely influenced by the presence of a powdered HRWR already incorporated into the cement. However, the results also suggest that the combination of VR10 and MG7920 exhibits the highest chemical compatibility, promoting the formation of stable, well-distributed air bubbles and efficient interaction between the AEA and HRWR.

Notably, although DA1000 and VR10 are both vinsol resin-based, their performance varied considerably—highlighting how even small chemical modifications within the same AEA base can lead to significant differences in air content, bubble characteristics, and rheological behavior. Overall, the observed differences in slump and HRWR demand across AEA types underscore the important role of AEA chemical composition in controlling not only workability, but also the stability and quantity of entrained air, which ultimately influences the mechanical properties of the hardened material.

For subsequent testing and applications, VR10 was selected due to its balanced performance in strength, air content, and workability. By 28 days, VR10 outperformed the other CSAP mixes and ranked among the strongest mixes in the LLP series. Its air content was comparable to that of the other AEAs, while achieving moderate workability with minimal HRWR demand.

4.1.1.5. Influence of Latex Modifier Dosage

In the final phase, Phase IV, latex quantity was studied independently of other parameters. The aggregate size and blend remained consistent with the preliminary CSA-LM mix, with only the latex dosage adjusted. This isolated approach provided clearer insight into how latex affected the performance of the mix, without influence from other parameters. The dosage levels selected were based on the ACI 548 guideline (American Concrete Institute, 2009), which recommends 3.5 gallons per sack (94 lbs) of cement for CSA systems. In this study, the latex doses were reduced to 25% (0.875 gal/sack) and 50% (1.75 gal/sack) of the standard. Note that the W/C ratio was increased to 0.38 for the 25% and 50% latex mixes, as the original 0.32 W/C ratio produced dry, unworkable mixes with no slump and a crumbly texture.

Figure 4-7, which presents both compressive strength and air content results, shows that the LM_100% mix—representing the standard latex dose—achieved compressive strength comparable to the LM_25% mix by 4 hours. However, by 3 days, the LM_25% mix surpassed LM_100% and continued to outperform LM_100% and LM_50% over time. Although the LM_50% mix exhibited the lowest early-age strength, it eventually exceeded LM_100% by the end of the testing period. This trend in early-age performance, despite the increased W/C ratio, highlights the potential of reduced latex dosages to maintain or even improve strength development. Such findings are particularly relevant for applications where cost efficiency or material limitations are critical considerations.

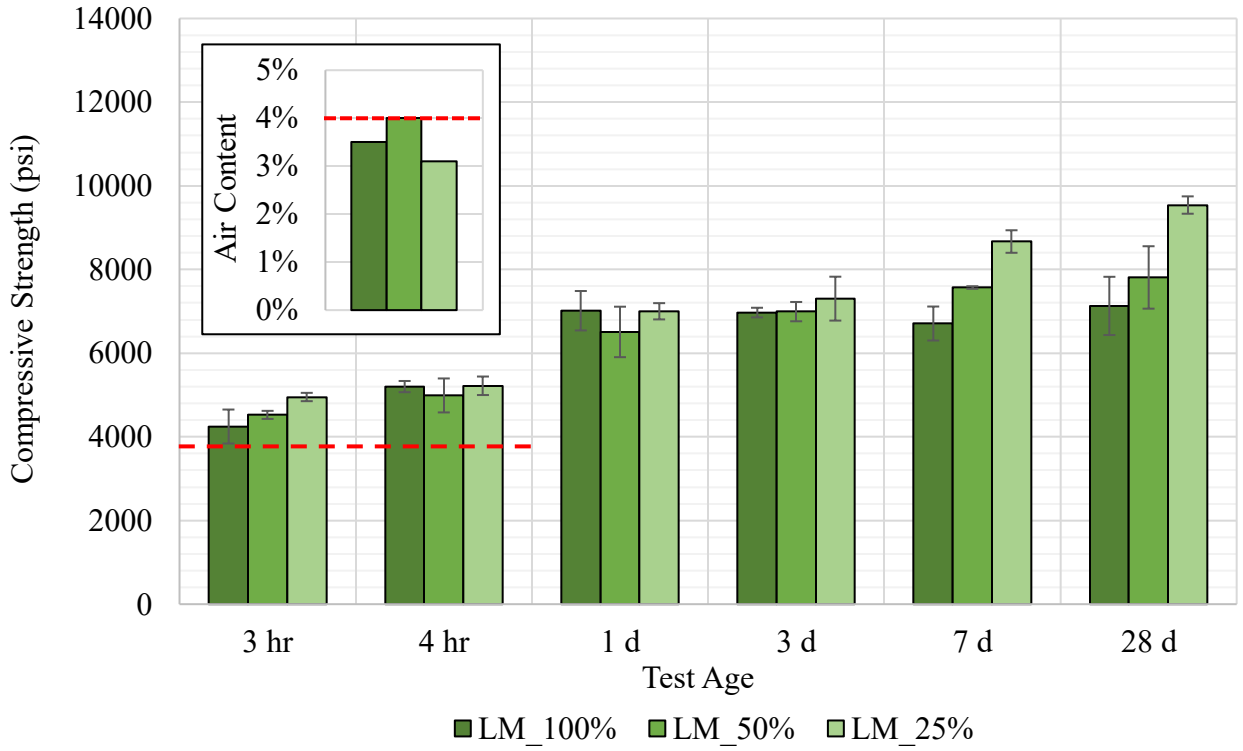

Figure 4-7: Compression results of the latex modifier dosage mix matrix

Figure 4-8 displays a trellis plot illustrating the relationships between CSA system, percentage of standard latex dosage, air content, and 28-day compressive strength. A combination of scatter plots, jitter plots, bar graphs, and histograms is used to visualize these interactions. In the jitter plots, darker regions indicate overlapping data points, reflecting areas of higher concentration.

The CSAP and LLP mixes shown were the mixes selected for further testing and have a CA/FA ratio of 48.9/51.1 along with an AEA dosage of 1.75% VR10. A red dashed line marks the minimum target air content of 4%. On average, these mixes reached 63% of their 28-day compressive strength at 4 hours (SD = 0.061), making the 4000 psi target at 4 hours equivalent to a 28-day strength of 6300 psi. This value is also highlighted with a red dashed line.

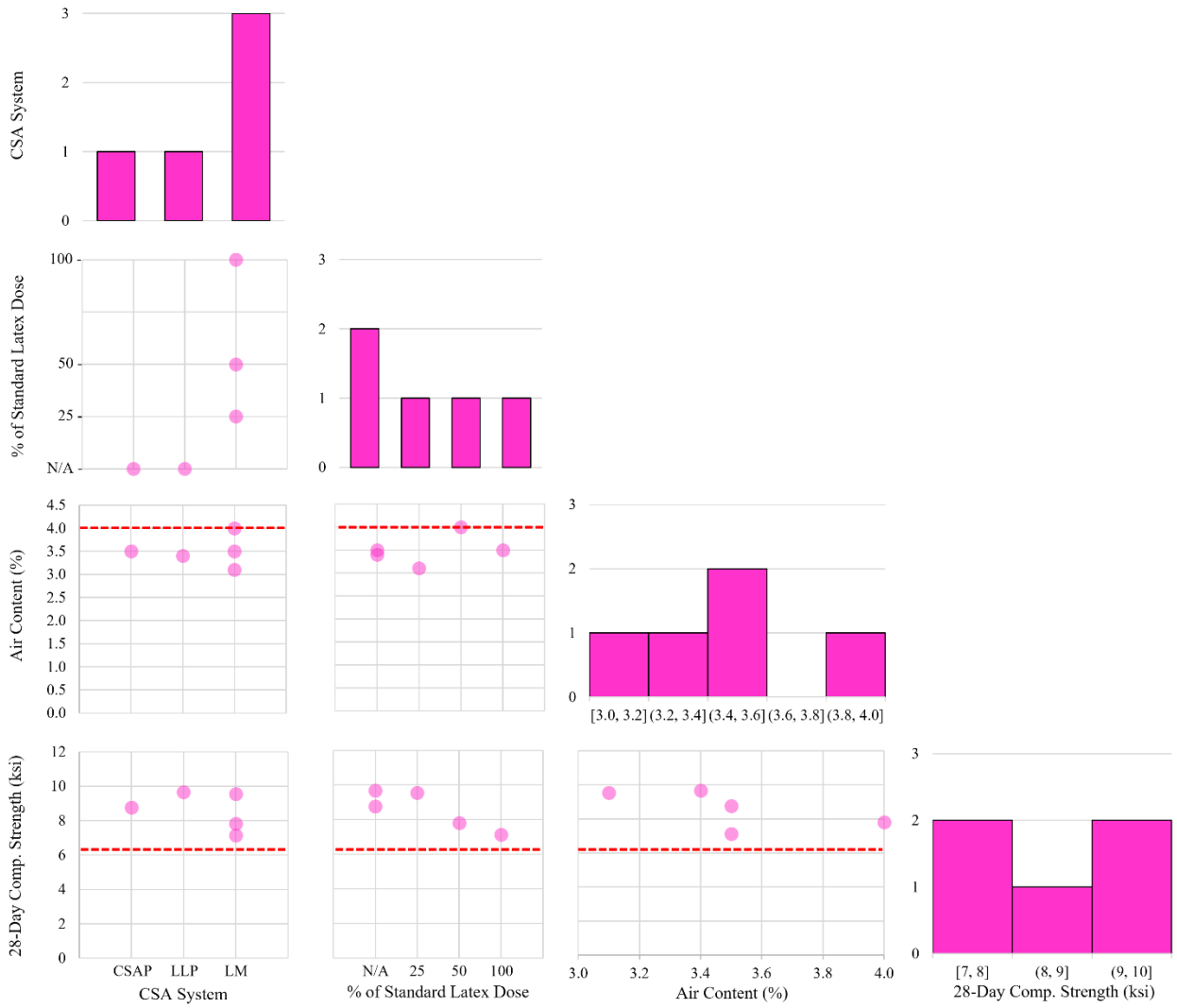

Figure 4-8: Trellis plot of latex modifier dosage and performance metrics

The mix with 25% of the standard latex dosage produced the lowest air content, while 50% resulted in the highest, followed by a decrease at the full 100% dosage. This trend may reflect variability in mixing but also suggests diminishing air content at higher dosages, similar to the reduction observed with elevated VR10 levels in the LLP mixes. Like traditional air-entraining agents, latex contains surfactants that can introduce significant amounts of entrained air into concrete (Choi & Yun, 2014). However, excessive latex has been associated with adverse

effects such as increased air content, delayed setting, and reduced mechanical strength (Eren et al., 2017).

In terms of compressive strength, the 25% latex mix performed comparably to the non-latex-modified mixes, while higher dosages led to a decline in strength, especially at 100%. These results suggest that lower latex dosages may help preserve compressive strength. Overall, the findings emphasize the need to carefully regulate latex dosage—not only to maintain mechanical performance but also to manage air content and ensure long-term durability. Both LM_25% and LM_100% mixes will be included in future testing to evaluate the long-term effects of extreme latex dosages

4.1.1.6. Characterization Study Summary

The characterization portion of this project investigated the influence of aggregate gradation, aggregate size, AEA dosage and type, and latex modifier dosage on compressive strength and air content of CSA-based concrete. Across all parameters studied, clear relationships emerged between mix and admixture compositions and their impact on air void stability and mechanical performance, underscoring the importance of carefully balancing mix components to achieve the desired concrete behavior.

- **Phase I (CA/FA aggregate ratio and maximum aggregate size):** A higher proportion of fine aggregate (35/65 blends) increased air content but reduced compressive strength, primarily due to the lower coarse aggregate content and diminished load-bearing capacity. Slight shifts in the CA/FA ratio toward coarser blends, such as 48.9/51.1, enhanced packing density and compressive strength while maintaining moderate air content.

  A larger NMSA of 3/4" consistently led to lower air contents, attributed to the reduced surface area available for air entrainment and a decrease in fine aggregate volume. Although compressive strength generally declined with the use of larger aggregates, latex modification

seemed to help offset these losses, indicating a beneficial role of polymer modifiers in reinforcing the interfacial transition zone, especially when coarse aggregate content is high.

Among the tested combinations, a CA/FA ratio of 48.9/51.1 with a 3/8" NMSA offered the best balance between compressive strength and air content retention.

- **Phase II (AEA dosage):** The effects of AEA dosage followed a parabolic trend, with strength and air content initially increasing before plateauing or declining at higher dosages. This behavior was especially evident in the LLP system, suggesting potential overdosage effects and bubble destabilization. A dosage of 1.75% AEA emerged as the optimal balance, providing adequate air content while preserving strong mechanical performance across both binder systems.
- **Phase III (AEA type):** The type of AEA had a significant impact on both air content and workability. Although the tested AEAs shared similar base chemistries, such as vinsol resin, their performance varied—likely due to differences in chemical formulations. VR10 demonstrated the most balanced performance, offering consistent strength, moderate air content, and good workability with minimal HRWR demand. Thus, VR10 was chosen to be used for subsequent testing.

  In contrast, synthetic AEAs such as AE90 improved workability but tended to reduce compressive strength and air entrainment, particularly when combined with the powdered Low-P™ polymer. This behavior suggests a complex interaction between AEAs and powdered polymers, potentially involving adsorption of AEA onto the polymer surface, similar to the known adsorption of AEAs onto carbon. However, the exact mechanisms remain unclear, and further research is needed to better understand AEA–polymer interactions and their impact on air entrainment and mechanical properties.

- **Phase IV (Latex modifier dosage):** A strong polynomial relationship between the air content and the strength development of varying latex dosages was found. Latex, with a reduced dosage of 25%, provided superior strength development over time, likely due to improved matrix integrity and reduced surfactant-induced destabilization.

  However, air content peaked at 50% latex before declining at 100%, paralleling trends seen with high AEA dosages, suggesting a common mechanism of bubble destabilization at high latex dosages. The LM_25% mix showed comparable strength to the LLP mix, while higher latex dosages decreased strength, highlighting the significance of latex dosage on mechanical performance.

Collectively, these findings demonstrate that performance in CSA-based concrete is governed by subtle interplays between aggregate gradation, admixture type/dosage, and polymer content. Small adjustments in these variables can significantly impact air entrainment, strength, and durability, highlighting the importance of integrated mix design approaches that consider the interactive effects among components rather than evaluating them independently.

Based on the characterization results, all subsequent testing used a 48.9/51.1 CA/FA blend with a 3/8" NMSA. For the CSAP and LLP mixes, VR10 was used at 1.75% by moc. Two latex-modified mixes were also evaluated: LM100, using the full standard dosage, and LM25, using 25% of the standard dosage. All mixes had a W/C ratio of 0.32, except LM25, which required an increased ratio of 0.38 to ensure workability.

4.2. Field Trials

To evaluate the field performance of the CSA mixtures, overlays were placed on mini-bridge deck substrates designed to replicate typical WSDOT bridge decks. A major objective of the study was to assess the compatibility between the overlays and substrates, with particular attention to bond strength and long-term volume stability. Additionally, the mechanical

properties of the field-scale specimens were tested to better understand their real-world behavior and potential limitations.

4.2.1. Field-Scale Testing

Field-scale specimens for the CSAP (CSAP_deck) and LLP (LLP_deck) overlay mixes were cast during their respective pours to track the development of their mechanical properties over time. Furthermore, field-scale specimens of the CSAP, LLP, LM100, and LM25 mixes were cast in the laboratory under controlled conditions to allow for a more accurate and consistent comparison of the four mixes.

It is important to note that the admixtures and CSAP cement used in the overlay mixes were supplied by the contractor operating the volumetric mixer for the pour. The CSAP cement used on-site included both a powdered HRWR and a powdered AEA. In contrast, the CSAP cement used in the laboratory contained only powdered HRWR and did not include AEA. These differences in admixture products deviated from those typically used in laboratory testing.

4.2.1.1. Fresh Properties

The slump, air content, temperature, and unit weight of the mini-bridge deck and lab mixes are summarized in

Table 4-1. Both had nominally the same design, with minor admixture and mix differences detailed in section 3.3.2.1. Deck mixes were cured outdoors for 24 hours before lime-water bath curing, while lab mixes were cured 24 hours in controlled conditions prior to the same lime-water treatment.

The deck mixes exhibited similar fresh properties, except for slump—CSAP_deck was significantly more workable than LLP_deck. This trend was also observed in the laboratory series and aligns with the findings from the characterization phase (section 4.1.1.4), suggesting influence from the powdered HRWR in the CSAP cement.

In the laboratory, the LLP mix produced considerably more air than the CSAP mix, which may support the previously discussed hypothesis of AEA adsorption by polymer particles (section 4.1.1.4). Interestingly, LLP_deck showed slightly lower air content than CSAP_deck, indicating that differences in admixture type, dosage, or mix proportions between the lab and field mixes may have contributed to these variations in fresh properties. For the latex-modified mixes, LM100 and LM25 had similar air contents, but LM25 exhibited lower slump. This suggests that higher latex content may improve workability, potentially by reducing interparticle friction within the mixture.

Table 4-1: Field-scale fresh properties

Mixture	Temperature (°F)	Air Content (%)	Slump (in)	Unit Weight (pcf)
CSAP_deck	62	4.5	8.50	N/A
LLP_deck	62	4.0	4.75	N/A
CSAP	65	4.0	9.50	149.2
LLP	67	5.7	7.50	147.2
LM100	63	3.1	9.25	148.0
LM25	67	3.1	6.50	146.8

In addition to recording the temperature at the time of casting, the internal temperature of the instrumented mini-bridge overlays was also monitored over time. The temperatures the deck overlays experienced can be used to understand the temperatures the outdoor deck cylinder specimens were exposed to during curing. Figure 4-9 presents the concrete temperature profiles of the overlays from the time of placement to 1 day. The maximum, minimum, temperature change, and 1-day temperatures experienced by each deck are shown in Table 4-2 for more precise comparison.

Decks 1 and 3 experienced similar temperature increases (6.54°F and 5.82°F, respectively), while Deck 5 exhibited the greatest increase (9.50°F) and Deck 4 showed a moderate change (7.46°F). This suggests that Deck 5 underwent the highest heat of hydration, while Decks 1 and 3 experienced the least. By the end of the first day, the temperatures had stabilized and were within 10°F of each other.

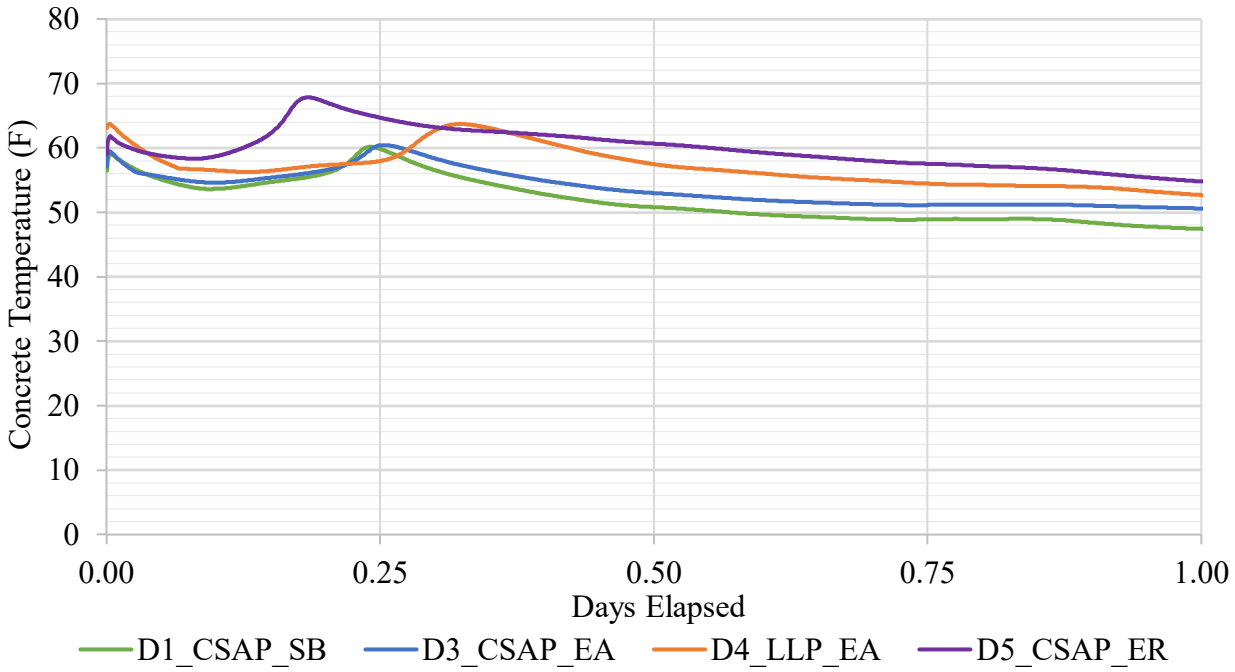

Figure 4-9: CSA overlay internal temperatures over 24 hours after placement

Table 4-2: Maximum, minimum, temperature change (ΔT), and 1-day temperatures for each deck from Figure 4-9

Deck	Max (°F)	Min (°F)	ΔT (°F)	1-Day (°F)
D1_CSAP_SB	60.16	53.62	6.54	48.99
D3_CSAP_EA	60.45	54.62	5.83	51.22
D4_LLP_EA	63.72	56.24	7.48	54.05
D5_CSAP_ER	67.84	58.34	9.51	57.05

4.2.1.2. Compressive Strength

Figure 4-10 presents the strength data for both the field-scale deck and laboratory specimens. The figure also indicates the curing conditions for the deck mix specimens, distinguishing between outdoor curing and indoor curing in a lime-water bath. Notably, neither

deck mix developed measurable compressive strength by 4 hours, likely due to the slower hydration caused by the colder outdoor curing conditions.

The figure includes horizontal lines indicating the minimum and maximum opening strength benchmarks for concrete pavements based on two surveys of state agency standard specifications (Cavalline et al., 2020; Van Dam et al., 2005). In general, states distinguished between the strength needed for construction equipment access and that required for regular traffic (Cavalline et al., 2020), while some specific strength thresholds based on the concrete age (Van Dam et al., 2005).

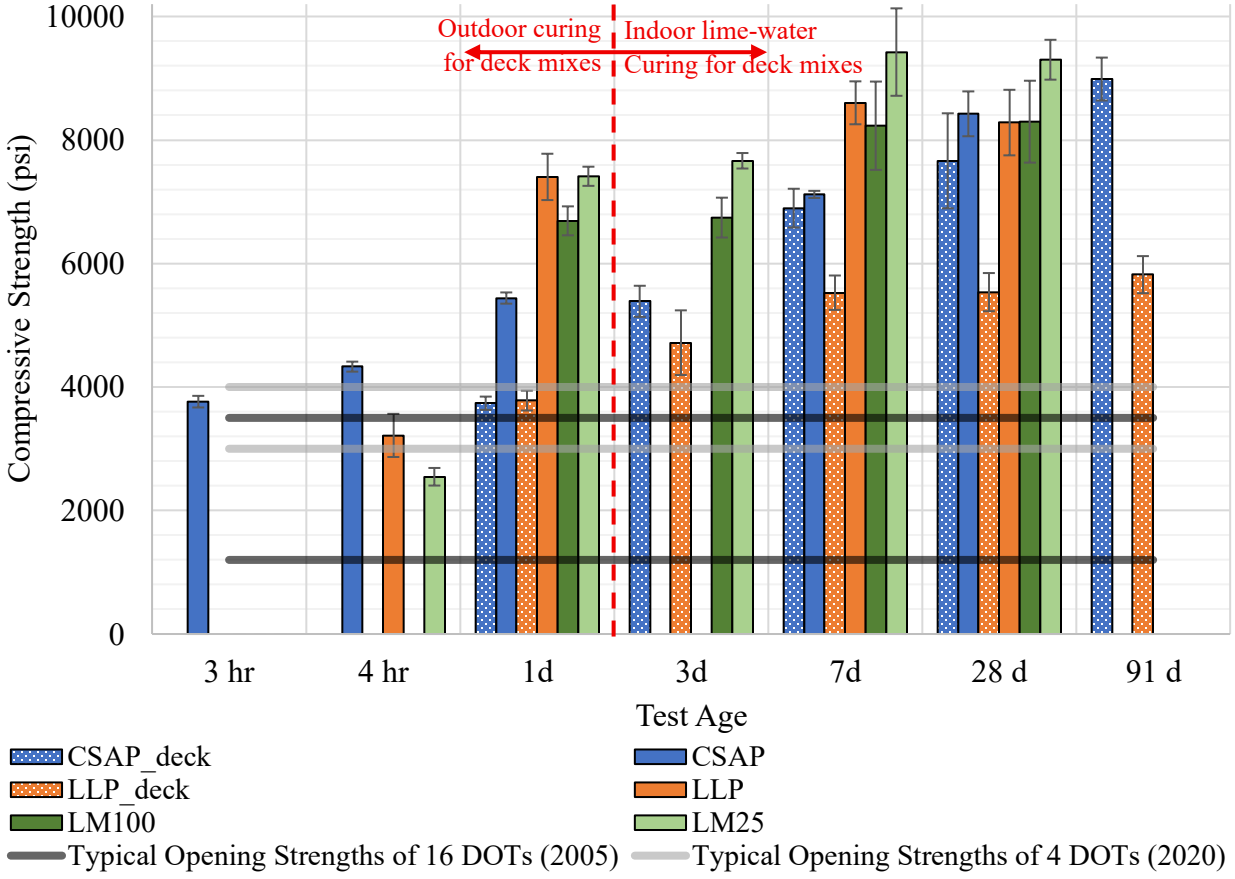

Figure 4-10: Compressive strength of field-scale specimens

By 1 day, both deck mixes reached just under 4000 psi. Over the following 28 days, both continued to gain strength, with CSAP_deck surpassing LLP_deck by day 3. At later ages,

CSAP_deck continued to gain significant strength, while LLP_deck only experienced a slight strength gain from 7 days to 91 days. These trends differ from those observed in the laboratory specimens.

In the laboratory field-scale tests, only the CSAP mix reached 4000 psi within 4 hours. However, all lab mixes were within range of the opening strengths of the sampled 2005 DOT standards (Van Dam et al., 2005), indicating that they could potentially be used for early opening to traffic. By 1 day, all mixes had exceeded 4000 psi, with CSAP exhibiting the lowest strength and being significantly outperformed by LLP. This trend contrasts with the deck mix results but aligns with earlier laboratory-scale characterization findings. Throughout the testing period, LLP outperformed CSAP until 28 days, after which their strengths became comparable.

The difference in strength gain between the laboratory and deck mixes may be attributed primarily to curing conditions. Since the deck mixes were cured outdoors, the ambient temperature was likely lower and more variable than in the controlled laboratory environment, contributing to slower initial hydration and delayed strength development. However, after this initial retardation, the hydration rate of the CSAP_deck appeared to align closely with that of the laboratory CSAP series, resulting in steady strength gain through 91 days. In contrast, the hydration rate for LLP_deck did not appear to recover to match that of the laboratory LLP mix.

This discrepancy may be attributed to chemical interactions between the liquid forms of Low-P^{TM} polymer, AEA, and/or HRWR and the cementitious system, in contrast to the powdered formulation in which Low-P^{TM}, AEA, and HRWR were pre-blended into the cement. The LLP system may also exhibit greater sensitivity to admixture compatibility and curing conditions, making it more susceptible to reduced performance in field applications—particularly in colder or drier environments. However, the temperature profiles shown in Figure 4-9 suggest that the rate of hydration was higher in the LLP mix, as indicated by the greater

change in internal temperature compared to the SB- or EA-applied CSAP mixes. Further investigation is needed to fully understand the differences between these systems.

Among the latex-modified mixes, LM25 consistently outperformed LM100 and achieved the highest strength of the lab mix series. This performance contrasts with the LM25 specimens cast during the characterization phase, which were consistently weaker than both the CSAP and LLP mixes. Furthermore, at 3 and 4 hours, the latex-modified mixes showed limited early strength development, consistent with the delayed setting behavior reported by Li et al. (2018). This delay is likely attributed to the presence of polymers, which may interfere with early hydration reactions by forming films around the cement particles.

Despite the slow early-strength development, latex-modified performance improved significantly after 1 day. By 7 days, LM25 had surpassed all mixes in strength. These results suggest that while latex-modified systems may be unsuitable for applications requiring rapid strength gain, they offer superior long-term strength potential, likely due to improved microstructural development and crack resistance contributed by the polymer phase.

4.2.1.3. Split Tensile Strength

The results of the split tensile strength test are presented in Figure 4-11. At 1 day, CSAP and LM25 exhibited similar tensile strengths, but were outperformed by LLP and LM100. By 28 days, LM100 minimal strength gain, while LM25 achieved strength comparable to LM100, reflecting the long-term strength development also observed in the compressive strength results. In contrast, the LLP mix experienced a notable decrease in strength, while the CSAP mix showed only marginal improvement. This reduction in the LLP mix's strength may be attributed to anomalies in the tested specimens, or it may indicate a poorly developed later-age microstructure that compromised tensile performance.

For the deck mixtures, both were significantly weaker than the laboratory mixes at 1 day, with LLP_deck performing slightly better than CSAP_deck. By 28 days, CSAP_deck had gained strength comparable to the CSAP lab mix, whereas LLP_deck showed little change from its 1-day strength. These tensile strength results are consistent with the compressive strength trends, further supporting the observation of delayed hydration in the CSAP_deck mix, but the limited strength development of the LLP_deck mix.

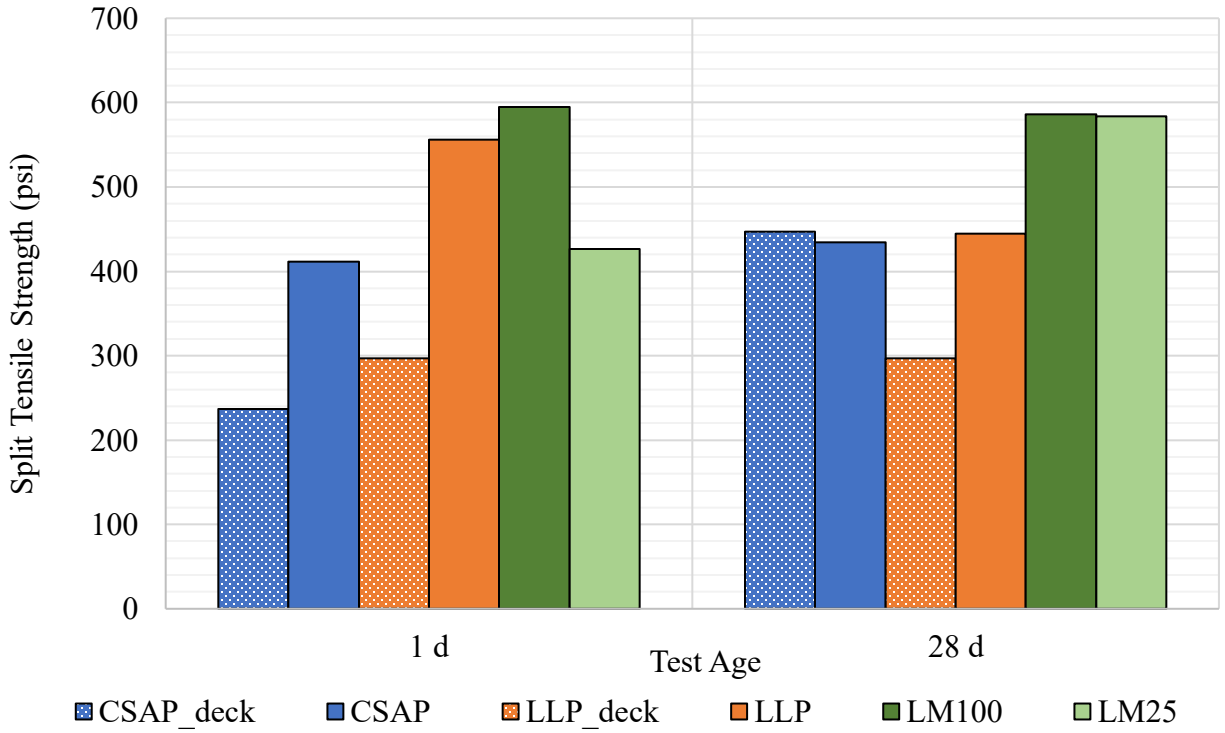

Figure 4-11: Split tensile strength of field-scale specimens

4.2.1.4. Flexural Strength

The modulus of rupture, calculated from flexural testing, is shown in Figure 4-12. The horizontal lines in the figure indicate the modulus of rupture thresholds specified by various state DOTs that must be met before reopening high-early strength concrete overlays to traffic (Cavalline et al., 2020; Van Dam et al., 2005).

All mixes fell within the range of flexural strengths sampled from the 2005 DOT standards (Van Dam et al., 2005), suggesting potential suitability for early traffic opening. However, the two latex-modified mixes did not meet the range sampled from the 2020 DOT standards (Cavalline et al., 2020), indicating they may not satisfy more recent strength requirements.

Both latex-modified mixes exhibited low strengths at 1 day, in contrast to the higher early-age compressive and tensile strengths observed. However, both mixes demonstrated substantial strength gains by 28 days, with LM100 achieving the highest strength among all laboratory and deck series mixes. This suggests that the full benefits of latex modification are realized over time as the polymer matrix continues to develop and integrate with the cement hydration products, improving flexural capacity among other mechanical properties.

At 1 day, the LLP mix showed the highest strength, followed by CSAP. The same trend was observed in the corresponding deck mixes, though with slightly reduced strengths, likely due to variability in field curing conditions. By 28 days, the trend reversed—CSAP surpassed LLP in flexural strength, while LLP experienced a slight decrease, consistent with the tensile strength results. This decline may, again, be due to anomalies in the tested specimens or could reflect a less-developed later-age microstructure that limited both flexural and tensile performance. The similar behavior observed in the deck mixes reinforces the reliability of these trends under both controlled laboratory and field conditions.

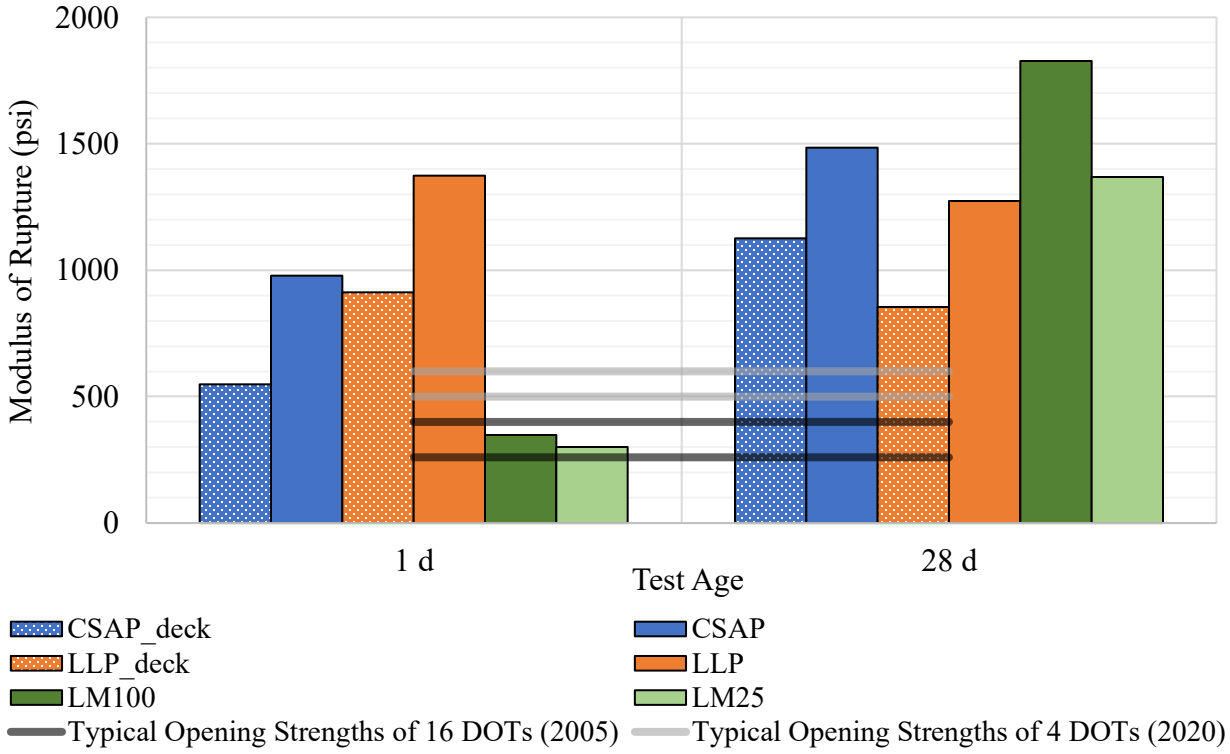

Figure 4-12: Flexural strength of field-scale specimens

4.2.1.5. Modulus of Elasticity

The modulus of elasticity (MOE) for each mix is shown in Figure 4-13. All mixes exhibited an overall increase in MOE over time. At days 1 and 3, LM25 was marginally stiffer than LM100; however, by day 28, LM25 showed a significant increase in stiffness, while LM100 exhibited only a slight improvement. Latex polymers form a flexible film within the cement, and this polymer phase is significantly less stiff than the cementitious phase, resulting in a more flexible composite material. This likely explains why the reduced latex dosage in LM25 led a higher MOE compared to LM100.

For the CSAP and LLP mixes, both had similar stiffness at day 1, but LLP gained stiffness at a much faster rate throughout the testing period, ultimately achieving the highest stiffness among all the mixes. In contrast, for the deck mixes, although LLP was initially stiffer at day 1, CSAP reached comparable stiffness by day 3 and eventually surpassed LLP by day 28,

indicating a faster rate of stiffness for CSAP than LLP. This difference may reflect the varying chemical interactions of the CSA systems with the admixtures used in the outdoor deck mixes compared to those used in the laboratory, similar to the trend seen with the compressive strengths.

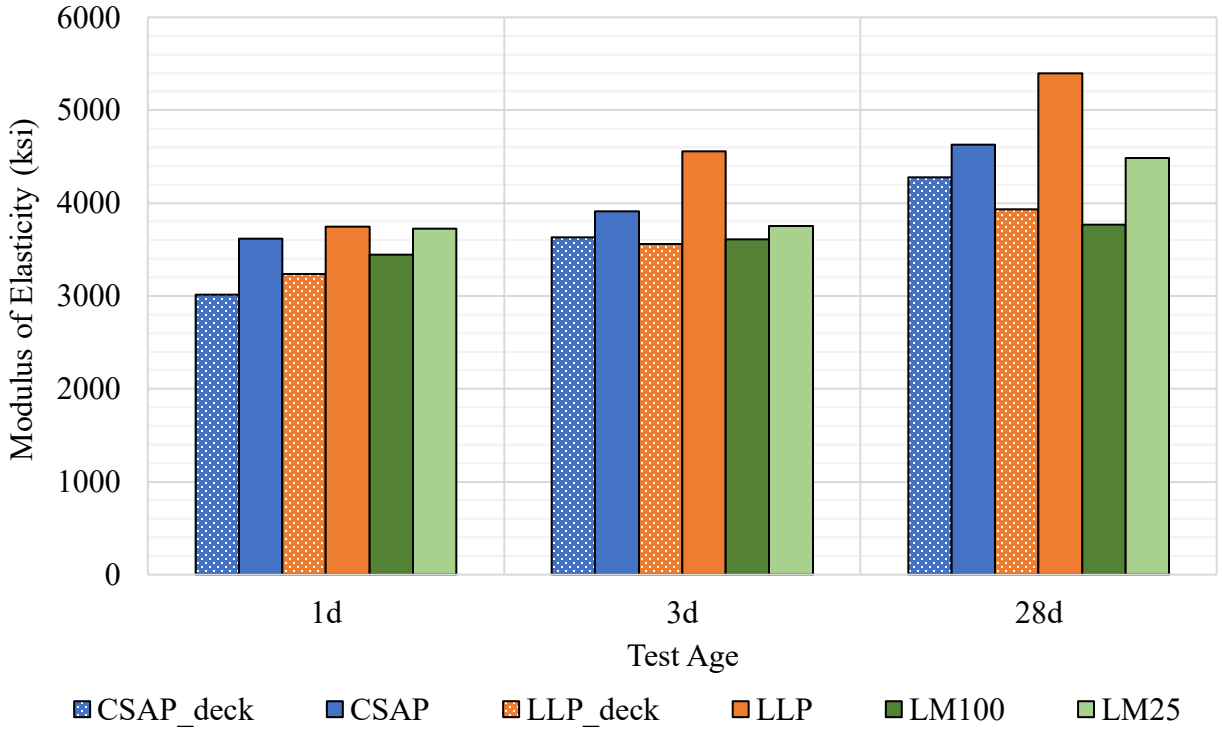

Figure 4-13: Modulus of elasticity of field-scale specimens

4.2.1.6. Drying Shrinkage

Figure 4-14 shows the drying shrinkage of the specimens. The drying shrinkage of the OPC substrate used in the mini-bridge decks was also plotted alongside the tested specimens for reference, revealing significantly greater shrinkage in the OPC mix compared to the CSA mixes.

CSAP and LLP each showed shrinkage trends similar to their corresponding deck mixes during the first two weeks, indicating that these materials closely replicated the early age drying behavior of the field mixtures. In contrast, the latex-modified mixes showed significantly higher shrinkage during this period, with the LM25 mix showing only slightly less shrinkage than

LM100. These results contrast the findings of Li et al. (2018) who observed that increasing latex content generally reduced shrinkage. Although styrene butadiene rubber (SBR), the same kind of latex used in this study, was noted in their work to have the smallest effect among the tested latexes, reducing its dosage from 100% to 25% of the standard led to about a 6% decrease in shrinkage.

The discrepancy between the two studies may be attributed to differences in CSA composition. Li et al. (2018) reported their cement contained 26.4% belite by weight, which falls short of the threshold to classify as BCSA cement under the proposed classification by Bescher and Kim (2019). Instead, their material may be better described as a Type A (accelerating additive) CSA cement, given its rapid-hardening characteristics. In contrast, the cement used in this project was classified as a BCSA, which may imply different chemical interactions with the latex and may explain the increased shrinkage at higher latex dosages observed here.

After two weeks, all laboratory series mixes exhibited a reduction in shrinkage rate, consistent with the CSA drying shrinkage curve seen by Sirtoli et al. (2020) where most deformation occurs at earl-ages. Interestingly, LM100 exhibited slight expansion by 56 days, possibly due to polymer film formation or delayed internal curing effects, while LM25 continued to shrink, potentially because its lower polymer content offered less restraint to drying stresses.

The deck series also showed a reduction in shrinkage after two weeks, though the decline was less pronounced than in the laboratory mixes. Since all the specimens were stored in the same conditions, this may suggest that there's a greater difference between the internal relative humidity of the deck mixes and the environmental relative humidity compared to the laboratory mixes. This may be due to the different degrees of hydration achieved at later ages in the deck mixes compared to the laboratory mixes.

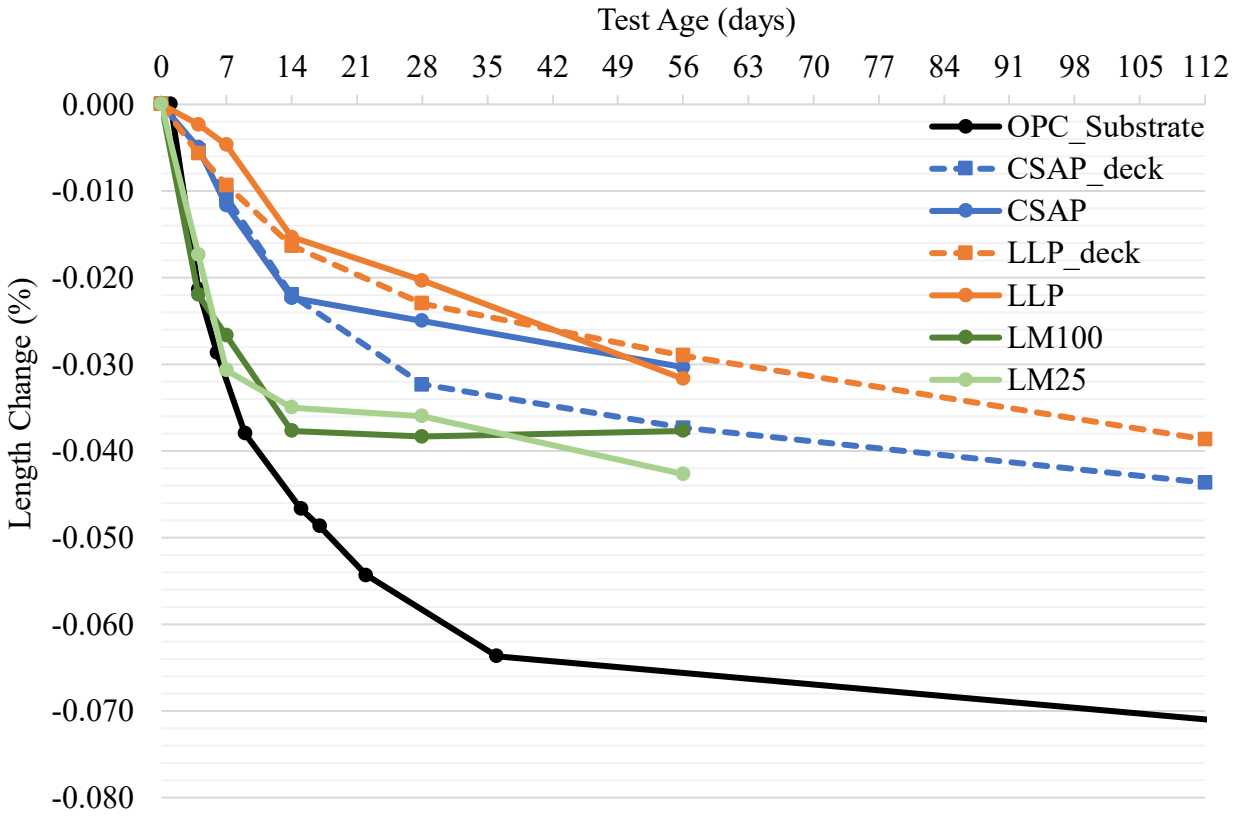

Figure 4-14: Drying shrinkage of field-scale specimens

4.2.1.7. Coefficient of Thermal Expansion

The coefficient of thermal expansion (CoTE) was measured for the field-scale specimens to evaluate their thermal sensitivity. Results are shown in Table 4-3, with higher CoTE values indicating greater response to temperature changes.

Table 4-3: Coefficient of thermal expansion of deck field-scale specimens

CSA Mixture	CoTE (in/in/°F)
CSAP_deck	$5.63x10^{-6}$
LLP_deck	$5.96x10^{-6}$
CSAP	$5.75x10^{-6}$
LLP	$5.63x10^{-6}$
LM100	$7.14x10^{-6}$
LM25	$5.76x10^{-6}$

The CoTE values of the laboratory CSAP_deck and LLP_deck mixes were relatively similar and within the same magnitude as the laboratory series mixes. Among the latex-modified mixes, LM25 had a CoTE comparable to the Low-P™ mixes. However, LM100 showed a significantly higher CoTE than all other specimens, possibly due to a testing error or an anomaly in the LM100 samples. Since the same aggregates were used for all the mixes, the similar CoTE values seen are not unexpected.

4.2.1.8. Field-Scale Testing Summary

To assess the mechanical performance of the CSA mixtures at a field scale, specimens were collected from the mini-bridge deck overlay pours and compared to those cast under controlled laboratory conditions. This approach provided consistency for comparing laboratory specimens while establishing a baseline for evaluating the field-cast specimens, highlighting the differences and limitations between controlled laboratory mixing and real-world field conditions.

- **Fresh properties:** The deck mixes showed similar trends in fresh properties compared to their corresponding lab mixes. However, the LLP lab mix produced significantly more air and exhibited greater slump than the deck mix, suggesting that the AEA used in the deck mix was less effective with the LLP system than with the CSAP system.

  Furthermore, the significant air content generated in the laboratory LLP mix, compared to the CSAP mix, further supports the hypothesis of AEA adsorption by polymer particles presented in the project's characterization study.

  Both latex-modified mixes produced similar air contents, but the lower slump observed in LM25 suggests that higher latex content may improve workability, potentially by reducing interparticle friction.

- **Compressive strength:** In the lab tests, LLP initially outperformed CSAP, but by 28 days their strengths became comparable. In contrast, the deck mixes reached just under 4000 psi at 1 day, significantly lower than the laboratory mixes. By 3 days, CSAP_deck surpassed LLP_deck and continued to gain strength throughout the testing period, showing trends similar to the CSAP lab mix, while LLP_deck plateaued after 7 days.

  The strength differences between lab and deck mixes are likely due to outdoor curing conditions, which slowed early hydration. Additionally, the limited strength gain in LLP_deck suggests that chemical interactions between the Low-P^{TM} polymer and admixtures may have suppressed hydration and the formation of key strength-gaining products.

  Among the latex-modified mixes, LM25 achieved the highest long-term strength despite delayed early strength development, consistent with prior findings that latex polymers can retard early hydration but improve long-term performance.

- **Split tensile strength:** The tensile strength results mirrored the compressive strength trends. At 1 day, LLP and LM100 outperformed CSAP and LM25, but by 28 days, LM25 matched

LM100, while LM100 showed minimal strength gain and LLP experienced a notable decrease, possibly due to specimen anomalies or a poorly developed later-age microstructure.

For the deck mixes, both were significantly weaker than the lab mixes at 1 day, with LLP_deck performing slightly better than CSAP_deck. However, by 28 days, CSAP_deck had gained strength comparable to its lab counterpart, while LLP_deck remained largely unchanged. These results further support observations of delayed hydration in CSAP_deck and limited strength development in LLP_deck.

- **Flexural strength:** Both latex-modified mixes exhibited low flexural strength at 1 day, but by 28 days, they demonstrated substantial strength gains, with LM100 achieving the highest flexural strength among all mixes. This indicates that the full benefits of latex modification are realized over time as the polymer matrix develops and integrates with cement hydration products, enhancing flexural capacity.

  At 1 day, LLP showed the highest flexural strength, followed by CSAP, with similar trends observed in the corresponding deck mixes, though field curing conditions likely reduced strength. By 28 days, CSAP surpassed LLP in flexural strength, while LLP experienced a slight decrease, consistent with tensile strength results. The similar behavior in both lab and deck mixes reinforces the reliability of these trends under both controlled and field conditions.

- **Modulus of elasticity:** All mixes showed increasing modulus of elasticity (MOE) over time. LM25 became significantly stiffer than LM100 by 28 days, likely due to its lower latex content, as the flexible polymer phase reduces stiffness.

  CSAP and LLP had similar stiffness at day 1 in the lab, but LLP gained stiffness more rapidly and achieved the highest MOE overall. In contrast, for the deck mixes, CSAP surpassed LLP in stiffness by 28 days, indicating different stiffness development trends in the

field. This reversal may be due to differing chemical interactions between the CSA systems and admixtures under outdoor curing conditions.

- **Drying shrinkage:** Results showed that CSAP and LLP closely matched their corresponding deck mixes during the first two weeks, indicating similar early-age behavior. In contrast, the latex-modified mixes exhibited significantly higher shrinkage, with LM25 showing only slightly less shrinkage than LM100. The increased shrinkage observed at higher latex dosages may be due to chemical interactions between the latex and the BCSA cement used in this study.

  After two weeks, shrinkage rates declined across all lab mixes, consistent with typical CSA behavior. Notably, LM100 showed slight expansion by 56 days, possibly due to polymer film formation or delayed internal curing, while LM25 continued to shrink, potentially due to lower polymer content providing less restraint to drying stresses. Deck mixes also showed a reduction in shrinkage over time, though the decline was less pronounced than in the lab mixes, possibly due to differences in internal relative humidity.

- **Coefficient of Thermal expansion:** The CoTE values for the laboratory and deck CSAP and LLP mixes were similar. Among the latex-modified mixes, LM25 had a CoTE similar to the Low-P™ mixes, while LM100 showed a much higher CoTE than all other specimens—likely due to a testing error or an anomaly in the LM100 samples.

The mixes demonstrated distinct performance trends influenced by composition, admixture compatibility, and curing conditions. Fresh properties were generally consistent between lab and deck mixes, though the LLP system showed sensitivity to admixture interactions, resulting in variations in workability and air content. In terms of strength development, the CSAP system outperformed LLP under field conditions, with LLP_deck exhibiting limited long-term gains likely due to suppressed hydration.

Among the latex-modified mixes, LM25, with reduced latex dosage, generally matched or exceeded the long-term mechanical performance of LM100, indicating that lower latex content can improve strength and stiffness while reducing shrinkage. These findings highlight the critical role of admixture compatibility and curing environment in optimizing CSA-based and polymer-modified concrete systems.

4.2.2. Concrete Embedded and Arc Welded Strain Gauges

To evaluate the short- and long-term performance of CSAP and LLP as overlays, strain gauges were used to monitor volume change and assess compatibility with different substrate finishes. Two types of strain gauges were employed: concrete-embedded strain gauges (CESGs) to measure strain within the CSA overlays, and arc-welded strain gauges (AWSGs) to measure strain in the substrate at the overlay-substrate interface. Figures 4-15 and 4-16 show the early-age and long-term volume change captured from the instrumented decks, respectively. Unless otherwise noted as "Substrate", the strain shown is of the CSA overlays.

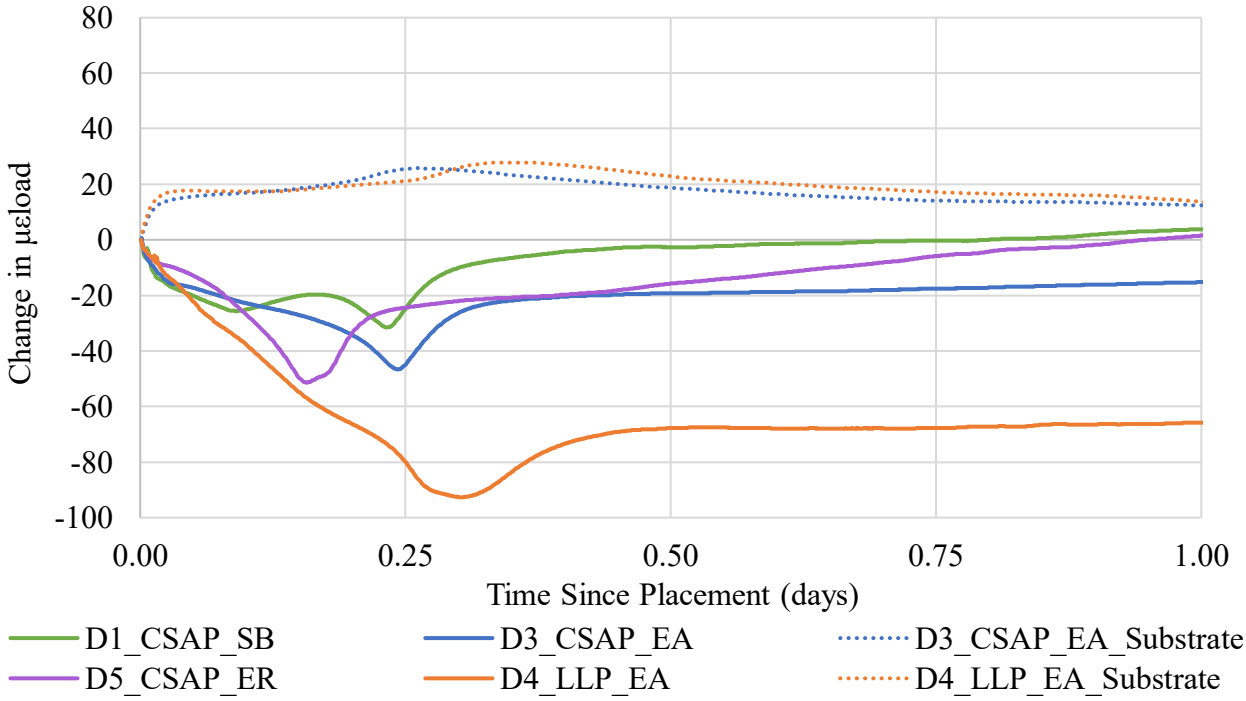

Figure 4-15: Early-age volume change of both the CSAP and LLP overlay decks

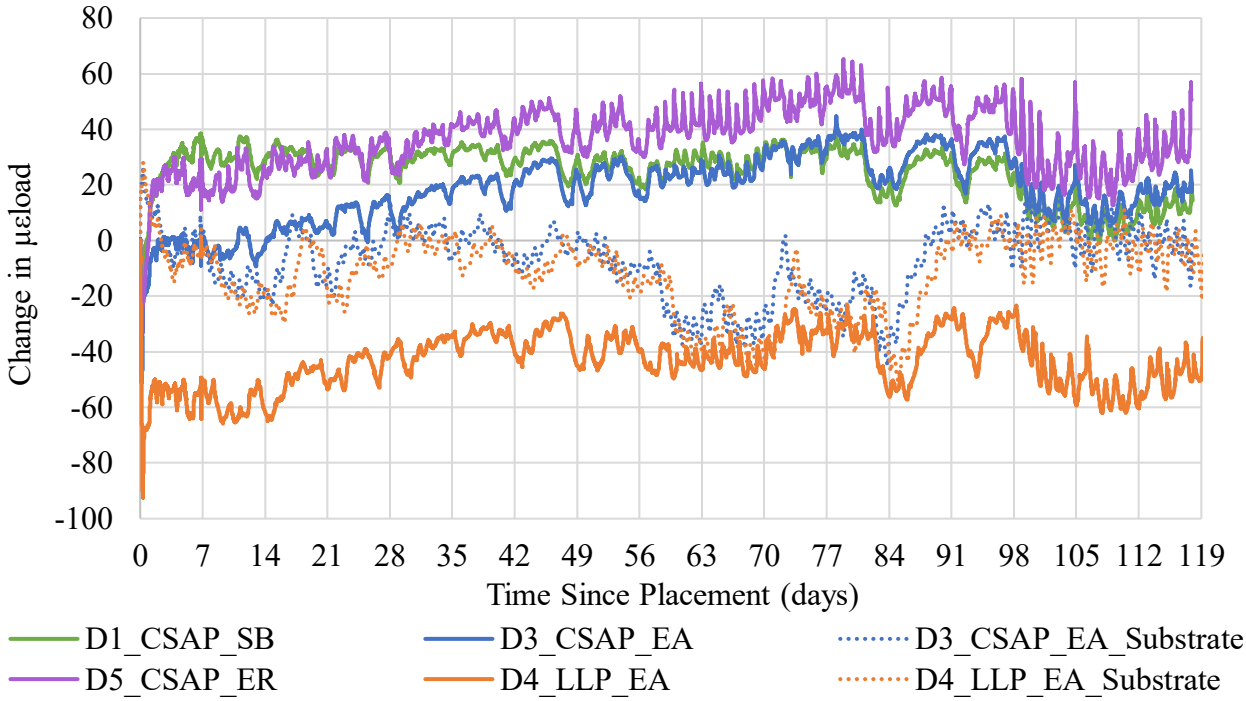

Figure 4-16: Long-term volume change of both the CSAP and LLP overlay decks

As shown in Figure 4-15, the LLP overlay experienced significant early-age shrinkage within the first 8 hours after casting, reaching a peak compressive strain of nearly -100 με. Following this initial contraction, the overlay exhibited a slight expansion of approximately 20 με before gradually stabilizing. All CSAP overlays followed a similar trend—initial shrinkage, followed by minor expansion and eventual stabilization. However, the magnitude of early-age shrinkage in the CSAP overlays was notably lower, ranging from approximately -50 με to -25 με.

These shrinkage behaviors differ from those described by Deo et al. (2023), where early expansion was expected due to 24 hours of wet burlap curing. The observed rapid contraction is more characteristic of autogenous shrinkage in BCSA cement-based systems, as noted by Sirtoli et al. (2020), suggesting that insufficient free water was available for complete hydration, leading to self-desiccation. The slight expansion observed afterward may be attributed to delayed

ettringite formation, potentially caused by the cooler ambient temperatures during casting, which can delay the hydration reactions responsible for early-age expansion.

The LLP overlay exhibited significantly greater shrinkage than the CSAP overlays. However, the shrinkage observed in the mini-bridge decks was inconsistent with the drying shrinkage measured from field-scale specimens cast using the same concrete. This discrepancy is likely due to differences in environmental exposure: the overlays were placed outdoors under natural conditions, while the shrinkage specimens were stored under controlled temperature and relative humidity. These findings suggest that both Low-P^{TM} systems are sensitive to early-age temperature effects.

Notably, the timing of shrinkage peaks varied across the overlays. Deck 5 reached its peak earliest at approximately 0.15 days (3.6 hours), while Deck 4 peaked latest at around 0.28 days (6.7 hours). Decks 1 and 3 peaked at roughly the same time, around 0.25 days (6 hours). These differences may be attributed to variations in CSA formulations and the presence or absence of exposed reinforcement. Steel reinforcement, with its higher thermal conductivity compared to concrete, may have accelerated local cooling and hydration, promoting earlier shrinkage. Additionally, the presence of rebar could have introduced moisture gradients that led to localized self-desiccation and early-age deformation.

It is also possible that some portion of the early-age deformation reflects not only autogenous and thermal effects but also minor contributions from plastic settlement or shrinkage. While not directly observed, the timing and magnitude of early strain in overlays with exposed rebar may be partially influenced by early differential settlement. As noted by Combrink et al. (2018), such behavior can arise from uneven settlement around rigid inclusions like reinforcing steel, particularly in flat elements like bridge decks that are exposed to drying conditions. Though autogenous shrinkage remains the dominant mechanism in these CSA-based systems,

localized plastic settlement could contribute to the observed variation in peak timing and magnitude across the overlays.

While Decks 1 and 3 peaked at similar times, the extent of shrinkage differed. Deck 1, which had a sandblasted (SB) finish, exhibited two shrinkage peaks: a small initial peak at 0.10 days (2.4 hours) and a larger one coinciding with Deck 3, which had an exposed aggregate (EA) finish. Despite the similar peak times, Deck 1 exhibited only about half the strain of Deck 3. Deck 5, which had both exposed rebar and an exposed aggregate (ER) finish, showed shrinkage similar in magnitude to Deck 3, further suggesting that surface finish significantly influences early-age shrinkage behavior.

The rougher, more porous texture of the EA finish may have increased the substrate's surface area, promoting greater moisture absorption and accelerating autogenous shrinkage. Additionally, the deeper grooves and irregular profile of the EA surface may have led to reduced mechanical restraint of the overlay. As reported by Manawadu et al. (2023), grooved or highly textured substrates do not always enhance bonding—particularly when overlay materials fail to adequately fill the deeper voids.

In such cases, the effective contact area is reduced, compromising mechanical interlock. Conversely, SB surfaces have been shown to provide stronger mechanical bonding due to more uniform and accessible surface roughness, which enhances overlay adherence. This difference in bond quality may have allowed greater unrestrained movement in the EA-finished overlays, contributing to the higher shrinkage observed in Decks 3 and 5 compared to Deck 1.

In contrast, the concrete substrates expanded by approximately 20 με immediately following overlay placement and showed minimal change in the subsequent hours. This early expansion is consistent with findings by Burris & Kurtis (2018), who reported rapid heat evolution during the early hydration of BCSA systems due to ettringite formation. The tensile

strain observed may reflect thermal expansion from this exothermic reaction. Interestingly, substrate shrinkage began around the same time as overlay expansion, possibly indicating the onset of strain equalization across the interface due to thermal and moisture gradients.

As shown in the long-term data in Figure 4-16, both overlay and substrate strains fluctuated in response to daily temperature cycles. Despite this variability, all systems gradually stabilized. The substrates returned to near-zero strain, hovering around their initial baseline of 0 με. Despite differences in early shrinkage, both Decks 1 and 3 eventually stabilized at approximately 30 με, though at different rates. Deck 1 reached stabilization within 7 days, whereas Deck 3 continued to expand before stabilizing at day 49. This delayed stabilization in Deck 3 may result from its rougher, more irregular EA finish, which could slow bond development and create localized stress concentrations that delay strain equalization.

Similarly, Deck 5 expanded continuously until stabilizing at around 40 με after 49 days. The combination of exposed aggregate and rebar likely contributed to both slower stabilization and slightly higher final strain. The presence of steel may have altered local thermal behavior and hydration kinetics, resulting in greater tensile strain due to differential thermal effects.

In contrast, the LLP overlay stabilized at a compressive strain of approximately -50 με. This may be attributed to an interaction between the LLP cement system and its admixtures that limited its expansive potential. Even if the admixtures did not directly inhibit expansion, the initial autogenous shrinkage was likely so significant that it caused the overlay to remain in residual compression despite subsequent expansion.

Notably, between days 63 and 91, the substrates of Decks 3 and 4 experienced significant shrinkage, while the overlay strains remained relatively stable. This divergence in behavior may be attributed to seasonal weather patterns in Seattle, WA—specifically, a period of snowfall and sustained low temperatures during early January and February. The pronounced shrinkage in the

substrates, in contrast to the minimal strain change in both CSAP and LLP overlays, suggests that the overlay systems are less sensitive to ambient temperature drops than the conventional PLC-based substrate concrete. This observation also suggests consistent early-age mechanical and chemical interaction between overlay and substrate across both types.

In summary, the results highlight clear differences in shrinkage behavior between LLP and CSAP overlay systems. All overlays exhibited early-age autogenous shrinkage followed by minor expansion and long-term stabilization; however, CSAP overlays consistently demonstrated lower shrinkage magnitudes and more favorable strain stabilization. This improved performance is likely due to the uniform dispersion of interground powdered polymer, increased air content, and the formation of a continuous polymer film that reduced capillary tension and internal drying.

Surface finish and the presence of exposed rebar were also shown to influence the timing and extent of shrinkage, with rougher or thermally conductive substrates accelerating early-age deformation. Overlays were generally more resilient to environmental temperature fluctuations than the PLC-based substrates, indicating effective strain buffering and interaction at the interface. Together, these findings suggest that CSAP systems offer more dimensional stability at early ages compared to LLP systems.

4.2.3. Crack Maps

In addition to collecting strain gauge data, the decks were manually inspected for cracks that developed after placement. Crack maps are presented in Figures 4-17 through 4-22. Each deck was assessed three times, with cracks from each assessment marked in a different color: red (1.5 weeks after casting), blue (approximately two months later), and green (approximately five months later).

For each assessment, the average crack width, crack frequency within each grid square, and crack orientation were recorded. Significant cracking occurred at an early age and was captured during the first assessment; therefore, only the first assessment data are presented in Table 4-4.

Due to aggregate distribution, some cracks appeared discontinuous; however, these smaller segments were considered part of a single, larger crack and were counted accordingly. The vertical direction was defined as the long side of the deck, while the transverse direction referred to the short side.

Table 4-4: Mini-bridge deck crack data from first assessment

Deck ID	Total Crack Count		Average Crack Width (in)	
	Vertical	Transverse	Vertical	Transverse
D1_CSAP_SB	0	0	N/A	N/A
D2_LLP_SB	10	5	0.005	0.004
D3_CSAP_EA	1	0	0.004	N/A
D4_LLP_EA	14	4	0.004	0.005
D5_CSAP_ER	1	0	0.004	N/A
D6_CSAP_EA	0	2	0.004	0.004

Among all the specimens, the decks with LLP overlays (D2 and 4) exhibited the most extensive early-age cracking, with significant cracking observed on all sides during the first assessment. This aligns with the large initial shrinkage measured in the LLP overlay strain gauges.

The SB CSAP deck (Deck 1) exhibited no visible cracks, while a vertical crack was observed on the EA CSAP deck (Deck 3), and a couple of transverse cracks on the other EA CSAP deck (Deck 6). While both LLP decks showed notable shrinkage, the EA-finished deck (Deck 4) exhibited more cracking than the SB-finished deck (Deck 2), as shown in Table 4-4. This is consistent with strain gauge results, which showed greater shrinkage in EA-finished overlays. The findings support the inference that EA finishing contributes to greater shrinkage development and cracking, whereas sandblasting provides better bonding and shrinkage restraint.

The ER CSAP deck (Deck 5) exhibited a similar degree of transverse cracking as the EA CSAP (Deck 3), which is consistent with their comparable shrinkage magnitudes as measured by the strain gauges. This suggests that while exposed rebar may have accelerated the rate of early-age shrinkage, it did not significantly affect the total amount of shrinkage.

Notably, no cracking was observed in the central regions of the decks (boxes 8–11), likely because the center was not subjected to the same level of shrinkage restraint and moisture loss as the edges, which were confined by formwork. Unique diagonal corner cracks were also observed, especially in the LLP decks. These are likely due to increased restraint and moisture loss where two edges meet, concentrating stress diagonally and resulting in corner cracking.

Decks 2, 3, 4, and 5 showed additional cracking in later assessments. Some of these were newly formed cracks, while others were existing cracks that had widened indicative of continued volume change as the overlays approached strain stabilization. These later-age cracks may have resulted from ongoing drying shrinkage but could also be influenced by daily and seasonal temperature fluctuations, as the decks were exposed to outdoor environmental conditions.

Among the instrumented decks, Decks 3, 4, and 5 experienced additional cracking, while Deck 1—the only SB-finished deck—did not. This is consistent with strain gauge data, which showed that the decks with additional cracking took longer to stabilize in strain, whereas Deck 1

stabilized more quickly. These findings suggest that EA surface finishing may contribute to delayed cracking and a prolonged period before strain stabilization.

In summary, the early-age cracking behavior observed across the decks closely aligned with measured shrinkage data from the strain gauges, highlighting the influence overlay material and substrate finish on crack development. Decks with LLP overlays (Decks 2 and 4) exhibited the most extensive early-age cracking, consistent with their high initial shrinkage. In contrast, the SB CSAP deck (Deck 1) showed no visible cracking and achieved early strain stabilization, underscoring the effectiveness of sandblasting in enhancing bonding and restraining shrinkage. EA finishing was associated with greater shrinkage and more cracking, particularly in LLP and CSAP overlays, suggesting it may contribute to prolonged strain development and delayed cracking.

The presence of transverse and vertical cracks, as well as unique corner cracks, reflected both material behavior and structural constraints such as formwork-induced edge restraint. Later-age cracking in several decks further pointed to the role of ongoing drying shrinkage and environmental exposure. Overall, the findings support the conclusion that CSAP systems exhibit greater early-age dimensional stability than LLP systems.

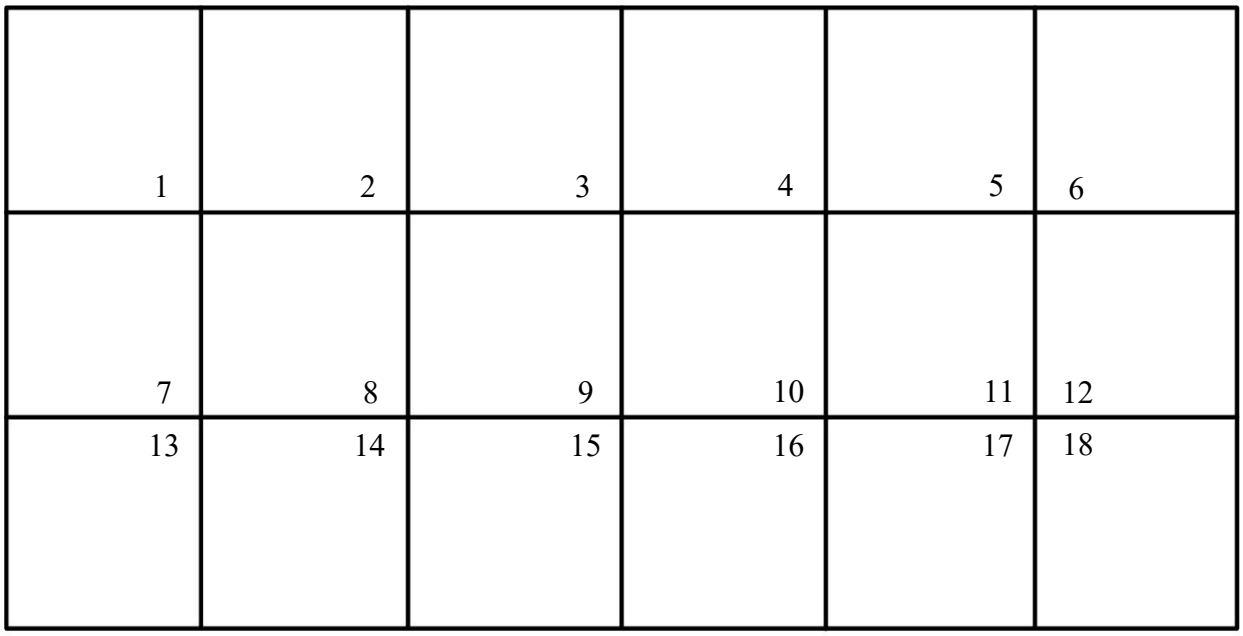

Figure 4-17: Crack map of Deck 1 – Sandblasted, CSAP

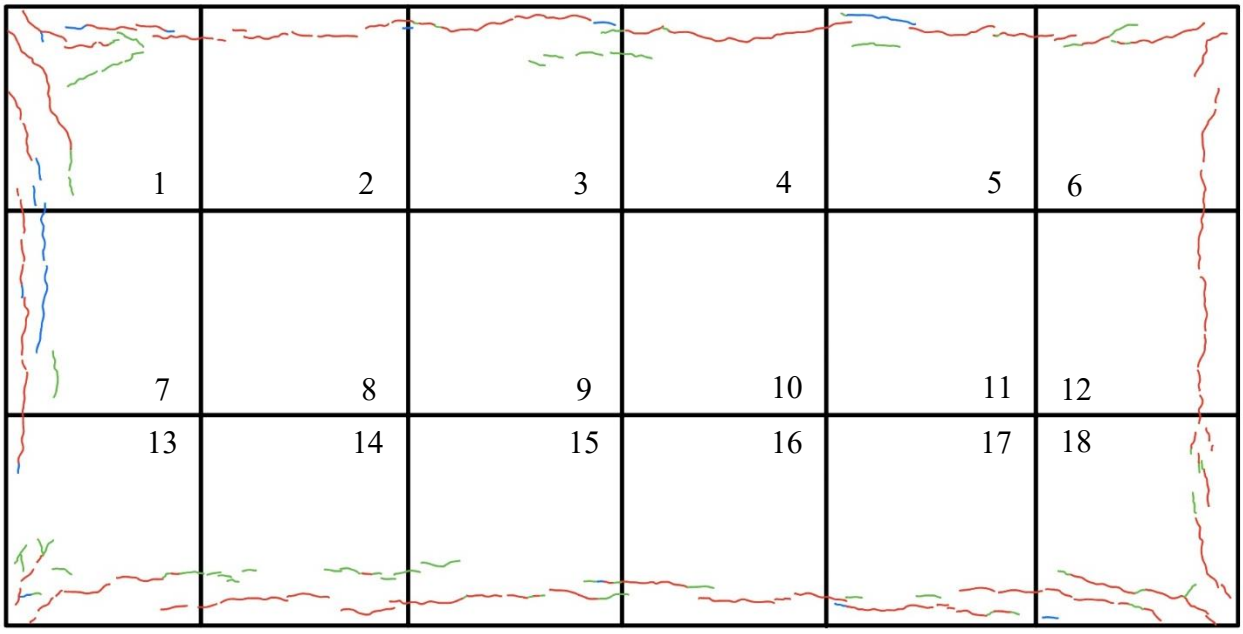

Figure 4-18: Crack map of Deck 2 – Sandblasted, LLP

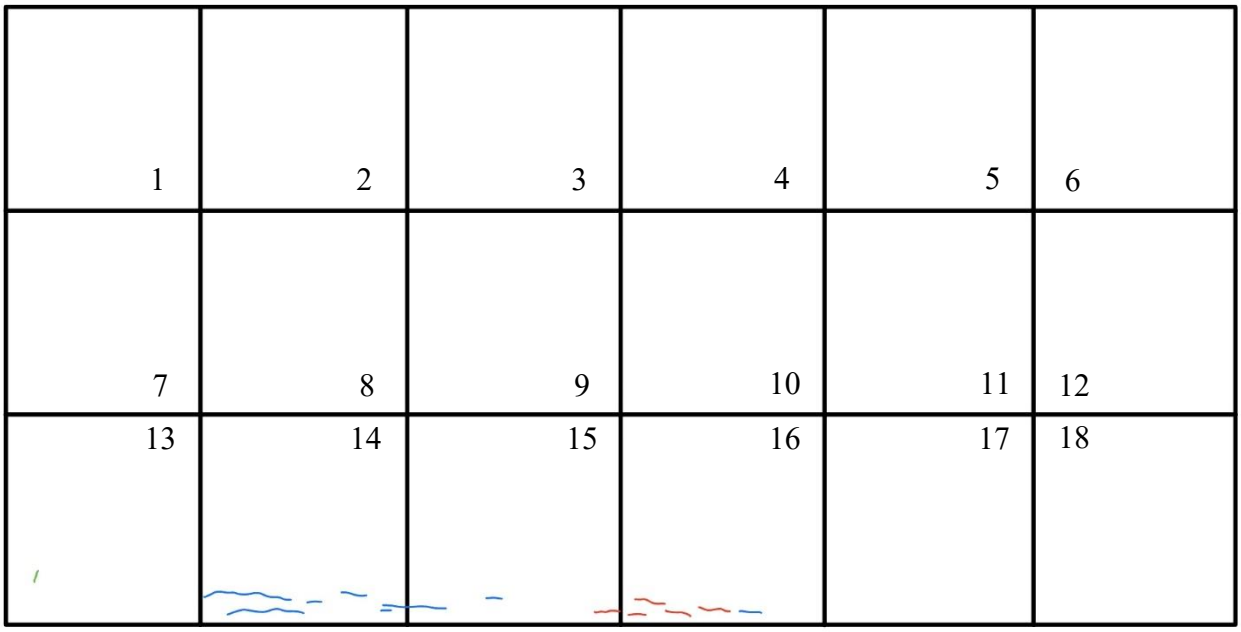

Figure 4-19: Crack map of Deck 3 – Exposed Aggregate, CSAP

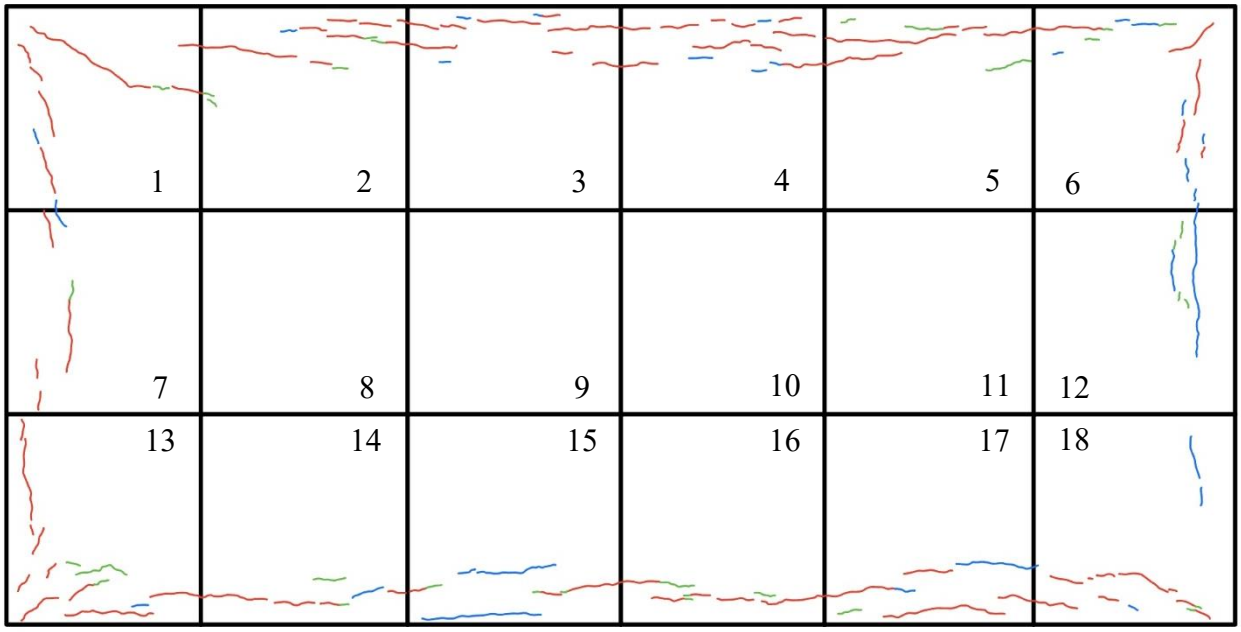

Figure 4-20: Crack map of Deck 4 – Exposed Aggregate, LLP

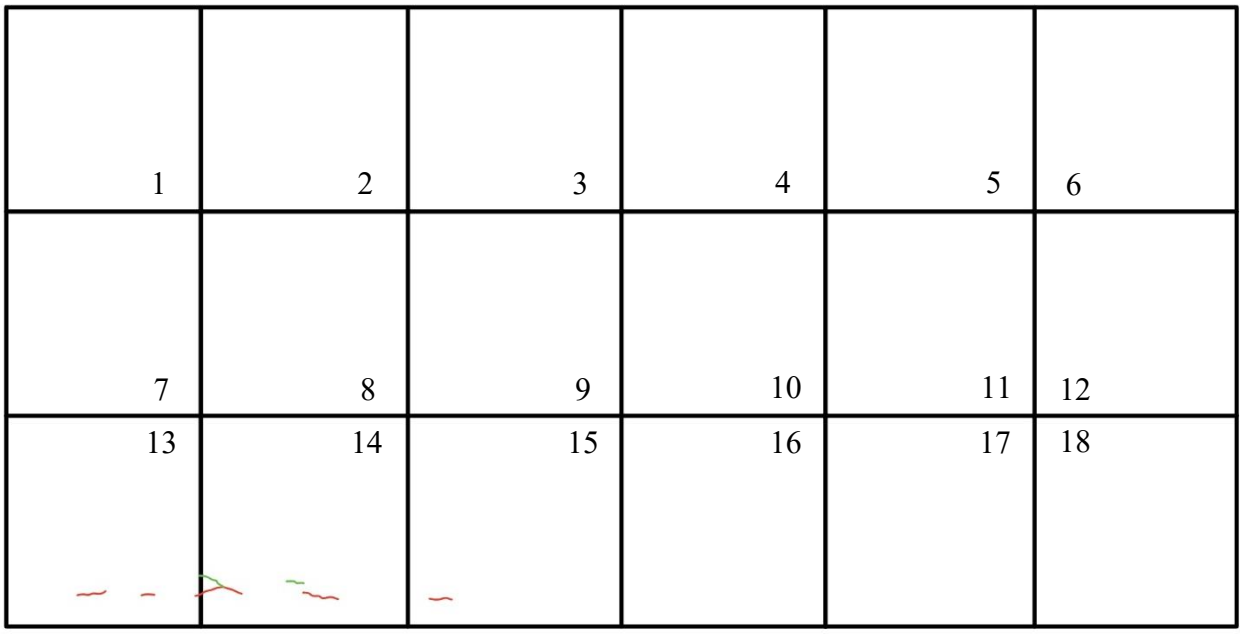

Figure 4-21: Crack map of Deck 5 – Exposed Rebar, CSAP

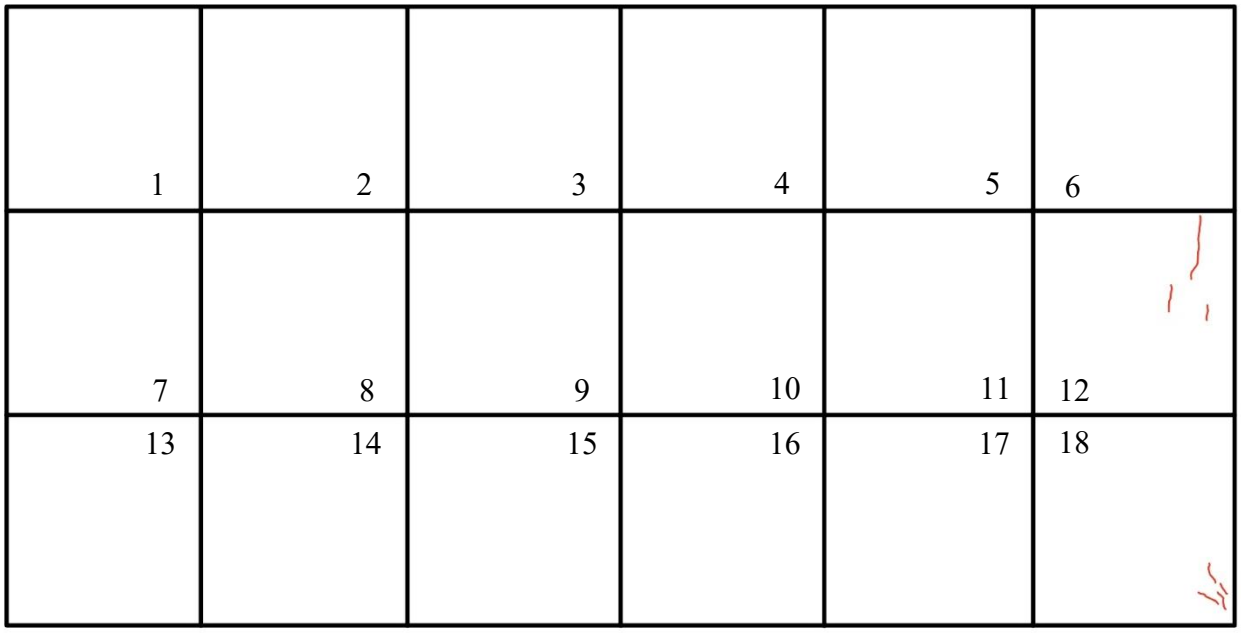

Figure 4-22: Crack map of Deck 6 – Exposed Aggregate, CSAP

4.3. Durability Study

CSA cements have been found to exhibit low permeability and minimal volume change, enhancing their durability and compatibility with existing substrates, making them an ideal

candidate for overlays. To thoroughly assess their performance, a series of durability tests were conducted, evaluating the CSA cements under various environmental and mechanical conditions.

4.3.1. Autogenous Deformation

The mixes were tested for autogenous deformation to evaluate the amount of self-desiccation experienced. The microstrain of the mixtures in the mortar series is presented in Figure 4-23, while the microstrain of the 23°C, 10°C, and 35°C cement paste series are presented below in Figures 4-23, 4-24, and 4-25 respectively.

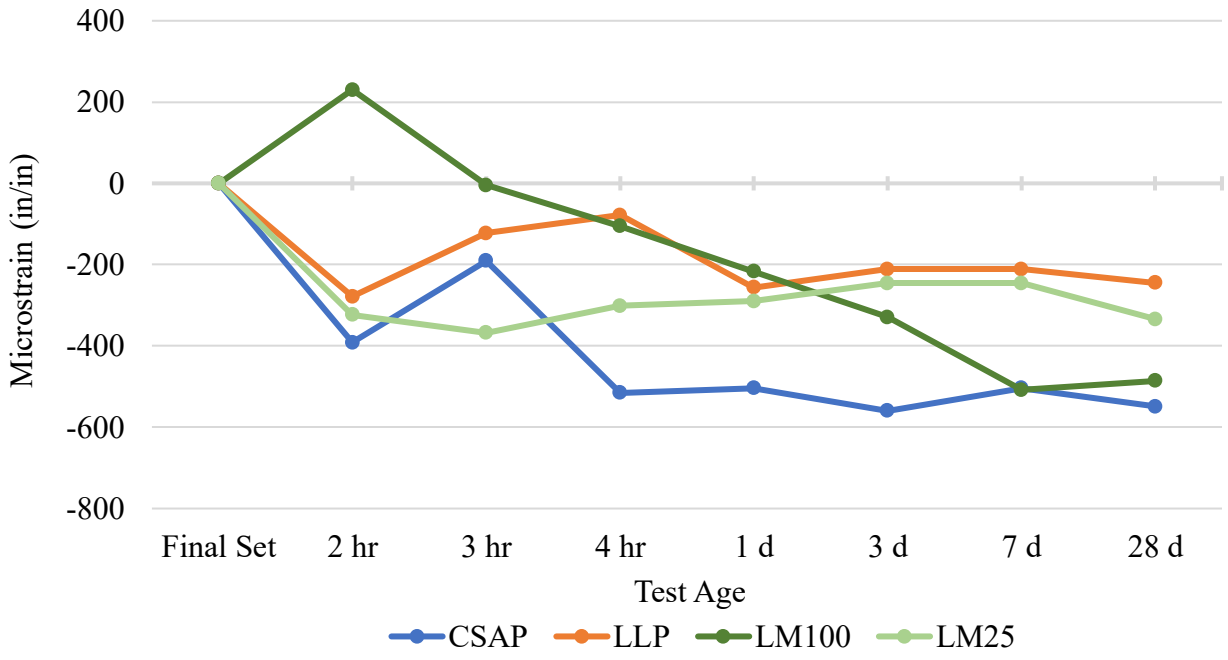

Figure 4-23: Microstrain of mortar mixes stored at 23°C

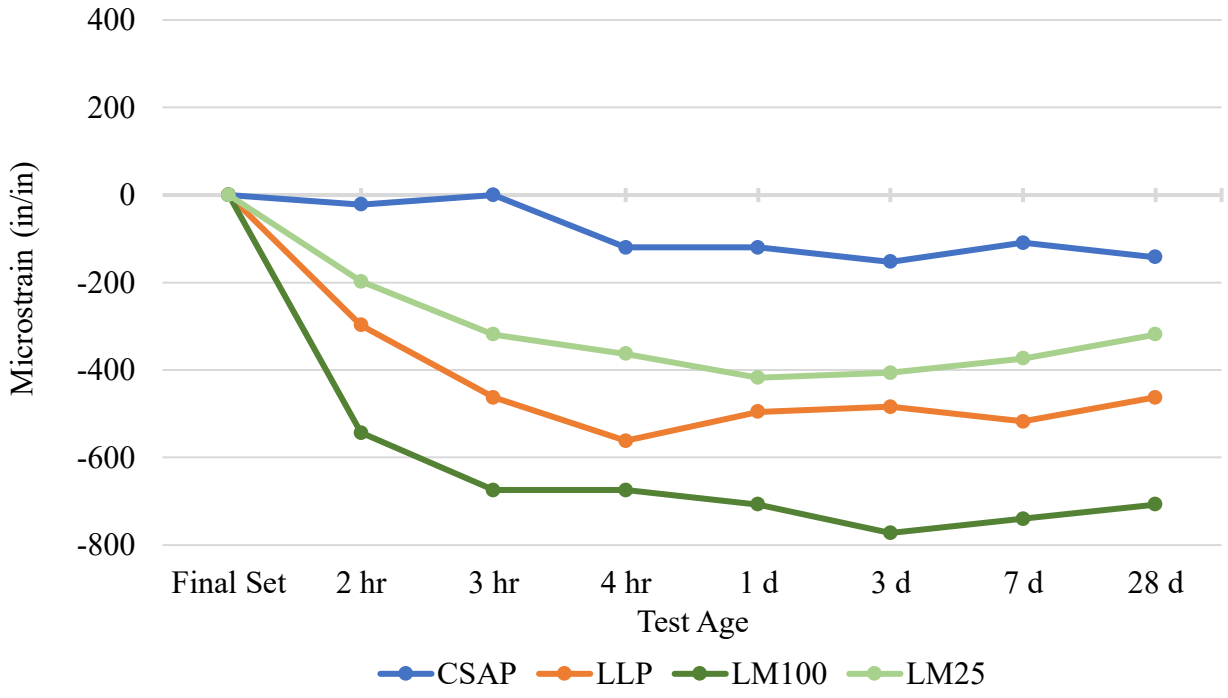

Figure 4-24: Microstrain of paste mixes stored at 23°C

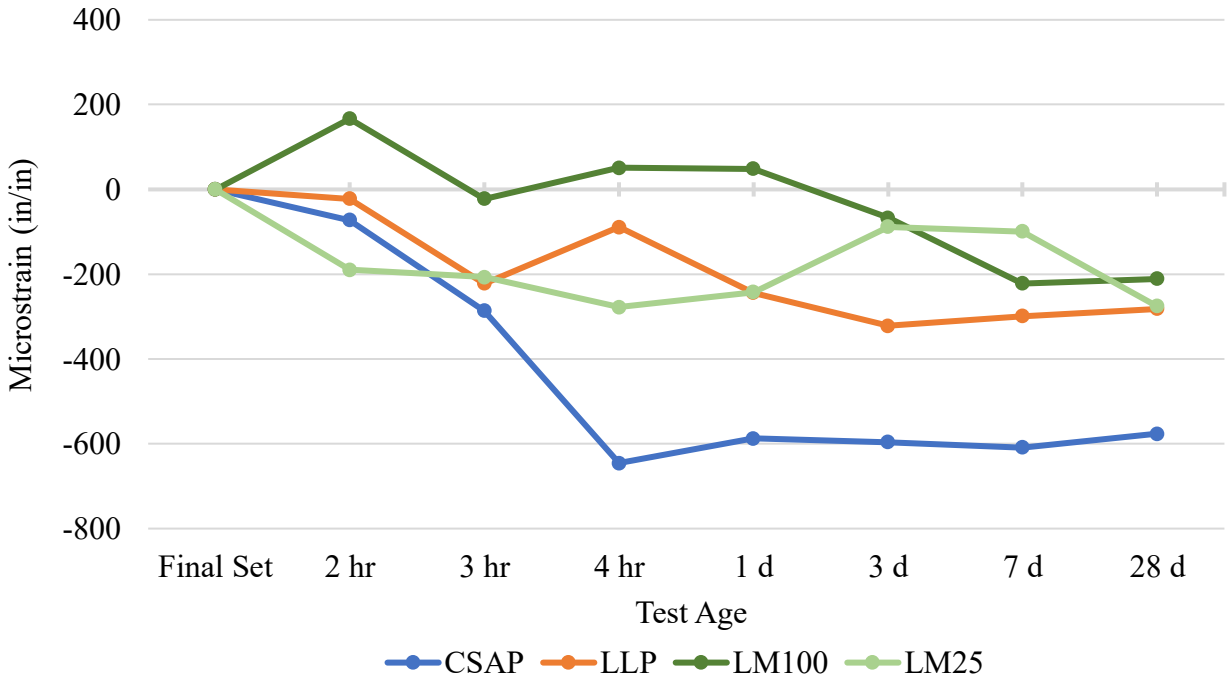

Figure 4-25: Microstrain of paste mixes stored at 10°C

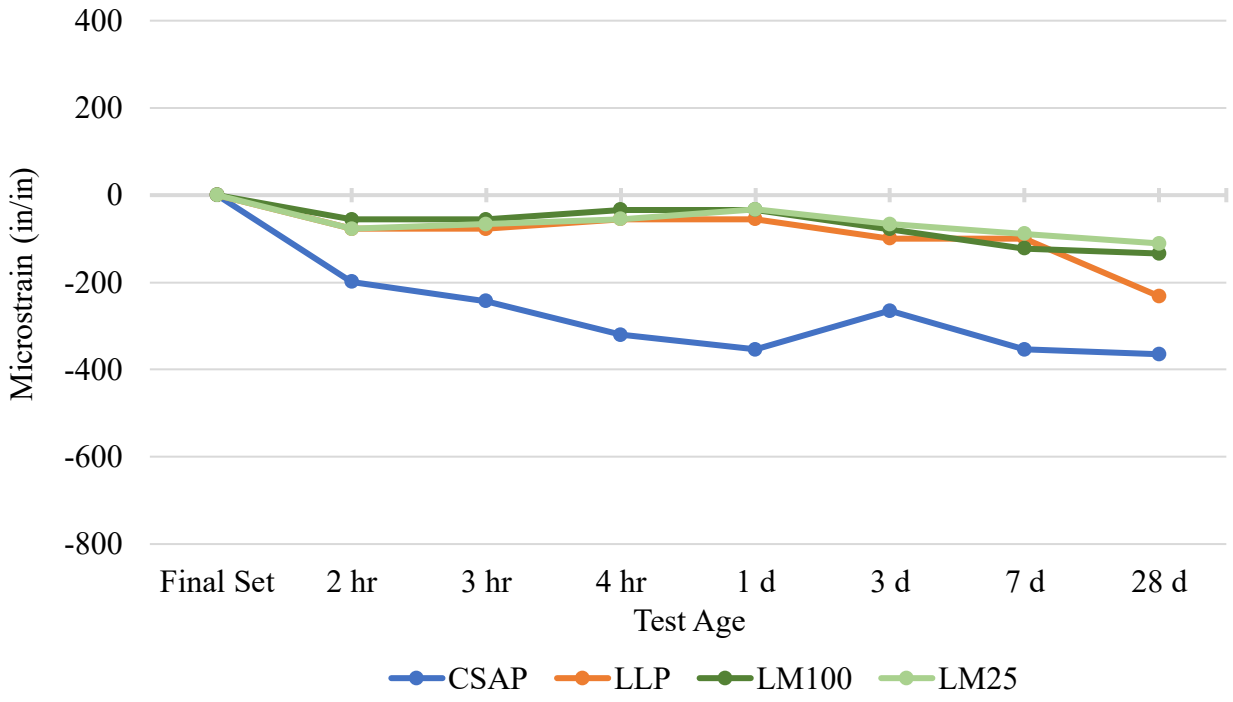

Figure 4-26: Microstrain of paste mixes stored at 35°C

Autogenous deformation was found to be lower in mortar samples than in cement pastes, which aligns with known behavior. The presence of aggregate in mortar reduces the overall volume of cement paste and restrains internal movement, resulting in reduced shrinkage. However, since the mortars were prepared by wet sieving concrete mixtures, the exact amount of paste present in each mortar sample is unknown, introducing some uncertainty into the results.

Among the mortars, the CSAP mixture experienced the greatest rate of shrinkage within the first 24 hours, after which it stabilized. In contrast, the LLP and LM25 mortars showed most of their shrinkage within the first two hours of testing and then remained relatively stable. The LM100 mortar behaved differently, continuing to shrink until about seven days before stabilizing. Some irregularities, such as small expansions observed in the data, may be attributed to the high sensitivity of the test method and are likely not representative of actual material behavior.

While direct comparisons between mortars and pastes are limited, some general observations can still be made. At 23°C, LLP and LM25 pastes behaved similarly, with steady shrinkage until about one day, followed by stabilization. LM25 exhibited slightly less shrinkage overall. The LM100 paste shrank more rapidly during the first few hours and began stabilizing around three hours. Interestingly, CSAP paste showed very minimal shrinkage at this temperature, which contrasts with its behavior in other test conditions.

Temperature had a noticeable effect on autogenous shrinkage. At 10°C, all mixes experienced more strain than at 35°C, indicating that lower temperatures increase autogenous shrinkage. LLP and LM25 pastes again showed similar trends, with slow shrinkage and stabilization starting around one day. LM100 paste exhibited minimal change during the first 24 hours but showed slight shrinkage at later ages. CSAP paste shrank quickly during the first four hours and remained stable afterward. At 35°C, shrinkage in all mixes, except CSAP, was minimal, likely due to faster hydration reactions that occurred before measurements began. CSAP, however, continued to shrink gradually over the first day before stabilizing, showing a different temperature sensitivity than the other mixtures.

As noted by Borštnar et al. (2020), BCSA cements tend to hydrate earlier and release more heat at higher temperatures, which likely occurred here and contributed to the reduced shrinkage at 35°C. The inverse can also appears to be true at 10°C, where slower reactions may have led to prolonged deformation. Although Shen et al. (2016) focused on high-performance OPC concrete, their findings also emphasize that curing temperature significantly affects the extent of hydration and microstructure development. These observations, while not specific to BCSA, help explain the marked differences in strain behavior observed across temperatures in this study.

The inconsistent behavior of the CSAP mixture across various tests may be due to the presence of the powdered HRWR integrated into its cement, while the other mixtures used plain CSA cement without such admixtures. The HRWR likely affects particle dispersion and hydration kinetics, although the specific influence is not fully understood. Nonetheless, its impact on the performance of CSAP is evident throughout the test results.

Across all conditions, LLP and LM25 consistently displayed similar shrinkage trends and magnitudes, aligning with the findings from Sirtoli et al. (2020). In contrast, LM100 generally shrank at a faster rate and to a greater extent, suggesting different hydration behavior and deformation characteristics compared to the other two blends.

4.3.2. Plastic Shrinkage

The mixes were also evaluated for plastic shrinkage behavior and surface cracking in concrete panels. Two specimens were tested for each mix. In all cases except LM100, only one of the two panels exhibited cracking. For LM100, both panels showed cracks. Table 4-5 presents the average crack width of the cracked panels in each mix; for LM100, the average of both panels was used. Additionally, Figures 4-27 through 4-30 show the crack maps of the panels. Cracks are lined in red, and in accordance with ASTM C1579 (ASTM International, 2021), the 1-inch boundary is marked with a black dashed line.

Table 4-5: Average crack width developed by plastic shrinkage

Mixture	Average Crack Width (in)	
	Vertical	Transverse
CSAP	N/A	0.0032
LLP	N/A	0.0025

LM100	0.0427	0.0521
LM25	N/A	0.0078

For the CSAP, LLP, and LM25 mixes, only one of the two specimens in each case exhibited cracking. These cracks appeared along the middle of the panels in the transverse direction, corresponding with the area of highest stress concentration. Among these three mixes, LM25 demonstrated the greatest average crack width—more than twice that of the LLP panel. CSAP also resulted in slightly larger crack widths than LLP. This trend aligns with the drying shrinkage results discussed in section 4.2.1.6.

The LM100 mix displayed a distinctly different behavior. Both of its specimens exhibited significant cracking in both transverse and vertical directions. Notably, the transverse cracks did not align with known stress riser locations, suggesting a different cracking mechanism was at play. Kuhlmann (1991) observed that latex-modified concrete can form a surface crust when exposed to air for prolonged periods while in the plastic state. Once this crust forms, the surface can become brittle and prone to tearing if disturbed, while the underlying material remains plastic. However, in this study, the small panel size allowed for finishing within minutes, making late-stage surface disturbance an unlikely cause.

Instead, the unusual cracking pattern in LM100 is likely attributable to differential shrinkage and setting behavior between the surface and interior of the panel. This behavior was only observed in LM100 and not in LM25, which suggests that the higher latex content in LM100 may have contributed to the formation of a surface crust, consistent with Kuhlmann's observations. In contrast, LM25 contained less latex, which was likely insufficient to induce the same crusting effect. As a result, LM25 exhibited the more typical transverse cracking aligned with the stress riser.

Interestingly, LM25 still showed larger average crack widths than either CSAP or LLP. Although the latex content in LM25 was lower, it may have been enough to cause slight shrinkage differentials, contributing to increased crack width relative to the other Low-P^{TM} CSA systems.

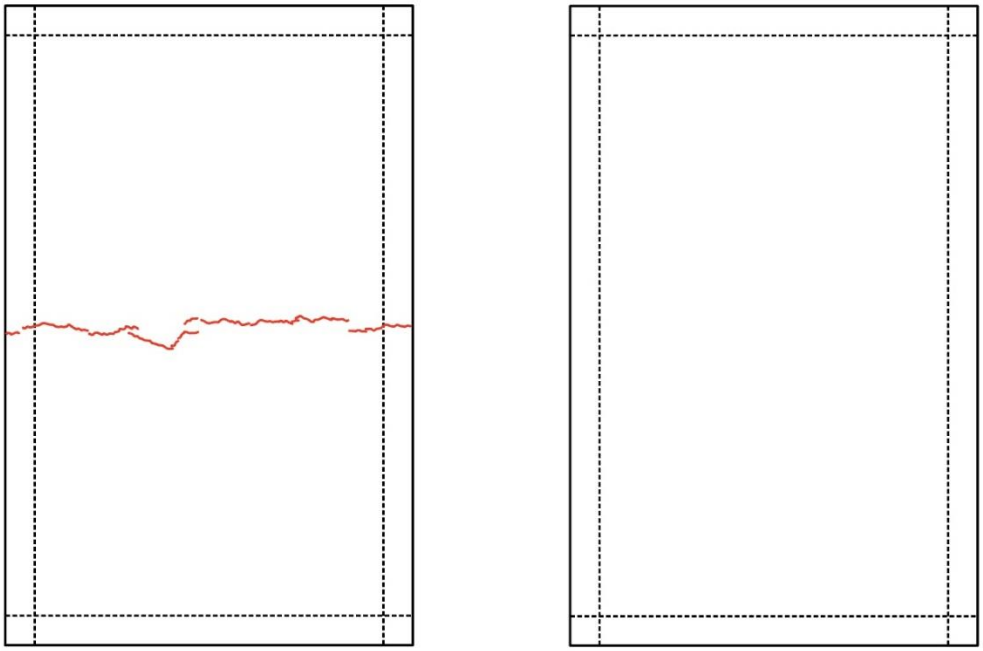

Figure 4-27: Crack map of CSAP plastic shrinkage panels

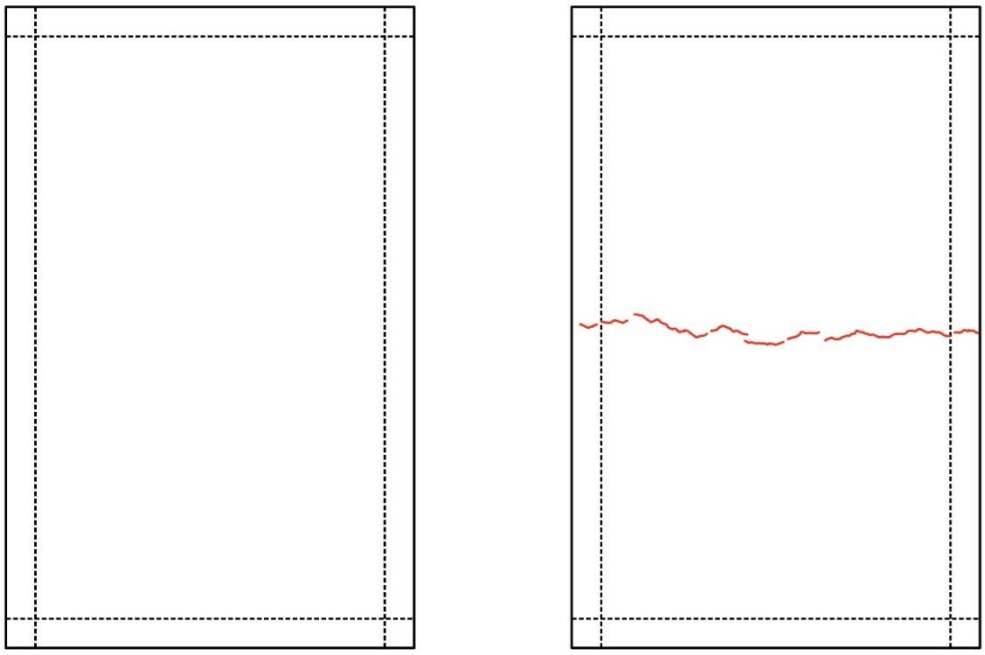

Figure 4-28: Crack map of LLP plastic shrinkage panels

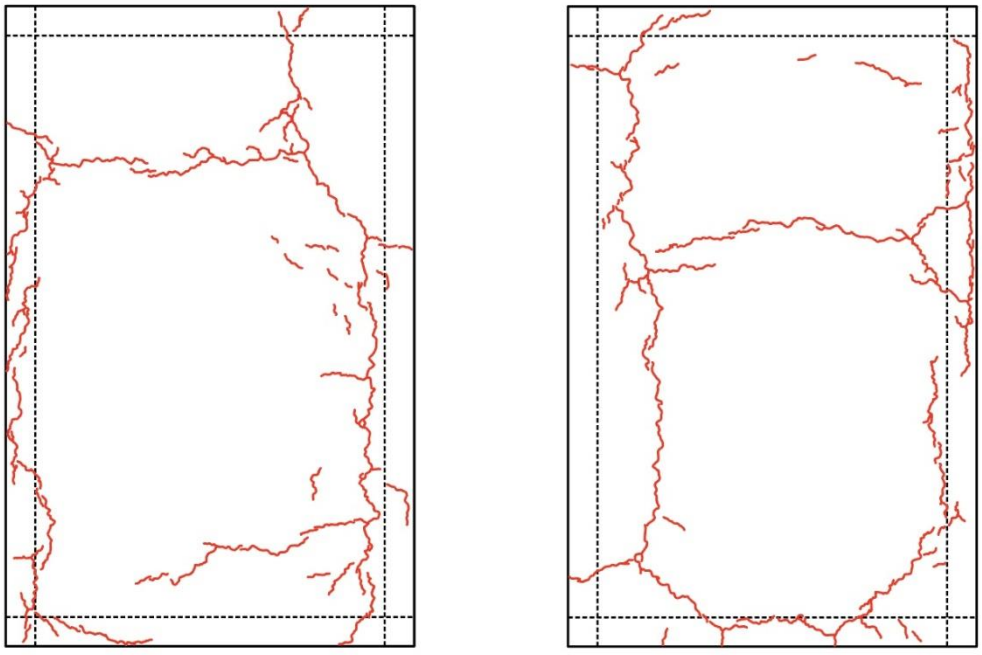

Figure 4-29: Crack map of LM100 plastic shrinkage panels

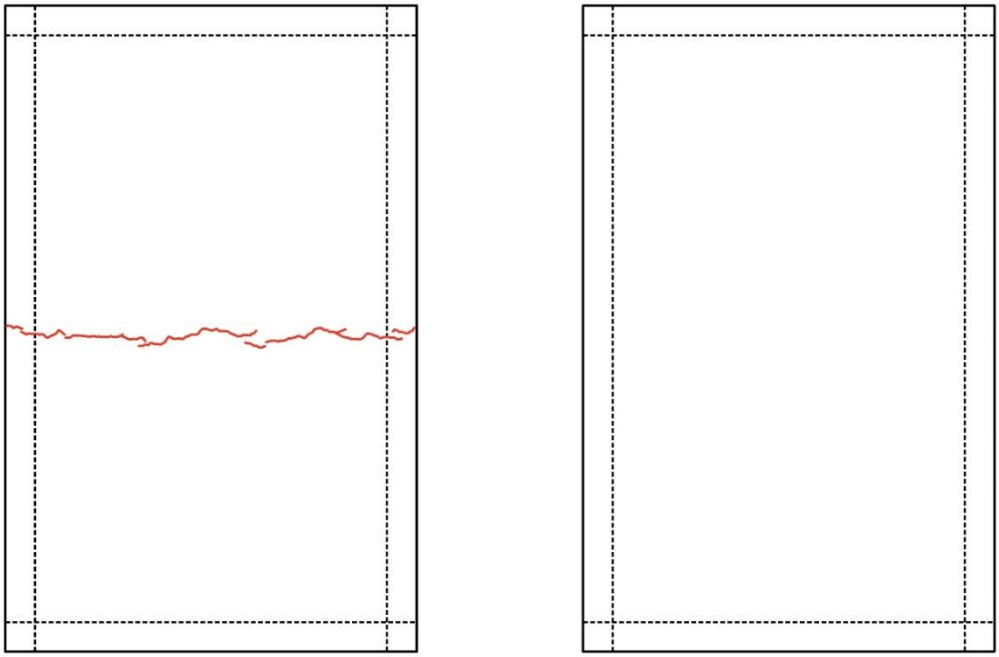

Figure 4-30: Crack map of LM25 plastic shrinkage panels

4.3.3. Freeze-Thaw Resistance

The concrete mixes were subjected to rapid freeze-thaw cycles to assess their performance under such environmental conditions. Table 4-6 presents the relative dynamic moduli of elasticity (RDME) and durability factors (DF) for each mix. RDME indicates stiffness retention during freeze-thaw cycles, with higher values indicating less internal damage. DF reflects the concrete's resistance to degradation under repeated cycles, with higher values signifying better durability.

Figure 4-31 visually compares the four mixtures by plotting RDME against the number of cycles, assuming exponential decay over the testing period. According to ASTM C666 (ASTM International, 2003), specimens should undergo 300 cycles or be stopped once RDME falls below 60%, indicating poor durability—whichever occurs first. In this study, all specimens

were tested until RDME became unmeasurable. The 60% threshold is indicated on the graph for reference.

Table 4-6: Freeze-thaw resistance test results

Mixture	% Relative Dynamic Modulus of Elasticity	Durability Factor
CSAP	37.9	38
LLP	100.5	100
LM100	97.2	97
LM25	57.1	57

Both CSAP and LM25 fell below the 60% RDME threshold, indicating poor durability. The CSAP mixture exhibited significantly lower performance compared to the LLP mixture, which may be attributed to its typically lower air content noted in sections 4.1.1. and 4.2.1.1.—a factor known to influence freeze-thaw resistance by affecting internal pressure relief mechanisms. However, the notable performance difference between the CSAP and LLP warrants further investigation. Interestingly, the % RDME for the LLP mixture exceeded 100%, likely due to the sensitivity or calibration of the testing equipment rather than actual increases in stiffness.

Among the latex-modified mixtures, LM100 outperformed LM25, likely due to the higher latex content. The increased latex dosage in LM100 likely formed a more continuous polymer film within the matrix, reducing porosity and improving the microstructure's resistance to water ingress and freeze-induced damage. These findings align with the results reported by Li et al. (2018), where the use of styrene-butadiene rubber (SBR) was shown to enhance freeze-thaw resistance in cement-based composites.

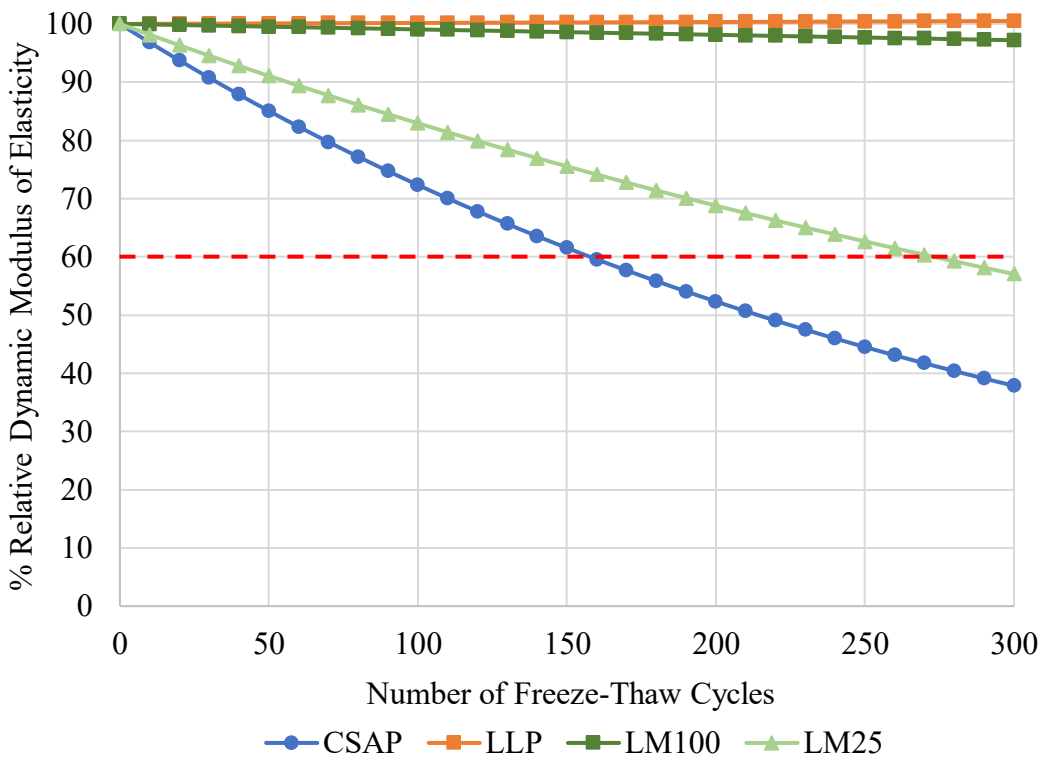

Figure 4-31: % Relative dynamic moduli of elasticity over freeze-thaw cycles

4.3.4. Salt-Scaling Resistance

The concrete mixes were also subjected to salt scaling to assess their performance in the presence of deicing salts. Two specimens of each mix were tested and visually evaluated according to the scale provided in ASTM C672 (ASTM International, 1998). The ratings of the specimens were averaged and are presented in Figure 4-32.

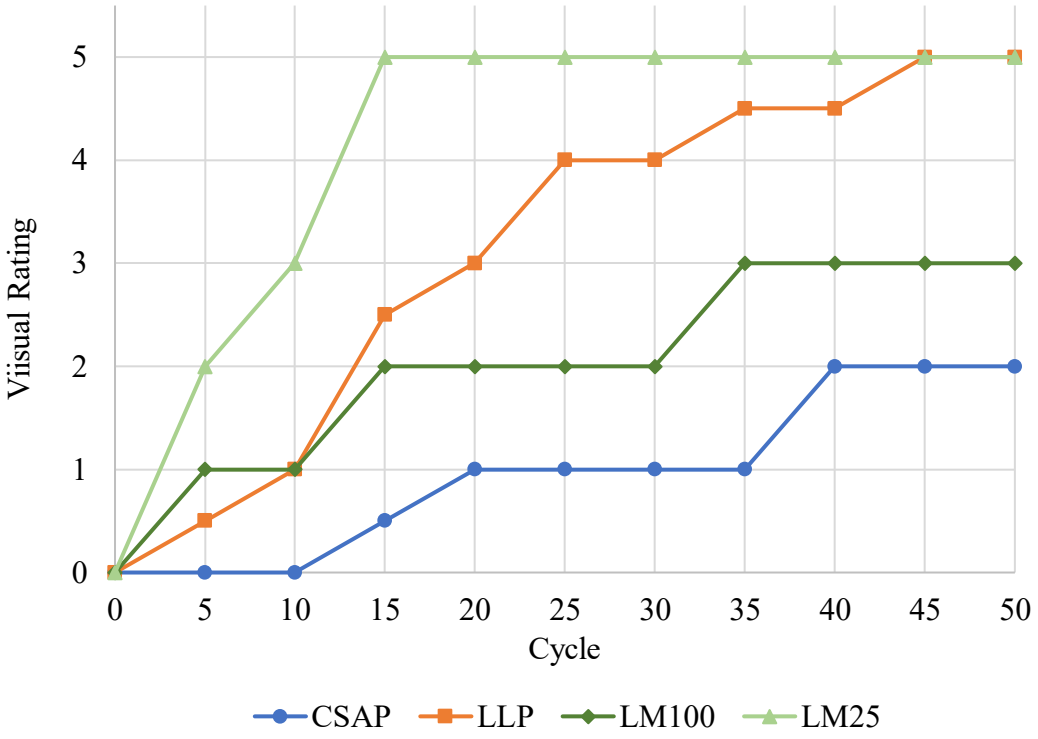

Figure 4-32: Visual rating of salt-scaling over cycles

In contrast to the freeze-thaw resistance results, the CSAP mix exhibited the least amount of salt scaling, indicating strong performance under exposure to deicing salts. On the other hand, the LLP mix demonstrated a steady progression of surface deterioration throughout the testing period. By the end of the test, LLP reached the highest and most severe salt-scaling rating. While the CSAP results are consistent with the findings reported by Moffatt (2016), the LLP results deviates from their observations. The contrasting results observed for CSAP and LLP highlight the need for further investigation into their performance differences.

The behavior of the latex-modified mixes in the salt scaling test closely aligned with their freeze-thaw resistance performance. LM25 exhibited significantly more surface degradation than LM100, likely due to LM100's higher latex content. Notably, LM25 was highly susceptible to salt scaling, showing substantial surface damage by cycle 15, at which point it received a rating of 5—the most severe level of scaling. These results are consistent with the findings of Yun et al.

(2004) who also observed improved salt scaling resistance with increasing latex content. This improvement is likely attributed to the formation of a more continuous polymer film at higher latex dosages, which reduces water penetration and enhances durability.

In Figure 4-33, the final visual ratings from the salt scaling test and the durability factors from the freeze-thaw test are plotted together. No clear trend was observed between the two. This lack of correlation may be attributed to the inherent sensitivity and limitations of both tests, particularly the salt scaling test. Despite best efforts to ensure consistency in specimen finishing and test observations, some variability may have occurred, potentially contributing to the differing results.

Additionally, it is important to recognize that, although the two tests assess durability under freezing conditions, they differ in methodology and in the mechanisms involved. In the freeze-thaw test, specimens are fully submerged, leading to internal hydrostatic pressure throughout the material. In contrast, the salt scaling test exposes only the surface to a salt solution, initiating a diffusion process from the top and creating a concentration gradient through the specimen. Therefore, while certain trends may appear to align between the two tests, a direct comparison or strong correlation cannot always be made due to the fundamental differences in test conditions and failure mechanisms.

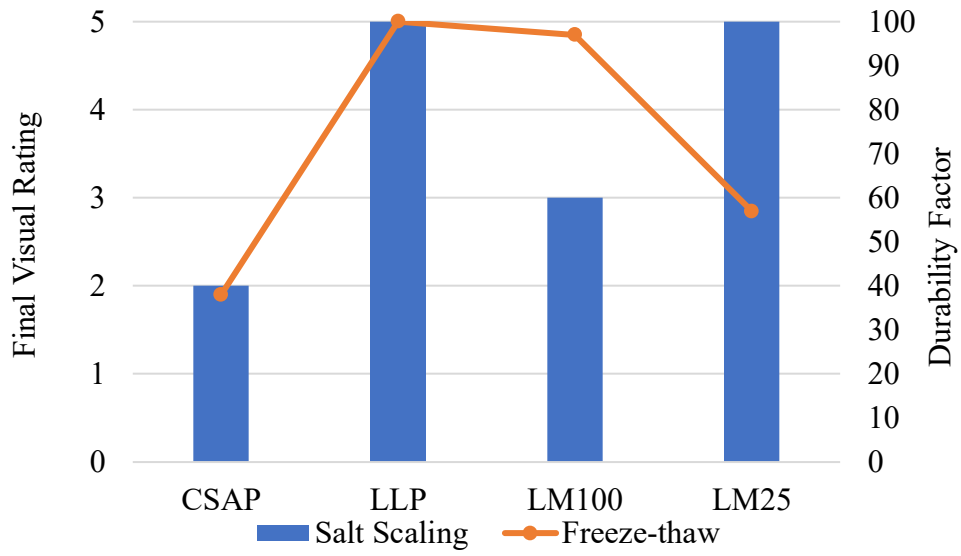

Figure 4-33: Comparison of freeze-thaw durability factor and salt-scaling visual rating

4.3.5. Slant-Shear Test

The mixes' overlay potential and compatibility with PLC substrates were evaluated using slant-shear tests at interface angles of 30°, 45°, and 60°. Figure X presents the measured shear and normal strengths at failure for each mix, test age, and angle. Figure Y shows the calculated bond strengths, with ultimate compressive strengths indicated as horizontal reference lines for comparison.

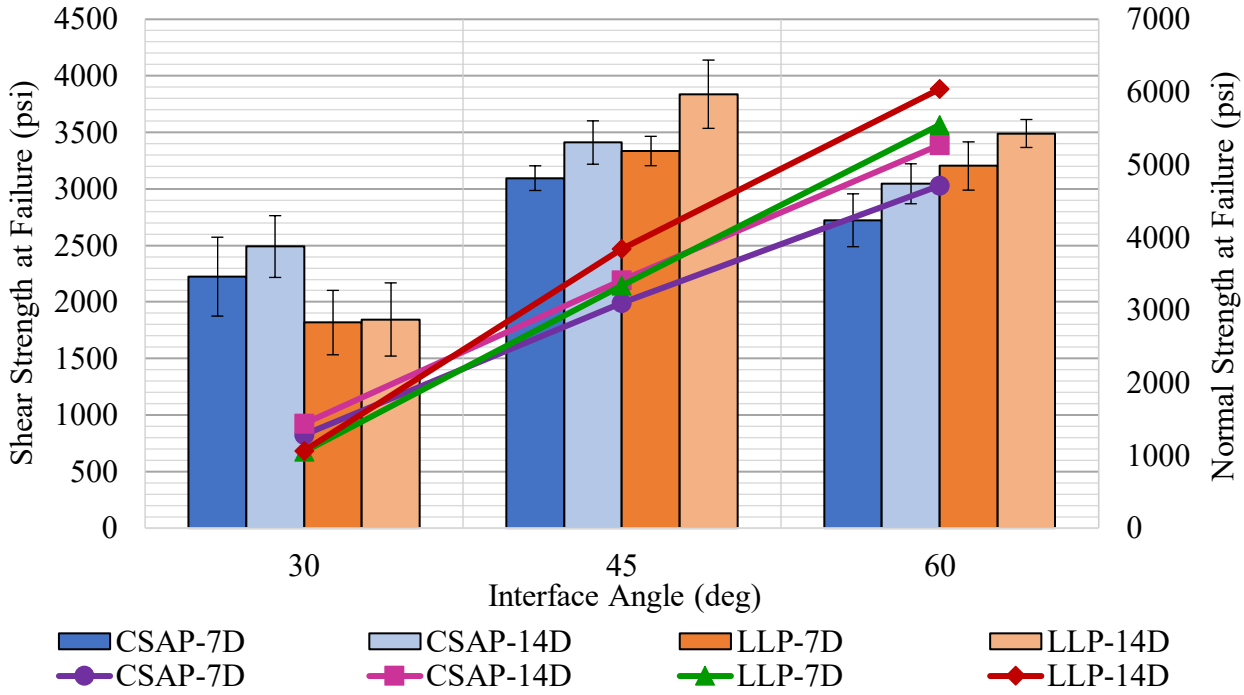

Figure 4-34: Shear and normal strengths at varying substrate-overlay interface angles

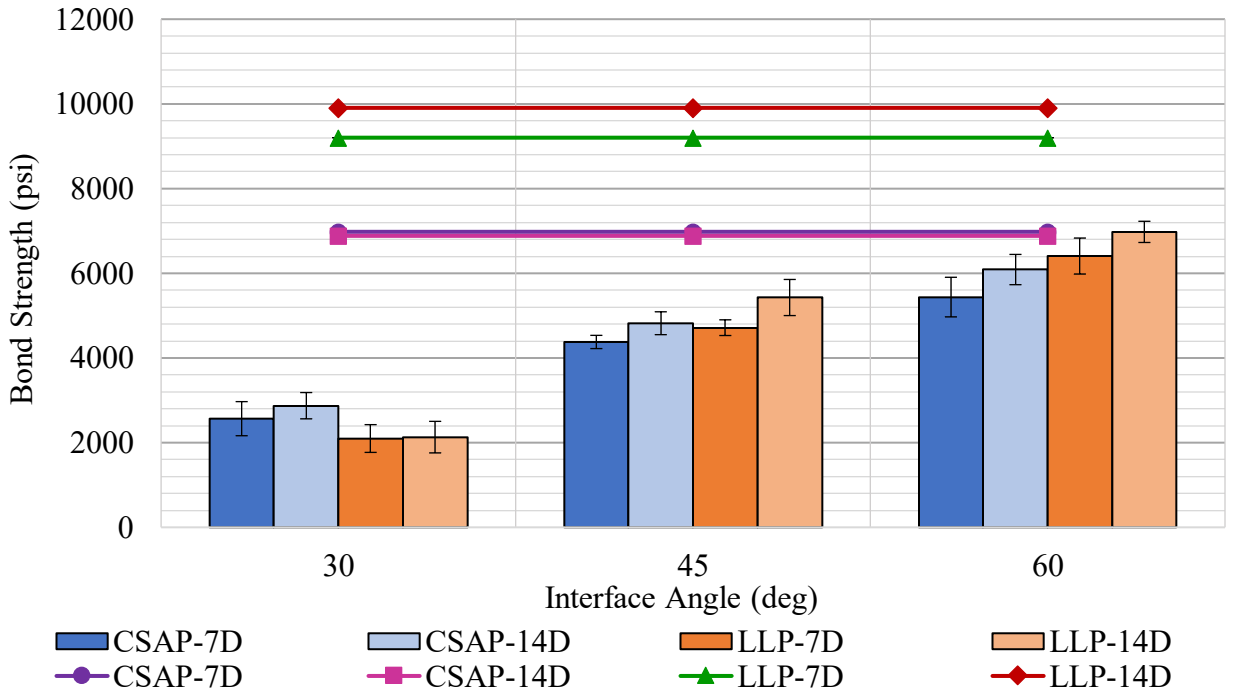

Figure 4-35: Bond strengths of at varying substrate-overlay interface angles

Specimens with larger interface angles typically exhibited higher compressive strengths, while lower shear strengths were generally associated with bond failures. This suggests that the geometry of the bonded interface plays a significant role in overall mechanical performance. When comparing materials, LLP demonstrated better performance over CSAP, with higher shear and normal strength values. This suggests that LLP provides greater bond strength than CSAP under slant-shear loading conditions. Notably, 28.2% of CSAP specimens experienced failure at the overlay interface, whereas none of the LLP specimens failed in this manner, highlighting a clear disparity in bonding reliability. Overall, the results underscore LLP's potential as a more reliable overlay material in applications where bond strength is critical.

4.3.6. Durability Study Summary

The durability phase of this research focused on evaluating the performance of CSA systems under various environmental and mechanical conditions to assess their long-term viability as overlay materials. Tests conducted included early-age autogenous and plastic shrinkage, freeze-thaw resistance, salt scaling, and bond strength via the slant-shear test. While some tests yielded clear and consistent results, others showed variability, highlighting both the sensitivity of the testing methods and the materials themselves.

- **Autogenous deformation:** Mortars showed lower autogenous shrinkage than pastes, as expected, though variability in paste content introduced some uncertainty. CSAP mortar had the highest early shrinkage, while LLP and LM25 stabilized quickly; LM100 shrank more gradually. Temperature strongly influenced behavior—shrinkage increased at 10°C and decreased at 35°C due to hydration kinetics. CSAP's inconsistent results likely stem from its powdered HRWR content. Overall, LLP and LM25 showed consistent, stable performance, while LM100 exhibited greater and prolonged shrinkage, indicating different hydration behavior.

- **Plastic shrinkage:** For CSAP, LLP, and LM25 mixes, only one specimen per mix cracked, with transverse cracks forming at stress concentrations. LM25 exhibited the widest cracks, followed by CSAP, with LLP showing the smallest; LM25's cracks were more than twice as wide as those in LLP. LM100 behaved differently, with both specimens cracking significantly in multiple directions. These cracks did not follow expected stress paths, likely due to surface crusting from high latex content causing differential shrinkage. LM25, with less latex, did not exhibit this behavior but still showed wider cracks than CSAP and LLP, possibly due to minor shrinkage differentials from its moderate latex content.
- **Freeze-thaw resistance:** CSAP performed significantly worse than LLP in freeze-thaw resistance, potentially due to its lower air content, which limits internal pressure relief. The stark difference between the two mixes suggests further investigation is needed. Notably, LLP's %RDME exceeded 100%, likely due to equipment sensitivity rather than actual stiffness gain. Among latex-modified systems, LM100 outperformed LM25, likely due to its higher latex content forming a more continuous polymer network, enhancing resistance to moisture and freeze damage.
- **Salt-scaling resistance:** Contrary to its poor freeze-thaw performance, CSAP showed the least salt scaling, suggesting strong resistance to deicing salts, while LLP experienced the most severe scaling—contradicting previous findings and warranting further study. Latex-modified mixes followed expected trends: LM100, with higher latex content, outperformed LM25 in salt scaling resistance, consistent with earlier freeze-thaw results and literature. However, no clear correlation was found between freeze-thaw durability and salt scaling ratings, likely due to the tests' differing mechanisms—submersion versus surface exposure—and the inherent sensitivity of each method.

- **Slant-shear test:** Specimens with steeper interface angles showed higher compressive strengths, while lower shear strengths were often linked to bond failures, emphasizing the impact of interface geometry. LLP outperformed CSAP in both shear and normal strength, with no bond failures observed, compared to a 28.2% bond failure rate in CSAP specimens. These findings highlight LLP's superior bonding reliability and its suitability for applications requiring strong overlay adhesion.

Overall, LLP consistently outperformed the other mixes, demonstrating stable shrinkage, strong freeze-thaw resistance, minimal cracking, and superior bond strength, making it ideal for overlays. CSAP showed mixed results, excelling in salt scaling but performing poorly in freeze-thaw tests, experiencing bond failures, and exhibiting variable autogenous shrinkage, which warrants further investigation. LM100 outperformed LM25 in both freeze-thaw and salt scaling resistance but displayed higher shrinkage and atypical cracking. These findings highlight the significant impact of polymer type and dosage on durability performance.

CHAPTER 5: CONCLUSIONS

Bridge deck cracking has become an increasingly significant concern in infrastructure maintenance. Calcium sulfoaluminate (CSA) cement has garnered growing interest as an alternative binder due to its rapid setting characteristics and inherent shrinkage-compensating behavior. Additionally, CSA cement tends to form a denser and more refined microstructure, which contributes to improved long-term strength and durability. Its lower production temperature also reduces energy consumption, enhancing its environmental sustainability.

This study focused specifically on belitic calcium sulfoaluminate (BCSA) cement, a subset of CSA known for its significant early-strength development. Two proprietary polymer-modified BCSA systems were investigated as potential alternatives to latex-modified BCSA cement (LM), as latex-modified concrete is commonly used for bridge deck overlay repairs. Both proprietary systems incorporated the same polymer, Low-P™—one interground with the BCSA as a powder (CSAP), and the other introduced as a liquid admixture (LLP). The cementitious systems were subjected to a comprehensive testing program to assess their mechanical properties and durability performance, with the goal of evaluating their suitability for application in bridge deck overlay repairs.

5.1. Characterization Study

Previously optimized CSA concrete mixes were further modified to investigate the effects of aggregate size and gradation, as well as air-entraining admixture (AEA) type and dosage, on compressive strength. A common challenge associated with polymer-modified CSA cement is achieving the target fresh air content of 5.5% ± 1.5%. To address this, the study evaluated multiple AEA types and dosages to achieve the desired air content while maintaining acceptable workability, mechanical strength, and durability. Additionally, while latex-modified concrete typically requires high dosages of latex, there is limited data supporting such levels for

modern binders like CSA. Consequently, this study also assessed whether reduced latex dosages could maintain performance in fresh and hardened states.

The key findings of this study include:

- Higher fine aggregate content (35/65 CA/FA) increased air content but resulted in reduced compressive strength likely due to less coarse aggregate load-bearing capacity. Additionally, slight changes in the aggregate blend (CA/FA 45/55 to 48.9/51.1) led to improvements in long-term strength development.
- Larger NMSA (3/4") consistently reduced air content and strengths generally declined; however, latex in the LM concrete seemed to have mitigated strength loss.
- AEA dosage showed a parabolic effect where initial increased in dosage resulted in increased air content, but at higher dosages, a plateau or decline were found. AEA formulation also significantly influenced performance, despite similar bases (e.g., vinsol resin).
- The synthetic AE90, performed particularly poorly with CSAP, possibly due to AEA adsorption onto polymer surface (analogous to carbon adsorption). Further research is needed to understand AEA-polymer interactions and their effects on air entrainment and strength.
- Latex dosage exhibited a strong polynomial relationship with strength and air content. Air content peaked at 50%, then declined at 100% dosage, suggesting high latex can destabilize bubbles, similar to AEA overdose effects. The 25% dosage mix shoed comparable strength LLP mix. While higher dosages led to strength loss.

Overall, CSA-based concrete performance was found to be highly sensitive to interactions among aggregate gradation, AEA type/dosage, and polymer content. Minor changes can cause significant shifts in air content, strength, and durability, emphasizing a need for holistic mix design rather than isolated parameter adjustments. For subsequent testing, a 48.9/51.1 CA/FA ratio with 3/8" NMSA was chosen with the AEA VR10 dosed at 1.75% by

mass of cement. Latex-modified CSA system was also studied at the full standard latex dosage (LM100) and at 25% latex dosage (LM25). All mixes used 0.32 W/C expect LM25 which was increased to 0.38 W/C as the reduction in latex resulted in decreased workability.

5.2. Field Trials

To evaluate the field performance of the CSAP and LLP mixes, they were applied as overlays to mini-bridge deck substrates with varying finishes designed to replicate typical WSDOT bridge deck conditions. The main goal of this portion of the project was to assess the compatibility between the overlay materials and the substrates, with particular focus on bond strength and long-term volume stability. Additionally, the mechanical properties of field-scale specimens from the overlay mixes and -scale specimens of CSAP, LLP, LM100, and LM25 cast in the laboratory were evaluated to gain insight into their mechanical properties and development over time. The mixes were evaluated for compressive, split tensile, and flexural strength, as well as drying shrinkage, modulus of elasticity, and coefficient of thermal expansion.

The key findings of this study are as follows:

- Compressive, tensile, and flexural strength differences were observed between CSAP_deck and LLP_deck, as well as between their corresponding laboratory mixes. These variations were likely influenced by mix composition, admixture compatibility, and curing conditions.
- Compressive strength findings in the laboratory CSAP and LLP mixes contrasted the findings in the earlier laboratory-scale characterization study. Suggesting variance in performance between field- and laboratory-scale testing.
- LM mixes exhibited significantly higher drying shrinkage over the first two weeks compared to both outdoor and laboratory CSAP and LLP mixes.
- LM25 generally matched or exceeded the long-term mechanical performance of LM100, suggesting that lower latex content can improve strength, stiffness, and minimize shrinkage.

- CSAP overlays demonstrated lower shrinkage and better strain stabilization than LLP overlays, indicating that CSAP systems offer superior early-age dimensional stability.
- Surface finish and exposed rebar influenced shrinkage behavior, with rougher, more thermally conductive substrates accelerating early-age deformation.
- LLP decks exhibited significant transverse and vertical cracking, while CSAP decks showed minimal cracking, consistent with strain gauge shrinkage data.
- Unique diagonal cracking at the corners is likely due to increased restraint and moisture loss where the edges meet.

Overall, notable differences were observed between the outdoor CSAP and LLP mixes and their laboratory counterparts, highlighting the sensitivity of these systems to mix composition, admixture compatibility, and environmental conditions. Additional research is recommended to better understand the variability in performance between field and lab-prepared CSAP and LLP mixes. Among the latex-modified concretes, LM25 matched or exceeded the mechanical performance of LM100, indicating that reduced latex dosage can improve both structural performance and dimensional stability. In overlay applications, CSAP demonstrated significantly lower shrinkage than LLP, suggesting superior early-age dimensional stability. Additionally, substrate surface finish was found to influence the strain behavior of the overlay, further emphasizing the importance of interface conditions in field performance.

5.3. Durability Study

The durability portion of this study evaluated the long-term suitability of CSA systems as overlay materials by testing their performance under various environmental and mechanical conditions. Tests included early-age autogenous and plastic shrinkage, freeze-thaw resistance, salt scaling, and slant-shear bond strength.

Notable outcomes from this investigation include:

- As expected, mortars exhibited less autogenous shrinkage than pastes. However, variability in paste content introduced a degree of uncertainty in the results.
- The CSAP paste showed inconsistent results at the varying temperatures, resulting likely from its powdered HRWR content. The influence of the HRWR on the CSAP system needs to be further investigated. The LLP and LM25 pastes showed relatively consistent autogenous shrinkage, while the LM100 paste exhibited greater and prolonged shrinkage.
- CSAP, LLP, and LM25 showed transverse cracking at the highest stress riser in the plastic shrinkage test, with the average crack width of the LM25 panel over twice that of the LLP panel.
- LM100 showed significant transverse and vertical cracks in the plastic shrinkage test, with the transverse cracks not following with the placement of the stress risers. A surface crust likely formed due to the high latex dosage, creating differential shrinkage between the surface and the interior of the panels and resulting in the cracking patterns observed.
- CSAP showed poor freeze-thaw resistance, it performed the best of all the mixes under salt-scaling, while LLP showed an inverse trend, warranting further study.
- LM100 performed well in both the freeze-thaw and salt-scaling testing, while LM25 did poorly in both. This is likely due to the higher latex content allowing for the development of a more continuous polymer network throughout the concrete microstructure, reducing porosity and freeze-damage.
- Slant-shear testing revealed that specimens with steeper interface angles generally exhibited greater compressive strength, whereas reduced shear strength was frequently associated with bond failure.

- LLP demonstrated superior performance over CSAP in both shear and normal strength tests, with zero bond failures observed—contrasting with a 28.2% bond failure rate in CSAP specimens.

Overall, LLP consistently outperformed the other mixes, showing controlled shrinkage, strong freeze-thaw resistance, minimal cracking, and excellent bond strength, making it ideal for overlays, despite field trial discrepancies. In contrast, CSAP showed mixed results: it excelled in salt scaling resistance but had poor freeze-thaw durability, bond failures, and inconsistent autogenous shrinkage. Among the latex-modified mixes, LM100 performed better than LM25 in freeze-thaw and salt scaling resistance but exhibited higher shrinkage and unusual cracking. The variability in CSAP's performance and the differing results for LLP in the durability study and field trials highlight the need for further research to fully understand the behavior of both systems.

5.4. Recommendations for Future Work

Based on the findings and limitations of this study, several key areas for future research have been identified to enhance the understanding and optimization of CSA-based overlay systems. These recommendations focus on addressing challenges related to material interactions, durability, and field performance to improve the reliability and effectiveness of CSA concrete in overlay applications:

- Further investigation is needed into the interactions between polymer modifiers, particularly the differences between powdered and liquid forms, and AEAs. A better understanding of adsorption effects and their impact on air void stability would improve control over fresh properties.

- While CSAP showed good performance in areas such as salt scaling, its poor freeze-thaw resistance and variable shrinkage behavior require deeper investigation to identify the causes of this variability and explore ways to mitigate it.
- The variability observed in LLP performance between outdoor overlays and laboratory tests calls for additional study to understand its sensitivity to outdoor application conditions.
- Following the overall positive performance of LM25 compared to LM100, further testing of intermediate latex dosages is warranted to refine optimal content that balances strength, shrinkage control, and durability.
- Expanding field-scale evaluations to include a wider range of environmental exposures would provide a more comprehensive understanding of long-term overlay behavior and its scalability.

BIBLIOGRAPHY

AASHTO Association. (2022). *AASHTO T336-22 Standard Method of Test for Coefficient of Thermal Expansion of Hydraulic Cement Concrete*. https://compass.astm.org/document/?contentcode=AASHTO%7CAASHTO%20T336-22%7Cen-US

Acarturk, B. C., & Burris, L. E. (2020). *Effects of combination of retarders on CSA cement systems*. Cement – Based Materials Tailored for a Sustainable Future, Istanbul, Turkey. https://doi.org/10.31224/osf.io/8ujyr

A.C.I. Committee. (2019). *Building code requirements for structural concrete: (ACI 318-19); and commentary (ACI 318R-19)*. http://refhub.elsevier.com/S0950-0618(22)02635-6/h0165

Adnan, T., Kienzle, A., & Thomas, R. J. (2022). Engineering properties and setting time of belitic calcium sulfoaluminate (BCSA) cement concrete. *Construction and Building Materials*, *352*, 128979. https://doi.org/10.1016/j.conbuildmat.2022.128979

Adnan, T., & Thomas, R. J. (2025). The alkali-silica reaction in belitic calcium sulfoaluminate (BCSA) cement concrete. *Construction and Building Materials*, *471*, 140726. https://doi.org/10.1016/j.conbuildmat.2025.140726

Ambrose, J., Shenbagam, V., Provis, J. L., & Hanein, T. (2023). *Belitic calcium sulphoaluminate (BCSA) cements and the current durability standards: What are we testing?*

American Concrete Institute. (2009). *ACI PRC-548.1-09: Guide for the Use of Polymers in Concrete*. https://www.concrete.org/store/productdetail.aspx?ItemID=548109&Format=DOWNLOAD&Language=English&Units=US_AND_METRIC

American Concrete Institute. (2012). *ACI 548.4M-11: Specification for Latex-Modified Concrete Overlays*.

ASTM International. (1998). *ASTM C672/C672M-98 Standard Test Method for Scaling Resistance of Concrete Surfaces Exposed to Deicing Chemicals*. ASTM International. https://compass.astm.org/document/?contentCode=ASTM%7CC0672_C0672M-12%7Cen-US

ASTM International. (2003). *ASTM C666/C666M-03 Test Method for Resistance of Concrete to Rapid Freezing and Thawing*. ASTM International. https://doi.org/10.1520/C0666_C0666M-03R08

ASTM International. (2015). *ASTM C127-15 Test Method for Relative Density (Specific Gravity) and Absorption of Coarse Aggregate*. ASTM International. https://doi.org/10.1520/C0127-15

ASTM International. (2017a). *ASTM C157/C157M-17 Test Method for Length Change of Hardened Hydraulic-Cement Mortar and Concrete*. ASTM International. https://doi.org/10.1520/C0157_C0157M-17

ASTM International. (2017b). *ASTM C496/C496M-17 Test Method for Splitting Tensile Strength of Cylindrical Concrete Specimens*. ASTM International. https://doi.org/10.1520/C0496_C0496M-17

ASTM International. (2019a). *ASTM C136/C136M-19 Test Method for Sieve Analysis of Fine and Coarse Aggregates*. ASTM International. https://doi.org/10.1520/C0136_C0136M-19

ASTM International. (2019b). *ASTM C1698-19 Test Method for Autogenous Strain of Cement Paste and Mortar*. ASTM International. https://doi.org/10.1520/C1698-19

ASTM International. (2020). *ASTM C143/C143M-20 Standard Test Method for Slump of Hydraulic-Cement Concrete*. ASTM International. https://doi.org/10.1520/C0143_C0143M

ASTM International. (2021). *ASTM C1579-21 Test Method for Evaluating Plastic Shrinkage Cracking of Restrained Fiber Reinforced Concrete (Using a Steel Form Insert)*. ASTM International. https://doi.org/10.1520/C1579-21

ASTM International. (2022a). *ASTM C78/C78M-22Test Method for Flexural Strength of Concrete (Using Simple Beam with Third-Point Loading)*. ASTM International. https://doi.org/10.1520/C0078_C0078M-22

ASTM International. (2022b). *ASTM C469/C469M-22 Test Method for Static Modulus of Elasticity and Poissons Ratio of Concrete in Compression*. ASTM International. https://doi.org/10.1520/C0469_C0469M-22

ASTM International. (2023a). *ASTM C29/C29M-23 Test Method for Bulk Density (Unit Weight) and Voids in Aggregate*. ASTM International. https://doi.org/10.1520/C0029_C0029M-23

ASTM International. (2023b). *ASTM C39/C39M-23 Test Method for Compressive Strength of Cylindrical Concrete Specimens*. ASTM International. https://doi.org/10.1520/C0039_C0039M-23

ASTM International. (2023c). *ASTM C403/C403M-23 Test Method for Time of Setting of Concrete Mixtures by Penetration Resistance*. ASTM International. https://doi.org/10.1520/C0403_C0403M-23

ASTM International. (2023d). *ASTM C882/C882M-23 Test Method for Bond Strength of Epoxy-Resin Systems Used With Concrete By Slant Shear*. ASTM International. https://doi.org/10.1520/C0882_C0882M-23

ASTM International. (2024a). *ASTM C 31/C31M-24a Practice for Making and Curing Concrete Test Specimens in the Field*. ASTM International. https://doi.org/10.1520/C0031_C0031M-24A

ASTM International. (2024b). *ASTM C33/C33M-24a Specification for Concrete Aggregates*. ASTM International. https://doi.org/10.1520/C0033_C0033M-24A

ASTM International. (2024c). *ASTM C231/C231M-24 Test Method for Air Content of Freshly Mixed Concrete by the Pressure Method*. ASTM International. https://doi.org/10.1520/C0231_C0231M-24

ASTM International. (2024d). *ASTM C494/C494M-24*. ASTM International. https://doi.org/10.1520/C0494_C0494M-24

Belhadi, R., Govin, A., & Grosseau, P. (2021). Influence of polycarboxylate superplasticizer, citric acid and their combination on the hydration and workability of calcium

sulfoaluminate cement. *Cement and Concrete Research*, *147*, 106513. https://doi.org/10.1016/j.cemconres.2021.106513

Bescher, E., & Kim, J. (2019, June). *Belitic Calcium Sulfoaluminate Cement: History, Chemistry, Performance, and Use in the United States*. 1st International Conference on Innovation in Low-Carbon Cement & Concrete Technology, London, United Kingdom. https://www.researchgate.net/publication/334204807

Borštnar, M., Daneu, N., & Dolenec, S. (2020). Phase development and hydration kinetics of belite-calcium sulfoaluminate cements at different curing temperatures. *Ceramics International*, *46*(18), 29421–29428. https://doi.org/10.1016/j.ceramint.2020.05.029

Burris, L. E., & Kurtis, K. E. (2018). Influence of set retarding admixtures on calcium sulfoaluminate cement hydration and property development. *Cement and Concrete Research*, *104*, 105–113. https://doi.org/10.1016/j.cemconres.2017.11.005

Carsana, M., Canonico, F., & Bertolini, L. (2018). Corrosion resistance of steel embedded in sulfoaluminate-based binders. *Cement and Concrete Composites*, *88*, 211–219. https://doi.org/10.1016/j.cemconcomp.2018.01.014

Cavalline, T. L., Tempest, B. Q., Biggers, R. B., Lukavsky, A. J., McEntyre, M. S., & Newsome, R. A. (2020). *Durable and Sustainable Concrete Through Performance Engineered Concrete Mixtures*. University of North Carolina at Charlotte.

Choi, P., & Yun, K.-K. (2014). Experimental analysis of latex-solid content effect on early-age and autogenous shrinkage of very-early strength latex-modified concrete. *Construction and Building Materials*, *65*, 396–404. https://doi.org/10.1016/j.conbuildmat.2014.05.007

Clear, K. C., & Chollar, B. H. (1978). *Styrene-Butadiene Latex Modifiers for Bridge Deck Overlays* (Interim Report No. FHWA-RD-78-35).

Combrinck, R., & Boshoff, W. P. (2015). Typical plastic shrinkage cracking behaviour of concrete. *Magazine of Concrete Research*, *65*(8), 486–493. https://doi.org/10.1680/macr.12.00139

Combrinck, R., Steyl, L., & Boshoff, W. P. (2018). Influence of concrete depth and surface finishing on the cracking of plastic concrete. *Construction and Building Materials*, *175*, 621–628. https://doi.org/10.1016/j.conbuildmat.2018.04.225

CSA. (2004). *Design of concrete structures*.

CTS Cement Manufacturing Corp. (2022). *CTS Cement Announces Environmental Product Declarations (EPD) for Flagship Brands*. https://www.ctscement.com/external/company/2022/EPD_press_release_R9.pdf

Cuberos, A. J. M., De la Torre, Á. G., Álvarez-Pinazo, G., Martín-Sedeño, M. C., Schollbach, K., Pöllmann, H., & Aranda, M. A. G. (2010). Active Iron-Rich Belite Sulfoaluminate Cements: Clinkering and Hydration. *Environmental Science & Technology*, *44*(17), 6855–6862. https://doi.org/10.1021/es101785n

De Bruyn, K., Bescher, E., Ramseyer, C., Hong, S., & Kang, T. H.-K. (2017). Pore Structure of Calcium Sulfoaluminate Paste and Durability of Concrete in Freeze–Thaw Environment. *International Journal of Concrete Structures and Materials*, *11*(1), 59–68. https://doi.org/10.1007/s40069-016-0174-3

Deo, O., Bhuskute, N., Paniagua, J., Guijosa, J., Rivera, J., & Bescher, E. P. (2023). A New Belitic Calcium Sulfoaluminate Cement. *Journal of Materials in Civil Engineering*, *35*(11). https://doi.org/10.1061/JMCEE7.MTENG-15950

Deo, O., Win, D., Bhuskute, N., Chung, D., deOcampo, N., & Bescher, E. (2022). Fast Setting, Low Carbon Infrastructure Rehabilitation Using Belitic Calcium Sulfoaluminate (BCSA)

Concrete. *MATEC Web of Conferences*, *361*, 00002. https://doi.org/10.1051/matecconf/202236100002

Dhahir, M. K., & Marx, S. (2023). Development of expansive concrete for chemical prestressing applications. *Case Studies in Construction Materials*, *19*, e02611. https://doi.org/10.1016/j.cscm.2023.e02611

Dolch, W. L. (1996). 8—Air-Entraining Admixtures. In V. S. Ramachandran (Ed.), *Concrete Admixtures Handbook (Second Edition)* (pp. 518–557). William Andrew Publishing. https://doi.org/10.1016/B978-081551373-5.50012-X

Dornak, M. L. (2014). *Mechanical Properties, Early Age Volume Change, and Heat Generation of Rapid, Cement-based Repair Materials* [The University of Texas at Austin]. http://hdl.handle.net/2152/26379

En 1992-1-1. (2004). *Eurocode 2: Design of concrete structures—Part 1–1: General rules and rules for buildings*. http://refhub.elsevier.com/S0950-0618(22)02635-6/h0175

Eren, F., Gödek, E., Keskinateş, M., Tosun-Felekoğlu, K., & Felekoğlu, B. (2017). Effects of latex modification on fresh state consistency, short term strength and long term transport properties of cement mortars. *Construction and Building Materials*, *133*, 226–233. https://doi.org/10.1016/j.conbuildmat.2016.12.080

Guerrero-Estrada, J. A. (2024). *High-Early Strength Concrete for Rapid Bridge Deck Repair and Rehabilitation*. University of Washington.

Huang, C., Cheng, Z., Zhao, J., Wang, Y., & Pang, J. (2021). The Influence of Water Reducing Agents on Early Hydration Property of Ferrite Aluminate Cement Paste. *Crystals*, *11*(71). https://doi.org/10.3390/cryst11070731

Ke, G., Zhang, J., & Liu, Y. (2022). Shrinkage characteristics of calcium sulphoaluminate cement concrete. *Construction and Building Materials*, *337*, 127627. https://doi.org/10.1016/j.conbuildmat.2022.127627

Kim, J. (2018, November 21). *How to Make the Most of Fast-Setting Concrete*. Concrete Construction. https://www.concreteconstruction.net/how-to/materials/how-to-make-the-most-of-fast-setting-concrete_o

Kosmatka, S. H., Kerkhoff, B., & Panarese, W. C. (2003). *Design and Control of Concrete Mixtures* (14th ed.). Portland Cement Association.

Kuhlmann, L. (1991). Cracks in Latex-Modified Concrete Overlays—How They Get There, How Serious They Are, and What To Do About Them. *Transportation Research Record*.

Kuhlmann, L. A. (1993). Using Styrene-Butadiene Latex in Concrete Overlays. *Transportation Research Record*. https://onlinepubs.trb.org/Onlinepubs/trr/1988/1204/1204-008.pdf

Li, L., Wang, R., & Lu, Q. (2018). Influence of polymer latex on the setting time, mechanical properties and durability of calcium sulfoaluminate cement mortar. *Construction and Building Materials*, *169*, 911–922. https://doi.org/10.1016/j.conbuildmat.2018.03.005

Ma, B., Ma, M., Shen, X., Li, X., & Wu, X. (2014). Compatibility between a polycarboxylate superplasticizer and the belite-rich sulfoaluminate cement: Setting time and the hydration properties. *Construction and Building Materials*, *51*, 47–54. https://doi.org/10.1016/j.conbuildmat.2013.10.028

Manawadu, A., Qiao, P., & Wen, H. (2023). Characterization of Substrate-to-Overlay Interface Bond in Concrete Repairs: A Review. *Construction and Building Materials*, *373*, 130828. https://doi.org/10.1016/j.conbuildmat.2023.130828

Markosian, N., Tawadrous, R., Mastali, M., Thomas, R. J., & Maguire, M. (2021). Performance Evaluation of a Prestressed Belitic Calcium Sulfoaluminate Cement (BCSA) Concrete Bridge Girder. *Sustainability*, *13*. https:// doi.org/10.3390/su13147875

McNerney, M. T., Khilfeh, S., & Bescher, E. P. (2020). *Rapid-Setting Belitic Calcium Sulfoaluminate Concrete Pavement at Seattle-Tacoma International Airport: A 25-Year History*. International Conference on Transportation and Development 2020. https://doi.org/10.1061/9780784483183.016

Mehta, P. K., & Monteiro, P. J. M. (2014). *Concrete: Microstructure, Properties, and Materials* (4th Edition). McGraw-Hill Education. https://www.accessengineeringlibrary.com/content/book/9780071797870

Moffatt, E. G. (2016). *Durability of rapid-set (ettringite-based) concrete*. University of New Brunswick.

Mrak, M., Winnefeld, F., Lothenbach, B., & Dolenec, S. (2021). The influence of calcium sulfate content on the hydration of belite-calcium sulfoaluminate cements with different clinker phase compositions. *Materials and Structures*. https://doi.org/10.1617/s11527-021-01811-w

Pedersen, K., Jensen, A., Skjothrasmussen, M., & Damjohansen, K. (2008). A review of the interference of carbon containing fly ash with air entrainment in concrete. *Progress in Energy and Combustion Science*, *34*(2), 135–154. https://doi.org/10.1016/j.pecs.2007.03.002

Péra, J., & Ambroise, J. (2004). New applications of calcium sulfoaluminate cement. *Cement and Concrete Research*, *34*(4), 671–676. https://doi.org/10.1016/j.cemconres.2003.10.019

Shen, D., Jiang, J., Shen, J., Yao, P., & Jiang, G. (2016). Influence of curing temperature on autogenous shrinkage and cracking resistance of high-performance concrete at an early age. *Construction and Building Materials*, *103*, 67–76. https://doi.org/10.1016/j.conbuildmat.2015.11.039

Sirtoli, D., Wyrzykowski, M., Riva, P., & Lura, P. (2020). Autogenous and drying shrinkage of mortars based on Portland and calcium sulfoaluminate cements. *Materials and Structures*, *53*(5), 126. https://doi.org/10.1617/s11527-020-01561-1

Soriano, E. (2019). *The Influence of Citric Acid on Setting Time and Temperature Behavior of Calcium Sulfoaluminate-Belite Cement*. University of Arkansas, Fayetteville.

Tan, B., Okoronkwo, M. U., Kumar, A., & Ma, H. (2020). Durability of calcium sulfoaluminate cement concrete. *Journal of Zhejiang University-SCIENCE A*, *21*(2), 118–128. https://doi.org/10.1631/jzus.A1900588

Taylor, P., Yurdakul, E., Wang, X., & Wang, X. (2015). *Concrete Pavement Mixture Design and Analysis (MDA): An Innovative Approach to Proportioning Concrete Mixtures* (Technical Report No. TPF-5(205)). Iowa State University. https://wisconsindot.gov/Documents/doing-bus/eng-consultants/cnslt-rsrces/tools/qmp/performance-based-PCC-mix-design-1-11-2017.pdf

Van Dam, T. J., Peterson, K. R., Sutter, L. L., Panguluri, A., Sytsma, J., Buch, N., Kowli, R., & Desaraju, P. (2005). *Guidelines for Early-Opening-to-Traffic Portland Cement Concrete for Pavement Rehabilitation* (No. 540; p. 13543). Transportation Research Board. https://doi.org/10.17226/13543

Wang, Y., Xiao, R., Hu, W., Jiang, X., Lu, H., & Huang, B. (2023). Influences of admixture combinations on the formation and stability of air bubbles in fresh cementitious

materials. *Journal of Building Engineering*, *76*, 107264. https://doi.org/10.1016/j.jobe.2023.107264

Washington State Department of Transportation. (2004). *Standard Specifications for Road, Bridge, and Municipal Construction (M 41-10)*. https://wsdot.wa.gov/publications/manuals/fulltext/M41-10/SS2004.pdf

Winnefeld, F., & Lothenbach, B. (2010). Hydration of calcium sulfoaluminate cements—Experimental findings and thermodynamic modelling. *Cement and Concrete Research*, *40*(8), 1239–1247. https://doi.org/10.1016/j.cemconres.2009.08.014

Winnefeld, F., & Lothenback, B. (2016). Phase equilibria in the system Ca4Al6O12SO4 – Ca2SiO4 – CaSO4 – H2O referring to the hydration of calcium sulfoaluminate cements. *RILEM Technical Letters*. https://doi.org/10.21809/rilemtechlett.2016.5

Wojciech, S., Szydłowski, J., Buchała, I., & Kapeluszna, E. (2024). Synthesis and Characterization of Calcium Sulfoaluminate Hydrates—Ettringite (AFt) and Monosulfate (AFm). *Materials*, *17*(21). https://doi.org/10.3390/ma17215216

WSDOT. (2025). *Standard Specifications M 41-10 Division 6 Structures*. https://wsdot.wa.gov/publications/manuals/fulltext/m41-10/division6.pdf

Yang, S., Acarturk, B. C., & Burris, L. E. (2022). Role of pore structure on resistance to physical crystallization damage of calcium sulfoaluminate belite (CSAB) cement blends. *Cement and Concrete Research*, *159*. https://doi.org/10.1016/j.cemconres.2022.106886

Yun, K.-K., Kim, D.-H., & Choi, S.-Y. (2004). Durability of Very-Early-Strength Latex-Modified Concrete Against Freeze-Thaw and Chemicals. *Transportation Research Record*. https://doi.org/10.3141/1893-01

Zhang, J., Guan, X., Wang, X., Ma, X., Li, Z., Xu, Z., & Jin, B. (2020). Microstructure and Properties of Sulfoaluminate Cement-Based Grouting Materials: Effect of Calcium

Sulfate Variety. *Advances in Materials Science and Engineering*, *2020*(1). https://doi.org/10.1155/2020/7564108

Zhou, Q., & Glasser, F. P. (2001). Thermal stability and decomposition mechanisms of ettringite at <120°C. *Cement and Concrete Research*, *31*(9), 1333–1339. https://doi.org/10.1016/S0008-8846(01)00558-0

APPENDIX

Appendix A: Field Trials

Mixture Proportions

Use WSDOT CLASS 4000D - OLD SPEC

Mix Properties

Slump	5.5" MAX	**Sack Content**	7.8	94 lb/sack	**Total Mass**	3967	lb
Air	6% (+/- 1.5%)	**Total Water**	30.0	gal	**Total Volume**	27.15	ft3
W/CM Ratio	0.34	**Water/Sack**	3.8	gal	**Unit Weight**	146.1	lb/ft3

Group	Material Description	Supplier	Absorption	Specific Gravity	Mass SSD lb	Volume ft3
Cement	TYPE_I-L - Type I-L Cement	Calportland-Vassai		3.11	660	3.401
Additive	Fly Ash FLYASH - FLYASH			2.4	75	0.501
Aggregate	Fine Aggregate MAN_SAND - BUILDING SAND	Manke Resources	1.6	2.69	1243	7.405
	Coarse Aggregate MAN_3/4 - AASHTO #57	Manke Resources	1.22	2.74	1735	10.148
Water	Potable Water WATER - WATER			1	250	4.006
Admixture	Air Entrainer AEA - AIR ENTRAINMENT-WR GRACE Range: 0.5-150 fl oz/100 lb CM	GCP Applied Tech.		1.35	0.647	0.00768
	Water Reducer WRA - WRDA64-WR GRACE Range: 0.5-5 fl oz/100 lb CM	GCP Applied Tech.		1	1.437	0.02303
	Water Reducer High Range ADVA - ADVA 195 WR GRACE Range: 0.5-25 fl oz/100 lb CM	GCP Applied Tech.		1	1.916	0.03070
Air	Air					1.626

Gradation

Sieve	% Passing	Specification
1 1/2" (37.5mm)	100.0	
1" (25mm)	99.4	
3/4" (19mm)	91.9	
1/2" (12.5mm)	67.0	
3/8" (9.5mm)	55.5	
#4 (4.75mm)	45.7	
#8 (2.36mm)	37.4	
#16 (1.18mm)	28.4	
#30 (.6mm)	19.3	
#50 (.3mm)	7.9	
#100 (.15mm)	1.9	
#200 (75µm)	0.47	

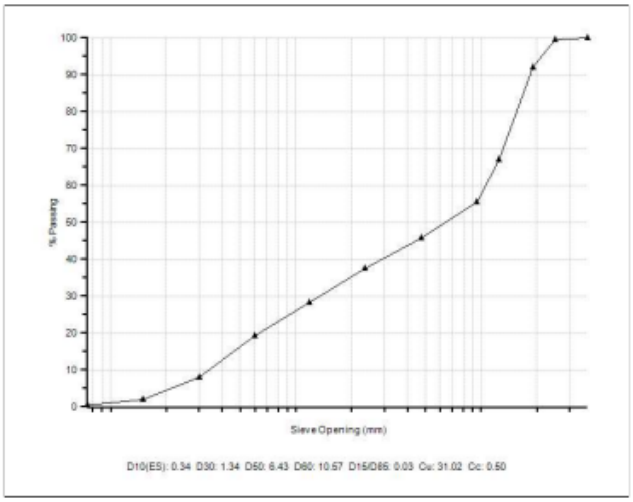

Figure A1: WSDOT concrete class 4000D batched weights for mini-bridge deck substrates

Ricci Quick & Easy Concrete

Date	11/15/2024	Total Concrete Poured	1.8 CY
Job Number			
Contract			
County	King		

	Product/Source	Weight(in lbs) Per Yard	Weight(lbs) for total pour
Cement	Rapid Set Juarez Plant	658	1184.4
Water	City	220	396
Stone	#8 Cal portland	1535	2763
Sand	Cal portland	1563	2813.4
Admixture	Combined/ See below for each	7.875	14.175
	Total	3983.875	7170.975

		Weight in Oz Per Yard
Admixture 1	Darcole dsa110	0
Admixture 2	Darcole Superflo1443	0
Admixture 3	Citric Acid	126
Admixture 4	CTS-Liquid Low P	0
	Total in pounds	7.875

Figure A2: Mini-bridge deck CSAP overlay batched weights

Ricci Quick & Easy Concrete

Date	11/15/2024	Total Concrete Poured	1.28 CY
Job Number			
Contract			
County	King		

	Product/Source	Weight(in lbs) Per Yard	Weight(lbs) for total pour
Cement	Rapid Set Juarez Plant	658	842.24
Water	City	220	281.6
Stone	#8 Cal portland	1520	1945.6
Sand	Cal portland	1548	1981.44
Admixture	Combined/ See below for each	18.9875	24.304
	Total	3964.9875	5075.184

		Weight in Oz Per Yard
Admixture 1	Darcole dsa110	42
Admixture 2	Darcole Superflo1443	126
Admixture 3	Citric Acid	70
Admixture 4	CTS-Liquid Low P	65.8
	Total in pounds	18.9875

Figure A3: Mini-bridge deck LLP overlay batched weights

Mini-Bridge Deck Cracks

Figure A4: First assessment cracks of Deck 1 – Sandblasted, CSAP

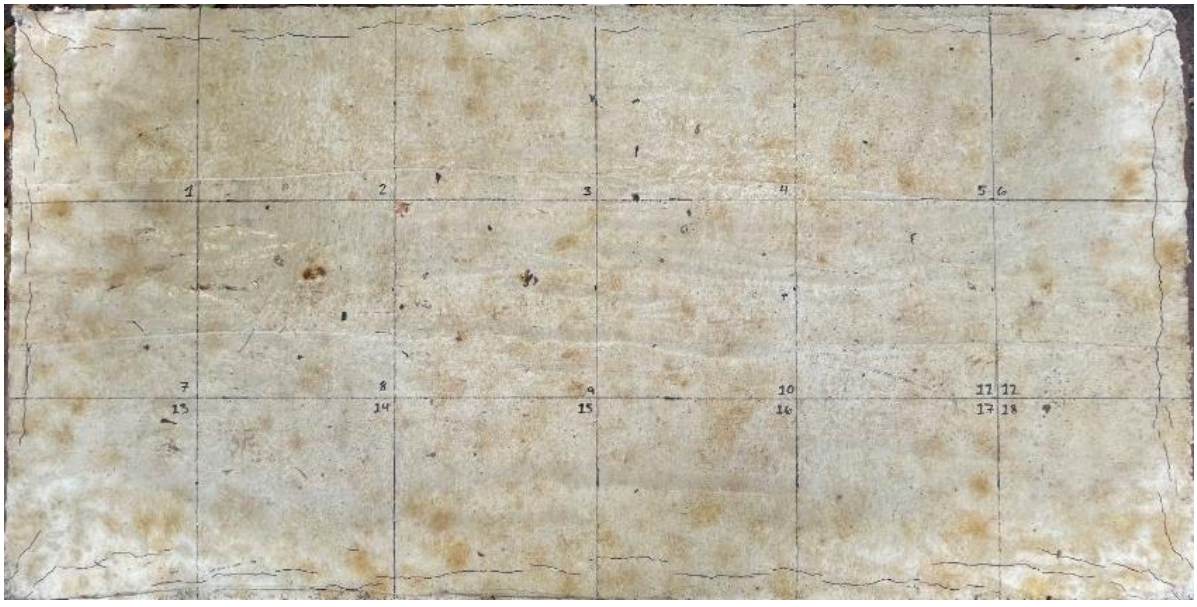

Figure A5: First assessment cracks of Deck 2 – Sandblasted, LLP

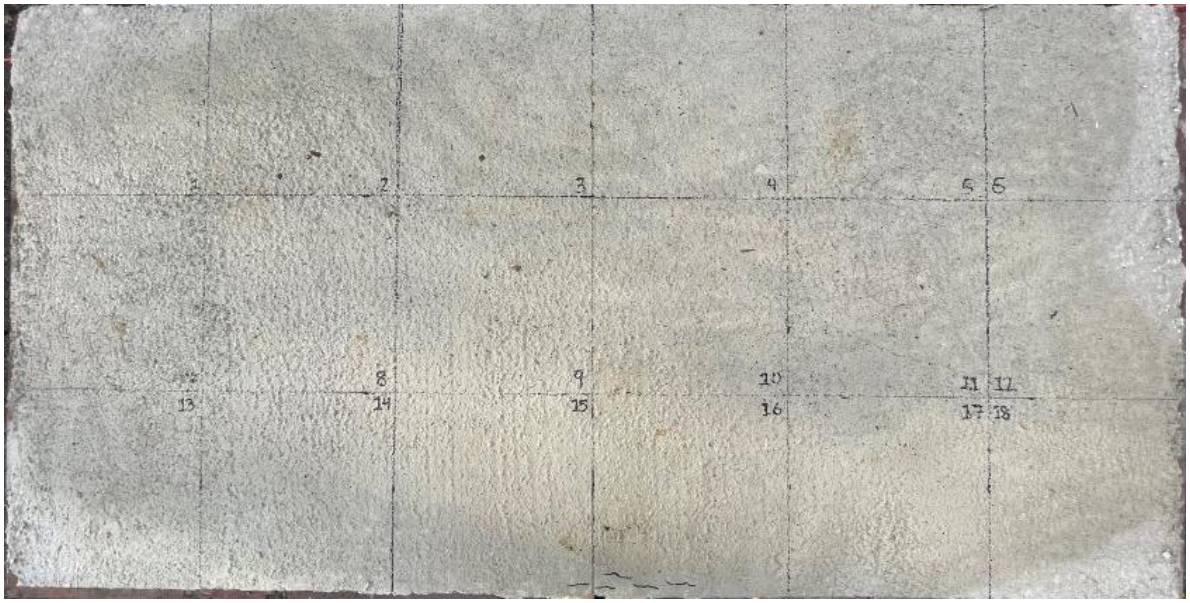

Figure A6: First assessment cracks of Deck 3 – Exposed Aggregate, CSAP

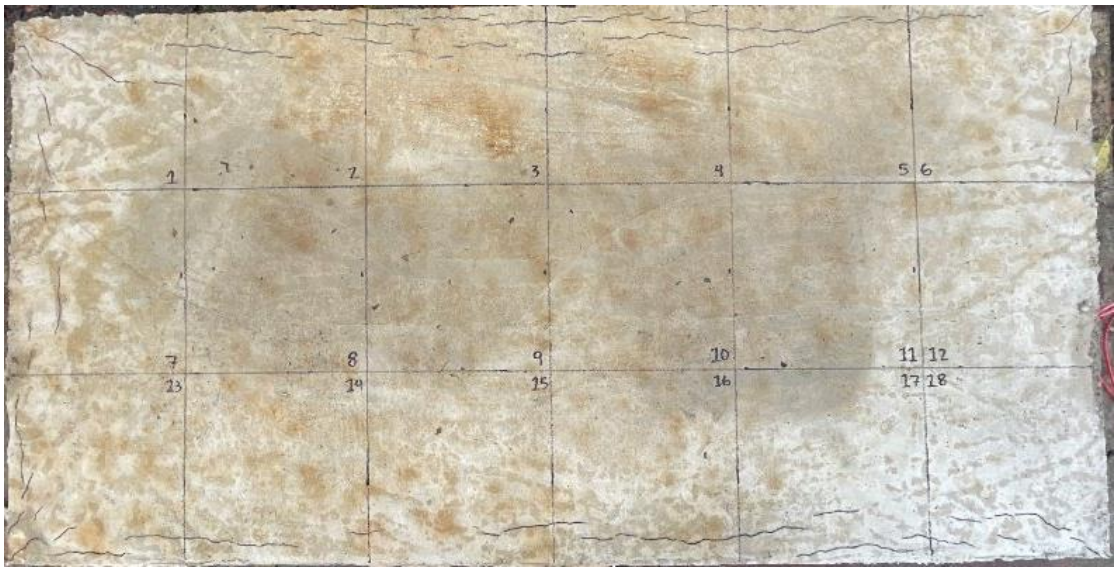

Figure A7: First assessment cracks of Deck 4 – Exposed Aggregate, LLP

Figure A8: First assessment cracks of Deck 5 – Exposed Rebar, CSAP

Figure A9: First assessment cracks of Deck 6 – Exposed Aggregate, CSAP

Appendix B: Durability Study

Plastic Shrinkage

Table B1: Plastic shrinkage environmental chamber evaporation rates

Mix	Velocity (m/s)		Temperature (°C)		Rel. Humidity (%)		Evaporation Rate (kg/m²/hr)
	Med.	Avg.	Med.	Avg.	Med.	Avg.	
CSAP	4.5	4.1	35.5	35.2	11.4	11.4	N/A
LLP	4.4	4.3	35.7	35.6	14.3	14.3	0.82
LM100	5.3	5.4	38.6	38.5	9.8	9.9	1.03
LM25	5.1	5.2	35.2	30.7	11.4	18.8	0.78

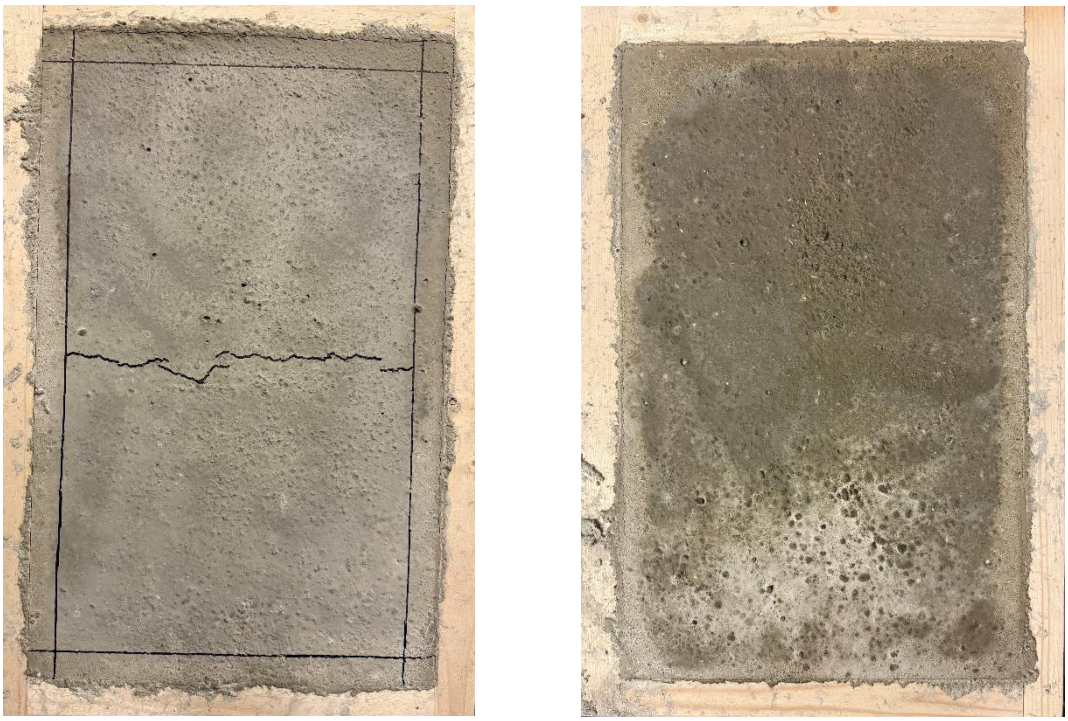

Figure B1: CSAP plastic shrinkage panels

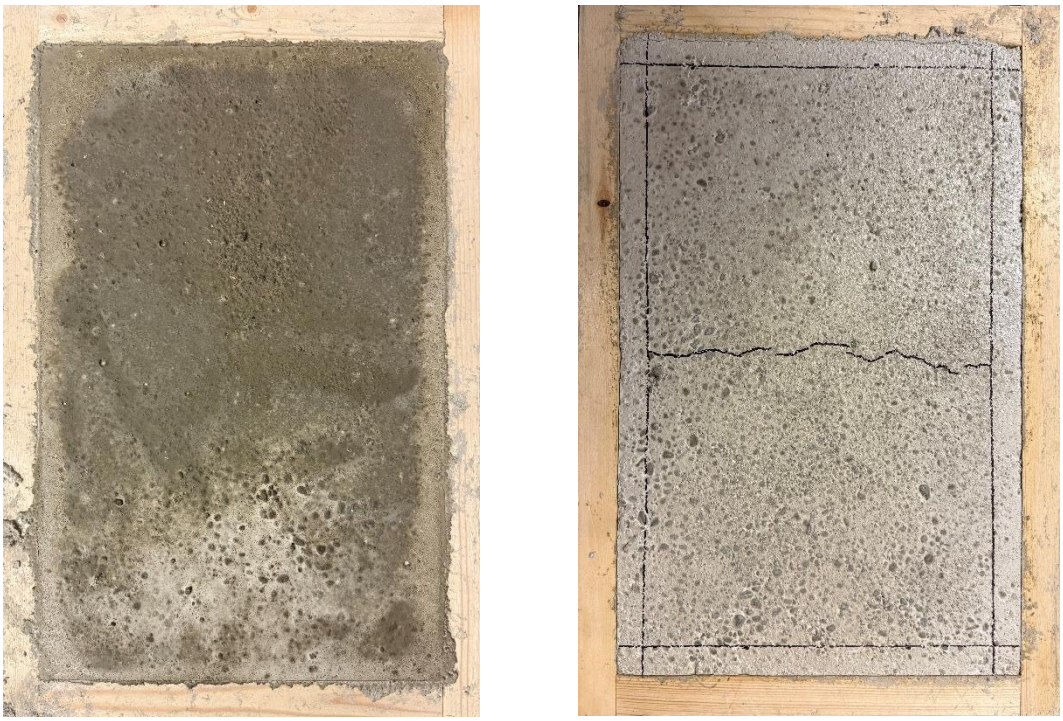

Figure B2: LLP plastic shrinkage panels

Figure B3: LM100 plastic shrinkage panels

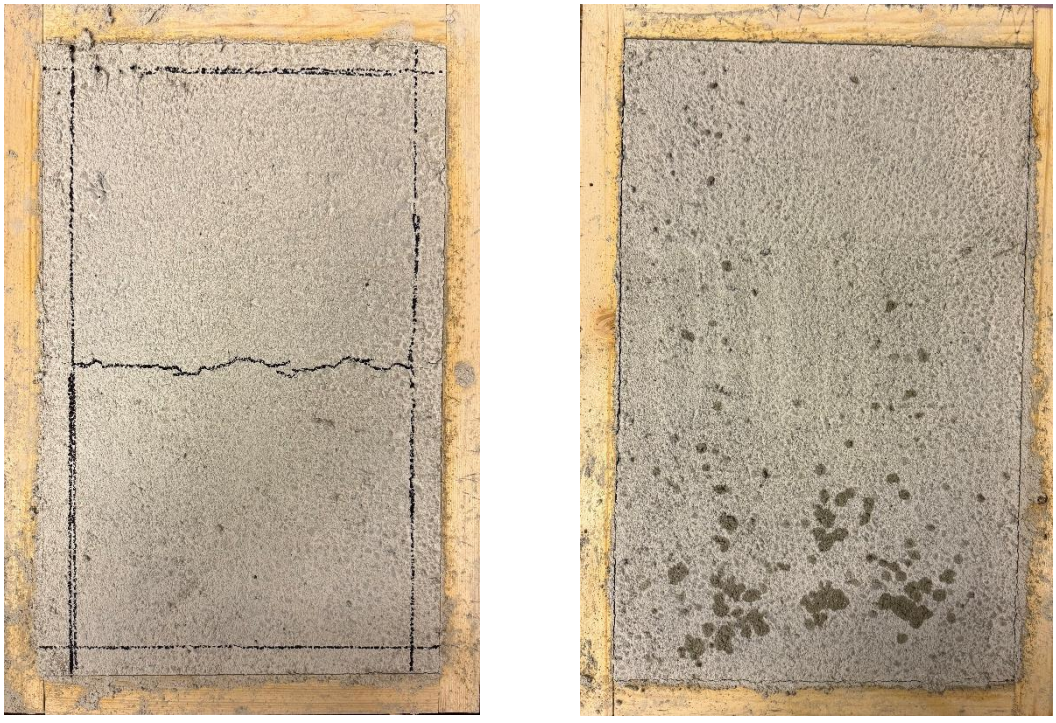

Figure B4: LM25 plastic shrinkage panels

Salt Scaling

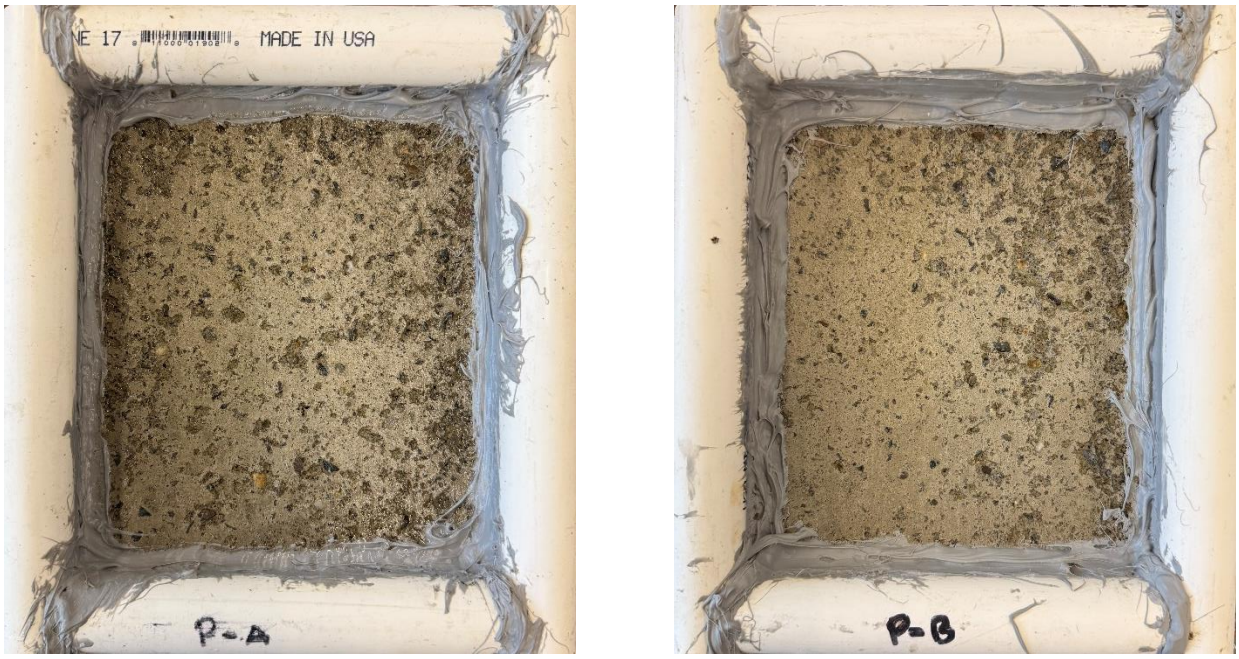

Figure B5: CSAP salt scaling specimens after 50 cycles

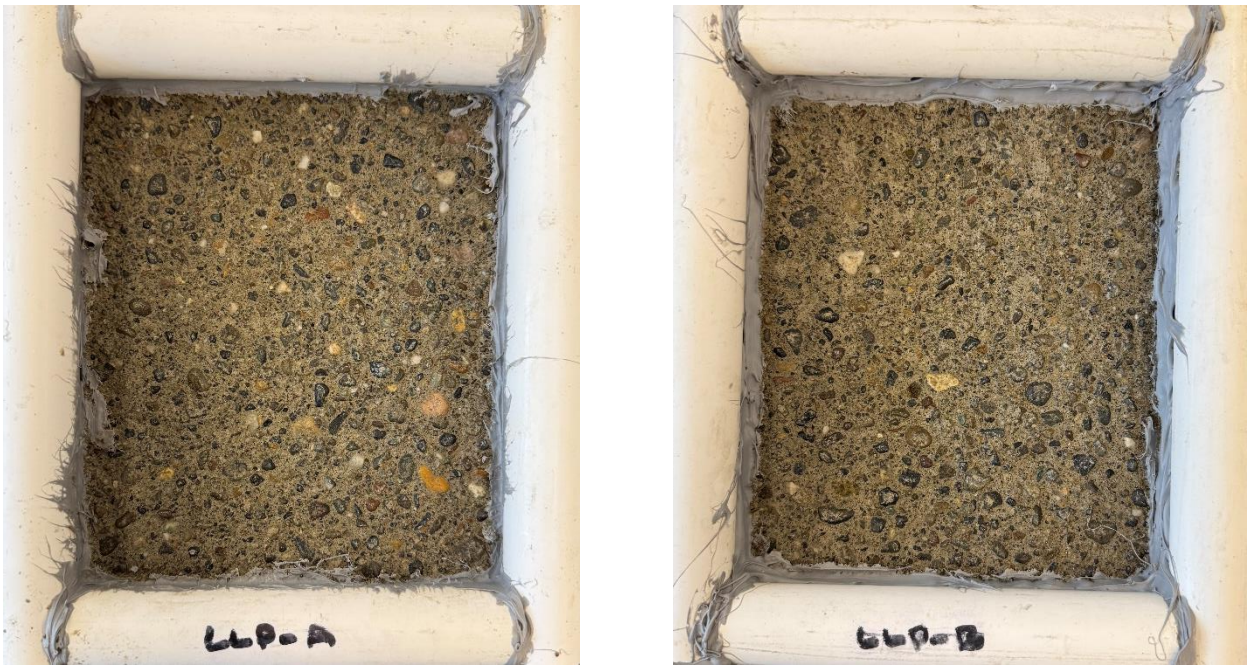

Figure B6: LLP salt scaling specimens after 50 cycles

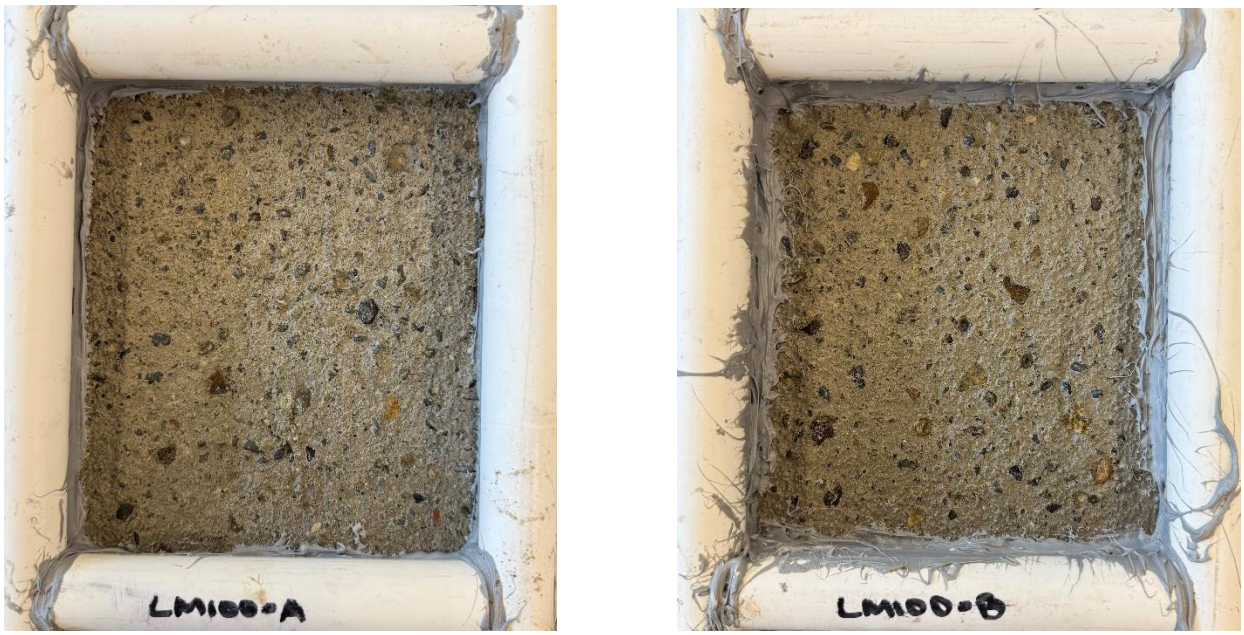

Figure B7: LM100 salt scaling specimens after 50 cycles

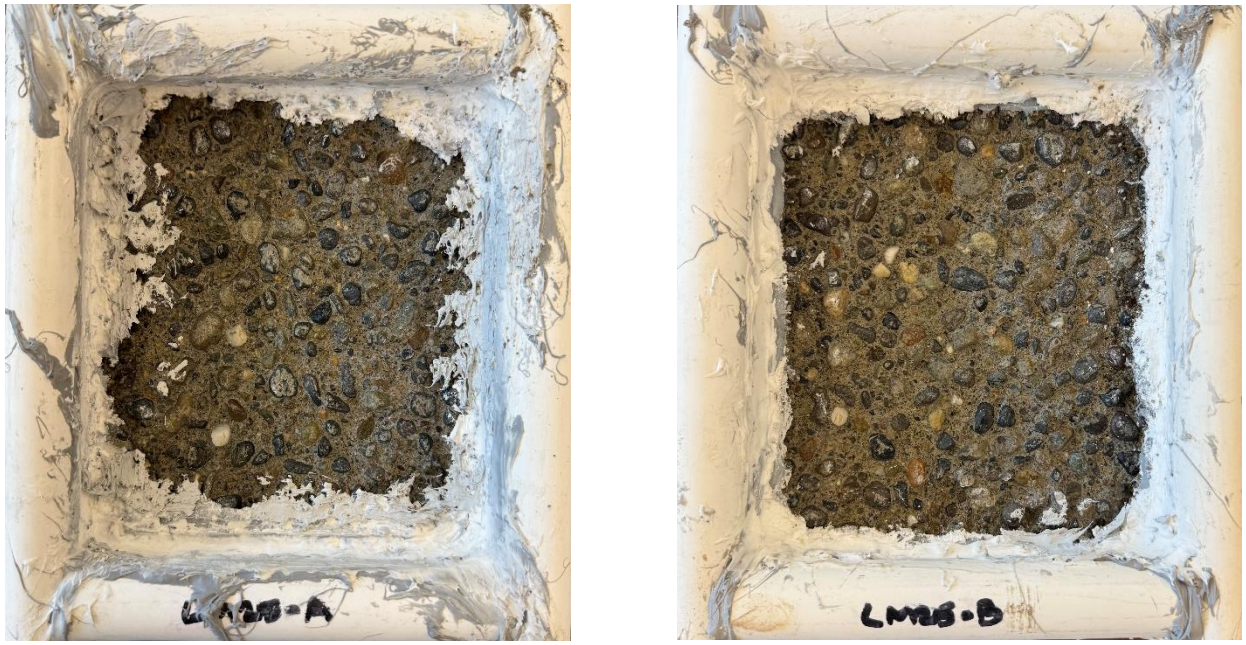

Figure B8: LM25 salt scaling specimens after 50 cycles